

SIGNAL PROCESSING BY THE CAT MIDDLE EAR:
ADMITTANCE AND TRANSMISSION, MEASUREMENTS
AND MODELS

by

Thomas Joseph Lynch III

B.S.E.E., University of Cincinnati
(1972)

S.M., Massachusetts Institute of Technology
(1974)

E.E., Massachusetts Institute of Technology
(1975)

SUBMITTED IN PARTIAL FULFILLMENT OF THE
REQUIREMENTS FOR THE DEGREE OF
DOCTOR OF PHILOSOPHY

at the

MASSACHUSETTS INSTITUTE OF TECHNOLOGY

February, 1981

© Massachusetts Institute of Technology 1981

Signature redacted

Signature of Author.....
Department of Electrical Engineering and Computer Science
February 27, 1981

Signature redacted

Certified by.....
William T. Peake
Thesis Supervisor

Signature redacted

Accepted by.....
Arthur C. Smith

ARCHIVES Chairman, Departmental Graduate Committee
MASSACHUSETTS INSTITUTE
OF TECHNOLOGY

JUL 30 1981

LIBRARIES

SIGNAL PROCESSING BY THE CAT MIDDLE EAR:
 ADMITTANCE AND TRANSMISSION, MEASUREMENTS
 AND MODELS

by

THOMAS JOSEPH LYNCH III

Submitted to the Department of Electrical Engineering
 and Computer Science on February 27, 1981
 in partial fulfillment of the requirements for
 the Degree of Doctor of Philosophy

ABSTRACT

A sound source designed to measure acoustic admittance at the cat tympanic membrane was constructed and tested. Measurements with a wide range of admittance magnitude (100 dB) and angle ($+90^\circ$) demonstrate an rms accuracy better than 1 dB in absolute admittance magnitude and 7° in angle over the frequency range of 10 Hz to 24.4 kHz.

The "source" consists of a sound generator (earphone), calibrated probe microphone, and acoustic elements which give it relatively small source admittance, Y_s . A Norton equivalent network was used to specify the source characteristics (i.e., Y_s , the source admittance, and U_t , the "short-circuit" volume velocity). This method has the advantage that the source need not generate constant volume velocity. Determination of "unknown" load admittances, Y_L , having magnitudes somewhat smaller than that of the source, $|Y_s|$, can be made precisely. Source specification was accomplished by measurement of sound pressure, P , in two "reference loads" of known admittance. Different reference loads were used for low and high ($f > 5$ kHz) frequency regions; cavities were used for low frequencies, while an acoustic transmission line and a very small cavity were used at high frequencies. This procedure allowed precise source specification over a broad bandwidth. A lumped-element electric network analog of the source was developed to provide insight into the detailed properties of the source; good agreement was obtained between model response (Y_s, U_t) and measured behavior.

The performance of the admittance measurement system was demonstrated in loads having resistive, mass, and compliant behavior (acoustic transmission line, free-space radiation, a long cavity, "parallel mass-compliance" network). The system was capable of tracking rapid magnitude and angle changes vs frequency, e.g., 60 dB in magnitude and 180° in angle over one octave. Other loads with cylindrical coupling space (between the load and source) terminated by a commercially available acoustic resistor were evaluated for five different resistor values. A section of lossless transmission line was used to account for this coupling space. Results indicate that some resistors have resistive impedance over a wide bandwidth (10 Hz to 15 kHz). The effects of small

variations in line length were examined.

The acoustic source was used to measure pressure (P_d) and admittance (Y_d) at the cat tympanic membrane. High impedance probe-microphones were used to measure pressure in the bulla (P_b) and tympanic (P_t) middle-ear cavities. Y_d and the pressure transfer ratio P_t/P_d were measured for "normal" and "experimentally modified" states of the middle-ear cavities (MECs). The modified states were 1) bulla cavity open widely, 2) the foramen between the tympanic and bulla cavities plugged, and 3) MECs opened widely. These input admittance and pressure transmission measurements were used to test a "series" model of the middle ear, $Z_d = Z_{mec} + Z_{doc}$, where the impedance of the MECs, Z_{mec} , is in series with the impedance measured with the cavities widely opened, Z_{doc} . The tests show the model to be valid for frequencies between 10 Hz and 22 kHz, except possibly in the frequency region near 13 kHz. Thus, Z_{doc} can essentially be interpreted as the impedance of the ossicular chain.

A lumped-element network model containing four elements (C_t , C_b , M_f , and $R_f(w)$) provides a good description of the impedance components of Z_{mec} for $10 \text{ Hz} < f < 10 \text{ kHz}$. Volumetric measurements of bulla-cavity and tympanic-cavity volumes are in excellent agreement with the acoustic measurements of the cavity compliances, C_t and C_b , indicating that the MECs are accurately represented by $C = V/pc^2$ for low frequencies. Average volumetric results are 0.66 cc for the bulla and 0.22 cc for tympanic cavity. Fair agreement was found between foramen dimensions and the model elements of acoustic mass, M_f , and acoustic resistance, $R_f(w)$.

Measurements are reported concerning the spatial variation in bulla cavity pressure, input admittance and MEC pressures with tympanic membrane perforations, and the effects of the ear canal coupling space.

Measurements of admittance at the tympanic membrane (TM) with the MECs opened, Y_{doc} , were made for various "experimental modifications" of the ossicular chain (e.g. removal of the cochlear "load", joint interruption, mass loading of the ossicles, fixation of the incus or malleus). Removal of the cochlear "load" or interruption of the incudo-stapedial joint, significantly affects Y_{doc} for frequencies in the 1 kHz to 2 kHz region. Our previous measurements of cochlear input impedance (Lynch et.al, 1981) were combined with average measurements of Z_{doc} to calculate an ideal "transformer ratio" ($T = 52$) which is a valid representation of the middle ear only for a narrow range of frequencies in the vicinity of 2 kHz to 3 kHz. The portion of the TM which is not coupled to malleus motion, Z_{tmu} , apparently controls Z_{doc} for frequencies above 4 kHz and is insignificant for $f < 1 \text{ kHz}$. The low-frequency compliance of Y_{doc} is primarily determined by 1) the annular ligament of the stapes and 2) the "coupled" TM and malleus compliance. Prominent inertial effects of the ossicles are not detectable in Y_{doc} for the normal intact ossicular chain; measurements of "mass loading" of the manubrium indicated effects in the 2 kHz to 3 kHz region. The input admittance at the TM with MECs intact, Y_d , was also measured when static pressures were applied to the middle-ear cavities.

Thesis Supervisor: Dr. William T. Peake

Title: Professor of Electrical and Bio-engineering

ACKNOWLEDGEMENTS

I would like to express gratitude to Professors William T. Peake, Thomas F. Weiss, and H. Steven Colburn and Dr. Nelson Y.-S. Kiang, Dr. John J. Rosowski, Dr. William M. Rabinowitz, and Dr. John J. Guinan of the Eaton-Peabody Laboratory of Auditory Physiology for their encouragement, suggestions, and criticisms, which have provided an environment conducive to scientific investigation. My association with the Laboratory has been most inspiring.

My sincerest thanks go to Professor William T. Peake, my thesis advisor, who has given me much advice, technical assistance and personal support during the years spent performing the research for my master and doctoral theses. It is truly a privilege to have worked with him.

Most members of the Eaton-Peabody Laboratory have provided assistance in various ways. I warmly thank you all. Some have provided key assistance and deserve special mention. Donald C. Galley wrote most of the software used to perform frequency-response measurements. Alan Crist designed, built, and maintained one of the meters used to measure phase angle. Lanelle Miller, Dianne Doot, Joanne Larrabee, and Betsy Marr performed the surgical preparations and measurements of ossicular masses. The figures for this thesis were drawn by Joanne Larrabee; their neatness and clarity reflect her excellent drafting skills. Susan Beckvold was extremely helpful in the final editing and production of this thesis document.

Finally, I would like to thank my family. My mother and father, Mary Ellen and Thomas Lynch Jr., have inspired me to pursue my education in terms of formal training, and practical experience; any experience,

whether positive or negative, can be viewed as a "learning experience." They have taught me the meaning of honesty, character, and "common sense" which are so much a part of the process of scientific investigation. My wife, Marjie Lovering-Lynch, also helped in the final production of this document. She has always been quite supportive and has made many sacrifices to allow the completion of this research. She also enthusiastically participated in our role as tutors in Burton House at M.I.T. and has substantially contributed to the quality of student life on Burton 5.

For most of the time spent on my doctoral research, financial support was provided by a M.I.T. Whitaker Health Sciences Fund Fellowship and by grants from the National Institutes of Health. I am grateful for this support.

TABLE OF CONTENTS

| | |
|------------------------|---|
| TITLE PAGE..... | 1 |
| ABSTRACT..... | 2 |
| ACKNOWLEDGEMENTS..... | 4 |
| TABLE OF CONTENTS..... | 6 |

Chapter I

A SYSTEM FOR AUDIO FREQUENCY
ACOUSTIC ADMITTANCE MEASUREMENTS

| | | |
|-----|--|----|
| I. | INTRODUCTION..... | 12 |
| | A. Methods and Applications..... | 12 |
| | B. The Approach..... | 14 |
| II. | METHODS..... | 16 |
| | A. The Measurement Scheme..... | 16 |
| | B. Acoustic Source Design..... | 19 |
| | 1. Specifications..... | 19 |
| | 2. Hardware Realization..... | 19 |
| | C. Stimulus Generation and Response Measurement..... | 22 |
| | D. Pressure Calibration..... | 24 |
| | E. Source Specification..... | 26 |
| | 1. Detailed Method..... | 26 |
| | 2. Choice of Reference Loads..... | 28 |
| | 3. Y_{sL} and U_{tL} : Low Frequency Calibration Procedure..... | 30 |
| | 4. Y_{sh} and U_{th} : High Frequency Calibration Procedure..... | 32 |
| | 5. Consistency of \bar{Y}_{sL} and Y_{sh} | 34 |

| | | |
|------|--|-----|
| 6. | Data Processing for Unknown Load Estimates, Y_L | 36 |
| 7. | Noise and Artifact Measurements..... | 38 |
| 8. | Source Stability..... | 39 |
| F. | Network Model of the Source..... | 42 |
| 1. | Model Topology and Element Values..... | 42 |
| 2. | The Source Admittance, Y_S^m and Y_S | 43 |
| 3. | Source Volume Velocity, U_t^m and U_t | 45 |
| III. | PERFORMANCE TESTS..... | 50 |
| A. | Admittance Predictions for Test Loads with No Coupling Space..... | 50 |
| 1. | Tygon Transmission Line..... | 51 |
| 2. | The "Long" Cavity..... | 53 |
| 3. | Radiation Admittance..... | 54 |
| 4. | A "Parallel Mass-Compliance" Load..... | 55 |
| B. | Test Loads with Cylindrical Coupling Space..... | 58 |
| 1. | Admittance Measurements..... | 58 |
| 2. | Effects of Small Variations in Line Length..... | 60 |
| C. | Measurement Summary and Error Limitations..... | 62 |
| 1. | Admittance Measurement Space and Error Limitations..... | 62 |
| 2. | Low Frequency Compliance Estimates and Measurement Imprecision..... | 63 |
| | APPENDIX A..... | 66 |
| | FOOTNOTES..... | 68 |
| | TABLES..... | 72 |
| | FIGURE CAPTIONS..... | 75 |
| | FIGURES..... | 81 |
| | REFERENCES..... | 107 |

Chapter II

ACOUSTIC PROPERTIES OF THE MIDDLE-EAR
CAVITIES OF CAT

| | | |
|------|---|-----|
| I. | INTRODUCTION..... | 110 |
| | A. Toward a Theory of the Mechanics of the Middle Ear..... | 110 |
| | B. Effects of the Middle-Ear Cavities: An Approach..... | 111 |
| II. | METHODS..... | 115 |
| | A. Animal Preparation..... | 115 |
| | B. Stimulus Generation and Response Measurement..... | 118 |
| | C. Admittance Measurements..... | 119 |
| | D. Middle-Ear Cavity Pressure Measurements..... | 119 |
| | 1. Construction of the Probe-Microphones..... | 119 |
| | 2. Calibration Procedure..... | 120 |
| | 3. Measurement Procedure..... | 123 |
| | E. Volumetric Measurements of Cavity Volumes..... | 123 |
| III. | RESULTS..... | 127 |
| | A. Admittance Measurements..... | 127 |
| | 1. Correction for the Source-Tympanic Membrane Coupling Space..... | 127 |
| | 2. Stability..... | 130 |
| | 3. Y_d : Manipulations of the Middle-Ear Cavities..... | 132 |
| | 4. Y_d and Y_{doc} : Measurement Summary Across Cats..... | 133 |
| | 5. Bulla Admittance: Y_d | 136 |
| | 6. Tympanic Membrane Holes and Z_{mec} | 137 |
| | B. Middle-Ear Cavity Pressure Measurements..... | 139 |

| | | |
|-----|---|-----|
| 1. | Intact Middle-Ear Cavities..... | 139 |
| 2. | Manipulations of the Middle-Ear Cavities..... | 140 |
| 3. | P_b/P_d : Effect of Bulla Pressure Probe Location..... | 142 |
| 4. | Measurements with a Tympanic Membrane Hole..... | 145 |
| IV. | DISCUSSION..... | 146 |
| A. | Interpretation of Measurements as Acoustic Admittance..... | 146 |
| B. | Comparisons to Previous Measurements..... | 148 |
| 1. | Impedance Measurements..... | 148 |
| 2. | MEC Pressure Measurements..... | 153 |
| C. | Wideband Test of the Series Model..... | 154 |
| D. | Correlation of Middle-Ear Cavity Admittance and Middle-Ear Cavity Volumes..... | 156 |
| E. | Network Model of the Middle-Ear Cavities..... | 159 |
| 1. | The Pressure Ratio: P_b/P_t | 159 |
| 2. | Estimates of the MEC Model Impedances..... | 160 |
| 3. | Correlation of Foramen Geometry with M_f and $R_f(w)$ | 165 |
| 4. | Comments Concerning M_f | 166 |
| V. | SUMMARY..... | 167 |
| | FOOTNOTES..... | 169 |
| | TABLE I..... | 171 |
| | FIGURE CAPTIONS..... | 172 |
| | FIGURES..... | 179 |
| | REFERENCES..... | 206 |

Chapter III

COMPONENTS OF THE ADMITTANCE OF
THE CAT OSSICULAR CHAIN

| | | |
|------|--|-----|
| I. | INTRODUCTION..... | 208 |
| II. | METHODS..... | 210 |
| | A. Input Admittance at the TM, Y_d , and Static MEC Pressure..... | 210 |
| | B. Surgical Preparation and Experimental Modificatins..... | 211 |
| | C. Measurements of Ossicular Mass..... | 212 |
| III. | RESULTS..... | 213 |
| | A. Experimental Modification of the Cochlea and Joints..... | 213 |
| | 1. Removal of the Cochlear "Load"..... | 213 |
| | 2. Interruption of the Incudo-Stapedial Joint..... | 214 |
| | 3. Interruption of the Manubrium of the Malleus..... | 216 |
| | B. "Mass Loading" of the Manubrium..... | 217 |
| | 1. "Mass Loading" of the Intact Ossicular Chain..... | 218 |
| | 2. "Mass Loading" on the Interrupted Manubrium..... | 219 |
| | C. "Blocking" of the Ossicles..... | 219 |
| | D. Effects of Positive and Negative Static MEC Pressures..... | 221 |
| IV. | DISCUSSION..... | 223 |
| | A. On the "Transformer Ratio" of the Middle Ear..... | 223 |
| | B. Z_{doc} : Implications for Models of Cat Middle-Ear Mechanics...226 | |
| | 1. Z_{jis} : The Incudo-Stapedial Joint Impedance..... | 226 |
| | 2. Components of the Low-Frequency Compliance, C_{doc} | 227 |
| | 3. High Frequencies: Effects of Z_{tmu} | 230 |
| | 4. Inertial Effects of the Malleus and Incus..... | 231 |
| | C. Implications from Measurements of Static MEC Pressure..... | 233 |

TABLE I.....236
FIGURE CAPTIONS.....237
FIGURES.....240
REFERENCES.....255
BIOGRAPHICAL NOTE.....257

Chapter I

A SYSTEM FOR AUDIO FREQUENCY ACOUSTIC ADMITTANCE MEASUREMENTS

I. INTRODUCTION

A. METHODS AND APPLICATIONS

Various experimental methods have been used to determine acoustic impedance. Some of these methods have been previously reviewed (Beranek, 1949; Gatley and Cohen, 1969). Beranek (1949) has classified these methods into three broad groups: 1) "SURFACE METHODS" which "utilize data taken at or very near the surface of the sample" (i.e., the unknown impedance element) "exposed to a plane wave sound field", 2) "TRANSMISSION LINE METHODS" in which "data are taken at various points somewhat removed from the surface of the sample", and 3) "COMPARISON METHODS" which require a known standard of acoustic impedance for comparison with the impedance to be determined."

Details of the implementation of these methods in terms of hardware, signals, and signal processing are usually dictated by the specific application. Several of these applications are surveyed below. Surface methods are the most direct; the coupling space between the source and load is essentially nonexistent. Mawardi (1949) used a constant volume velocity source (assuming infinite source impedance) and a single "pressure" measurement to determine the acoustic impedance of an acoustic

absorber material. Others have used a similar approach for measurement of acoustic impedance at the tympanic membrane (Møller, 1960, 1963, 1965; Rabinowitz, 1981) but have accounted for the finite source impedance; however, the coupling space was not negligible and was modelled as a lossless transmission line. The transmission line method has been extensively used with various types of excitation signals (e.g., sinusoids, impulses, tone bursts, noise). Recent applications include measurements of acoustic impedance in the ear (Blauert and Platte, 1974; Mehrgardt and Mellert, 1977), the lung (Fredberg, Jackson and Dawson, 1975), automotive mufflers (Seybert and Ross, 1977), ocean bottom sediment samples (Martin, 1974), and fluid machinery manifolds (Singh and Soedel, 1978). The first experimental determination of impedance in the ear used the comparison method in the form of an acoustic bridge (Metz, 1946; Zwislocki, 1963). Currently, the electroacoustic bridge (Terkildsen and Neilson, 1952) is widely used in clinical environments to measure impedance at the tympanic membrane.

In summary, there are several approaches to measurement of acoustic impedance. The choice of a method depends upon a number of factors including the type of sample, measurement requirements, available hardware, and computational power. The purpose of this paper is to describe an approach (basically a surface method) which we have used to measure a wide variety of acoustic impedances. This approach, historically, was not used extensively because of the effort required for the complex-number arithmetic; the availability of digital computers reduces this effort dramatically.

B. THE APPROACH

Our approach is to characterize the acoustic source in terms of its Norton equivalent network (FIGURE 1A). If the source is a linear system, its terminal behavior may be completely described in terms of a constant volume velocity, $U_t(f)$, and internal source admittance, $Y_s(f)$ (Bose and Stevens, 1965; Møller, 1960; Egolf and Leonard, 1977; Rabinowitz, 1981). Thus, specification of the source involves a calibration procedure used to determine the complex amplitudes of $U_t(f)$ and $Y_s(f)$. These quantities are obtained by measuring the complex amplitude of the pressure response, P_r , in two "reference" loads whose admittances are known theoretically (FIGURE 1B). In principle, once the source is specified, we may determine any unknown load admittance, $Y_L(f)$, through measurement of the pressure, $P_L(f)$, when connected to the source (FIGURE 1C). In practice, error in the source specification limits the magnitude of load admittances which may be determined to approximately $|Y_L| > 0.1|Y_s|$ for reasonable measurement precision. Another practical problem is the characterization of the coupling space between the source and load.

The particular hardware configuration of our source was primarily determined by our desired application--measurement of acoustic impedance at the tympanic membrane in cat. Our system provides relatively quick and precise determination of the acoustic impedance for frequencies between 10 Hz and 22.4 kHz over a wide range of impedance values. It represents a significant improvement in terms of useful bandwidth, dynamic range, and precision over methods reported previously to

determine admittance in cat (Møller, 1960, 1963, 1965; Tonndorf and Khanna, 1967; Khanna and Tonndorf, 1972; Margolis et al., 1978). Our system is suitable for evaluating small samples of sound absorbing material and acoustic filter structures, such as those used in hearing aids and hearing protectors.

The approach of specifying the Norton equivalent network of the source is potentially useful in other applications. The transducer used to generate the sound stimulus must be a linear device, but it need not generate either constant volume velocity or constant volume displacement. Thus, other mechanical configurations and transducers (with correspondingly different values of U_t and Y_s) may easily be used to meet other requirements. In general, it is necessary to determine U_t and Y_s ; under some conditions ($Y_s \ll Y_L$) only U_t need be determined. Also, in nonphysiological environments it is usually possible to precisely control the mechanical dimensions of the coupling space; thus, the acoustical effects of this space may be theoretically specified and taken into account in a straightforward manner, as demonstrated in Section III.

II. METHODS

A. THE MEASUREMENT SCHEME

In principle, the source admittance, Y_s , and total source volume velocity, U_t (FIGURE 1A), can be determined by measurement of sound pressure, P_{ri} , in two ($i = 1,2$) different "reference" loads of known admittance, Y_{ri} , (FIGURE 1B) giving

$$U_{t1} = P_{r1}(Y_s + Y_{r1}) \quad (1)$$

$$\text{and } U_{t2} = P_{r2}(Y_s + Y_{r2}) \quad (2)$$

Assuming that the volume velocity, U_t , remains constant (corresponding to constant voltage excitation, E_o , and constant source characteristics, K_s ; $K_s E_o = U_t$), we equate the right hand sides of Equations (1) and (2) and solve for the source admittance

$$Y_s = (P_{r2}Y_{r2} - P_{r1}Y_{r1}) / (P_{r1} - P_{r2}) \quad (3)$$

Once Y_s is known, we may calculate the source volume velocity, U_t , using either Equation (1) or (2).

With the source specified, an unknown load admittance, Y_L , can be determined by measurement of the pressure, P_L , in this load (FIGURE 1C):

$$Y_L = (U_t/P_L) - Y_s \quad (4)$$

Substituting for U_t either Equation (1) or (2), ($i = 1,2$), we have

$$Y_L = ((Y_{ri} + Y_s)(P_{ri}/P_L)) - Y_s \quad \text{or rewriting,}$$

$$Y_L = Y_{ri}(P_{ri}/P_L) + Y_s\{(P_{ri}/P_L) - 1\}. \quad (5a)$$

Substituting Equation (3) into Equation (5a), choosing the $i = 1$ reference condition we obtain

$$Y_L = Y_{r1}(P_{r1}/P_L) + \{Y_{r2} - Y_{r1}(P_{r1}/P_{r2})\} \frac{\{(P_{r1}/P_L) - 1\}}{(P_{r1}/P_{r2}) - 1}. \quad (5b)$$

Thus, to determine Y_L , it is sufficient to measure pressure ratios or alternatively to measure the output-voltage ratios of a linear pressure transducer (see Section II E 1).

The accuracy of the Y_L estimate obtained from Equation (5b) depends on the relative values of the admittances Y_L , Y_s , Y_{r1} , and Y_{r2} . If $|Y_s|$ is "negligibly small" (i.e., $|Y_s| \ll |Y_{ri}|$ and $|Y_s| \ll |Y_L|$; the limiting case is $|Y_s| = 0$, Equation 5a) the estimate of the load admittance can be obtained from measurements in only one reference load (Y_{ri}), and the load admittance can be calculated as $Y_L = Y_{ri}(P_{ri}/P_L)$. In this case, errors in the Y_L estimate can result from two factors: 1) error in the theoretically specified value for the reference load, Y_{ri} , and 2) errors in the measured pressure ratio P_{ri}/P_L , which depend upon the linearity and precision of the measurement system, and

signal-to-noise ratio (S/N) of the measurements.

When Y_s is not negligible, errors in the load estimate may arise from both terms of Equation (5) and the accuracy of the Y_L estimate depends on the accuracy of the Y_s estimate. It is clear that three sets of conditions can lead to large errors in the Y_L estimation, even if the reference loads, Y_{r1} and Y_{r2} , and the pressure ratios are quite precise (Egolf and Leonard, 1977): 1) If $Y_{r1} \cong Y_{r2}$, then $P_{r1} \cong P_{r2}$ and two of the factors of the second term of Equation (5b) will be small and will produce errors which are much larger than the error in the pressure measurement. 2) If both $|Y_{r1}| \gg |Y_s|$ and $|Y_{r2}| \gg |Y_s|$, then $P_{r1}Y_{r1} \cong P_{r2}Y_{r2}$ and the term, $Y_{r2} - Y_{r1}(P_{r1}/P_{r2})$, of Equation (5b) will be small and may cause errors. This conclusion is intuitively reasonable. Since, for this condition Y_s has little effect on the reference load pressure measurements, estimation of Y_s from these measurements will be inaccurate. 3) If both $|Y_{r1}| \ll |Y_s|$ and $|Y_{r2}| \ll |Y_s|$, then $P_{r1} \cong P_{r2}$ and the denominator of the second term of Equation (5b) is small and inaccurate.

All of these conditions are avoided if $Y_{r1} \ll Y_s \ll Y_{r2}$, and a simplification of the above results is possible. Equating Equation (1) and (2), $P_{r1}(Y_s + Y_{r1}) = P_{r2}(Y_s + Y_{r2})$. Since $|Y_{r1}| \ll |Y_s|$, $P_{r1}Y_s \cong P_{r2}(Y_s + Y_{r2})$ and $Y_s = P_{r2}Y_{r2}/(P_{r1} - P_{r2})$. Also $|P_{r1}| \gg |P_{r2}|$, so that $(P_{r1} - P_{r2}) \cong P_{r1}$, and we have the result

$$Y_s \cong Y_{r2}(P_{r2}/P_{r1}) . \quad (6)$$

In this case it is not necessary to compute any differences between complex numbers. We have used this situation to increase the precision

of our Y_s estimate (Section II E 4).

B. ACOUSTIC SOURCE DESIGN

1. Specifications

The design goals for the source were as follows: 1) SMALL SOURCE ADMITTANCE relative to the input admittance of the cat (cat equivalent volume $\cong 0.3$ cc, $f < 1$ kHz); 2) WIDE BANDWIDTH (10 Hz to 20 kHz, if possible); 3) capability for admittance measurements over a LARGE RANGE in magnitude and angle with stimulus pressures as high as 105 dB SPL across the above frequency range; 4) PRECISION of approximately 10% in magnitude and 10° in angle, which is influenced by the measurement system's resolution, linearity, signal-to-noise ratio, etc., and the source transducers (earphone, microphone) that were selected; and 5) appropriate MECHANICAL CONFIGURATION to allow (a) good acoustic coupling to the cat earcanal (a function of earcanal diameter and length, skull geometry, etc.), and (b) convenient modifications of the source in order to accomodate different types of experiments, to remove foreign matter from the probe tube, and to replace damaged parts.

2. Hardware Realization

The acoustic system is a closed sound system which consists of a

sound source (earphone) and a pressure measurement transducer (FIGURE 2). E_e is the electrical input to the earphone which generates a sound pressure, P_L , at the acoustic load. This pressure response is measured using the probe-microphone (output voltage, E_p). The earphone is a Bruel & Kjaer 1/2" condenser microphone (4134, equivalent volume V_0) which was placed near (0.010 cm) the end of its enclosure, leaving an air space, V_1 . The pressure transducer is an electret microphone (Knowles EA-1842) of equivalent volume V_5 , coupled to a probe tube (0.1 cm o.d.; \cong 0.06 cm i.d.; length \cong 1 cm) which is damped with a short (0.3 cm) piece of 29 gauge hypodermic needle (0.018 cm i.d.) inserted into the probe tube. R_5 and M_5 represent the combined characteristics of both probe tube and damper. A tube, R_3 (\cong 14 cm x 29 gauge), is used to prevent static pressure build-up (calculated break frequency \cong 1.9 Hz).

Two acoustic resistors are used to decrease the source admittance, Y_s ; each decouples a portion of the total air space between the earphone diaphragm and the tip of the acoustic system. R1 (Knowles BF-1923; fused-mesh type, 4700 ohm) is used to decouple the volume V_1 from V_2 , and is mounted in a plexiglass or aluminum holder that force fits into the sound tube, also removing some volume from the system. R2 is "homemade" from resistance screen material similar to that of R1 (Killion, 1980). Five minute epoxy (at room temperature) was used to glue the screen material to a small aluminum ring (o.d. \cong 0.400 cm, i.d. \cong .364 cm, length \cong 0.064 cm); a hole was made in the center of the screen using a hot soldering iron with a fine tip. The probe tube passed through the hole and was fastened to the screen with the epoxy. The resistance of R2 could be manipulated somewhat by controlling the

spread of the epoxy over the area of the screen. R_2 is used to decouple $(V_1 + V_2)$ from $(V_3 + V_4)$. Placement of R_2 near the tip of the sound tube is important because it minimizes $(V_3 + V_4)$. Since R_2 is a relatively high impedance at high frequencies, the high-frequency source admittance, Y_s , is controlled by the volume at the tip $(V_3 + V_4)$. Note that R_2 was mounted such that the screen material was slightly recessed, leaving a volume V_3 at the tip of the sound tube. This space reduced the possibility of contact between grease (used to seal loads to the source) and the screen; plugging of the screen could result upon contact.

Two nichrome wire (0.002" diameter; 168 ohm/ft.) heater coils were wound onto the system. One was used to reduce condensation on the diaphragm of the 1/2" earphone; the other was used to keep the probe tube damper patent. These heaters were only necessary for measurements in humid environments such as a cat ear; in this situation the heater currents were: earphone heater ($R = 364$ ohms) $I = 35$ ma, and probe-tube heater ($R = 66$ ohms) $I = 55$ ma.

Note that the probe tube extends 0.15 cm beyond the actual tip of the sound tube. This extension was used to decrease the coupling space between the source and load by moving the plane of pressure measurement closer to the load. The volume due to this extension (V_4 , enclosed by dashed line; diameter equal to that of the inner diameter of the sound tube) is included in the source admittance of the acoustic system, Y_s . In other words, the plane of source specification and admittance measurement is at the plane of the probe-tube tip, rather than at the end of the sound tube.

C. STIMULUS GENERATION AND RESPONSE MEASUREMENT

A computer-controlled system (Weiss et al., 1969) was used to control stimulus presentation, measurements, data storage and display, and manipulation of frequency responses (FIGURE 3). The stimulus section used to generate a sinusoidal sound pressure of complex amplitude, P_L , consists of a programmable oscillator (Wavetek Model 157) and attenuator (Charybdis Model D), earphone amplifier, and the 1/2" condenser earphone of the acoustic system. The measurement section consists of a programmable gain amplifier (7 steps of 6 dB gain, accurate to within 0.3 dB, from 10 Hz to 20 kHz), tracking filter (Spectral Dynamics SD101B-1 with 2 Hz bandwidth), log converter (Spectral Dynamics SD112-1), phase meter (Dranetz 305B with PA-3002), multiplexer, and 12 bit A/D converter. The frequency response of the measurement system itself (i.e., $E_o \bar{=} E_p$ in FIGURE 3) was routinely measured and used to correct subsequent measurements. Also, the frequency responses of various components of the system (amplifiers, etc.) were measured, stored, and used to make corrections. After the system was calibrated, it was used to determine the magnitude and angle of the fundamental component of the probe-microphone response, E_p .

Magnitude and angle data were taken at discrete frequencies starting at 10 Hz, with a frequency spacing of 40 points/decade. Measurements were made at 149 frequencies (10 Hz to 50.1 kHz); 10 magnitude<angle> samples were taken at each frequency and were averaged to obtain each magnitude<angle> "data point". After each frequency change, a delay of 1.5 seconds allowed the tracking filter and phase meter outputs to settle

before taking magnitude<angle> samples. Approximately 6.5 minutes were required to complete a single frequency response with the above parameters.

The resolution of this measurement system is limited¹ by the integer storage mode of our software rather than by the A/D converter. Thus, the system resolution limit is ± 0.1 dB and $\pm 0.36^\circ$. The precision of the admittance estimate is partially determined (Section II A) by the ratio of the voltage measurements, E_{ri}/E_L , which assuming system linearity, would lead to ± 0.2 dB and $\pm 0.72^\circ$ precision for this quantity. Measurements of system output voltage vs system input voltage (amplitude sweeps) at 32, 100, 316, 1000, 10,000 Hz, show the maximum deviations from linear behavior to be ± 0.35 dB, $\pm 1.8^\circ$ for the voltage levels used in our admittance measurements. Amplitude sweeps of the measurement system plus the acoustic source at the above frequencies did not differ significantly from those of the measurement system alone. Thus, maximum bounds on the linearity and imprecision of the measurement system and source are ± 0.55 dB and $\pm 2.5^\circ$. Since most of our measurements are made using a small portion of the system dynamic range, the precision of the ratio E_{ri}/E_L is probably close to the limits set by the system resolution.

All measurements reported in this paper were performed with the source located in a low-noise chamber (Ver et al., 1975), which provides at least 80 dB of acoustic isolation.

D. PRESSURE CALIBRATION

As stated above, it is not necessary to determine the voltage/pressure calibration of the probe-microphone in order to determine admittances. However, it is sometimes convenient to use this calibration to display the measurement results in terms of pressure rather than voltage.

The calibration procedure is essentially the same as that described by Weiss and Peake (1972). The acoustic system is inserted into a small cylindrical duct terminated by a 1/8" diameter condenser microphone (B & K, 4138) which is used as a reference pressure transducer (the absolute sensitivity and relative frequency response of this microphone² are determined with a pistonphone and electrostatic actuator, respectively; Bruel, 1964, 1965). A sinusoidal sound pressure is generated in the duct by applying a constant signal, E_e , to the earphone; the output voltages of the probe-microphone/amplifier (E_p) and reference microphone are measured as frequency is swept. Using the reference transducer E/P calibration, and assuming the pressures at both transducers are equal, we calculated the E_p/P calibration of the probe-microphone system $H_p(f) = E_p(f)/P(f)$ (FIGURE 4). This frequency response was stored in the computer system and used automatically to convert measured probe-microphone output voltage, E_p , to pressure.

The assumption of equal pressures at the reference and probe-microphones can easily be examined theoretically. The radius of the circular duct is $r = 0.278$ cm. The cutoff frequency for the first mode above the fundamental is $f_{1,0} = (X_0 c)/(2\pi r) = 36.3$ kHz,

($c = 3.4 \times 10^4$ cm/s, $X_0 = 1.84$, for the first asymmetric mode; $X_0 = 3.83$, first circularly symmetric mode, $f_{0,1} = 75.6$ kHz; Eriksson, 1980). Thus, for the audio frequencies of interest we assume that uniform plane wave propagation is predominant. The impedance of the reference microphone, Z_{rm} (which can be approximated by a compliance; Frederiksen, 1977), is high relative to the characteristic impedance of the duct,

$$Z_0 = \rho c/A = 168 \text{ d-s/cm}^5 \ll |Z_{rm}| = (\rho c^2)/(2\pi fV) = (2.24 \times 10^9)/f,$$

$$\text{or } |Z_{rm}/Z_0| = (1.3 \times 10^7)/f,$$

for $V = 10^{-4}$ cc and $\rho = 1.18 \times 10^{-3}$ g/cm³. Thus, for most audio frequencies we may assume that the pressure distribution is equal to that for a tube with a rigid termination. In our calibration cavity the distance from the tip of the probe tube to the diaphragm of the reference microphone is $y = 0.075$ cm. Thus, the magnitude ratio of the pressure at the probe-tube tip to that at the 1/8" reference microphone should be given by $\cos\{(2\pi yf)/c\} = 0.954$ or -0.41 dB, for $f = 22.4$ kHz. Therefore, longitudinal spatial variation of pressure is small and the assumption of equal pressure at both transducers introduces only small error. 22.4 kHz was used in the above calculation since it is the high frequency limitation imposed upon our data by "artifact" (Section II E 7).

The precision of the calibration might also be affected by changes in barometric pressure and temperature. Fluctuations observed in barometric pressure are approximately 760 ± 5 mm Hg (0.7% or 0.06 dB) and may be ignored. Temperature changes are usually less than $\pm 3^\circ$ C and may also be ignored. In summary, the precision of the relative frequency

response of the E_p/P calibration is probably within ± 0.8 dB and $\pm 3.2^\circ$ for low frequencies where the pressure at the probe-tip equals that at the 1/8" reference microphone. At 22.4 kHz the magnitude precision may be degraded to ± 1.2 dB by the spatial variation in pressure (0.4 dB) between these microphones. The value of absolute pressure sensitivity is not important for our measurements; however, it is probably correct to within ± 1.5 dB.

E. SOURCE SPECIFICATION

1. Detailed Method

We may expand the calibration procedure outlined in Section II A to allow for different levels of U_t , and to explicitly show the computation of Y_s , U_t , and Y_L in terms of the measured pressures or voltages.

Measurements show the probe-microphone to be linear with transfer function, $H_p = E_p/P$. Equation (5) may be rewritten in terms of the probe-microphone calibration and the particular level of earphone excitation, E_{oi} , as follows for each reference load condition ($i = 1,2$):

$$U_{t1} = K_s E_{o1} = P_{r1} (Y_s + Y_{r1}) = (E_{p1}/H_p) (Y_s + Y_{r1}) \quad (7)$$

$$U_{t2} = K_s E_{o2} = P_{r2} (Y_s + Y_{r2}) = (E_{p2}/H_p) (Y_s + Y_{r2}) \quad (8)$$

We may take the ratio of U_{t1}/U_{t2} and solve for Y_s obtaining

$$Y_s = \frac{(P_{r1}/E_{o1})Y_{r1} - (P_{r2}/E_{o2})Y_{r2}}{(P_{r2}/E_{o2}) - (P_{r1}/E_{o1})} , \quad (9)$$

or expressing Y_s in terms of measured probe output voltage,

$$Y_s = \frac{(E_{p1}/E_{o1})Y_{r1} - (E_{p2}/E_{o2})Y_{r2}}{(E_{p2}/E_{o2}) - (E_{p1}/E_{o1})} . \quad (10)$$

Source specification consists of measuring the two pressure (P_{r1}/E_{o1} and P_{r2}/E_{o2}) or voltage transfer functions (E_{p1}/E_{o1} and E_{p2}/E_{o2}), and using the theoretical values of Y_{r1} and Y_{r2} to compute Y_s and U_t .

It is clear that Y_s is independent of the probe-microphone transfer function, H_p ; this factor appears in both numerator and denominator of Equation (10) and cancels out. We found the measurements expressed in terms of pressures to be useful in that it was easier to detect defects in the acoustic seal of the reference loads to the source; note that the voltage sweeps at low frequencies are not flat vs frequency (see the E_p/P calibration, FIGURE 4).

To calculate the actual source volume velocity, we must use H_p (Equations 7, 8). Note, however, that when U_t is substituted into Equation (4) to calculate an unknown load admittance, Y_L , the expression in terms of our pressure measurements becomes

$$Y_L = \frac{(P_r/E_{or})(Y_s + Y_r)}{(P_L/E_{oL})} - Y_s \quad (11)$$

or in terms of voltage ratios,

$$Y_L = \frac{(E_{pr}/E_{or})(Y_s + Y_r)}{(E_{pL}/E_{oL})} - Y_s ,$$

and the H_p factor also cancels out of the Y_L computation. Thus, computing Y_s and Y_L in terms of the measured voltage ratios or using H_p to correct the probe output voltage to load pressure, does not effect these results. We normally do not calculate U_t directly using Equations (7) or (8); Y_s and Y_L (Equations 9 and 11) are the only calculations necessary.

The only assumption we have made is that the earphone and earphone amplifier are linear devices, i.e., their combined transfer function, K_s , is independent of level (see APPENDIX A for an experimental verification of this assumption). When making calibration measurements, we have kept the input voltage constant and have not changed any gain setting in the measurement section of our system (with the exception of the programmable gain amplifier in some instances). This helps to minimize small errors in magnitude and angle that might arise due to any small nonlinearity or imprecision in the input attenuator or measurement amplifiers, etc..

2. Choice of Reference Loads

The precision of the source calibration depends heavily upon the extent to which the admittance of the actual reference load equals the theoretically specified admittance for this load. The most convenient

type of acoustic load to construct is a cavity. Its admittance for low frequencies is easily specified from the cavity geometry ($Y = (j\omega V)/(\rho c^2)$, where V is cavity volume). Additionally, for an earphone which is a source of constant volume displacement, the resulting pressure signal is constant vs frequency and, thus, easy to measure. However, calibrating with cavities may not be practical for frequencies near quarter wave resonances, since the resonant characteristics (e.g., damping) may not be well defined. Additionally, use of cavities whose inner radius is different from that of the inlet opening can be complicated, since higher-order modes significantly effect the sound field in the cavity and must be taken into account when calculating the input admittance of these loads³ (Ingard, 1948; Burkhard and Sachs, 1977). Therefore, for calibrations that are valid at high frequencies, one would like to use cavities whose length is short enough to keep the resonances well above 30 kHz (cavity length $\cong 0.29$ cm), while keeping the cavity diameter equal to that of the inner diameter of the acoustic source (0.4 cm, area $\cong 0.12$ cm²). This obviously constrains the volume of the cavity (to approximately 0.035 cc or less), which must also satisfy the admittance constraints discussed in Section II A. For our value of $|Y_s|$ (equivalent volume, $V_s \cong 0.12$ cc) we found that calibration above 8 kHz was not practical using only cavities as reference loads. Thus, another type of reference load was necessary to obtain a high-frequency calibration. We found that an acoustic transmission line could be used to obtain a constant resistive admittance over a wide bandwidth. Therefore, two calibration procedures were used to obtain two estimates of Y_s and U_t . 1) The low-frequency source

estimate, Y_{sL} and U_{tL} , was obtained with cavity reference loads; 2) the high-frequency estimate, Y_{sh} and U_{th} , was obtained with an acoustic transmission line and a very small cavity.

3. Y_{sL} and U_{tL} : Low Frequency Calibration Procedure

The low-frequency calibration of the source was obtained using three reference cavity loads of volume 0.052, 0.082, and 0.133 cc. The cavities were cylindrical, each having the same cross-sectional area, but differing in length, l' . The dimensions and geometry of these cavities⁴ are given in TABLE I. All were machined from plexiglass and the interior walls were made smooth by polishing with optical polishing compound mixed with a light oil. The cross-sectional area of each cavity was made equal to that of the source in order to minimize excitation of higher-order modes in the cavities, thus making the theoretical specification of these loads relatively simple.

The theoretical admittance of each reference load was specified as

$$Y_r = (jA/\rho c)\tan(2\pi fl'/c) \quad , \quad (12)$$

where A is the cavity cross-sectional area, and l' is the acoustic length of the reference cavity. The dimensions of each finished cavity were measured and used to calculate A and l' . The frequency of the first quarter-wave resonance of these loads ($f = c/4l'$, TABLE I) ranges from 7.7 kHz to 20.3 kHz. Thus, we will restrict the validity of our low-frequency calibration procedure to "low" frequencies well below the

first resonance of the longest cavity (i.e., $f = 7.7$ kHz for the 0.13 cc), or approximately 5 kHz. Deviations from the theoretical representation of the cavity admittance can also occur at very low frequencies due to heat transfer through the cavity walls (Biagi and Cook, 1954). This phenomenon has the effect of increasing the admittance magnitude at sufficiently low frequencies by a factor of 1.4 or 2.9 dB, as the compression changes from an adiabatic to an isothermal process at very low frequencies. For our cavities we estimate this effect to be less than 0.5 dB at 18 Hz; we have, therefore, neglected it in all specifications of cavity admittance.

Our low-frequency calibration procedure is similar to that of Rabinowitz (1981). We first made pressure measurements in each of the three reference cavities (0.05 cc, P_{r1}/E_o ; 0.082 cc, P_{r2}/E_o ; 0.13 cc, P_{r3}/E_o), keeping the stimulus voltage, E_o , constant (see FIGURE 5A). Each cavity was acoustically sealed to the acoustic system using silicone stopcock grease (Dow Corning). {These data are limited at high frequencies by artifact (22.4 kHz); measurements were accepted only when they were 15 dB above the noise floor (Section II E 7).} Next, the data were taken pairwise and substituted into Equation (9), using the appropriate Y_r calculations (Equation 12) to obtain three estimates⁵ of Y_{sL} (FIGURE 6). These three estimates are not independent (Rabinowitz, 1981). The three estimates were then averaged (magnitude in dB, angle in degrees) to obtain our low-frequency source estimate, \bar{Y}_{sL} (FIGURE 7). Note that the effects of the quarter-wave resonances in these reference cavities are clearly apparent in the pairwise and average estimates of Y_{sL} .

The low-frequency source admittance estimate has a magnitude slope of +6 dB/octave and an angle near 90° at low frequencies and is therefore compliance dominated. The low-frequency equivalent volume of the source calculated from $|Y_{sL}|$ is approximately 0.12 cc. The values of the reference volumes (0.052, 0.082, 0.133 cc) range about this value and satisfy the conditions of Section II A.

The spread in the magnitude of the pairwise estimates shown in FIGURE 6 is somewhat larger than that obtained in many calibrations. We think that most of the variations are due to small differences in the placement and sealing of the reference cavities upon the tip of the source during the different calibrations. The averaging procedure used to obtain Y_{sL} tends to reduce their effect.

As noted above, the source volume velocity, U_t , was not calculated directly. Rather, Y_{sL} and the reference condition for the 0.05 cc cavity (P_{p1}/E_o , and Y_{r1}) were substituted into Equation (11) when a load estimate, Y_L , was computed. We could have calculated U_t in a "pairwise" manner (using Equation (7) or (8) with each pairwise Y_{sL} estimate) and averaged the three resulting U_t estimates. This is not necessary, since this process results in an estimate of U_t that is $-0.2 \text{ dB} \pm 0.2 \text{ dB}$ different from the estimate using the above procedure. Our procedure reduces the amount of calculation required to specify the source.

4. Y_{sh} and U_{th} : High Frequency Calibration Procedure

Our procedure for specifying the source at high frequencies produced

only one estimate of Y_s and U_t . Two reference loads were used: a very small cylindrical cavity of volume 0.005 cc, and an acoustic transmission line.

The dimensions of the cavity are given in TABLE I. Its cross-sectional area is equal to that of the source. The cavity is quite short; the frequency of its theoretical first quarter-wave resonance is outside our range of interest, although Equation (12) was used to calculate cavity admittance.

The acoustic transmission line (TL) was constructed from a 10.9 m length of copper tubing. It is circular in cross-section with inner diameter (0.476 cm) approximately matching that of the source (0.40 cm). The tubing was smoothly coiled with a diameter of about one foot. The far end of the tube was terminated⁶ with an acoustic conductance (Sintered Specialties, S-1416, $G = 1/226$ mhos) which equaled the characteristic admittance of the line,

$$Y_0 = A/(\rho c) . \quad (13)$$

Equation (9) was used to specify the reference admittance, Y_r , for the acoustic TL ($Y_0 = 1/227 = 4.4 \times 10^{-3}$ mhos or 12.9 dB re 1 mmho).

A plexiglass adapter (FIGURE 9) was used to couple the TL to the source. Its cross-sectional area was identical to that of the source. Functionally, it extends the end of the acoustic system to the plane of the probe-tube tip, so that the TL admittance measurements are referenced to this plane.

The steps taken to determine the high-frequency source specification, Y_{sh} and U_{th} , parallel those used in the low-frequency

calibration procedure. Each reference load was acoustically sealed to the source with silicone grease and the pressure response was measured (0.0052 cc , P_{r1}/E_o ; TL, P_{r2}/E_o) (FIGURE 5B). The pressure measurements in the TL load approached the noise floor of our measurement system at low frequencies; data are shown only for frequencies where the S/N exceeds 15 dB. Both measurements are limited to frequencies below 22.4 kHz by artifact. Y_{sh} was calculated using Equation (9) with the reference load data and the above theoretical reference admittances (Equations 12 and 13). As in the low-frequency calibration scheme, U_{th} was calculated implicitly via Equation (11); the TL reference condition (P_{r2}/E_o and Y_o) was always used when making unknown load calculations.

The very small cavity, 0.005 cc, was used as a reference load in this calibration procedure in an attempt to improve the precision of the Y_{sh} estimate. Equation (6) of Section II A showed that the Y_s calculation could be made insensitive to the theoretical value of one reference load, becoming dominated by the measured pressure ratio rather than the pressure difference. The extent to which this simplification is realized depends upon the degree to which the requirement $|Y_{r1}| \ll |Y_s| \ll |Y_{r2}|$ is satisfied. We have chosen these two reference loads to potentially maximize⁷ this effect while maintaining the approximate equality of source and load diameters.

5. Consistency of Y_{sL} and Y_{sh}

The low- and high-frequency source admittances were generally found

to agree (FIGURE 7) over some frequency range ($20 \text{ Hz} < f < 3 \text{ kHz}$). The consistency of load predictions using these two source specifications was tested two ways: 1) The low-frequency source specification (Y_{sL}, U_{sL}) was used as the "calibration", and the TL measurement (P/E_o) was treated as "data" from an "unknown" load. Equation (11) was then used to compute this "load" admittance and it was compared to our theoretical specification for the TL to determine the resulting "error". 2) The high-frequency source specification (Y_{sh}, U_{th}) was used as the "calibration", and the 0.052, 0.082, and 0.133 cc cavity pressure measurements were treated as the "data" and processed with Equation (11). The "error" was again found by comparison of the theoretical cavity specifications (Equation 12) to the predicted results. It was found that a small adjustment in the theoretical value for the transmission line (from $1/227$, 12.9 dB re 1 cgs mmho to $1/257$, 11.8 dB re 1 cgs mmho) decreased the differences between Y_{sL} and Y_{sh} (FIGURE 7) (rms magnitude differences over the bandwidth 20 Hz to 5.0 kHz, went from 1.3 dB to 0.85 dB; rms angle differences remained constant). This adjustment also decreased the apparent "errors" observed in the above consistency checks (FIGURES 8 and 9) while making the "errors" symmetrical about zero. The resulting rms differences between these measurements and theoretical specifications were computed for the bandwidth 20 Hz to 5.0 kHz, and are: 0.052 cc, 0.6 dB and 5.7° ; 0.082 cc, 0.8 dB and 6.6° ; 0.133 cc, 0.6 dB and 6.9° ; copper TL, 0.7 dB and 7.0° .

The above adjustment in TL admittance is an arbitrary but convenient way of accounting for some errors in reference load specification. Other methods could be used to allocate a percentage of the total error

observed to each particular reference load. For example, it was found that small adjustments in the theoretical value of each reference cavity (0.052, 0.082, 0.133 cc) could be used to decrease the range of variation observed in the pairwise Y_{sL} estimates. However, it is also possible to do this by adjustment of only one cavity volume, 0.082 cc, since the three estimates are dependent.

In summary, a small adjustment in the theoretical value of Y_0 was used to make the two source specifications and their resulting load predictions consistent. All results shown in this paper were processed using this adjusted TL admittance. Considering both $\overline{Y_{sL}}$ and Y_{sh} and their respective frequency regions of validity (FIGURE 7), we conclude that for frequencies below 1 kHz, the source admittance appears compliance dominated; at mid frequencies, $1 \text{ kHz} < f < 4 \text{ kHz}$, Y_s becomes nearly resistive; above 4 kHz, Y_s again becomes compliant, but deviates from this behavior above 10 kHz. Note the large differences in the two Y_s estimates for frequencies above 4 kHz, where Y_{sh} is the valid calibration. A more detailed model and interpretation of the source characteristics will be discussed in Section F.

6. Data Processing for Unknown Load Estimates, Y_L

Measurements obtained in unknown loads (excluding the consistency checks above) were always processed using both low- and high-frequency source specifications, resulting in two load estimates, Y_{LL} and Y_{Lh} . The load estimates were usually in excellent agreement over some

mid-frequency band, generally in the frequency region where both Y_s estimates agreed. In this case the two load estimate curves were combined into a single frequency response using the following algorithm: retain the low-frequency load estimate (magnitude and angle) for frequencies less than or equal to a transition frequency f_t , and retain the high-frequency load estimate (magnitude and angle) for frequencies larger than f_t . The transition frequency was selected after detailed comparison of the magnitude and angle curves of both load estimates. Values of f_t varied from curve to curve since it approximately represents a frequency where the two load estimates are in "best" agreement. In these cases no "noticeable" discontinuity can be detected when plotting the combined frequency responses; thus, discontinuities are less than 0.4 dB and 3.5° . It is, therefore, unnecessary to record f_t for these cases.

In some instances, the two load estimates differed significantly. Application of the above algorithm would produce a "noticeable" magnitude and/or angle discontinuity in the resulting frequency response. Under these circumstances both load estimates will be shown or application of the algorithm will be accompanied by specification of f_t .

All source and load computations were performed using FOCAL on our Digital Equipment Corp. PDP8/E computer. Calculation of \bar{Y}_{sL} and Y_{sh} took approximately 18.5 minutes. Computation time for the first pair of load estimates, Y_{LL} and Y_{Lh} (including the time required to calculate U_{tL} and U_{th}), is approximately 8 minutes; successive pairs of load estimates (U_t need not be recomputed) require an additional 4 minutes. Computation time for Equation (14) was 4 minutes per data curve. Thus, most

processing is done off line; this is especially true for our animal experiments, where as many as 200 pairs of load estimates are sometimes made. Significant improvement in computation time could be obtained using FORTRAN, but this does not outweigh the considerable inconvenience and lost time in I/O operations required to use FORTRAN on this machine at present. Our computational procedures are such that intermediate results are obtained, rounded to the nearest 0.1 dB in magnitude and 0.001 T (0.36°) in angle, and stored in our standard I/O format before use in subsequent computational steps. This procedure does not introduce detectable imprecision in our final result; therefore, this form of "computational noise" is less than 0.1 dB in magnitude and 0.001 T (0.36°) in angle.

7. Noise and Artifact Measurements

All of the pressure measurements reported here meet specific signal-to-noise ratio (S/N) and artifact⁸ criteria. Measurements were always made over the frequency range 10 Hz to 50.1 kHz. All reported results are limited to frequencies below 22.4 kHz because the "artifact" became large at higher frequencies; the S/N criteria sometimes limit the reported measurements at low frequencies.

For the measurements that led to source specification (FIGURE 5), data were accepted only if the S/N exceeded 15 dB, and for the "unknown" load measurements (Section III) a S/N > 10 dB was required. These limits were somewhat arbitrarily chosen; a more stringent limitation was used

for the source-specification measurements because they were subsequently used in the computation of the "unknown" load admittances.

Artifact was determined by measurement of the probe output when the probe-tube tip was mechanically plugged. A tapered metal pin was inserted into the probe tip and sealed with a rubbery silicone sealant (General Electric, "clear silicone glue and seal"). Measurements were made for several load conditions (0.005, 0.052, 0.082 cc, Copper TL); the artifact level was not very load dependent (less than 10 dB variation). Measurements in the 0.005 cc cavity are shown in FIGURE 10. The unplugged pressure magnitude is 10 dB above the plugged response at all frequencies below 22.4 kHz. The probe noise floor was also measured and is essentially identical to the plugged tip response for $f < 3$ kHz. For $f > 4$ kHz, the plugged tip response is more than 20 dB larger than the noise floor, and is, therefore, clearly "artifact". The artifact measurement in the copper TL load was 10 dB below the corresponding unplugged response at all frequencies below 28 kHz. Since these two loads are used to specify the high-frequency characteristics of the source, we will apply the frequency limitation of 22.4 kHz to our source specification (Y_{sh} , U_{th}). In addition, we will use this frequency as an upper limit for all succeeding pressure measurements.

8. Source Stability

The stability of the acoustic source was excellent for pressure measurements made "on the bench" to determine the source specification

(Section II E) and to test system performance in "unknown" loads (Section III). At constant temperature conditions, repeated pressure measurements in any particular load usually agreed within ± 0.1 dB and $\pm 1.1^\circ$ and were considered "stable". One could also remove and replace a load with the resulting change in pressure measurements being less than ± 0.1 dB and $\pm 1.1^\circ$. Y_s was determined on two occasions with no intervening modifications of the source. The differences between the two results were less than Y_{sL} : ± 0.7 dB and $\pm 7^\circ$, and Y_{sh} : ± 0.5 dB and $\pm 1.5^\circ$, except at 17.8 kHz where the differences were 2.5 dB and 14.5° .

The effects of temperature changes on the source (with no R_1 and R_2 resistors) were examined for several cavity loads. Variation of the ambient temperature from 18° C to 30° C produced an increase in the pressure measurement, P_L/E_o , of 0.75 dB and 0° for frequencies below 5 kHz. For these measurements, the earphone and probe tube heaters were turned off. For constant ambient temperature of 17° C, turning on the earphone and probe tube heaters (with the R_1 and R_2 source resistors present and using the currents of Section II B 2) had little effect for frequencies below 10 kHz (± 0.3 dB and $\pm 1.5^\circ$). The largest change was 1.2 dB and 14.5° at 13 kHz. Thus, it is desirable to keep the source temperature constant during measurement sessions.

A static pressure vent was present in the source during the measurements described above. Therefore, the changes observed were not induced via changes in static pressure associated with the temperature variations⁹.

The stability of the measurements in cats was the same as that of our "bench" measurements when the acoustic source was initially placed in

the ear. However, changes in the characteristics of the source often occurred after several hours (2 to 13 hours). Changes in the pressure measurements usually took the form of a frequency dependent loss that increased slowly with time. The loss was usually negligible at low frequencies ($f < 100$ Hz) and increased with increasing frequency to a maximum loss of 2 to 3 dB for $f > 10$ kHz. Plugging of the probe tube was probably not responsible for these changes, since plugging usually occurs over a relatively short time span and results in large signal loss at all frequencies. In some situations the silicone grease used to acoustically seal the source in the earcanal became soft and contacted the R_2 resistor screen, possibly plugging some of its pores and increasing the resistance. It is also possible that the high humidity of the cat's earcanal caused a similar blocking of the resistor screen. In fact, we were able to experimentally induce a pressure loss similar to that described above by placing the source in a heated cavity partially filled with water. This load provided a humid environment; water droplets formed on the cavity walls after several hours of heating. Measurements made in the 0.052 cc cavity before and after exposure to this humid load were used to determine the change in pressure response. A heat gun was used to dry the resistor screen after the pressure loss had been determined. This process did not improve the pressure response; rather, it caused the pressure loss at 10 kHz to increase 1 dB. Thus, the application of heat to the resistor screen may also alter its properties.

In summary, excessive heat, humidity, or grease may degrade the state of the resistor screen. In almost every animal experiment, stability problems forced us to remove this element and replace it with a

fresh resistor. Fabrication and installation of the resistor were time consuming; installation could take 1.5 hours, and the construction process was such that 8 hours were often used to make several resistors. Our success rate for resistor production was roughly 60-70%. It is clear that a major drawback to the use of our acoustic source is the effort required to produce and replace these resistors and to keep them in stable operating condition during measurements in the ear canal.

F. NETWORK MODEL OF THE SOURCE

1. Model Topology and Element Values

A network model was developed to provide insight regarding the detailed properties of the acoustic source. The model is a lumped-element electric circuit analog in which voltage is analogous to sound pressure and current is analogous to volume velocity. The geometry of the source (FIGURE 2A) was used to specify the network topology (FIGURE 2B). Most network elements were defined in Section II B 2; the acoustic mass M_1 is associated with the resistor R_1 , and M_2 with the resistor R_2 .

Mechanical dimensions of the source and known properties of some components of the source (e.g., earphone and acoustic resistance, R_1) were used to establish a set of "nominal" element values (TABLE II). These "nominal" values were modified, if necessary, to obtain a better fit between the model response (U_t^m, Y_s^m) and measured source

specification (U_t, Y_s) (FIGURES 11 and 12). Final element values are listed in FIGURE 2B and TABLE II. Our curve-fitting procedure was that of trial and error, with a "good fit" being determined by eye. Element values were first adjusted to obtain a good fit to Y_s ; small changes in these values were made to better fit U_t .

Relatively good agreement was obtained between the model response and the measured behavior. Although no systematic measurements were used to test the model, we have used computations on the model to identify the network elements that control important features of U_t and Y_s . These results and the differences between the model and measurements are discussed below.

2. The Source Admittance, Y_s^m and Y_s

We first chose the source admittance measurements to be fit by our model. Since Y_{sL} and Y_{sh} (Sections II E 3-4) are essentially identical at 2 kHz, we have used the algorithm of Section II E 6 with $f_t = 2$ kHz to combine these admittance estimates into the single curve shown in FIGURE 11. This curve is used as the "best" estimate of Y_s .

The model response using our "final" element values is also shown in FIGURE 11. The agreement between Y_s and Y_s^m is excellent, with rms errors being

$$0.8 \text{ dB and } 10.1^\circ \quad (10 \text{ Hz to } 22.4 \text{ kHz})$$

$$0.6 \text{ dB and } 4.7^\circ \quad (10 \text{ Hz to } 10.0 \text{ kHz}).$$

The only significant discrepancy occurs at frequencies above 12 kHz. At

these frequencies the angle of the model response approaches $+90^\circ$ while the data decrease to $+45^\circ$ at 20 kHz; the magnitude also deviates by as much as 3 dB in this range. The reasons for these differences are not clear.

Comparison of this Y_s curve to those obtained from many other calibrations indicates that the above discrepancies are approximately the largest that we have encountered. After animal experiments, we routinely disassembled and cleaned the source. Different elements and components (e.g., R_1 , R_2 , the plexiglass or aluminum holder for R_1) were often used to reconstruct the source. It is conceivable that changes in source geometry and/or element values caused this variation in Y_s from calibration to calibration.

Our model may also be inadequate at these high frequencies. In the next section we note that U_t^m and U_t have even larger differences for frequencies above 10 kHz. Thus, the present form of our model does not simultaneously match Y_s and U_t at $f > 10$ kHz to the same level of precision that was achieved for $f < 10$ kHz. Perhaps resolution of the U_t^m and U_t discrepancies at $f > 10$ kHz will provide better Y_s^m and Y_s agreement in this same frequency region.

The network elements that control the primary characteristics of Y_s will now be considered. Y_s^m and Y_s are compliance dominated at low frequencies. For frequencies below 100 Hz, the model compliance is that due to the total volume of the source (i.e., $V_0 + V_1 + V_2 + V_3 + V_4 + V_5$). At very high frequencies ($f > 4$ kHz) the impedance of R_2 and also that of the probe-microphone branch, $R_5 + j(\omega M_5 + 1/\omega C_5)$, are both large and Y_s^m is dominated by the volume at the tip of the source ($V_3 + V_4$).

At mid-frequencies ($f = 1.66$ kHz) the source admittance has a series resonance due to the probe-microphone branch. The damping, and therefore admittance level at this frequency, is controlled by R_5 . A parallel resonance in Y_S^m occurs at 2.7 kHz due to the probe-microphone branch in parallel with $(V_3 + V_4)$. Note that for the frequencies between the series and parallel resonances, the source admittance magnitude has a negative slope ($\cong -6$ dB/octave). The admittance magnitude in this frequency region is controlled by the value of the probe tube mass, M_5 .

Y_S^m is quite sensitive to the value chosen for R_2 . Small changes ($\cong 10\%$) relative to its final value of 8500 ohms primarily effect the magnitude of the mid-frequency source admittance. Larger changes can effect Y_S^m over most of the audio frequency range. The value of R_2 also determines the degree to which the $|Y_S^m|$ deviates from +6 dB/octave in the frequency region between 100 Hz and 1 kHz (i.e., small increases in R_2 cause the slope in this frequency region to decrease somewhat).

3. Source Volume Velocity, U_t^m and U_t

The computation of the source volume velocity estimates, U_{tL} and U_{th} , has been previously described in Section II E 3-4. These data are shown in FIGURE 12. We did not use the algorithm of Section II E 6 to combine U_{tL} and U_{th} into a single curve. The magnitude and angle differences at low to mid frequencies would cause a "noticeable" discontinuity in the resulting curve if the algorithm were used. Therefore, we arbitrarily decided to fit U_{tL} for $f < 20$ Hz, and U_{th} for

$f > 20$ Hz.

We must first specify a model for our earphone, U_0 , in order to calculate the short circuit volume velocity, U_t^m . The 1/2" B & K condenser earphone was modelled as an ideal constant displacement source, $U_0 = j\omega(\text{constant})$ (Frederiksen, 1977). In particular, $U_0 = j\omega C E_e M_p$, where C is the polarized cartridge capacity, M_p the cartridge open-circuit sensitivity, and E_e is the a.c. signal voltage. For our earphone, $M_p = 1.25 \times 10^{-3}$ V/d/cm² and $C = 20 \times 10^{-5}$ d-cm/V². In our measurements we have used a drive level of $|E_e| = 20$ volts rms. Thus at 100 Hz, $|U_0| = 20 \log_{10} \{ \omega C E_e M_p / (1 \text{ cc/s}) \} = -50.1$ dB re 1 cc/s rms. The agreement between $|U_t|$ and $|U_t^m|$ ($|U_t^m| \cong |U_0|$, $f = 100$ Hz) at 100 Hz is excellent (FIGURE 12).

The agreement between the model and measured volume velocity is good. The rms errors are listed below:

| | | |
|------------|------------------|---------------------|
| U_{tL} : | 0.9 dB and 16.8° | (10 Hz to 20 Hz) |
| | 0.9 dB and 11.6° | (10 Hz to 5.0 kHz) |
| U_{th} : | 0.6 dB and 18.8° | (20 Hz to 10 kHz) |
| | 1.3 dB and 80.8° | (20 Hz to 22.4 kHz) |

The principal difference between model and data occurs in the frequency range $14 \text{ kHz} < f < 18 \text{ kHz}$. Note that the angle disagreement approaches 90° in this region. Y_s^m and Y_s also disagreed at these frequencies. The reasons for these differences are not clear. One possibility might be that our model for the earphone volume velocity, $U_0 = j\omega C E_e M_p$, breaks down in this frequency region. The mechanical resonance of the diaphragm of this earphone is 20 kHz (B & K calibration chart). Our model for U_0 is only valid for frequencies well below this

resonance. This hypothesis could be tested by substituting a 1/4" B & K earphone, with resonant frequency of 70 to 100 kHz, for our 1/2" earphone during the calibration procedure. Other preliminary measurements concerning the high-frequency characteristics of similar acoustic sources (Peake, private communication) imply that some of these differences could be due, in part, to the fact that the tip of our acoustic system is near the edge of the earphone diaphragm rather than near its center. Our lumped parameter assumptions in this frequency region may be invalid. The largest mechanical dimension in our source is that of the earphone diameter (1.27 cm). This dimension was used to characterize the space between the earphone and its housing, $V_1 = \text{Area} \times \text{Length}$. Since $1.27 \text{ cm} \cong 0.33$ wavelength at 10 kHz, significant spatial pressure variations across the earphone diaphragm for $f > 10$ kHz are likely.

At present, we have no firm explanation for the low-frequency angle discrepancies between U_{tL} and U_{th} . The angle of the model response is $+90^\circ$ at these frequencies and matches the angle of U_{th} very well. However, $|U_{tL}|$ and $|U_{th}^m|$ are very close at low frequencies.

The source network model simplifies somewhat for the computation of U_t^m . U_t^m , the "short circuit volume velocity", was computed as the volume velocity in the R_2 branch with the load terminal pair shorted. Therefore, the network reduces to the volume velocity source, U_0 , a pair of compliances, $C_a = (C_0 + C_1)$ and C_2 , essentially two resistances R_1 and R_2 ($R_3 \gg R_2$), and the mass M_1 . At low frequencies the compliances have high "shunt" impedances and $U_t^m = U_0$. At mid frequencies, 600 Hz to 7 kHz, $|U_t^m|$ is approximately constant. The value of R_2 and total compliance, $C_a + C_2$, directly control this constant value. At

approximately 630 Hz, $R_2 \cong |1/j\omega C_2|$; at higher frequencies C_2 shunts volume velocity away from R_2 . At very high frequencies ($f > 10$ kHz), U_t^m decreases at -12 dB/octave and the angle approaches -180° . Note that the network itself is third order but the volume velocity source has a $j\omega$ frequency dependence. The value of R_1 controls the damping of the parallel resonance at 8.5 kHz between M_1 and C_a, C_2 ; the resonance appears to be slightly overdamped for these element values. The effects of including the acoustic mass M_2 were also studied. We found that for reasonable values of M_2 , it had the effect of sharpening the $|U_t^m|$ decrease at very high frequencies. However, its inclusion in the model did not significantly decrease the error in the U_{th} curve fit. Admittance measurements that we have made on similar resistor structures do not show a significant mass component. We have, therefore, used a value of $M_2 = 0$ in our final model computations.

A more complicated network could be used to model our measurements of U_t and Y_s . This would be interesting, but is not necessary since our model is not used in making load admittance predictions or in the calibration of the source. Its present use was to gain insight into the acoustics of the design and performance of the source. Further constraints on the model elements could be generated by manipulating the source (e.g., removing R_2 and/or R_1) while calibrating it to determine the changes in U_t and Y_s due to these manipulations. We have made measurements of this sort, but have not yet integrated them into the modelling procedure. Resolution of the high-frequency differences between the measurements and the model would be quite useful. The precision of our load estimates at high frequencies is constrained by the

precision of our source specification. Future work in this area should be performed.

III. PERFORMANCE TESTS

In this section we discuss admittance measurements made in two cases: 1) with no coupling space between load and source, and 2) with a cylindrical coupling space of the same diameter as the source. Limitations and errors in the admittance measurements are examined as a function of admittance magnitude and angle and frequency. Data presented in this section met a signal-to-noise ratio criterion of $S/N > 10$ dB and are limited to frequencies below 22.4 kHz because of the artifact criterion.

A. ADMITTANCE PREDICTIONS FOR TEST LOADS WITH NO COUPLING SPACE

The performance of our admittance measurement system was first evaluated by making measurements in several types of "unknown" loads in which there was no "coupling space". These loads include a small diameter transmission line, a "long" cavity, the free-space radiation admittance, and a "parallel mass-compliance" load. The geometry of the air space of each load was used to specify a theoretical admittance that is compared to the measurements.

It is not our intention to carry out detailed acoustic modelling of these loads. Some of their acoustic characteristics are not simply described or precisely known. In a few instances it is clear that a more sophisticated model could be used to better fit the measurements (e.g.,

the damping at resonances or the very low-frequency resistive character of the parallel mass-compliance load). The purpose of these tests is to use a simple model that is valid over some frequency range, to demonstrate the precision with which the system can measure acoustic admittance as a function of admittance magnitude and angle, and frequency.

Generally, the measured admittances are in excellent agreement with our theoretical specifications. The particular source specification (U_t , Y_s) used for these computations was previously discussed in Section II. Measurements in most of these loads have been made on many occasions with other source specifications. The curves shown below are also representative of results obtained from these other measurement sessions.

1. Tygon Transmission Line

A second transmission line was particularly useful to test the measurement of absolute admittance magnitude and the very high frequency performance of the system.

The "tygon line" was constructed from a 15.2 m (50') length of plastic tubing (Norton, Plastics and Synthetics Division) of 1/8" (0.318 cm) nominal inner diameter. From the measured inner diameter (0.302 cm) the characteristic admittance of this line was calculated, $Y_0 = 1/568 = 1.76 \times 10^{-3}$ mhos, or 4.9 dB re 1 cgs mmho. The adapter of FIGURE 9 was used to couple this line to the source. Input admittance measurements with "open" and "short circuit" terminations of the tube

were virtually identical above 30 Hz; however, the data shown in FIGURE 9 were obtained with the line terminated with an acoustic "resistance" (Sintered Specialties, S-2337, $G = 1/684$ mhos, 3.3 dB re 1 cgs mmho), which approximately equals the characteristic admittance of the line. The theoretical input admittance was assumed to be equal to Y_0 .

Both low- (Y_{LL}) and high- (Y_{Lh}) frequency load estimates for the tygon TL are shown in FIGURE 9. We have not combined these results (per Section II E 6), since differences exist in angle at low frequencies. Note that the angle of Y_{Lh} is closer to 0° for $f < 200$ Hz. This discrepancy is a manifestation of angle differences observed between U_{tL} and U_{th} in our source specification (FIGURE 12). From Equation (4) it is easy to see that $Y_L \cong U_t/P_L$ when $|Y_s| \ll |Y_L|$. This inequality is satisfied for the tygon TL at low frequencies and, therefore, variations in the angle of Y_L are simply related to U_t angle differences.

Note that both estimates are approximately resistive (Y_{Lh} to 22.4 kHz); the magnitudes are nearly constant vs frequency and the angles are near 0° . Minimum-mean-square-error resistance estimates (MMSEE) for these measurements were computed by averaging all magnitude<angle> data points in a specified bandwidth (\hat{Y}_{LL} , \hat{Y}_{Lh}). These estimators are \hat{Y}_{LL} : 4.1 dB re 1 cgs mmho, 7.2° ($12 \text{ Hz} < f < 5.0 \text{ kHz}$); and \hat{Y}_{Lh} : 4.0 dB, 0.36° ($20 \text{ Hz} < f < 22.4 \text{ kHz}$). The standard deviations are Y_{LL} : 0.7 dB, 6.5° , and Y_{Lh} : 0.4 dB, 1.8° . Thus, the MMSE estimates for magnitude and angle of these load predictions are within 0.9 dB and 7.2° of the theoretical values for this TL.

This level of agreement ($\approx 10\%$ in absolute $|Y|$) is considered to be good. The reasons for the discrepancies are not clear. The theoretical specification for this load, $Y_0 = A/(\rho c)$, was calculated using values of A and c at 22°C and 75.1 cm Hg . Temperature and static pressure fluctuations during measurement sessions cannot account for more than 0.25 dB of the discrepancy. Note that the admittance magnitude of this load at high frequencies is comparable to that of the source, $|Y_s|$.

2. The "Long" Cavity

A relatively "long" cavity ($l' \approx 0.3\text{ cm}$, $V' = 0.357\text{ cc}$) was found to be an interesting test load because of its large admittance variations vs frequency. Cavity dimensions are given in TABLE I; the frequency of its first quarter-wave resonance is 2.9 kHz . Equation (12) was used to specify the theoretical admittance of this load. The measured and theoretical admittances are shown in FIGURE 13. The rms magnitude and angle differences between these curves are 0.4 dB and 1.5° , computed for the frequency range $10\text{ Hz} < f < 2\text{ kHz}$. We have not attempted to compute these errors at the higher frequencies because the results would be dominated by the deviations near the resonant frequencies where our model is known to be inaccurate, since it includes no damping. The model admittance magnitude at the resonances and anti-resonances is theoretically infinite or zero; our computational point density (12 points/octave) is such that many of the model resonances appear finite and not much different from our measurement. Note that the

frequencies of resonance and anti-resonance are well predicted even at very high frequencies (to 22.4 kHz, FIGURE 13B). This comparison demonstrates that our system can precisely measure admittance over a wide range of magnitude (75 dB) and angle ($+90^\circ$). In addition, it can "track" rapid magnitude and angle changes vs frequency: 60 dB in magnitude and 180° in angle over one octave. The admittance magnitude of this load is larger than that of the source at most frequencies.

3. Radiation Admittance

A load with high admittance magnitude was desired to test the measurements over a wide range of admittance magnitude. The radiation admittance, Y_{rad} , proved to be useful for this purpose. A piece of flat sheet metal 2' x 3' x 1/32" with a hole at its center (diameter \cong 0.76 cm) was used as an "infinite" baffle for the source. The baffle and source were coupled with the adapter shown in FIGURE 14 to place the tip of the probe tube in the plane of the baffle surface.

The admittance of this load was modelled as the radiation admittance for a plane circular piston in an infinite baffle. An equivalent circuit model approximation (Beranek, 1954, pg. 121; see FIGURE 14) was used to calculate Y_{rad} with a piston diameter of 0.40 cm.

The model response and predicted load data are shown in FIGURE 14. Again, the agreement is excellent. The rms differences (and associated bandwidths) are 0.8 dB and 5.5° (119 Hz to 22.4 kHz), and 0.7 dB and 2.9° (119 Hz to 15.8 kHz).

The difference observed at low frequencies ($f < 200$ Hz) results from the low S/N for the pressure measurement; in this frequency region, S/N increased as frequency was raised. At extremely high frequencies ($f > 137$ kHz) Y_{rad} theoretically approaches a conductance, $G = A/(\rho c) = (\pi 0.2^2)/(\rho c) = 3.08 \times 10^{-3}$ mhos or 9.8 dB re 1 cgs mmho. The data are consistent with a trend towards conductive behavior. However, appreciable magnitude and angle deviations from the model response occur above 17 kHz. In this frequency region $|Y_{\text{rad}}|$ approaches $|Y_s|$; it is likely that imprecision in source specification at very high frequencies is responsible for these deviations.

4. A "Parallel Mass-Compliance" Load

It is important to determine the performance of our system when the load admittance magnitude is much smaller than that of the source, $|Y_s|$. Additionally, a test load that would mimic the resonant behavior¹⁰ of the admittance at the cat tympanic membrane is also desirable. We used a "parallel mass-compliance" load (PMC) to test both issues.

The PMC consists of a plexiglass cavity terminated with a narrow tube (FIGURE 15). The theoretical model for this load is that of the cavity admittance, Y_1 , in parallel with the admittance of the tube, Y_2 . Y_1 was computed using Equation (12). Use of Equation (12) rather than that for a compliance, $Y_1 = j\omega C$, is justified, since $|Y_2| \ll |Y_1|$ at high frequencies ($f > 10$ kHz) where the resonances of Equation (12) are possibly important. The model used for $Z_2 = 1/Y_2$ was that of an

"intermediate-sized tube" (Beranek, 1954, p. 137) which is valid for $280 < f < 16.9$ kHz for a tube of diameter 0.118 cm. Z_2 consists of a frequency-dependent resistance ($R_{a2} = 3.05 f^{0.5} \text{ d-s/cm}^5$) in series with an acoustic mass ($M_{a2} = 0.126 \text{ g/cm}^4$). End corrections (two) for a flanged tube were used ($\cong 10\%$ mass increase). In addition, it was necessary to increase the net mass term 15% ($M'_{a2} = 1.15 M_{a2}$) in our final computations to better fit the resonant frequency and low-frequency admittance magnitude.

The theoretical and measured admittances agree quite well (FIGURE 15). The rms magnitude and angle differences in the frequency range where both model and data are valid are 4.1 dB, 14.3° ($280 \text{ Hz} < f < 22.4 \text{ kHz}$) and 0.9 dB, 5.6° ($280 \text{ Hz} < f < 12.6 \text{ kHz}$). Note that these computations include the frequency region of resonance (near 2 kHz).

The above model is not valid for $f < 280$ Hz. Another model for the tube (Beranek, 1954, "tube of very small diameter", p. 135) can be used to examine the very low-frequency ($f < 12$ Hz) admittance of this load. At these frequencies the resistive term dominates, and the admittance of the load approaches $G = 1/41.7 = 2.4 \times 10^{-2}$ mhos, or 27.6 dB re 1 cgs mmho for $f < 12$ Hz (FIGURE 15). The data clearly show a trend toward resistive behavior at low frequencies and appear to be approaching this value.

At resonance, the admittance magnitude of this load is very small ($\cong -27$ dB re 1 cgs mmho), being approximately 17 dB smaller than $|Y_s|$; even so, the measurement is well behaved in this region and agrees with the model. The measured Q from the data is $\cong 13$; the model Q is

$Q \cong (1/R_{a2}(f))(M'_{a2}/C)^{0.5} = 14.4$ {f = 2.2 kHz, C = (cavity
 volume)/(ρc^2); we assumed $R_{a2}(f)$ to be approximately constant over the
 bandwidth of resonance}. These roughly agree and are comparable to those
 of our admittance measurements in cat, $Q \cong 16$.

The agreement between measurement and model is also good at
 frequencies above resonance where the compliance controls the load
 admittance. Note, however, that the model fails to predict the
 anti-resonance (14 kHz) and resonance (16 kHz) at very high frequencies.
 The reasons for this have not been investigated. The rms differences
 between model and measurement are significantly influenced by this
 discrepancy. We will therefore restrict the subsequent use of these
 results to frequencies below 12.6 kHz.

In summary, the results from these four test loads have demonstrated
 that our system can precisely determine acoustic admittance (rms
 differences < 0.9 dB, 5.6°) over a wide bandwidth (10 Hz to 22.4 kHz) and
 large range of admittance magnitude ($\cong 75$ dB at 119 Hz; with
 -17 dB $< |Y| < 58$ dB re 1 cgs mmho) and angle ($+90^\circ$). We have found
 that resonances with Q's on the order of 14 (and as high as 40 in "long"
 cavity at high frequencies) are precisely measured. All three basic
 types of acoustic elements have been examined (i.e., acoustic mass,
 resistance, and compliance).

B. TEST LOADS WITH CYLINDRICAL COUPLING SPACE

1. Admittance Measurements

Under some circumstances it is desirable to use our admittance measurement in the plane of the probe-tube tip, Y_L , to infer the admittance at another location, Y'_L . For example, when making measurements in an ear, one cannot make admittance measurements in the plane of the tympanic membrane. There is a coupling space between the probe-tube tip and the tympanic membrane which must be taken into account. The load configuration that we have used to test such inferences is a short, cylindrical, rigid-walled cavity terminated with an acoustic resistor (FIGURE 16). In this case one can attempt to compute the admittance in the plane of the resistor. We shall describe a method used to characterize this coupling space and discuss its performance.

We have made measurements on five such loads, each with the same cavity (diameter = 0.40 cm; length $l' = .090$ cm; volume = .0113 cc) but terminated with different resistors (Knowles BF series, fused-mesh type; 680, 1500, 2200, 3300, 4700 ohm, nominal values). The measured admittances of these loads at the plane of the probe-tube tip (Y_L) are shown in FIGURE 16. Each load is clearly resistive at low frequencies. For frequencies above 10 kHz, the admittances of the five loads are nearly identical, becoming compliance dominated as frequency increases. The 680 ohm load is the exception; it has a magnitude minimum near 9 kHz and becomes compliance dominated at higher frequencies.

If we assume that the cavity can be represented as a rigid-walled cylinder of length l' and uniform cross sectional area A , then the measured admittance at the probe tip, Y_L , and the admittance terminating the cavity, Y'_L , are related by the lossless transmission line transformation (Kinsler and Frey, 1962)

$$Y'_L(f) = \frac{Y_L(f) - j(A/\rho c)\tan(2\pi fl'/c)}{1 - j(Y_L(f)\rho c/A)\tan(2\pi fl'/c)} . \quad (14)$$

Using the above values of l' and A in Equation (14) we have computed the admittance Y'_L in the plane of the resistor for these loads (FIGURE 17). Note that all of the loads (with the exception of the 680 ohm load) are approximately resistive over a wide bandwidth ($10 \text{ Hz} < f < 15 \text{ kHz}$). Our best estimate of the resistance of each load was computed by averaging the magnitude<angle> data over a specified bandwidth. This procedure yields the MMSE data estimator, \hat{Y} (TABLE III). Standard deviations were also computed for both magnitude and angle. The value of $|\hat{Y}|$ relative to the supplier's nominal admittance magnitude $|Y_n|$ was calculated ($\underline{\Delta}|Y| = 20\log_{10}\{|\hat{Y}/Y_n|\}$) and the results are listed in TABLE III.

In general, there is good agreement between the nominal and measured resistance values. Resistive results are obtained over a wide bandwidth even at admittance magnitudes that are much smaller than that of the source, $|Y_s|$ (e.g., 4700 ohm at $f > 7 \text{ kHz}$). The supplier (Knowles Electronics, Inc.) specifies a magnitude precision of roughly $\pm 2.0 \text{ dB}$. Four of our measurements (680, 1500, 2200, 3300 ohm loads) fall within

their tolerance. The only discrepancy exists for the 4700 ohm load; results from several other measurements using different 4700 ohm elements were closer to the supplier's nominal value. This level of agreement is considered to be adequate for our purposes; we have not attempted to assess the amount of variability existing in admittance magnitude across a population of these resistors.

All of the Y'_L results have larger variation in magnitude and angle for frequencies between 15 kHz and 22.4 kHz. For two loads (3300, 4700 ohm), the angle of the admittance becomes more negative than -90° at the highest frequencies. These variations in Y'_L result from imprecision in the source specification and the effects of the TL transformation upon a relatively lossless input admittance, Y_L (the angle of Y_L is close to $+90^\circ$ at these frequencies). Therefore, we will restrict these Y'_L results to frequencies below 15 kHz for our succeeding discussion (Section III A 2) of line length variations.

Note that the smallest resistance (680 ohms) appears to have a significant mass component that cannot be accounted for solely on the basis of the acoustic mass associated with the length and diameter of the tube supporting the resistor¹¹. The other resistors appear to have negligible mass.

2. Effects of Small Variations in Line Length

The sensitivity of the Y'_L admittance estimate to variation in transmission line length, l' , was examined for each of the loads of

FIGURE 16. Y'_L was computed from Y_L using three different line lengths (0.07, 0.09, 0.11 cm) corresponding to a $\pm 22\%$ variation about the measured length, 0.09 cm. The results for the load with smallest admittance magnitude (4700 ohm) are shown in FIGURE 18. Large differences are seen at high frequencies: 4 dB in magnitude (between $l' = 0.09$ and 0.11 cm) and 50° in angle (between $l' = 0.09$ and 0.07 cm). Angles are clearly affected at frequencies as low as 1 kHz. Similar trends were seen in the other loads; however, the differences decreased as the nominal resistance of the load decreased. Thus, as the magnitude of the resistive load admittance approached that of the characteristic admittance of the line ($Y_0 = 9.8$ dB re 1 cgs mmho), the variation in Y'_L vs distance became smaller.

In summary, we have made input admittance measurements in five loads using resistive elements that are commercially available. The coupling space was theoretically accounted for using a model for a short section of lossless transmission line. Our results indicate that these resistive elements do indeed have a resistive impedance over a wide bandwidth. In the case of the 4700 ohm load, this procedure allowed us to determine the resistive component of the load admittance for frequencies where the total load admittance was compliance dominated (for nearly a decade in frequency from 2 kHz to 15 kHz). Results can be significantly influenced by the value chosen for line length. This is especially true for terminations causing large pressure standing wave ratios.

C. MEASUREMENT SUMMARY AND ERROR LIMITATIONS

1. Admittance Measurement Space and Error Limitations

The range in admittance magnitude and angle over which we have made measurements is summarized in FIGURE 19. Measurements from four of the calibration loads (Section II E 5; excluding the 0.0052 cc cavity), the four "unknown" loads (Section III A), and the five RC networks (Section III B), have been used to define this "measurement space". Within the shaded magnitude and angle regions our results indicate that the rms accuracy of our measurements is better than 1 dB in absolute magnitude and 7.0° in angle. These values are the maximum rms differences found between measurement and theory for all of the above loads. For some loads we have used the small bandwidth statement of rms differences (or standard deviations) to establish this result, since our simple models are clearly valid over this restricted frequency range. We expect measurements upon other loads whose admittance falls within this "measurement space" to be accurate to these tolerances.

Admittance measurements were also made in several other regions of our "measurement space" where we have not attempted to precisely specify the magnitude and angle errors. For example, the regions enclosed by dashed lines are the resonant peaks of the cavity loads. No error specifications were made in these regions. The region enclosed by the dotted line represents the 15 kHz to 22.4 kHz admittance predictions from the transmission line computations for the RC loads. The standard deviation for magnitude measurements in this region is less than 2.5 dB.

We have also made admittance predictions for the 0.005 cc cavity using six independent low-frequency source specifications ($\overline{Y_{sL}}$, U_{tL}). The rms differences between measurement and theory ranged from 5.7 dB to 2.8 dB in magnitude and 71° to 26° in angle. These results are quite "noisy". Imprecision in the source specification is a major factor in this "noise", since the theoretical admittance of the 0.005 cc cavity (FIGURE 19) is approximately 27 dB smaller than $|Y_s|$ at low frequencies. To make precise admittance measurements in this region (with the current source design), the precision of the measurement system must be increased. These issues are examined briefly in the next section.

2. Low Frequency Compliance Estimates and Measurement Imprecision

At low frequencies, errors in $|Y_L|$ estimation can be simply related to the ratio $|Y_L/Y_s|$ and to the precision of the pressure measurement. Y_s is clearly compliance dominated (FIGURE 7) at low frequencies. If we measure the low-frequency admittance of an "unknown" compliance load, $Y_L = j\omega V_L/\rho c^2$, using a known compliance as a reference load, $Y_r = j\omega V_r/\rho c^2$, the following simplifications occur. In general,

$$U_t = P_r(Y_s + Y_r) = P_L(Y_s + Y_L), \quad \text{which may be rewritten}$$

$$P_r/P_L = (Y_s + Y_L)/(Y_s + Y_r). \quad (15)$$

Substituting the compliance relations for Y_s , Y_L , and Y_r into

Equation (15) we obtain

$$P_r/P_L = (1 + V_L/V_s)/(1 + V_r/V_s) , \quad \text{or}$$

$$(P_r/P_L)(1 + V_r/V_s) - 1 = V_L/V_s . \quad (16)$$

If we take the logarithm of both sides of Equation (16) and substitute $\alpha = 20\log_{10}(P_r/P_L)$ and $\beta = 20\log_{10}(V_L/V_s)$ into the result, we may obtain an expression between the quantities α and β :

$$\beta = 20\log_{10}\{ 10^{\alpha/20} (1 + V_r/V_s) - 1 \} . \quad (17)$$

The desired result is the sensitivity of the load estimate, β (actually V_L , since V_s is assumed to be constant), to "errors" (of $\pm \delta$ dB) in the measured pressure ratio, α . Taking the derivative $\frac{d\beta}{d\alpha}$ we obtain

$$\frac{d\beta}{d\alpha} = \frac{10^{\alpha/20} (1 + V_r/V_s)}{10^{\alpha/20} (1 + V_r/V_s) - 1} . \quad (18)$$

The "error" in the "unknown" load estimate, γ , was calculated $\gamma = \delta \left(\frac{d\beta}{d\alpha}(\alpha_0) \right)$ and is shown in FIGURE 20 for several values of measurement precision, δ .

The precision, δ , of the measured pressure ratio, P_r/P_L , may be estimated to be approximately 0.2 to 0.4 dB (Section II C). Thus errors, γ , in the "unknown" load estimate for the 0.005 cc cavity

($\beta = -27$ dB) discussed in the preceding section are predicted to be between 4.5 and 8.5 dB (FIGURE 20). The observed rms differences between measurement and theory were 2.8 to 5.7 dB, which is consistent with the above prediction.

This analysis graphically depicts the degradation in load estimation as the "unknown" load admittance (volume) becomes "significantly" smaller than the source admittance (volume). Therefore, if we wish to make accurate measurements of these small load admittances (volumes), we must either increase the precision of the system used to measure P_r/P_L or decrease the source admittance (volume).

APPENDIX A

EXPERIMENTAL VERIFICATION OF THE CONSTANCY OF U_t
 FOR A WIDE RANGE OF LOADS

The excellent agreement between theory and measurement observed in Section III A may be alternatively viewed as confirmation of our assumption of constant source volume velocity, U_t , for a wide range of load conditions. For example, we have computed U_t for the "infinite baffle" radiation admittance load, U_{trad} , and for the 0.05 cc reference cavity load, U_{tc} . The ratio $\underline{R} = U_{\text{trad}}/U_{\text{tc}}$ is plotted in FIGURE A1 and is essentially unity over the whole frequency range and a wide (but variable) dynamic range. The dynamic range plot in FIGURE A1 was computed as the ratio of the theoretical admittances of these two loads: $20\log_{10}\{|Y_{\text{rad}}/Y_{\text{c}}|\}$. The average value and standard deviation (S.D.) of the volume velocity ratios are:

$$\underline{R}_L: 0.1 \text{ dB}, -1.1^\circ \text{ with S.D.: } 0.6 \text{ dB}, 1.4^\circ \\
 (119 \text{ Hz} < f < 5.0 \text{ kHz})$$

$$\underline{R}_h: 0.7 \text{ dB}, 3.2^\circ \text{ with S.D.: } 0.6 \text{ dB}, 5.0^\circ \\
 (119 \text{ Hz} < f < 22.4 \text{ kHz})$$

$$\underline{R}_h: 0.6 \text{ dB}, 2.5^\circ \text{ with S.D.: } 0.2 \text{ dB}, 1.1^\circ \\
 (200 \text{ Hz} < f < 10.0 \text{ kHz})$$

In summary, our assumption of constant source volume velocity, U_t , is justified; in fact, it is valid over a very large range of admittance magnitudes and angles.

FOOTNOTES

(1) Magnitude data are stored in increments of 0.1 dB; angle data in increments of 0.001 periods (T). The 12 bit A/D resolution is 0.02 dB and 0.00062 T, or 0.22° .

(2) Included in this frequency response are the transfer functions for the microphone preamplifier (B & K 2619) and microphone amplifier (B & K 2608).

(3) For audio frequencies the primary effect is to significantly lower the resonant frequencies of the cavities.

(4) Note that the mechanical length of each cavity, l , is 0.15 cm longer than the acoustical length, l' . This is to allow our measurements to be referenced to the plane of the probe-tube tip. The 0.005 cc cavity is also used as a reference load (Section II E 4), while the 0.357 cc cavity is used as a test load (Section III A). The materials and construction methods used for all of the cavities in TABLE I were the same. The heavy dashed line in the figure depicting cavity cross section (below TABLE I) indicates the location of the probe-microphone tip. This convention is used in subsequent sectional figures.

(5) All admittance magnitude data are expressed in dB re 1 cgs mmho, i.e., $20\log_{10}\{|Y|/(1 \text{ mmho})\}$ where $1 \text{ cgs mmho} = 10^{-3} \text{ cm}^5/\text{dyn-s}$.

(6) Input admittance measurements of the line when terminated with an acoustic open or short circuit (a rigid wall or open end, respectively) show the appropriate systematic oscillations about Y_0 vs frequency for frequencies below 200 Hz. Above 200 Hz the measured input admittance is independent of the line termination. This implies that the losses are sufficient to provide a line with essentially no reflections for $f > 200$ Hz. The theoretical attenuation factor increases with frequency. At 200 Hz it is approximately 0.015 dB/cm for a tube diameter of 0.400 cm. Thus, the round trip attenuation for this tube would be > 36 dB for $f > 200$ Hz (Zuercher, 1977).

(7) For our reference loads we have approximately $(2\pi f V_{r1})/(\rho c^2) \ll (2\pi f V_s)/(\rho c^2) \ll 1/227$. At low to mid frequencies ($20 \text{ Hz} < f < 2 \text{ kHz}$) $V_s \cong 0.12 \text{ cc}$, $V_{r1} = 0.005 \text{ cc}$, and $V_s/V_{r1} \cong 23$; the admittance of the cavity is much less than the source admittance in this frequency region. Also, the admittance of the TL is much larger than that of the source at these frequencies. Thus, use of these particular reference loads helps to give a precise estimate of Y_s (provided that the S/N of the TL measurement is acceptable). At high frequencies ($3 \text{ kHz} < f < 20 \text{ kHz}$) the inequalities are realized, but to a lesser extent, since the source volume becomes smaller, $V_s \cong 0.022 \text{ cc}$ ($V_s/V_{r1} \cong 4.2$), and the admittance of the source comes to within a factor of 3 to that of the TL at 20 kHz. A smaller cavity might be used to improve this situation; however, it is unlikely that one would obtain more than a factor of 2 decrease in V_{r2} by decreasing the already short cavity length while maintaining the cavity

diameter. A larger diameter TL could be used to decrease its admittance, but it is desirable to keep the diameter close to that of the source. Note that the TL diameter is already 20% larger than that of the source. Another approach might be to increase the Y_0 of the line by filling it with a gas which is less dense than air (e.g., helium). We could also use the source free space radiation admittance (Section III) as a high admittance reference load. In summary, we found that these two reference loads gave adequate precision; the values we have chosen for these loads give performance close to the optimal condition.

(8) Artifact is the component of E_p resulting from signals other than pressure at the probe-tube tip, P_L . These extraneous signals may arise from mechanical vibration, sensitivity to electromagnetic fields, sound transmission to the microphone via the walls of the probe tube and/or microphone, etc..

(9) The cavity compliance is $C = V/\Gamma P$, where Γ is the ratio of specific heat of air at constant pressure to that at constant volume, P is static pressure, and V the volume. The static pressure is related to temperature by the ideal gas law, $P = RT/V$, where R is a constant and T is absolute temperature.

(10) Admittance measurements at the cat tympanic membrane show an admittance minimum near 4 kHz, with $Q \cong 14$. The admittance magnitude at resonance is $\cong -10$ dB re 1 cgs mmho.

(11) We calculate the acoustic mass of the supporting tube to be $M = 1.6 \times 10^{-2} \text{ g/cm}^4$, counting both end corrections for a flanged tube; a mass increase of approximately a factor of 2.8 is needed to match the data. Killion (private communication) suggests that the acoustic mass of this tube might be slightly larger, $2.3 \times 10^{-2} \text{ g/cm}^4$, making the discrepancy less than a factor of two. It is likely that the differences in diameter between the cavity and resistor introduce an additional mass component (Ingard, 1948) that could account for this discrepancy.

TABLE I
DIMENSIONS OF CAVITY LOADS

| NOMINAL VOLUME (cc) | ACOUSTIC VOLUME (cc) | DIAMETER (cm) | AREA (cm ²) | MECHANICAL LENGTH (cm) | ACOUSTIC LENGTH (cm) | $\lambda/4$ RESONANT FREQUENCY (KHZ) |
|---------------------|----------------------|---------------|-------------------------|------------------------|-----------------------|--------------------------------------|
| $V = A\ell$ | $V' = \ell'A$ | d | A | ℓ | $\ell' = \ell - 0.15$ | $f = c/\ell'^4$ |
| 0.0233 | 0.0053 | 0.391 | 0.120 | 0.194 | 0.044 | 196.0 |
| 0.0700 | 0.0517 | 0.394 | 0.122 | 0.575 | 0.425 | 20.3 |
| 0.1001 | 0.0823 | 0.389 | 0.119 | 0.844 | 0.694 | 12.4 |
| 0.1512 | 0.1334 | 0.389 | 0.119 | 1.275 | 1.125 | 7.7 |
| 0.3748 | 0.3569 | 0.391 | 0.120 | 3.119 | 2.969 | 2.9 |

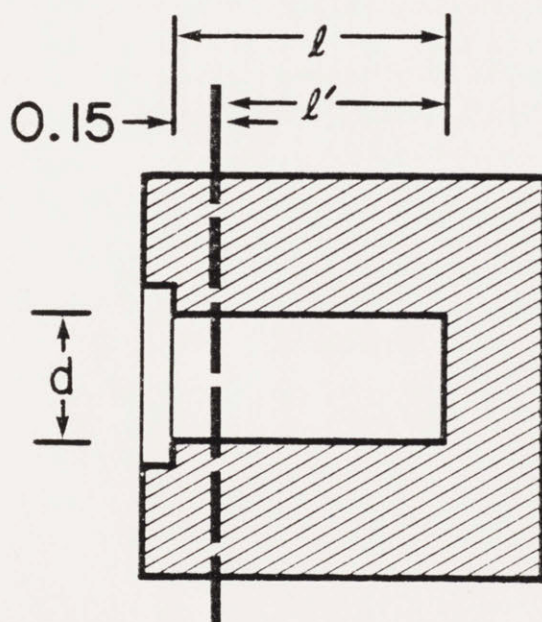


TABLE II
SOURCE NETWORK MODEL ELEMENT VALUES

| NETWORK ELEMENT | FINAL VALUE | NOMINAL VALUE | REASON FOR THE CHOICE OF THE NOMINAL VALUES |
|-----------------|-------------------------|-------------------------|---|
| V_0 | 0.010 cc | 0.010 cc | 1/2" B-K earphone equivalent volume |
| V_1 | 0.015 | 0.019 | Geometry of source and R_1 resistor |
| V_2 | 0.042 | 0.018 | Geometry of source |
| V_3 | 0.006 | 0.006 | Geometry of source and R_2 resistor |
| V_4 | 0.015 | 0.018 | Geometry of source 0.15 cm extension |
| V_5 | 0.030 | 0.022 | Eq. vol. of microphone (from acoustic measurements) + the probe tube volume |
| R_1 | 2.5 kohm | 4.7 kohm | Nominal value specified by supplier |
| R_2 | 8.5 kohm | 5.0 kohm | Guess initial value-choose close to R_1 |
| R_3 | 3.0 Mohm | 1.1 Mohm | Geometry of DC pressure release tube |
| R_5 | 4.5 kohm | 7.5 kohm | Geometry of #29 damper in probe tube. Large diameter probe tube is negligible |
| M_1 | 0.032 g/cm ⁴ | 0.016 g/cm ⁴ | Geometry of R_1 supporting tube |
| M_2 | 0.000 | 0.000 | Nothing known re mass of the resistor |
| M_5 | 0.430 | 1.70 | Geometry: total mass of probe tube and and #29 gauge damper |

TABLE III

TRANSMISSION-LINE RESISTOR TERMINATIONS:
MMSE CONDUCTANCE ESTIMATE AND STANDARD DEVIATIONS

| NOMINAL RESISTOR VALUE(OHMS) | $\Delta Y $ DATA RE NOMINAL (dB) | BANDWIDTH | | \hat{Y} CONDUCTANCE ESTIMATE | | STANDARD DEVIATION | |
|------------------------------------|--|---------------|--------------|--------------------------------|--------------------|---------------------------|--------------------|
| | | START (HZ) | END (kHz) | MAGNITUDE dB re 1 mmho | ANGLE (DEGREES) | MAGNITUDE dB re 1 mmho | ANGLE (DEGREES) |
| 4700 | -3.3 | 10 | 15 | -16.7 | 2.2 | 1.0 | 5.8 |
| 3300 | -0.6 | 10 | 15 | -11.0 | -0.7 | 0.5 | 7.9 |
| 2200 | -1.0 | 10 | 15 | - 7.8 | -1.4 | 0.7 | 8.3 |
| 1500 | -1.8 | 11 | 10 | - 5.3 | -2.2 | 0.8 | 10.4 |
| 680 | -1.0 | 20 | 2 | 2.3 | -0.7 | 0.4 | 7.9 |

FIGURE CAPTIONS

FIGURE 1: Procedures for specification of the Norton equivalent network of the acoustic source and measurement of "unknown" load admittances. Part A is the Norton equivalent network model. Part B illustrates the calculations used to obtain the source specification, Y_s , and U_t . Part C gives the calculation for a measurement of an unknown load, Y_L .

FIGURE 2: Schematic diagram of the acoustic source and its associated electric network analog. Part A illustrates the mechanical construction of the source (not to scale). Part B is the electric network analog and the element values that were found to provide a good match to measurements of the source admittance, Y_s , and "short-circuit" volume velocity, U_t . The load admittance, Y_L , is shown as a short circuit to illustrate U_t ; Y_L is nonzero for all measurement conditions.

FIGURE 3: The computer-controlled measurement system.

FIGURE 4: Frequency response calibration for the probe-microphone, $H_p(f) = E_p(f)/P(f)$. All frequency response curves reported are made up of straight-line segments connecting data points with a density of 40 points/decade.

FIGURE 5: Pressure measurements used for source specification. P_r/E_o

is the complex ratio of pressure in the reference load to excitation voltage. Part A illustrates measurements in three reference cavities used for the low-frequency source specification (Y_{sL}, U_{tL}). Part B gives measurements in the very small cavity and copper transmission line used for the high-frequency source specification (Y_{sh}, U_{th}). Symbols are used to identify the curves only where necessary. This policy will be followed throughout this document.

FIGURE 6: Three pairwise estimates of Y_{sL} . The volumes in parentheses indicate the pair of cavities used to obtain the particular Y_{sL} estimate.

FIGURE 7: Comparison of the average low-frequency ($\overline{Y_{sL}}$) and high-frequency (Y_{sh}) source admittance estimates. $\overline{Y_{sL}}$ is shown over the entire frequency range for purposes of comparison. See text for its frequency region of validity. Y_{sh} is shown only for its valid frequency range. In this and in subsequent figures, angle scales for plots of admittance are only given for the range $\pm 90^\circ$ even if the measurements exceed this range. Admittance angle results in excess of $\pm 90^\circ$ result from measurement imprecision.

FIGURE 8: "Load" admittance estimates of the three low-frequency reference cavities using the high-frequency source specification. Figures A, B, and C illustrate results for the 0.05, 0.08, and 0.13 cc cavities, respectively. Curves labeled "MEASUREMENT" are load admittance estimates, while those labeled "THEORETICAL" are the cavity admittances calculated from theory (Equation 12).

FIGURE 9: Admittance measurements in transmission line (TL) loads.

The curve labeled "COPPER TL" is the "load" admittance estimate using the low-frequency source specification. The horizontal straight lines are the theoretical characteristic admittance curves for the two TLs. Both low- and high-frequency load estimates (Y_{LL} and Y_{Lh} , respectively) are given for the "TYGON TL". A sectioned view (to scale) of the adapter used to couple the transmission lines to the acoustic source is in the upper portion of the figure. It is circularly symmetric and its dimensions are in cm.

FIGURE 10: Typical 0.005 cc reference cavity pressure measurement and the associated artifact level. The "PROBE TIP NORMAL" curve represents the normal response. The "PROBE TIP PLUGGED" measurement is artifact for $f > 4$ kHz. At 22.4 kHz the artifact magnitude is 10 dB less than the normal response magnitude. Both curves are shown to 50.1 kHz and are nearly identical for $f > 35$ kHz.

FIGURE 11: Comparison of the "MEASURED" source admittance, Y_s , and the "MODEL" result, Y_s^m . The model curve was calculated from the network model of FIGURE 2B. The "MEASURED" curve is a combination of Y_{sL} and Y_{sh} results.

FIGURE 12: Comparison of measurements of the source "short-circuit" volume velocity, U_t , and the network model prediction, U_t^m . Results for calculations using either the low-frequency (U_{tL}) or high-frequency (U_{th}) source admittance estimates are given.

FIGURE 13: Measured and theoretical admittances for the 0.357 cc "long" cavity test load. The "THEORETICAL" curve was computed from Equation

(12). Part B is an expanded view of the results for frequencies above 1 kHz.

FIGURE 14: Measured and theoretical free-space radiation admittance of the acoustic source. The network model approximation (upper left) for the radiation admittance, Y_{rad} , of a plane circular piston in an infinite baffle (Beranek 1954, p. 121) was used to compute the "THEORETICAL" curve. Model elements are $M_z = 0.27\rho/r \text{ g/cm}^4$, $R_x = 0.1404\rho c/r^2$, $R_y = 0.318\rho c/r^2 \text{ dyn-s/cm}^5$, and $C_w = 5.94r^3/\rho c^2 \text{ cm}^5/\text{dyn}$ with piston radius $r = 0.40 \text{ cm}$. The mass element clearly dominates Y_{rad} at most frequencies with the resistance elements having a small effect at very high frequencies. The circularly symmetric adapter used to couple the source to a 2' x 3' baffle for our measurement condition is shown in cross-section (upper right). This section is drawn to scale and dimensions are in cm.

FIGURE 15: Measured and theoretical admittance of a "parallel mass-compliance" load. The sectioned view of the acoustic load (top) illustrates the tube terminated by a narrow tube. The dashed line indicates the position of the tip of the probe-microphone when the source is coupled to this load. The section is to scale and dimensions are in cm. Only the dimensions relevant to the acoustic specification of the load are given; dimensions of the portion of the load that mates with the acoustic source are similar to those of the TL and baffle couplers.

FIGURE 16: Acoustic admittance measurements for a short, cylindrical cavity terminated by an acoustic resistor element. The nominal resistance values (cgs acoustic ohms) for the five different resistor

terminations are given in the legend. The horizontal, $|Y_0|$, is the theoretical characteristic admittance of the tube. The arrow marked " f_t " denotes the frequency where low- and high-frequency load admittance estimates were combined. The sectional diagram of the acoustic load (top right) is to scale except for the resistor element which has been enlarged for clarity. Dimensions are in cm.

FIGURE 17: The admittance measurements of FIGURE 16 referenced to the plane of the acoustic resistor, Y_L' . The effects of the coupling space have been accounted for using a lossless transmission line model for the cylindrical, rigid-walled cavity.

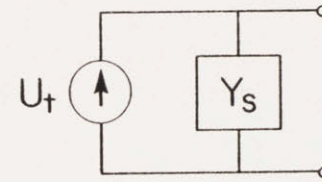
FIGURE 18: Sensitivity of the 4700 ohm Y_L' admittance estimate to small variations in transmission line length, l' .

FIGURE 19: Admittance "measurement space" summarizing the frequencies, magnitudes, and angles for which measurements have been reported. The shaded area indicates the range in magnitude and angle for which the rms accuracy is better than 1 dB and 7° . Measurements have been reported, but without a statement of precision, in the dashed and dotted regions. The magnitude and angle of the source admittance, Y_s , is shown for comparison to the range of measured "load" admittances. The dot-dash line is the theoretical admittance magnitude of the 0.005 cc cavity.

FIGURE 20: Error in load volume, γ , estimated from admittance measurements versus the ratio of the load volume to source volume, $\beta = 20 \log_{10}(V_L/V_S)$. The parameter, δ , is the measurement precision. Typical values of $V_r = 0.052$ cc and $V_s = 0.11$ cc were used.

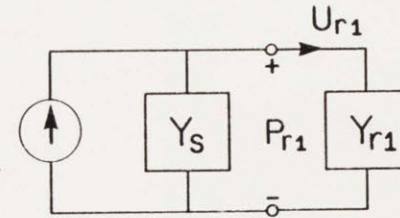
FIGURE A1: Experimental verification of constant source volume velocity. The low- and high-frequency volume velocity ratios, \underline{R}_L and \underline{R}_h , were computed as follows. The relation $U_{tx} = P_x(Y_s + Y_x)$, was used to calculate the volume velocity for each load condition ($x = \text{rad}$ or $x = \text{c}$ for 0.05 cc), with Y_s being the low-frequency source estimate, \underline{Y}_{sL} . \underline{R}_L is the complex ratio of the results, $U_{\text{trad}}/U_{\text{tc}}$. \underline{R}_h was computed in a similar manner using $Y_s = Y_{sh}$. The magnitude plot is $20 \log_{10} \{ |U_{\text{trad}}/U_{\text{tc}}| \}$ for both low- and high-frequency source specifications. The angle plot is the angle of U_{trad} relative to that of U_{tc} .

A. NORTON EQUIVALENT OF ACOUSTIC SOURCE

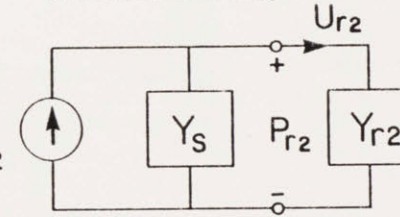


B. SOURCE SPECIFICATION

REFERENCE LOAD Y_{r1} : $U_{t1} = K_s E_{o1}$



REFERENCE LOAD Y_{r2} : $U_{t2} = K_s E_{o2}$



$$U_t = U_{t1} = U_{t2}$$

$$U_{t1} = P_{r1}(Y_s + Y_{r1})$$

$$U_{t2} = P_{r2}(Y_s + Y_{r2})$$

$$Y_s = \frac{Y_{r2}P_{r2} - Y_{r1}P_{r1}}{P_{r1} - P_{r2}}$$

C. MEASUREMENT CONDITION

$$Y_L = \frac{U_t}{P_L} - Y_s$$

$$U_t = K_s E_o$$

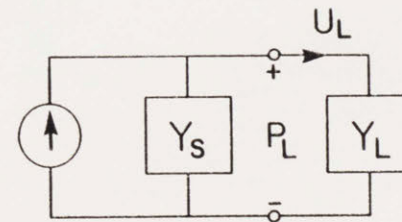
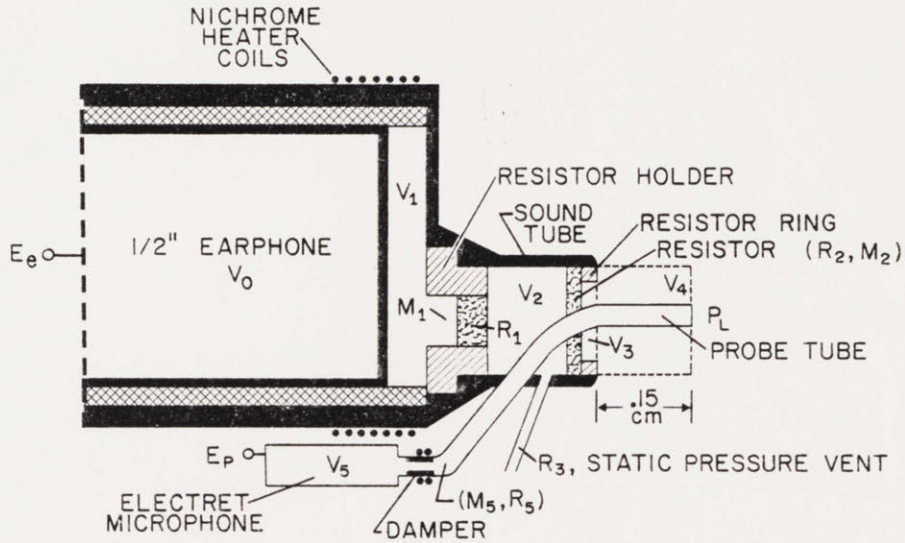


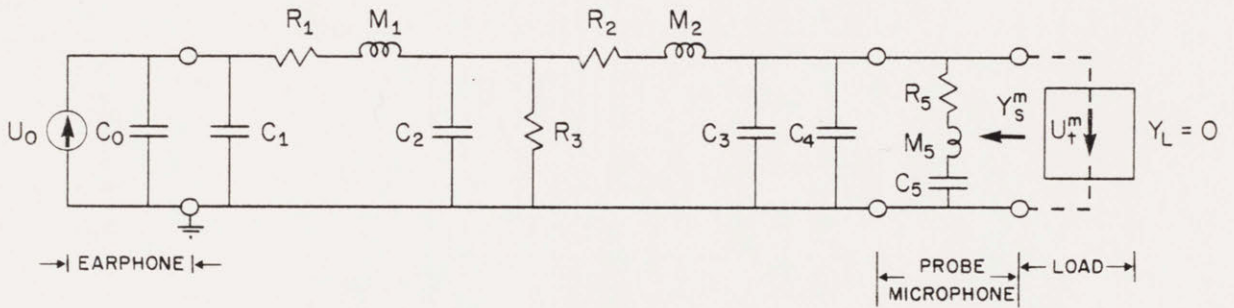
FIGURE 1

FIGURE 2

A. ACOUSTIC SOURCE



B. NETWORK MODEL



ELEMENT VALUES

| EQUIVALENT VOLUMES (cc) | AND | ACOUSTIC COMPLIANCES (cm ⁵ /dyn) | ACOUSTIC RESISTANCES (dyn-s/cm ⁵) | ACOUSTIC MASSES (g/cm ⁴) |
|-------------------------|-----|---|---|--------------------------------------|
| V ₀ = 0.010 | | C ₀ = 7.12 × 10 ⁻⁹ | R ₁ = 2.5 × 10 ³ | M ₁ = 0.032 |
| V ₁ = 0.015 | | C ₁ = 10.7 × 10 ⁻⁹ | R ₂ = 8.5 × 10 ³ | M ₂ = 0 |
| V ₂ = 0.042 | | C ₂ = 29.9 × 10 ⁻⁹ | R ₃ = 3.0 × 10 ⁶ | M ₅ = 0.430 |
| V ₃ = 0.006 | | C ₃ = 4.27 × 10 ⁻⁹ | R ₅ = 4.5 × 10 ³ | |
| V ₄ = 0.015 | | C ₄ = 10.7 × 10 ⁻⁹ | | |
| V ₅ = 0.030 | | C ₅ = 21.4 × 10 ⁻⁹ | | |

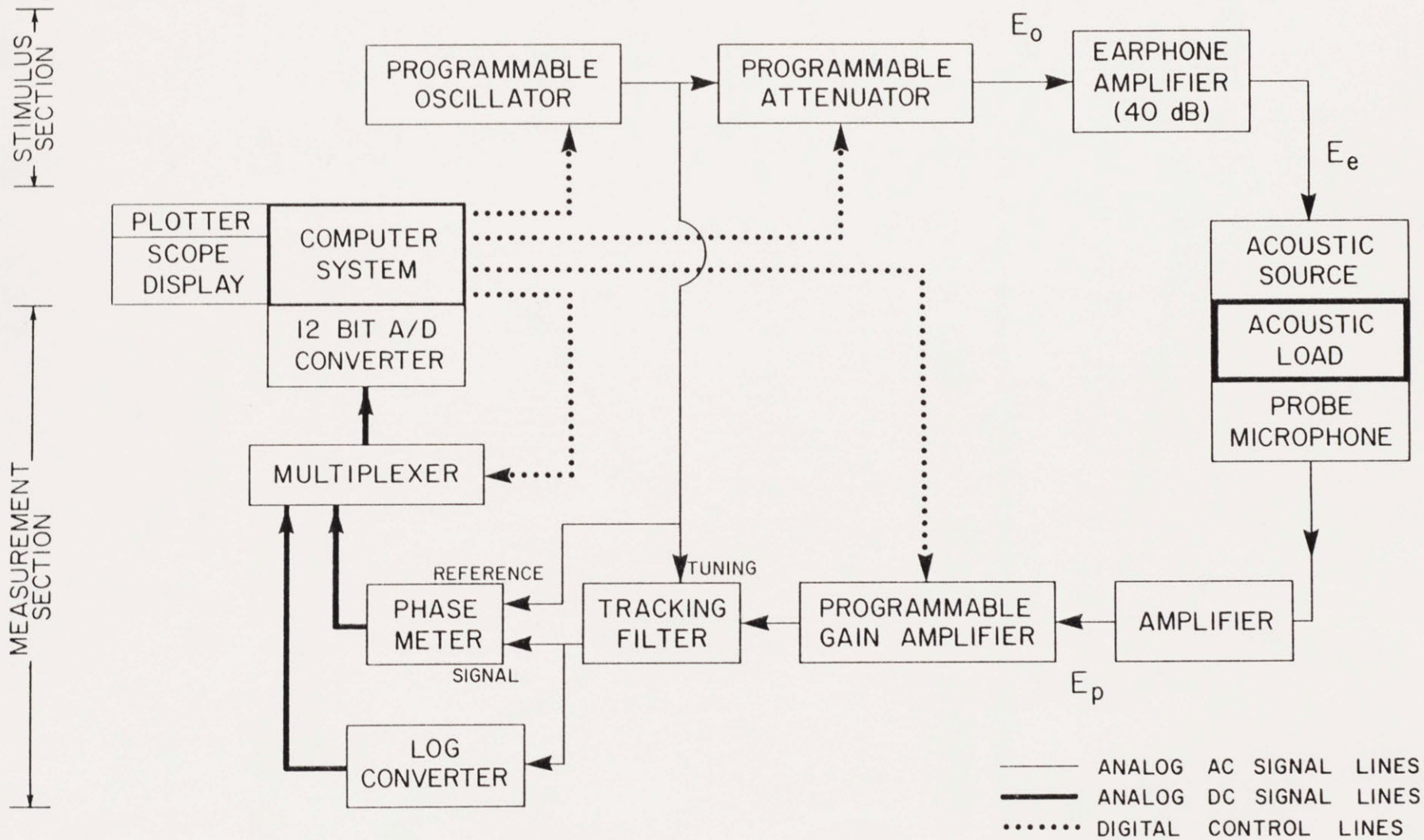


FIGURE 3

FIGURE 4

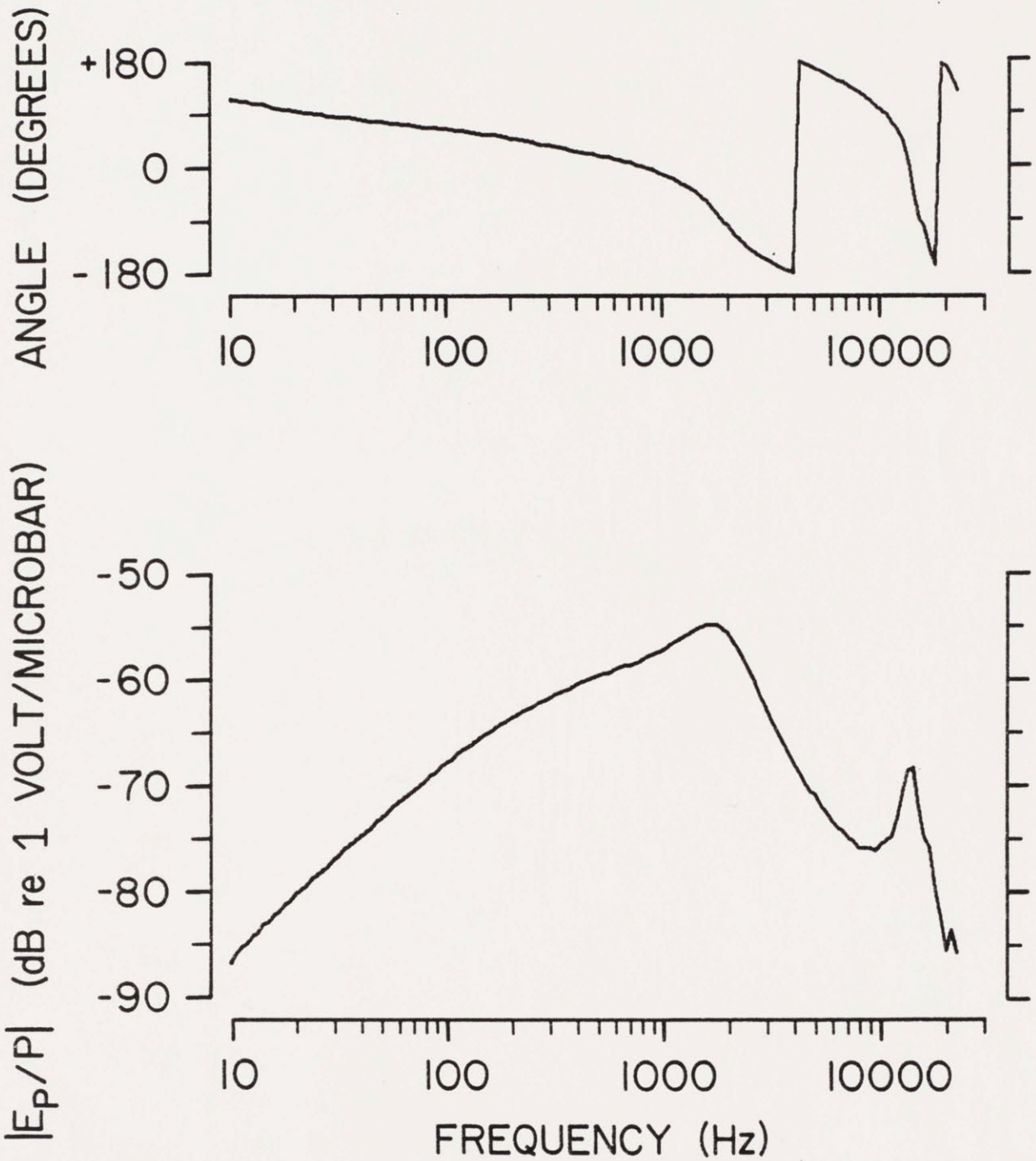


FIGURE 5A

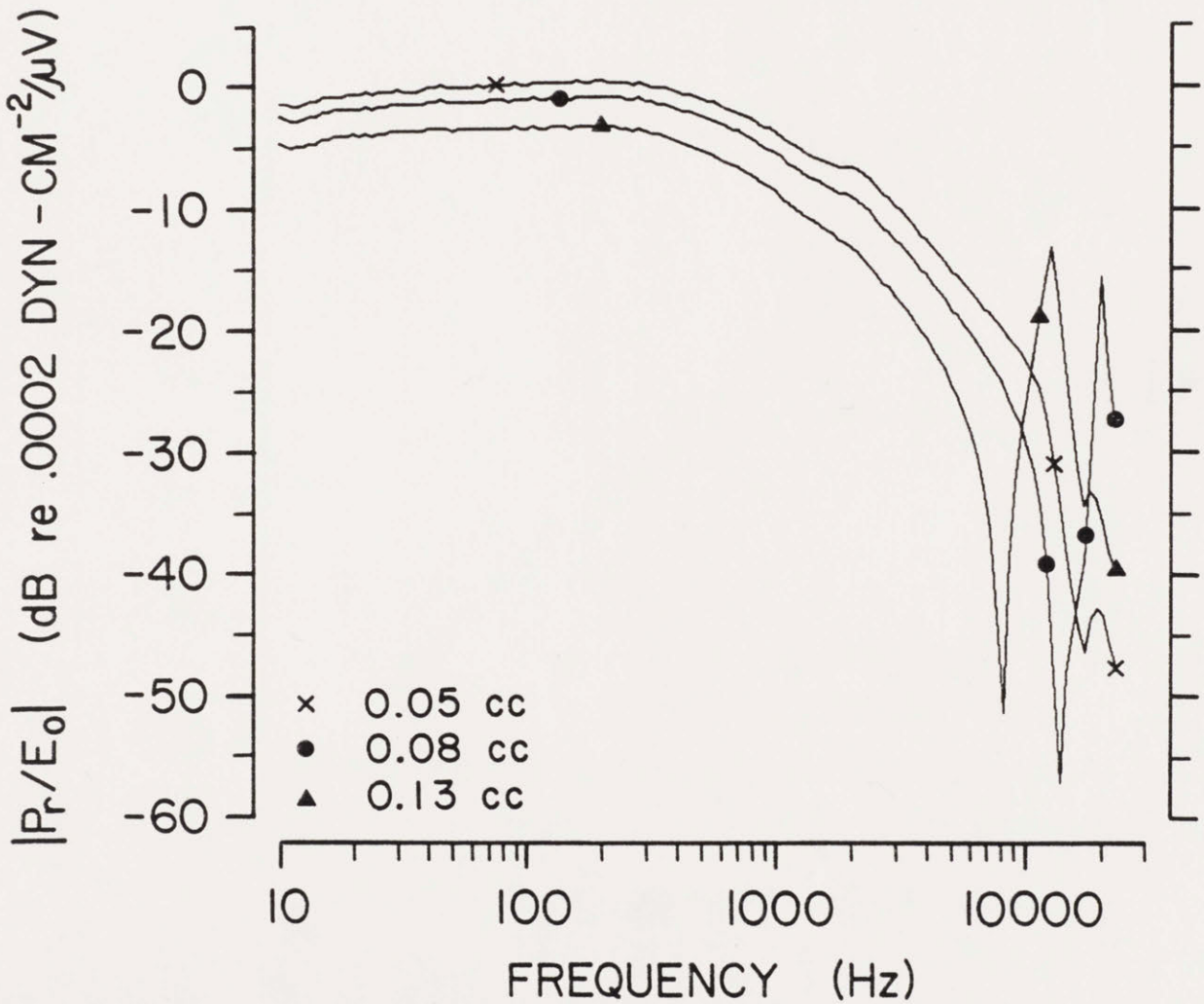
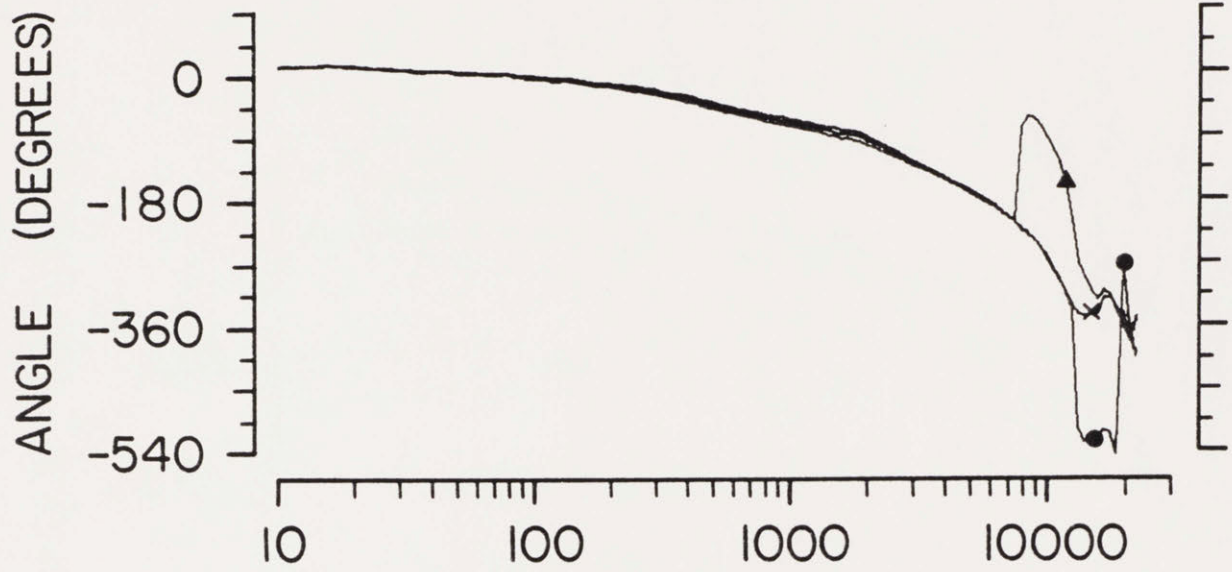


FIGURE 5B

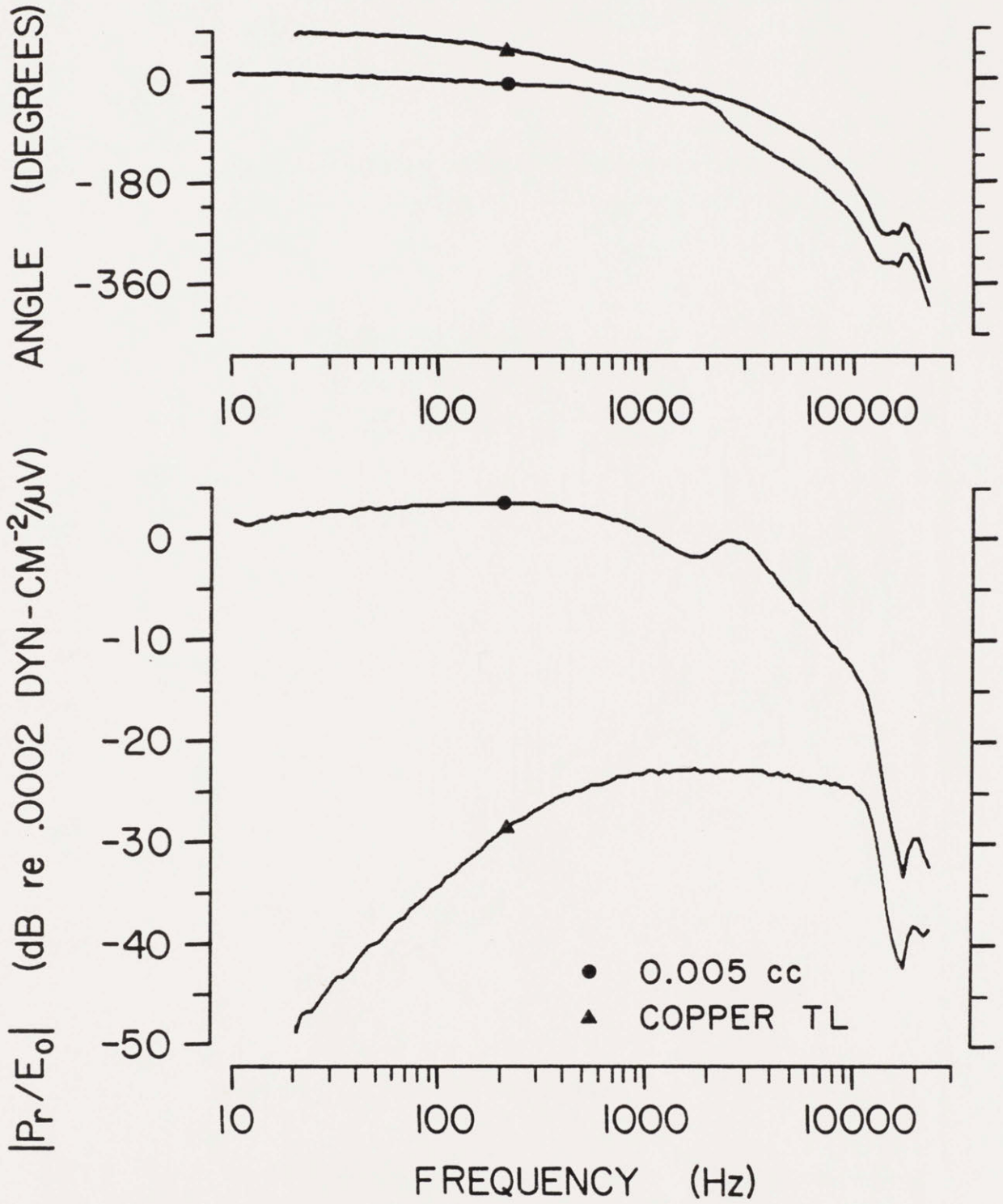


FIGURE 6

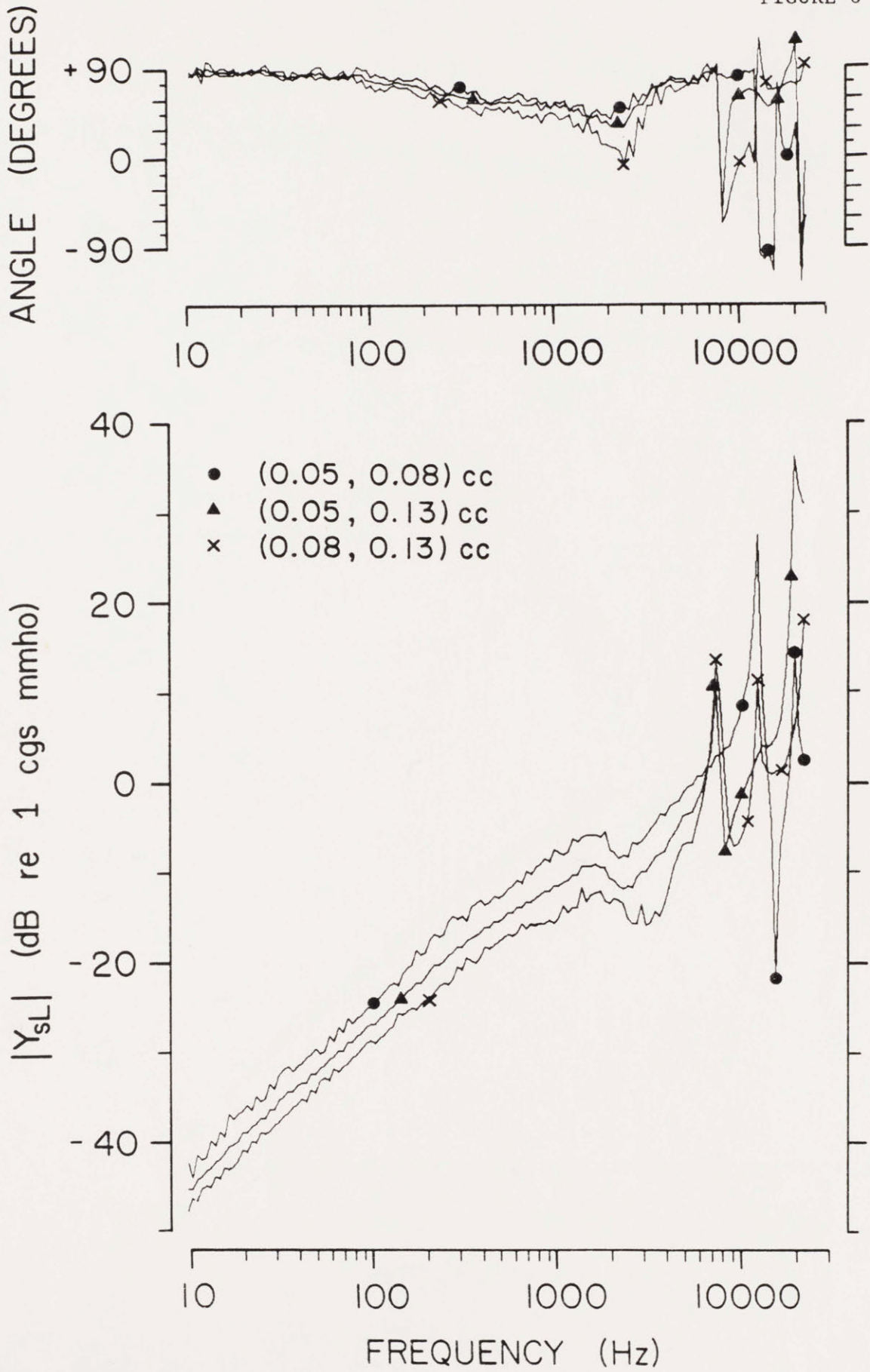


FIGURE 7

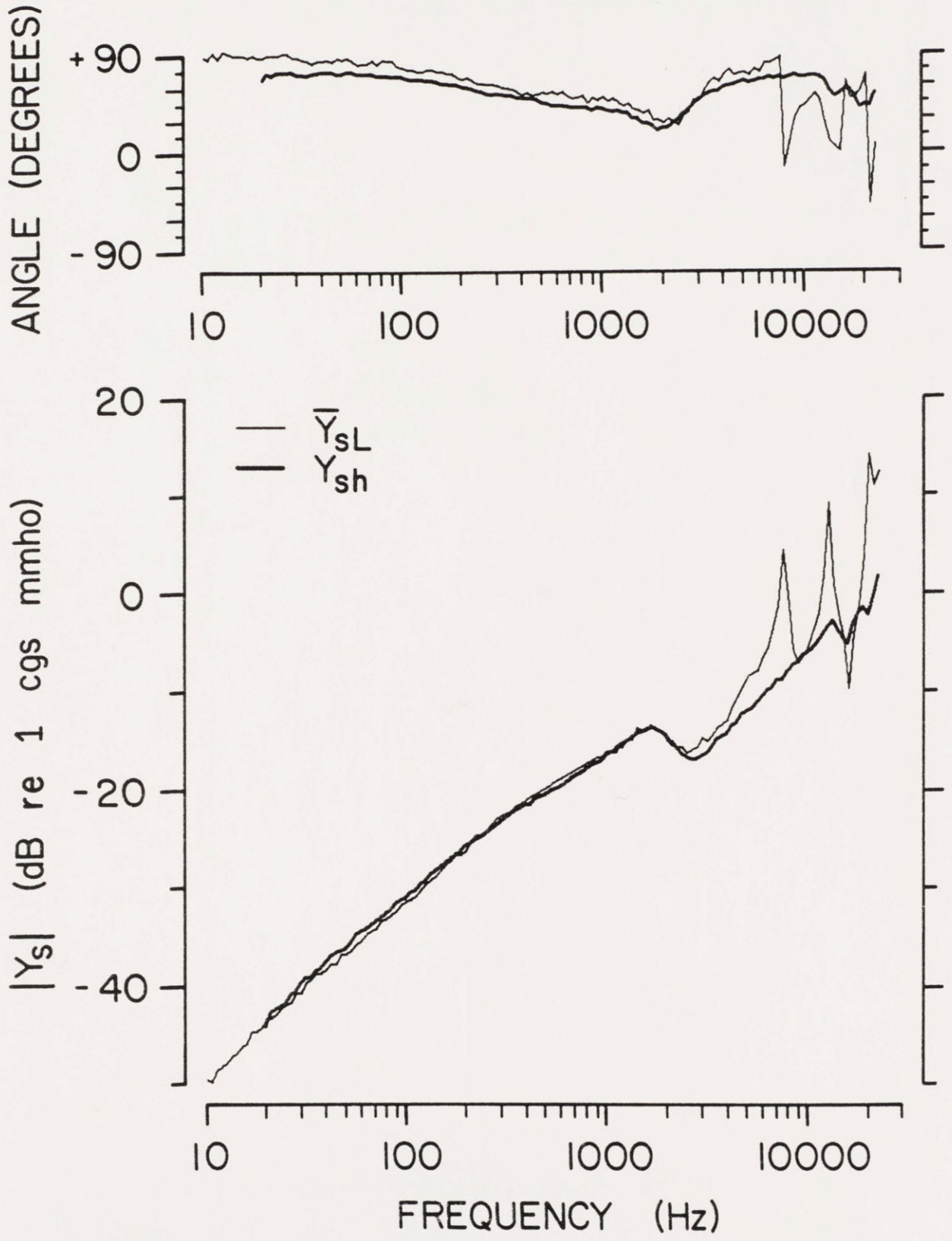


FIGURE 8A

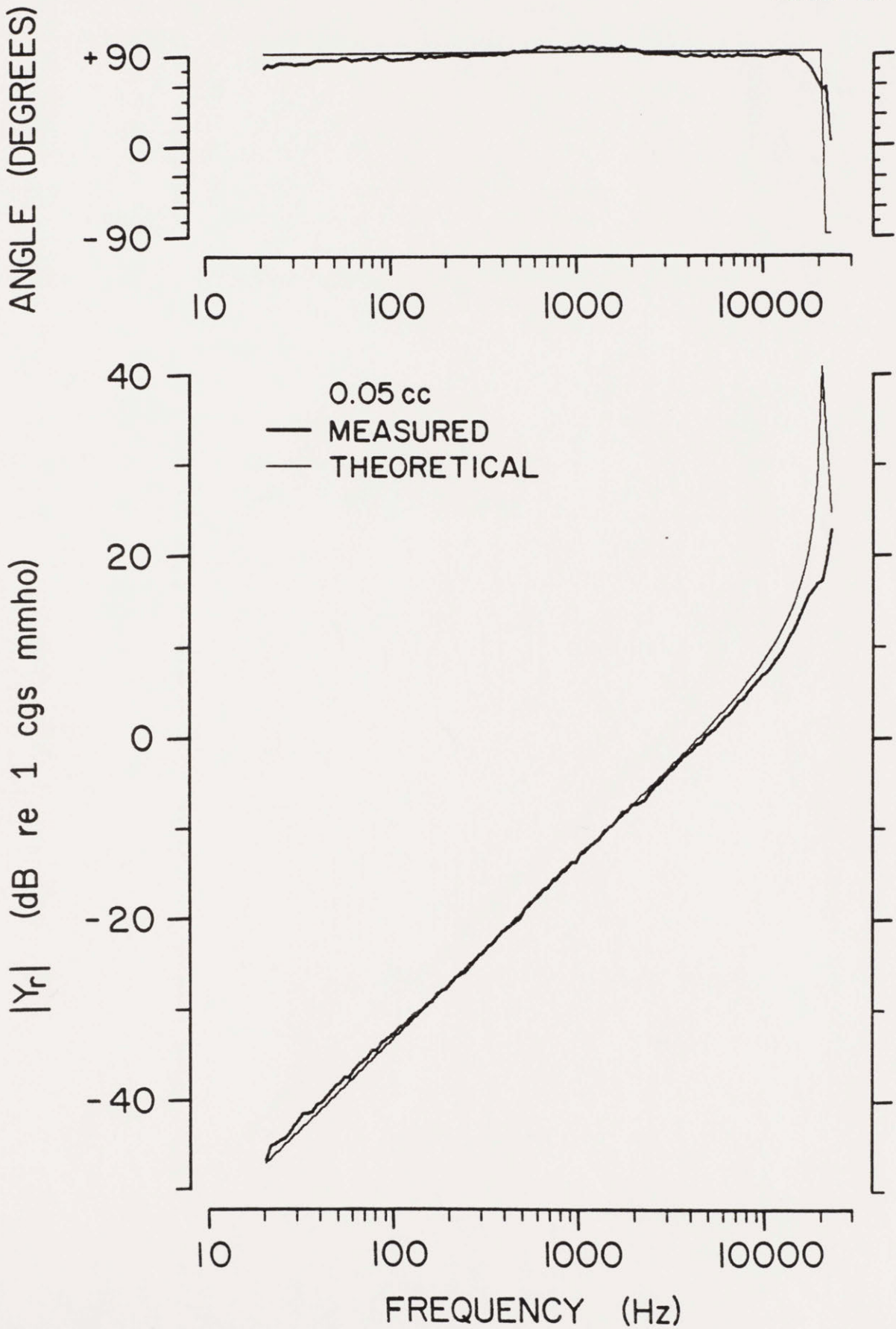


FIGURE 8B

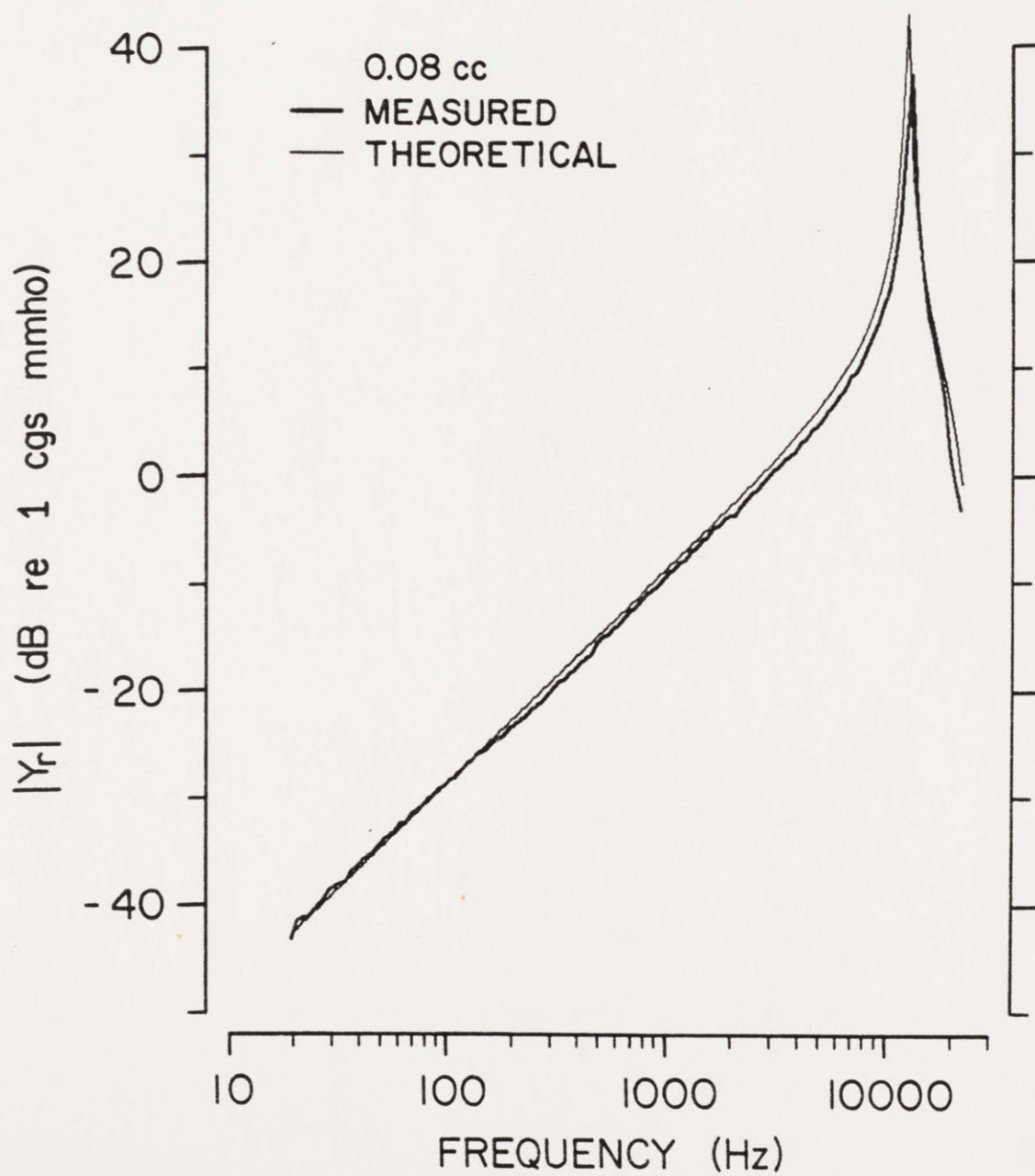
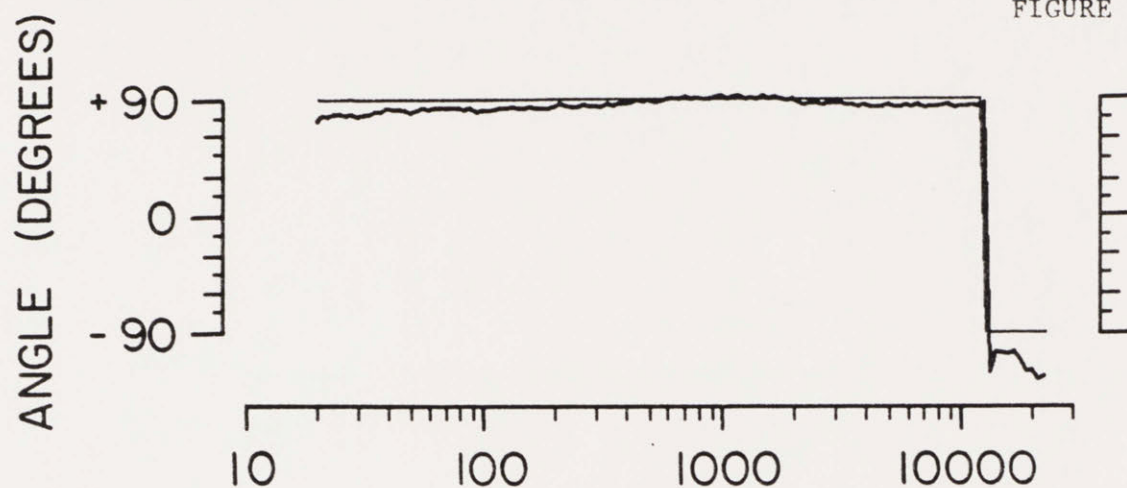


FIGURE 8C

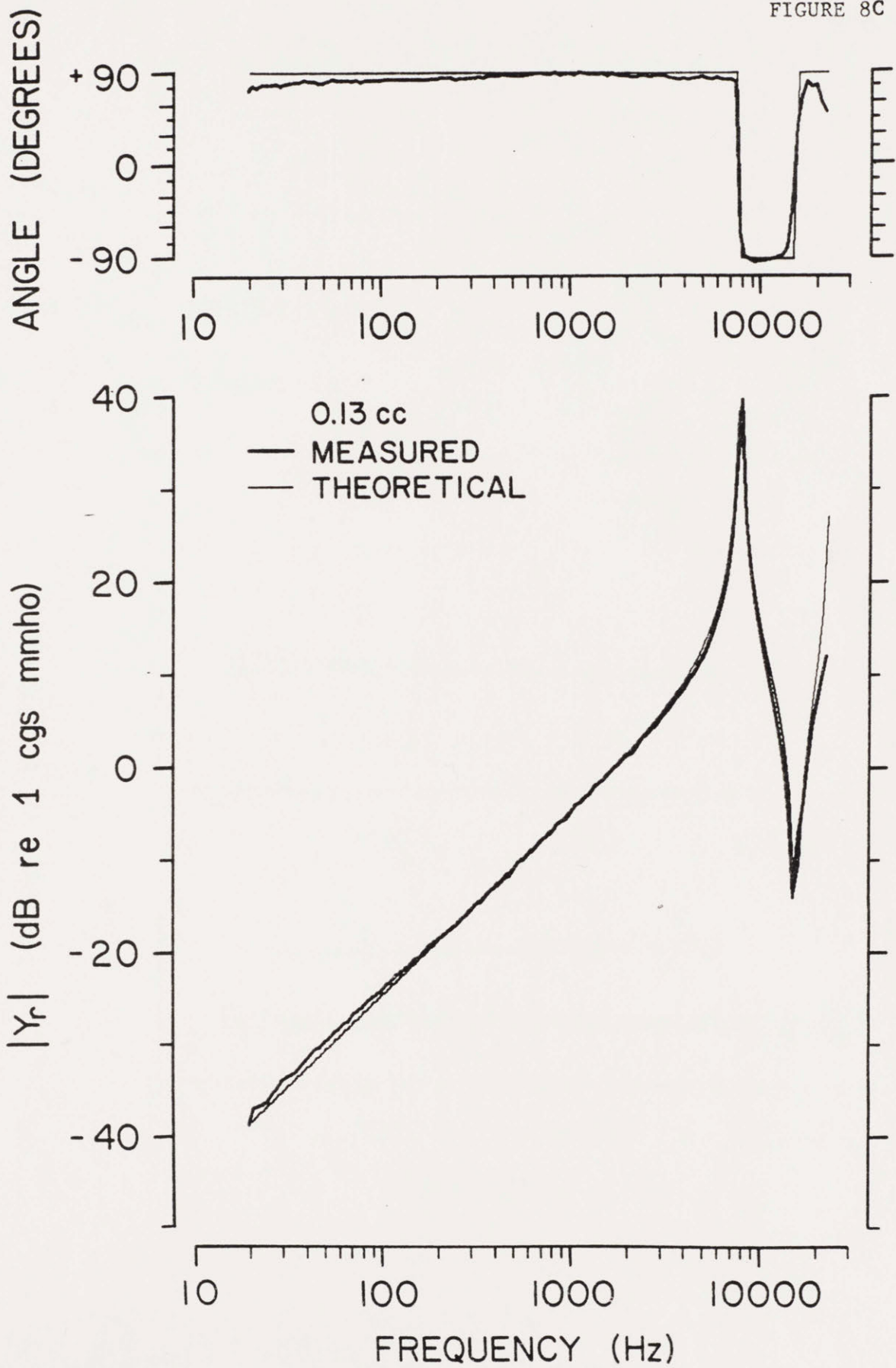


FIGURE 9

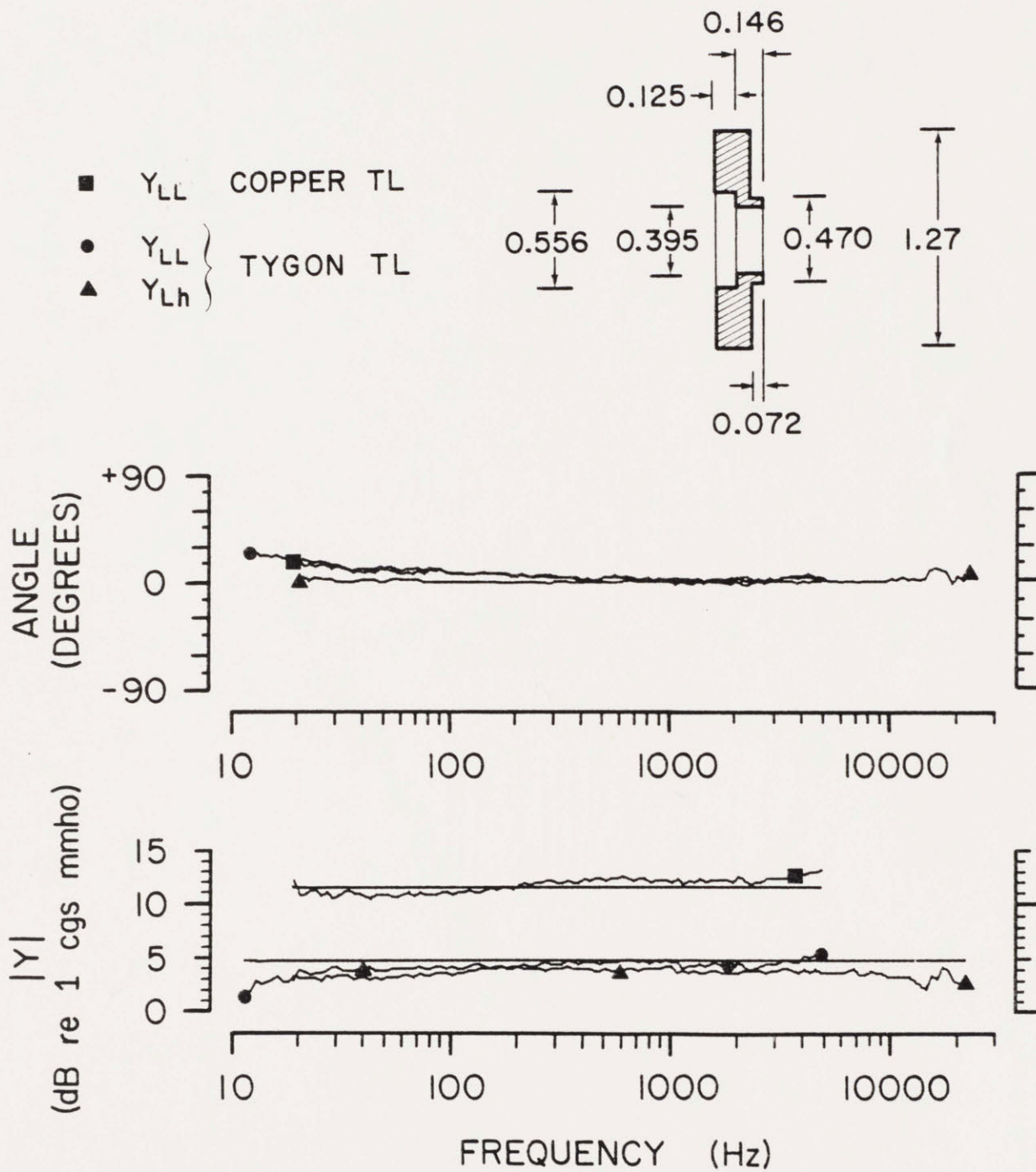


FIGURE 10

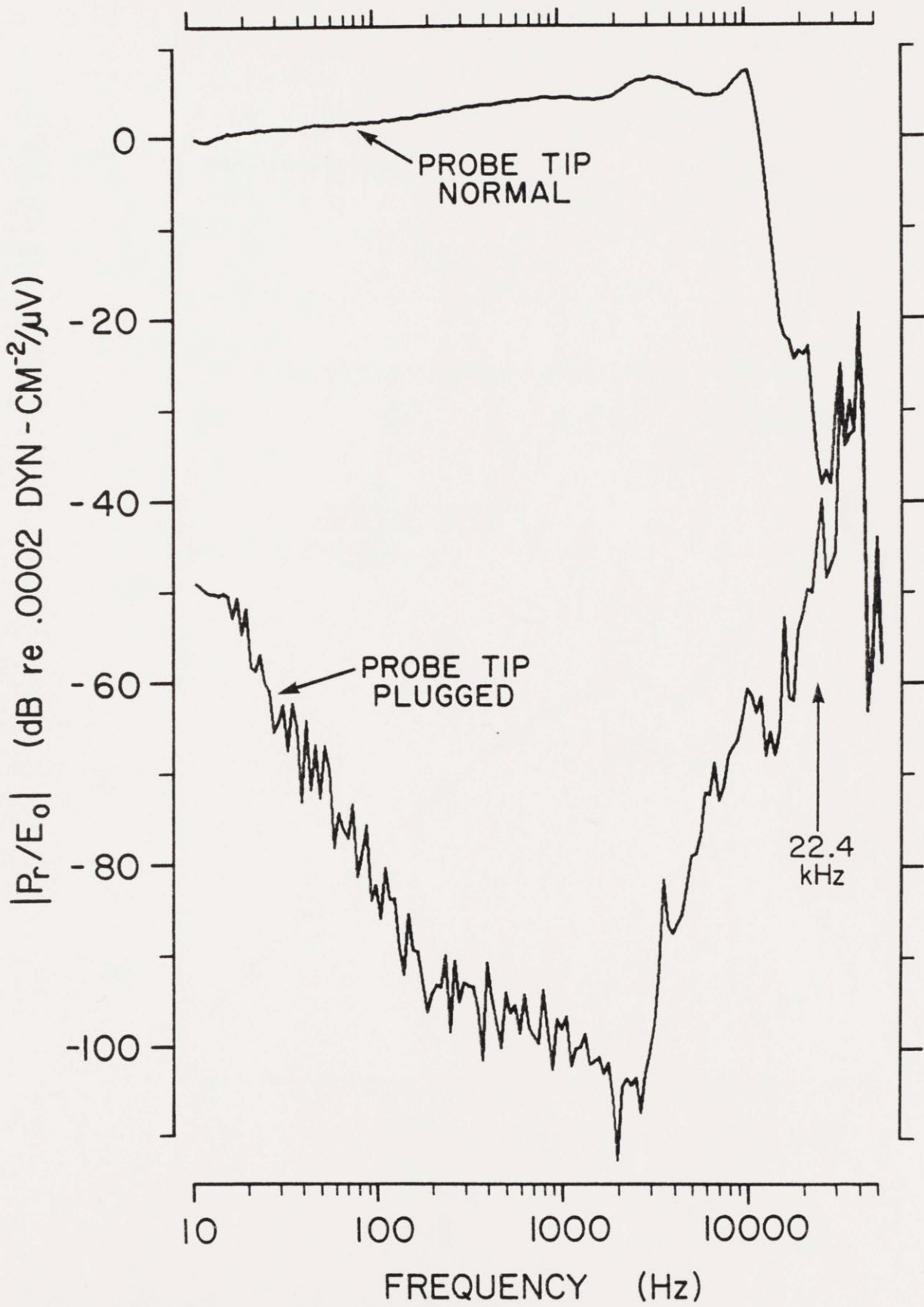


FIGURE 11

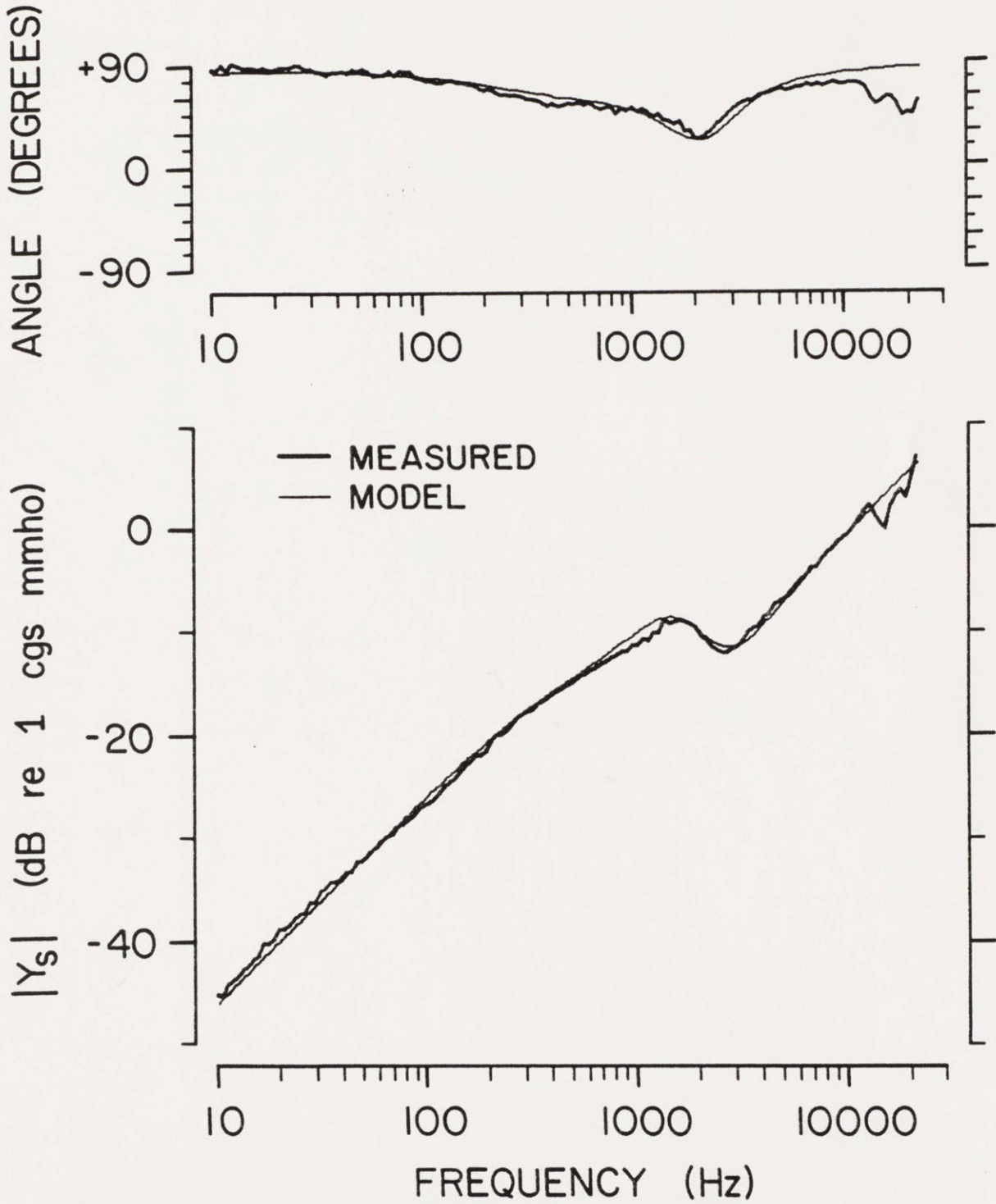


FIGURE 12

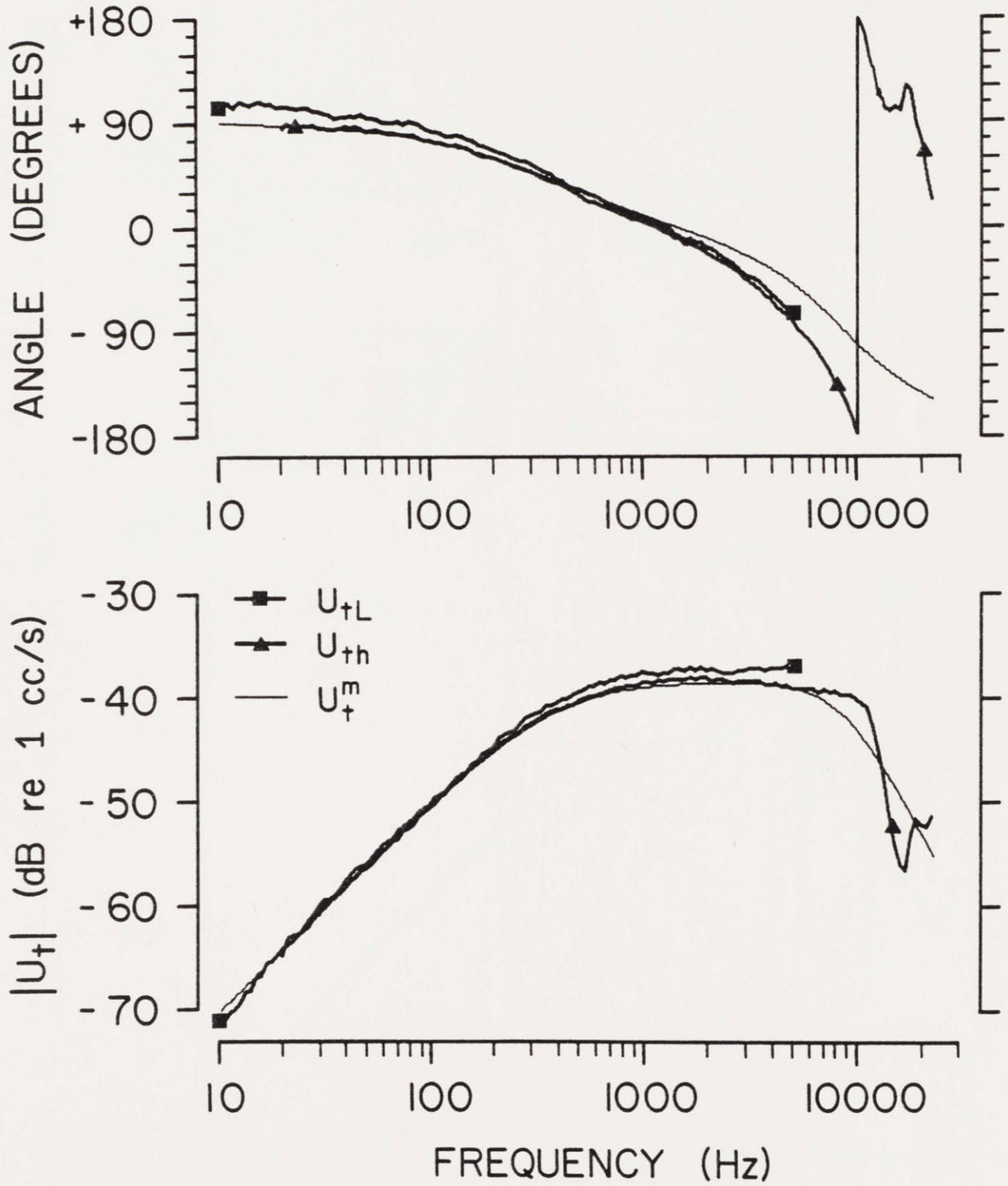


FIGURE 13A

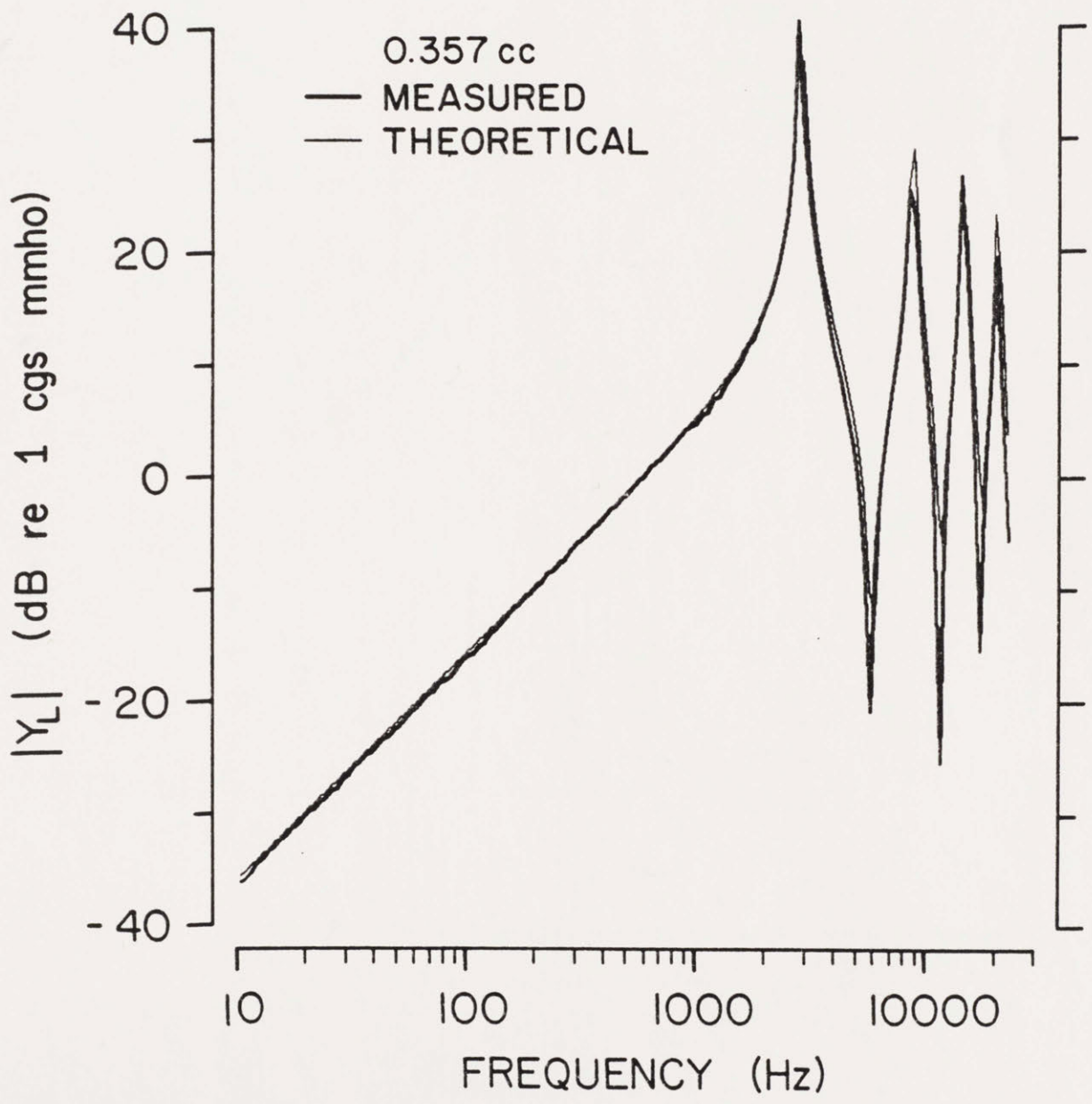
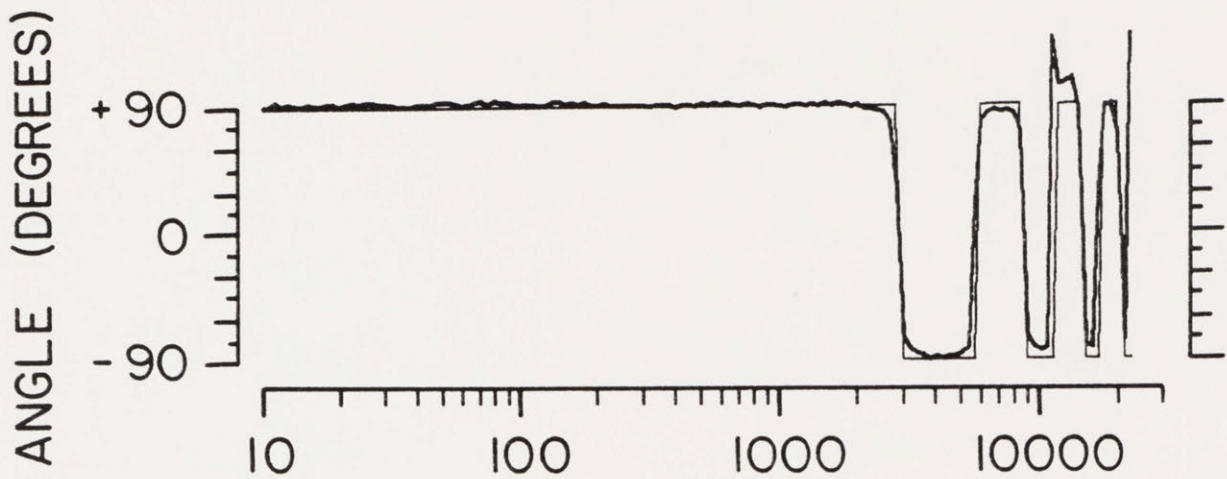


FIGURE 13B

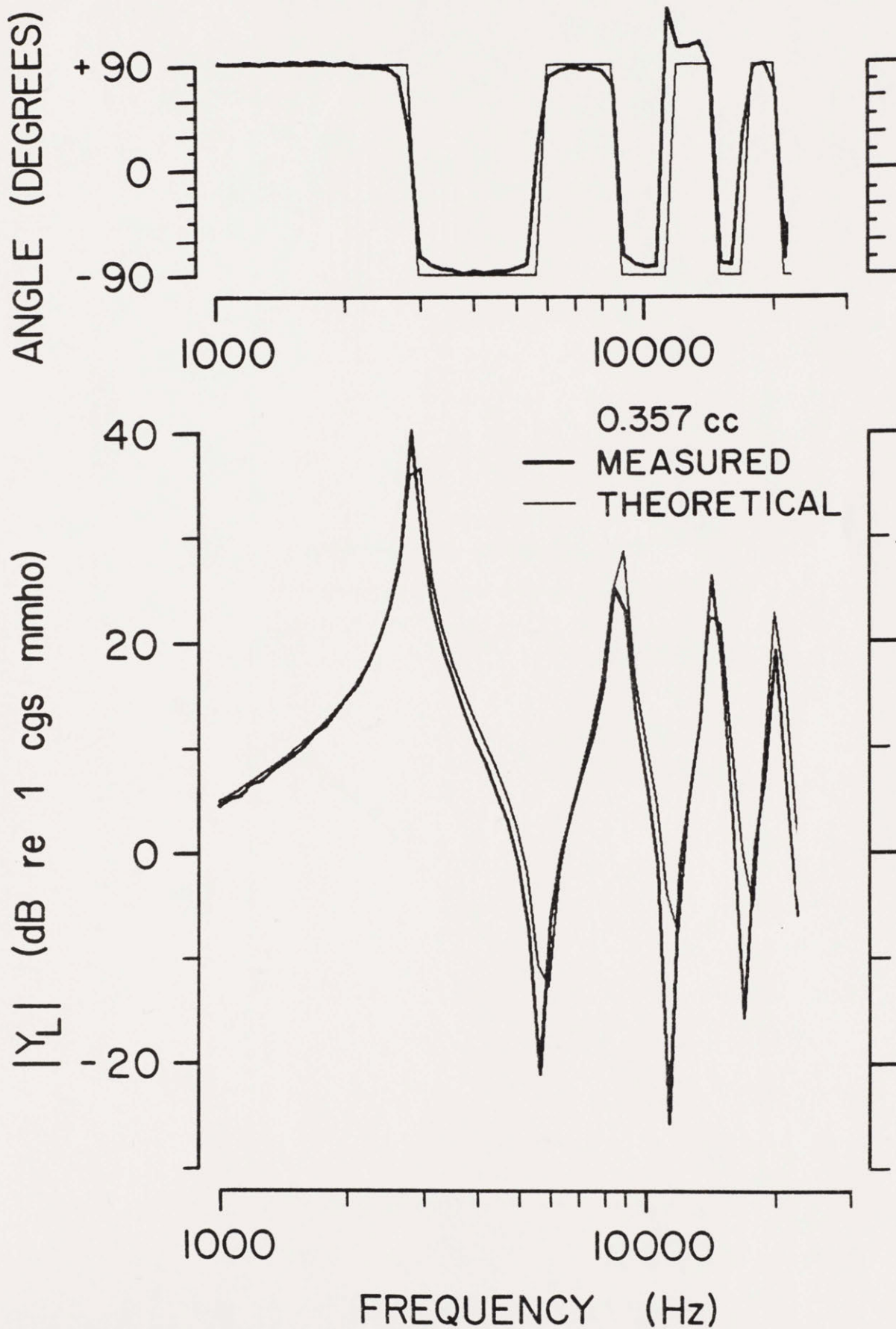


FIGURE 14

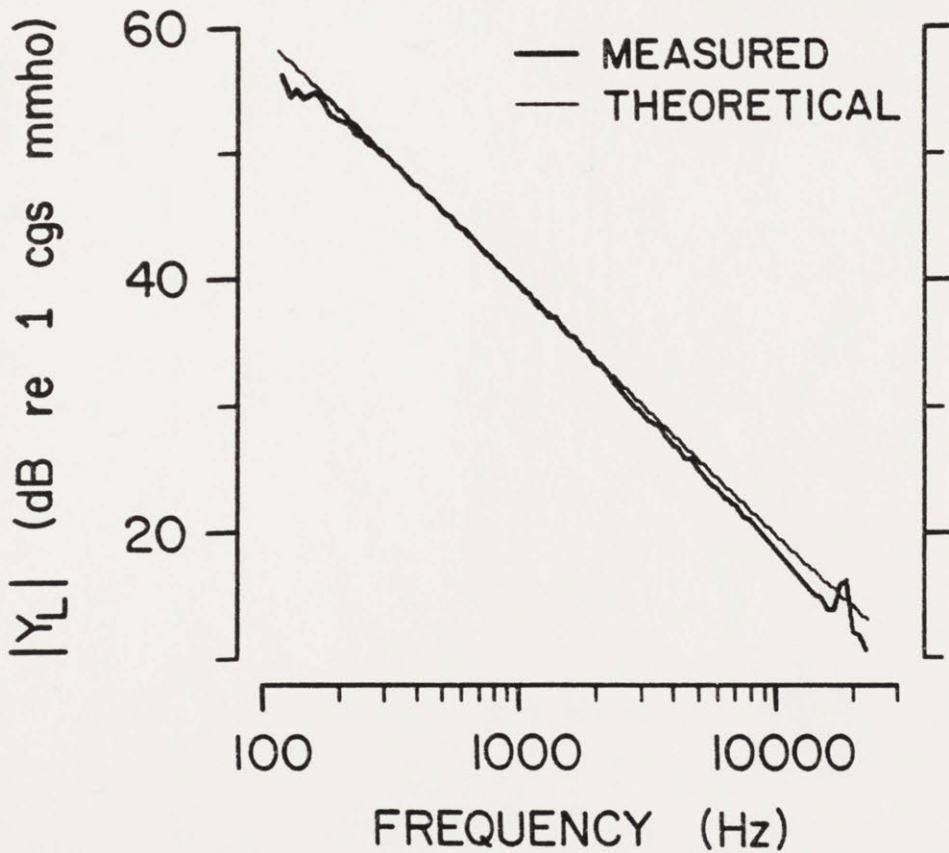
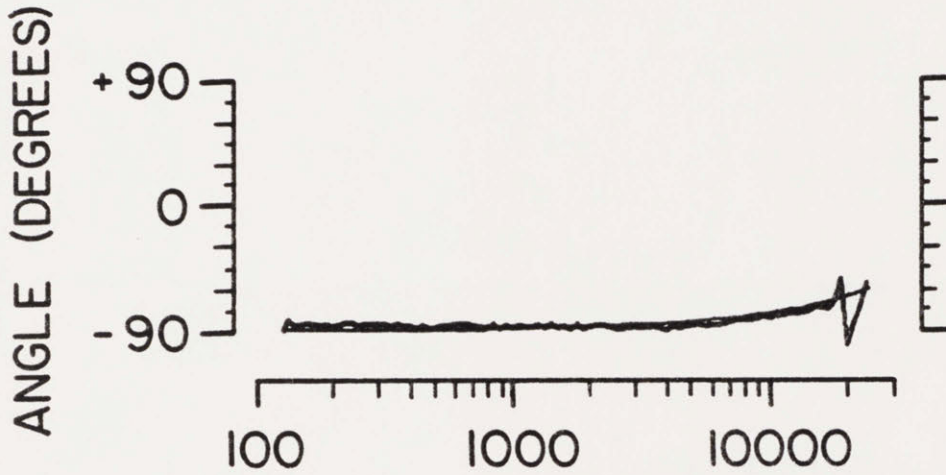
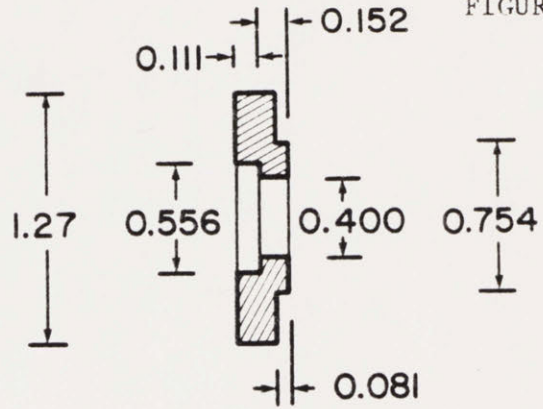
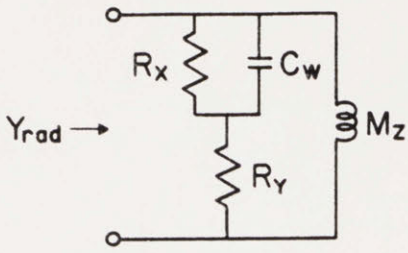


FIGURE 15

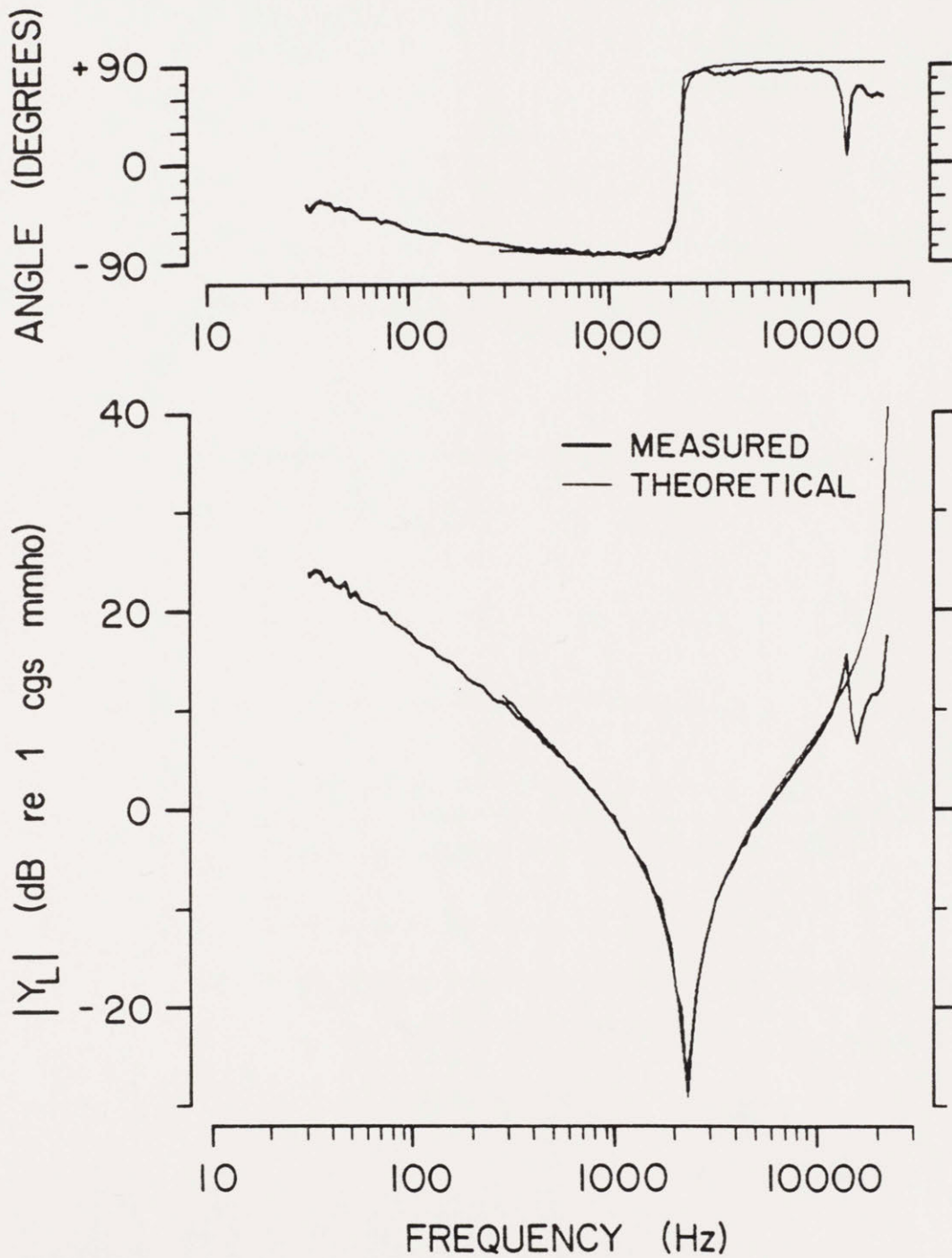
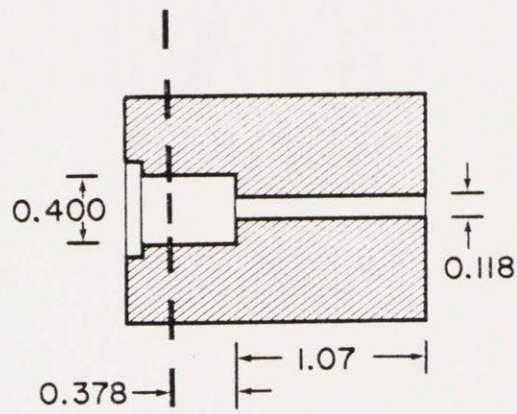


FIGURE 16

| NOMINAL RESISTANCE (OHMS) | |
|---------------------------|------|
| ● | 680 |
| ▲ | 1500 |
| ■ | 2200 |
| × | 3300 |
| ◆ | 4700 |

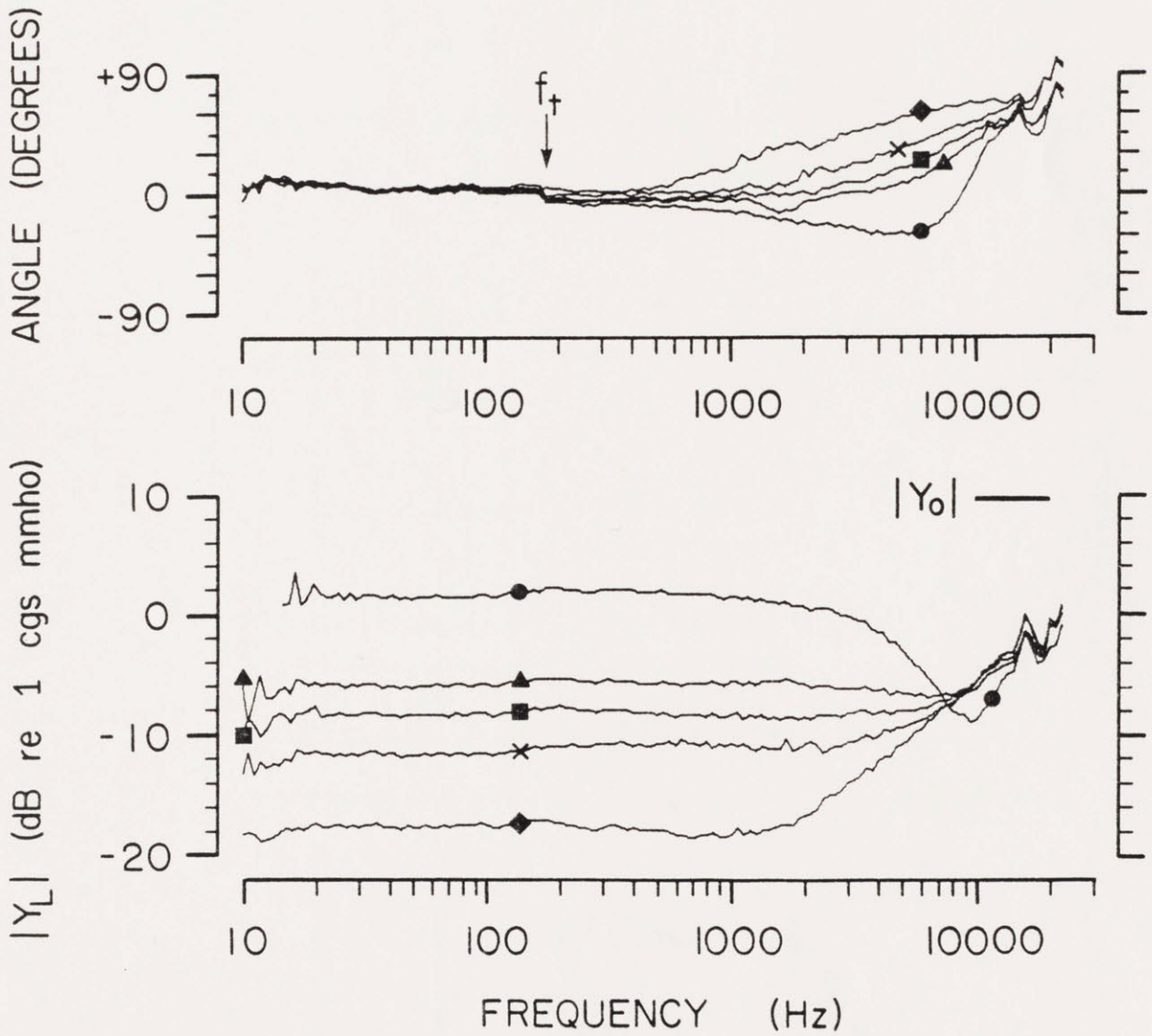
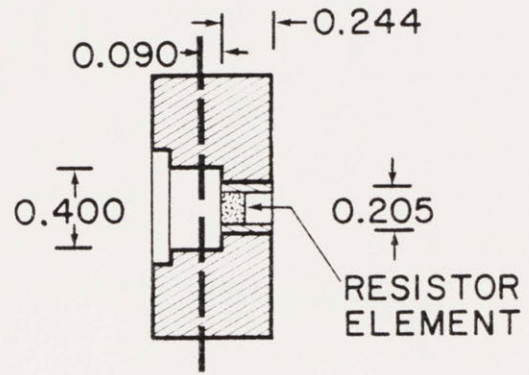
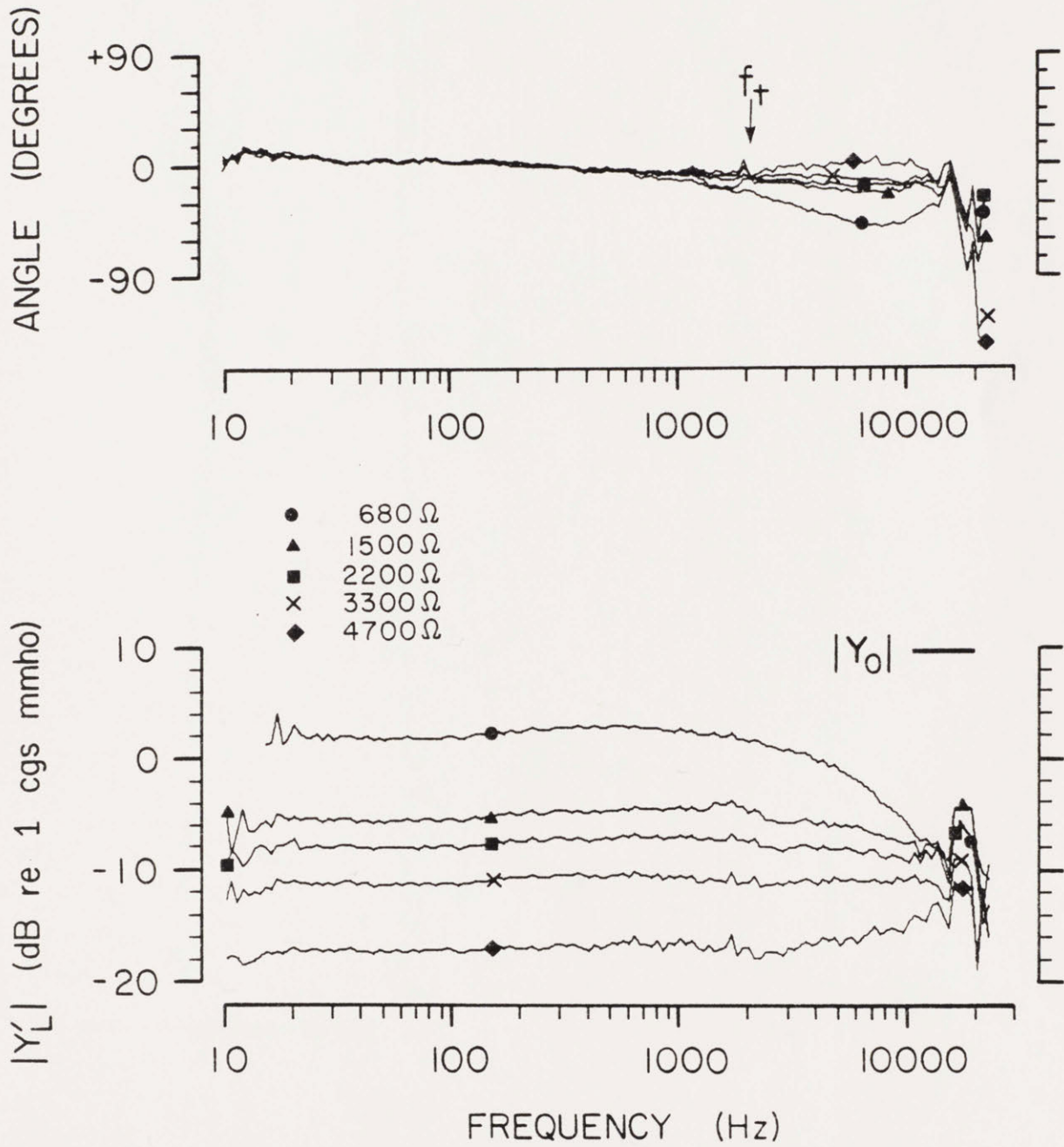


FIGURE 17



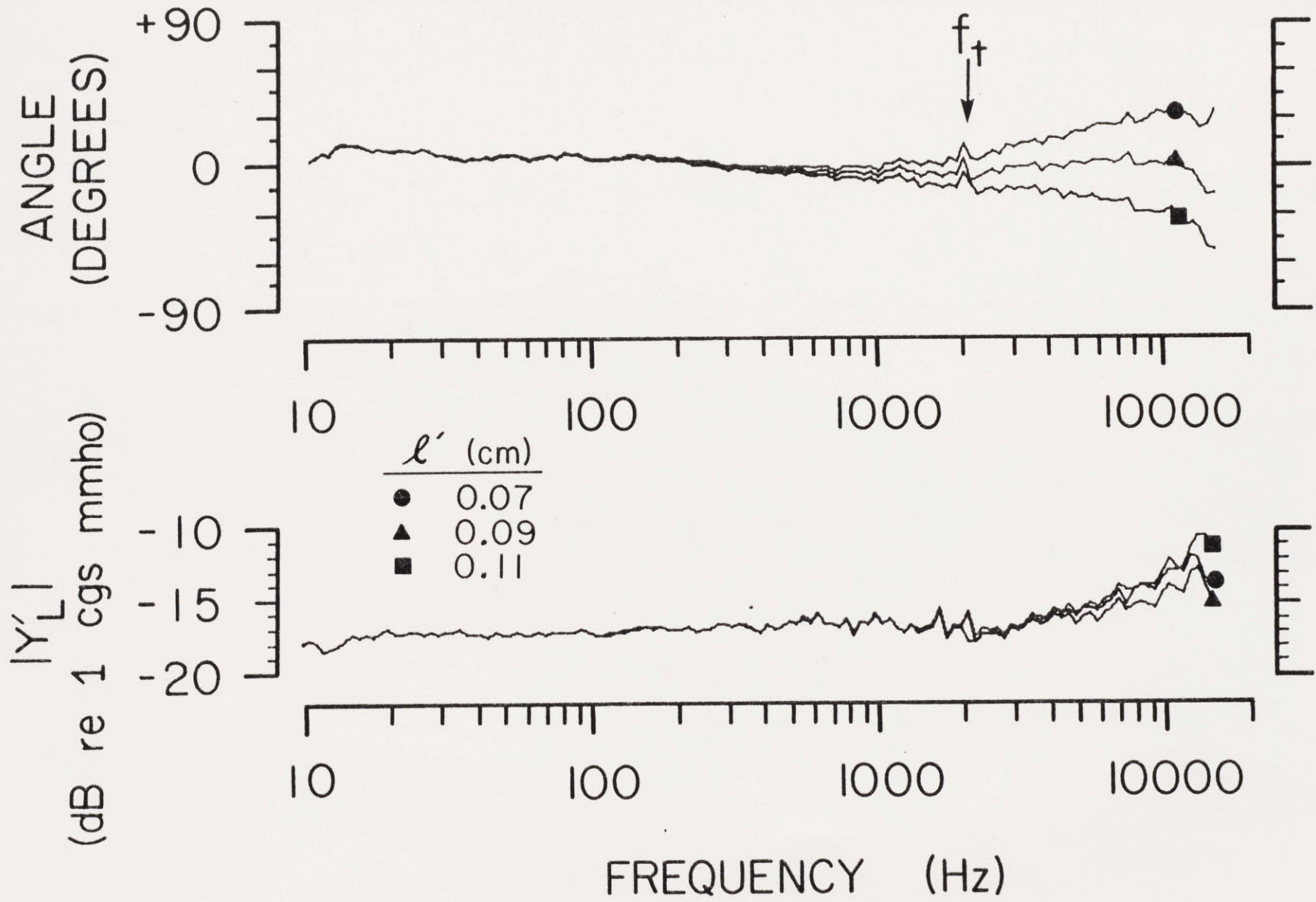
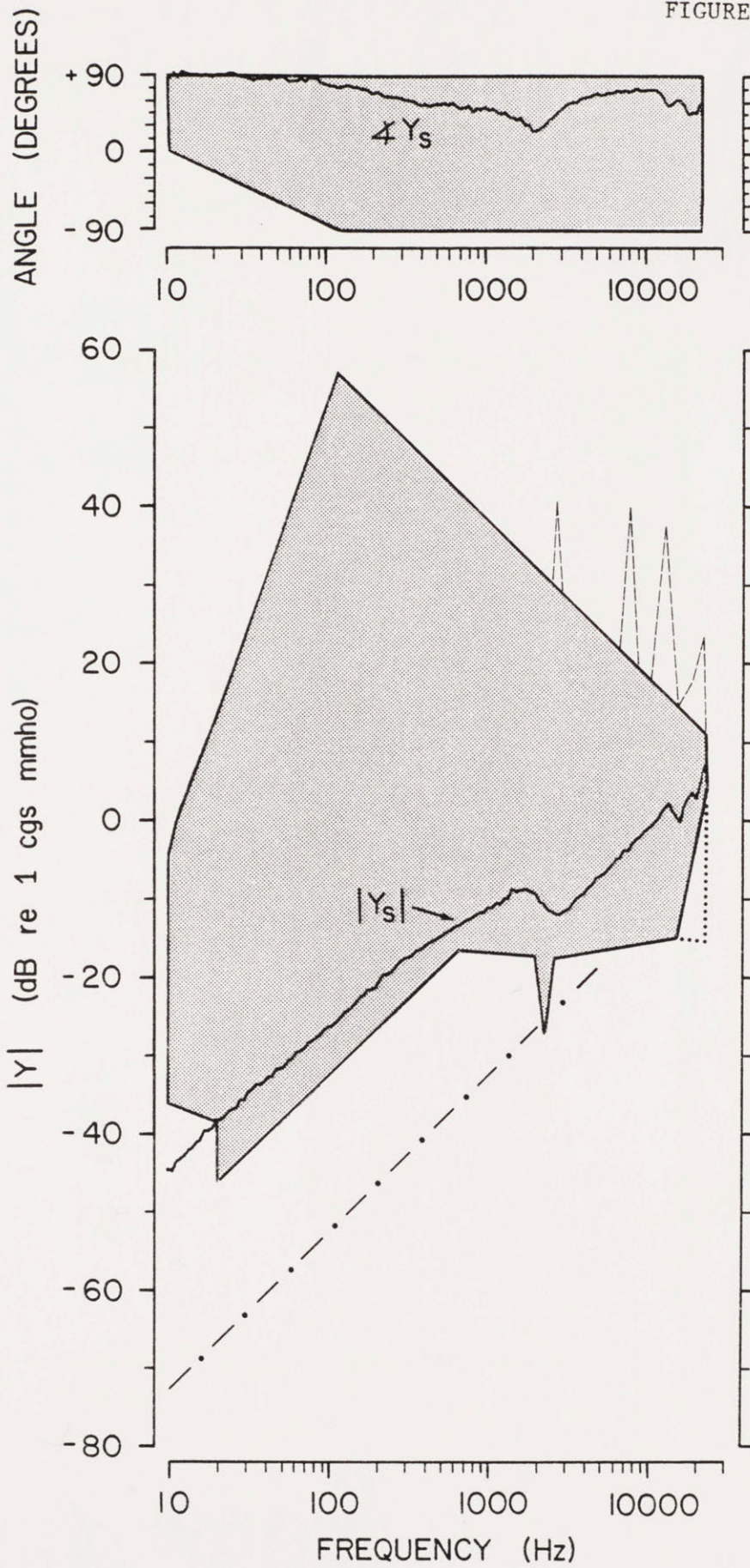


FIGURE 18

FIGURE 19



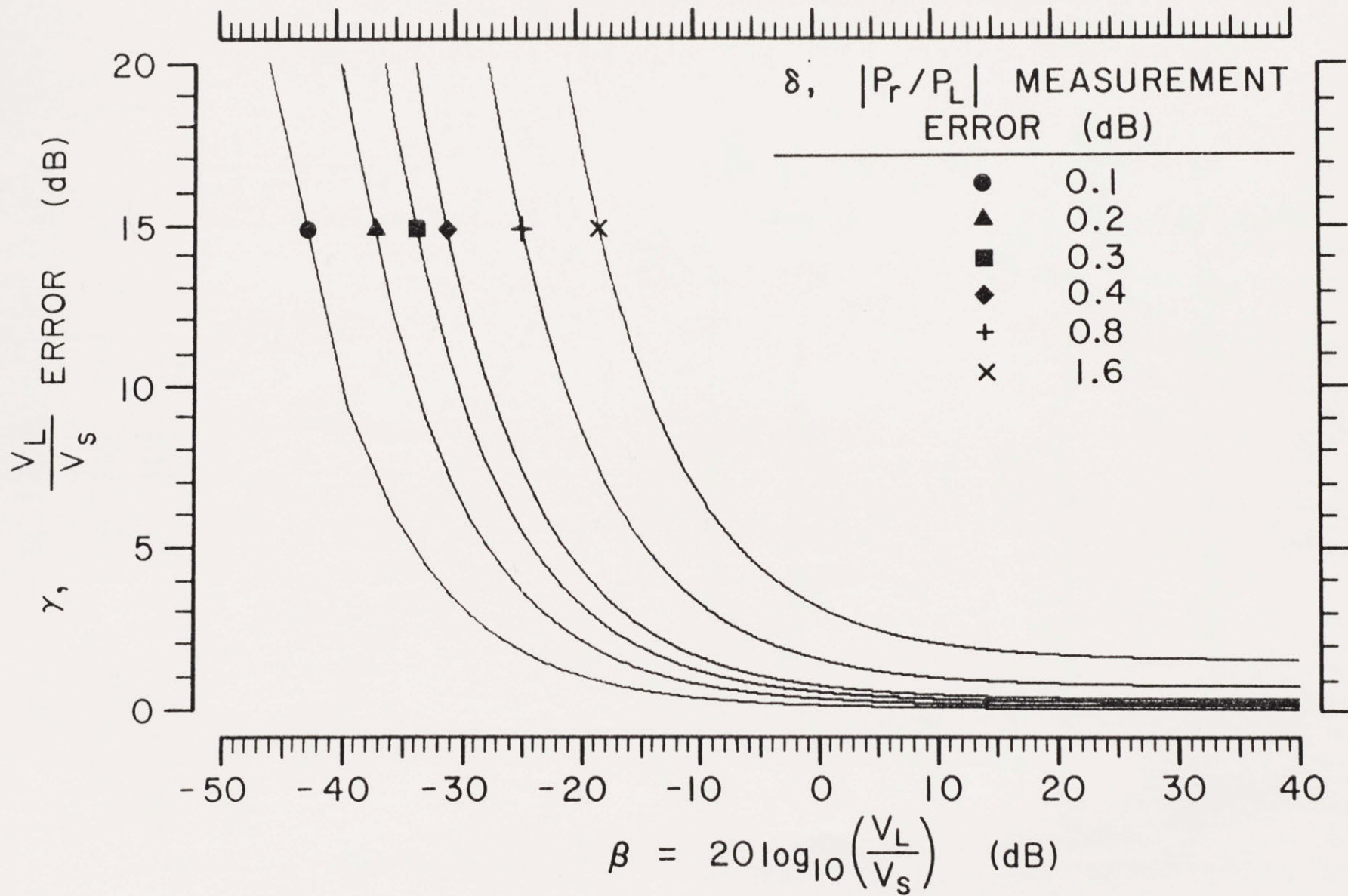
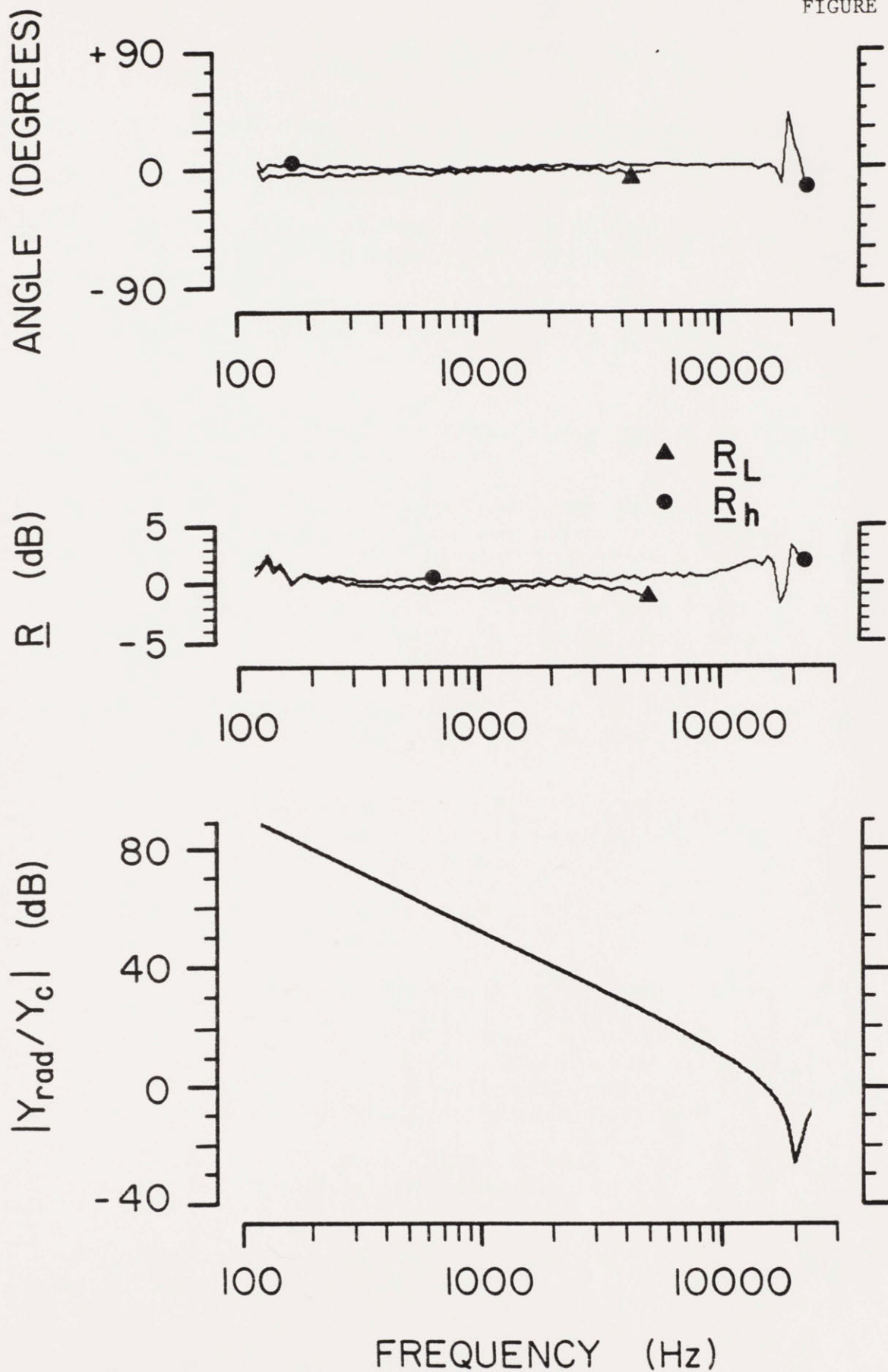


FIGURE 20

FIGURE A1



REFERENCES

- Beranek, L.L. (1949). Acoustic Measurements (Wiley, New York).
- Beranek, L.L. (1954). Acoustics (McGraw-Hill, New York).
- Biagi, F., and Cook, R.K. (1954). "Acoustic impedance of a right circular cylindrical enclosure," *J. Acoust. Soc. Am.* 26(4), 506-509.
- Blauert, J., and Platte, H.-J. (1974). "Impulse measurements of human eardrum impedance", *Proc. Eighth Int. Cong. Acoust.* (London) 1, 1972.
- Bose, A.G., and Stevens, K.N. (1965). Introductory Network Theory (Harper & Row, New York).
- Bruel, P.V. (1964). "The accuracy of condenser microphone calibration methods, part I," *Bruel and Kjaer Instruments, Inc., Technical Review No. 4*, 3-29.
- Bruel, P.V. (1965). "The accuracy of condenser microphone calibration methods, part II," *Bruel and Kjaer Instruments, Inc., Technical Review No. 1*, 3-26.
- Burkhard, M.D., and Sachs, R.M. (1977). "Sound pressure in insert earphone couplers and real ears," *J. Speech & Hear. Res.* 20(4), 799-807.
- Egolf, D.P., and Leonard, R.G. (1977). "Experimental scheme for analyzing the dynamic behavior of electroacoustic transducers," *J. Acoust. Soc. Am.* 62(4), 1013-1023.
- Eriksson, L.J. (1980). "Higher order mode effects in circular ducts and expansion chambers," *J. Acoust. Soc. Am.* 68(2), 545-550.
- Fredberg, J.J., Jackson, A.C., and Dawson, S.V. (1975). "Measurement of acoustic input impedance of an excised canine pulmonary system by transient excitation," *J. Acoust. Soc. Am.* 58(Suppl. #1), S128.
- Frederiksen, E. (1977). "Condenser microphones used as sound sources," *Bruel and Kjaer Instruments, Inc., Technical Review No. 3*.
- Gatley, W.S., and Cohen, R. (1969). "Methods for evaluating the performance of small acoustic filters," *J. Acoust. Soc. Am.* 46(1, Pt. 1), 6-16.
- Ingard, U. (1948). "On the radiation of sound into a circular tube, with an application to resonators," *J. Acoust. Soc. Am.* 20(5), 665-682.
- Killion, M.C. (1980). Private communication.

- Kinsler, L.E., and Frey, A.R. (1962). Fundamentals of Acoustics, 2nd edition. (Wiley & Sons, New York).
- Margolis, R.H., Osguthorpe, J.D., and Popelka, G.R. (1978). "The effects of experimentally-produced middle ear lesions on tympanometry in cats," *Acta Otolaryngol.* 86, 428-436.
- Martin, F.D. (1974). "Air impedance-tube technique for measuring the acoustic properties of wet sediment samples," *J. Acoust. Soc. Am.* 56(Suppl. #1), S51
- Mawardi, O.K. (1949). "Measurement of acoustic impedance," *J. Acoust. Soc. Am.* 21, 84-91.
- Mehrgardt, S., and Mellert, V. (1977). "Transformation characteristics of the external human ear," *J. Acoust. Soc. Am.* 61, 1567-1576.
- Metz, O. (1946). "The acoustic impedance measured on normal and pathological ears," *Acta Otolaryngol. Suppl.* 63, 1-254.
- Møller, A.R. (1960). "Improved technique for detailed measurements of the middle ear impedance," *J. Acoust. Soc. Am.* 32(2), 250-257.
- Møller, A.R. (1963). "Transfer function on the middle ear," *J. Acoust. Soc. Am.* 35(10), 1526-1534.
- Møller, A.R. (1965). "An experimental study of the acoustic impedance of the middle ear and its transmission properties," *Acta Otolaryngol.* 60, 129-149.
- Peake, W.T. (1981). Private communication.
- Rabinowitz, W.M. (1977). "Acoustic-Reflex Effects on the Input Admittance and Transfer Characteristics of the Human Middle-Ear," Ph.D. Thesis, Massachusetts Institute of Technology, Cambridge, Ma., pp. 1-250.
- Rabinowitz, W.M. (1981). "Acoustic immittance of the human middle ear," (Unpublished).
- Seybert, A.F., and Ross, D.F. (1977). "Experimental determination of acoustic properties using a two-microphone random-excitation technique," *J. Acoust. Soc. Am.* 61(5), 1362-1370.
- Singh, R., and Soedel, W. (1978). "An efficient method of measuring impedances of fluid machinery manifolds," *J. Sound Vib.* 56, 105-125.
- Terkildsen, K., and Nielsen, S. (1960). "An electroacoustic impedance measuring bridge for clinical use," *Arch. Otolaryng. (Chicago)* 3, 339-346.
- Tonndorf, J., and Khanna, S.M. (1967). "Some properties of sound transmission in the middle and outer ears of cats," *J. Acoust. Soc.*

Am. 41(2), 513-521.

Ver, I.L., Brown, R.M., and Kiang, N.Y.S. (1975). "Low-noise chambers for auditory research," J. Acoust. Soc. Am. 58(2), 392-398.

Weiss, T.F., Goldmark, G.M., Altmann, D.W., and Brown, R.M. (1969). "Automated system to control stimulus and measure response variables in experiments on the auditory system," M.I.T. Research Laboratory of Electronics, Quarterly Prog. Rep. No. 95, 122-127.

Weiss, T.F., and Peake, W.T. (1972). "Cochlear potential response at the round-window membrane of the cat -- A reply to the comment of G.R. Price," J. Acoust. Soc. Am. 52, 1729-1734.

Zuercher, J.C. (1977). "The calculation of isothermal and viscous effects in acoustic tubes," Presented at the 94th Meeting of the Acoustical Society of America, Miami Beach, Fla., December, 1977.

Zwislocki, J. (1962). "Analysis of the middle-ear function. Part I: Input impedance," J. Acoust. Soc. Am. 34(8, Pt. 2), 1514-1523.

Chapter II

ACOUSTIC PROPERTIES OF THE MIDDLE-EAR CAVITIES OF CAT

I. INTRODUCTION

A. TOWARD A THEORY OF THE MECHANICS OF THE MIDDLE EAR

Transmission of acoustic signals from the external ear canal to the inner ear is accomplished by the mechanical system of the middle ear. The acoustic and mechanical responses of the structures comprising this system have been represented by an analog electric network in FIGURE 1A. This approach has been used by others to describe the mechanics of the middle ear in human (Onchi, 1949, 1961; Zwislocki, 1957, 1962), guinea pig (Mundie, 1963; Zwislocki, 1963; Nuttall, 1974), and cat (Møller, 1961; Peake and Guinan, 1967; Geisler and Hubbard, 1975). Although mechanical responses of this system have been measured in cat, existing experimental evidence is not sufficient to formulate a detailed theory of middle-ear mechanics. Our goal is to work toward such a theory based on systematic measurements of the forces and motions associated with the various structures of the middle ear.

Our approach is comprised of two steps. The first is to experimentally determine the impedance and/or transmission characteristics of various isolated structures of the cat middle ear. For example, the acoustic impedance of the stapes and cochlea

(FIGURE 1A, boxes 7 and 8) have been previously determined (Lynch, et al., 1981). The present report is concerned with the specification of the acoustics of the middle-ear cavities (box 1). Results pertinent to the mechanics of the remaining blocks will be described in CHAPTER III. The second step is the integration of these results into a complete theory of middle-ear mechanics, which can be tested using independent measurements of the middle ear (e.g., Guinan and Peake, 1967; Nedzelnitsky, 1980; Møller, 1963, 1965).

B. EFFECTS OF THE MIDDLE-EAR CAVITIES: AN APPROACH

"Functional" anatomy of the middle ear is often used to propose network models, such as those of FIGURE 1, which account for measurements of input impedance and/or middle-ear transmission. It is important to experimentally test the validity of the model topology. Also, elements in the models are often associated with specific anatomical entities; these associations must also be tested.

Assuming that the network of FIGURE 1A is appropriate, we may simplify the model to the form shown in FIGURE 1B, where Z_d is the complex acoustic input impedance at the tympanic membrane for the condition of an intact middle ear,

$$Z_d = P_d/U_d = Z_{doc} + Z_{mec} \cdot \quad (1)$$

Z_{mec} is the acoustic impedance of the middle ear cavities (MEC) and Z_{doc} is the acoustic impedance at the tympanic membrane for the condition of

open cavities (i.e., Z_{mec} is assumed to be "shorted" by opening the cavities; Z_{doc} is the input impedance of the remaining blocks). P_d is the complex amplitude of the sound pressure at the tympanic membrane, and U_d is the complex amplitude of the tympanic membrane volume velocity.

FIGURE 2A schematically shows the anatomical and experimental arrangement for the intact ear. The tympanic membrane (TM) is part of the lateral wall of the tympanic cavity (volume = $V_t \cong 0.25$ cc) which encloses the ossicular system. A short, narrow foramen leads from the tympanic cavity through the boney septum to the larger bulla cavity ($V_b \cong 0.8$ cc). The actual geometry of both cavities and the foramen is irregular.

We propose to test the "series" aspect of the model (FIGURE 1B) by measurement of the acoustic input impedance, Z_d , and the pressure transmission ratio, P_t/P_d , for "normal" and "experimentally modified" states of the MECs. In particular, the conditions are (FIGURE 2) 1) intact MECs (Z_{di}), 2) bulla cavity opened widely with the foramen open (Z_{dob}), and 3) foramen mechanically plugged (Z_{dpf}). These experimental conditions are denoted below by the addition of an x to the subscript of the impedances and pressure ratios. From FIGURE 1B it is clear that

$$(P_t/P_d)_x = \frac{Z_{mecx}}{Z_{mecx} + Z_{doc}} = \frac{Z_{dx} - Z_{doc}}{Z_{dx}} \quad (2)$$

which can be rewritten

$$1 - (P_t/P_d)_x = Z_{doc}/Z_{dx} = Y_{dx}/Y_{doc} \quad (3)$$

where Y is complex admittance. Thus, we can test the "series" model

structure with measurements of $(P_t/P_d)_x$ and Y_{dx}/Y_{doc} to obtain independently each side of Equation (3). Additionally, we can use these data to compute estimates (\hat{Z}) of the total middle-ear cavities impedance, \hat{Z}_{mecx} , for each of the above conditions from

$$Z_{dx} (P_t/P_d)_x = P_{tx}/U_{dx} = \hat{Z}_{mecx} . \quad (4)$$

The lumped-impedance model corresponding to the MEC's anatomical arrangement (FIGURE 1C) is composed of Z_t , Z_b , and Z_f --the acoustic impedances of the tympanic cavity, bulla cavity, and foramen, respectively. A proposed detailed model of the cat middle-ear cavities is shown in FIGURE 1D. Bulla and tympanic cavity impedances are modelled by acoustic compliances ($Z_b = 1/j\omega C_b$ and $Z_t = 1/j\omega C_t$, where $C = V/\rho c^2$ is the compliance, V = cavity volume, ρ = density of air, and c = the speed of sound in air). The foramen is modelled as a narrow tube represented by an acoustic mass, M_f , and resistance, R_f , in series. Note the following aspects of the model impedance, Z_{mec} . 1) For very low frequencies, $Z_{mec} \cong 1/j\omega(C_b + C_t)$. 2) For very high frequencies, $Z_{mec} \cong 1/j\omega C_t$. 3) At an intermediate frequency, $f_s = 1/\{2\pi(M_f C_b)^{0.5}\}$, there is a series resonance between C_b and M_f , resulting in a relative minimum in $|Z_{mec}|$ (if R_f is small, i.e., low damping). 4) At a slightly higher frequency, $f_p = 1/\{2\pi(M_f C_{eq})^{0.5}\}$, where $C_{eq} = C_b C_t / (C_b + C_t)$, a parallel resonance, produces a relative maximum in $|Z_{mec}|$.

The \hat{Z}_{mec} estimates (Equation 4) will be used to determine values for the component elements of Z_b , Z_t , and Z_f and to evaluate the validity of the model. We have also measured the pressure ratio, P_b/P_d , for the condition of intact MECs. P_b/P_t was calculated using the corresponding

measurement of P_t/P_d . This result tests the detailed behavior of Z_b and Z_f (independent of Z_{doc}), since the model prediction is $P_b/P_t = Z_b/(Z_b + Z_f)$. We will also attempt to correlate the geometry of the anatomical components of the MECs with the measured acoustic properties (e.g., cavity volumes or foramen dimensions with acoustic impedances).

II. METHODS

A. ANIMAL PREPARATION

Adult cats weighing between 2.1 and 3.9 kg were initially anesthetized by an intraperitoneal injection of Dial (0.75 ml/kg). Additional doses of 0.2 ml were administered as needed. Each cat received 50,000 units of penicillin intramuscularly and approximately 50 ml of physiological saline subcutaneously. A cannula was inserted into the trachea. Rectal temperature was monitored and maintained at $38 \pm 2^{\circ}$ C through control of the ambient room temperature ($30 \pm 3^{\circ}$ C) and intermittent use of a heating pad located under the animal.

A ventral surgical approach was used to expose the lateral and ventral surface of the bulla and tympanic cavities. The pinna and most of the external ear canal were removed, leaving a short length (≈ 0.3 cm) of cartilaginous ear canal attached to the bony tympanic ring. Approximately two hours were required to complete these procedures. As soon as the bulla was exposed, a hole (0.06 to 0.15 cm diameter) was drilled into its ventral side to prevent static pressure build-up (Guinan and Peake, 1967) and resultant fluid accumulation in the middle-ear cavities. Petrolatum or a damp gauze pad was often placed on the ear canal to prevent the cartilage from stiffening. In addition, a moist piece of cotton was usually inserted into the ear canal to maintain the humidity of the air space near the tympanic membrane; the cotton was removed when the sound source was placed in the ear canal. In some

instances, excessive fluid accumulated on the dorsal edge of the tympanic membrane. In these cases moist cotton was not placed in the earcanal; exposure to the cooler and less humid environment of the room often reduced this fluid accumulation. A short incision (0.15 cm) was made in the posteroventral edge of the earcanal to allow the insertion of the acoustic source. The tympanic membrane, earcanal, and middle ear of the cats used in these experiments appeared "normal" (i.e., no middle-ear infection or inflammation of the earcanal was apparent).

Initial admittance measurements at the tympanic membrane, Y_d , were performed to assess the stability of the preparation. Silicone stopcock grease was used to seal the sound source to the earcanal. Repeated measurements were made with the bulla hole both open and sealed. Measurements with the hole sealed with either dental cement ("Grip", S.S. White Co.) or silicone grease and a small piece of glass indicated that the latter technique was acceptable. If measurements of each condition were repeatable, the preparation was judged "stable". If the measurements appeared "unstable" (changes greater than 0.5 to 1 dB), a permanent vent was placed in the bulla. A hole (0.10 cm diameter) was made in the medioventral edge of the bulla and the vent tube (18 cm long, 0.033 cm i.d.) was inserted and sealed with zinc cement (S.S. White Co.). A nichrome wire (0.002" diameter; 168 ohm/ft.) coil wound on the tube was used as a heater to prevent condensation in the tube. The heater resistance was 326 ohms and the current was between 50 and 60 ma. Y_d measurements before and after the insertion of the vent tube generally differed by less than 1 dB.

Holes were also drilled in the ventral surfaces of the bulla and

tympanic cavities for the MEC probe-microphones. The exact location of the bulla hole varied from experiment to experiment, but was on the posterolateral portion of the bulla within approximately 1 cm of the foramen. The bulla holes were 0.15 cm in diameter. Tympanic cavity holes were smaller in diameter (0.10 cm), and were always located on the anterolateral edge of the ventral surface of tympanic cavity between the tympanic ring and septum. It was important to make this hole as far medial as possible to avoid damage to the tympanic membrane. Both microphones were mounted on micromanipulators, and the probe tubes were inserted into the holes (≈ 0.05 cm), which were then sealed with dental cement or silicone grease. Admittance and MEC pressure measurements were used to test the quality of the seal, which was good in all cases.

Additional surgical procedures were required to manipulate the middle ear cavities. First, the bulla hole was enlarged to a diameter of approximately 0.5 cm; Y_d and P_t/P_d measurements were then made with the foramen open and plugged (FIGURE 2B). With the foramen plug in place, colored saline was injected into the bulla to measure cavity volume. The bulla was then opened as widely as possible (FIGURE 2B), the foramen plug was removed, and admittance and pressure measurements were repeated. The foramen was then replugged and saline was injected into the tympanic cavity hole to determine cavity volume. Next, the boney septum, chorda tympani nerve, styloid projection, and the ventral wall of the tympanic cavity were removed to open the tympanic cavity as widely as possible. This last condition is referred to as the "cavities open widely" condition (FIGURE 2C). During the above procedures, care was taken to completely remove the injected fluid or secretions. Surgical

manipulations were carried out using a dissecting microscope.

The Eustachian tube of these animals is thought to be closed during all measurements. We found that static pressure appeared to build up in the MEC's of most animals if the MEC's were sealed for periods of ≈ 30 minutes or more. Also, measurements in two cats in which the cavities were connected to a source of static pressure demonstrated that positive and negative static pressures were maintained.

B. STIMULUS GENERATION AND RESPONSE MEASUREMENT

The computer-controlled system used to generate stimuli and measure pressure responses has been described in CHAPTER I, Section II C. In the animal experiments described here, the number of signal processing channels was increased. Voltage outputs from the bulla and tympanic cavity pressure probes were amplified using amplifiers (Grass Instrument Co., Model P511) similar to that of the P_d channel (CHAPTER I, FIGURE 3); the three response signals, E_p (TM pressure-probe output voltage), E_b (bulla pressure-probe output voltage), and E_t (tympanic cavity probe output voltage), were multiplexed into two channels that could be simultaneously measured by the computer system. The equipment used in the second channel is identical to that of the channel used for E_p processing, with the exception of the phase meter. The performance (linearity, resolution, etc.) of the two channels is identical. "Two channel" frequency sweeps took approximately 9.3 minutes; the additional time required to sample and store data from the second channel was

responsible for the increase in sweep time (6.5 minutes, single channel). Data point density was 40 points/decade.

C. ADMITTANCE MEASUREMENTS

The procedure used to compute input admittance, Y_d , from the measurement of P_d/E_o was described in CHAPTER I. Sound pressure levels used for measurements in intact ears were approximately 90 to 100 dB SPL. P_d data presented in this report are limited to frequencies below 22.4 kHz; "source artifact" imposed this limitation (CHAPTER I). P_d data are reported only if the signal-to-noise ratio (S/N) exceeded 10 dB.

Note that the earphone and probe-tube heaters were used in the experiments described here; the static pressure vent of the source was also present. Measurements for the source specification for animal experiments were carried out at relatively high room temperatures ($30 \pm 3^\circ$ C). The effects of the heaters and ambient temperature were described in CHAPTER I, Section II. The method used to account for the coupling space (V_{ec} = earcanal volume) between the source and tympanic membrane is similar to that described in CHAPTER I, Section III; details of this procedure will be discussed in Section III A 1.

D. MIDDLE-EAR CAVITY PRESSURE MEASUREMENTS

1. Construction of the Probe Microphones

The tympanic cavity (P_t) and bulla cavity (P_b) pressure probe-microphones are identical. An electret condenser microphone (Knowles Electronics Inc., EA-1842) is used as the pressure transducer. It is coupled to a long, narrow probe tube (4 cm by 29 gauge; 0.018 cm i.d.), which gives the resulting probe-microphone a high input impedance. However, the probe tube also introduces a pressure attenuation of approximately 20 dB at low frequencies. The "windscreen" (located inside the larger probe tube attached to the microphone body by the manufacturer) was removed and the long, narrow probe tube was attached to the microphone with epoxy. A nichrome wire (0.002" diameter; 168 ohm/ft.) heater coil was wound onto the tube and covered with a thin layer of epoxy. The heater keeps the probe tube patent during "long" measurement sessions (9 hours) in the humid environment of the MECs. The coil resistances and heater currents were: P_t microphone, $R = 163$ ohms, $I = 35$ ma; and P_b microphone, $R = 139$ ohms, $I = 30$ ma.

2. Calibration Procedure

The procedure used to calibrate these probe-microphones is identical to that described in CHAPTER I, Section II D for the P_d microphone, but some of the hardware is different. The probe-microphone was inserted into a small cylindrical duct (similar to that of Nedzelnitsky, 1971) terminated by a 1/8" diameter reference microphone. A 1" diameter condenser earphone (B & K, 4144) was located at the other end of the duct and was used to generate a sinusoidal sound pressure. The calibrations

$E_t(f)/P(f)$ and $E_b(f)/P(f)$ for the probe-microphones are shown in FIGURE 3. Each frequency response was stored in the computer system and used automatically to convert measured voltages to pressures.

The analysis of CHAPTER I, Section II D, used to verify the assumption of equal pressures at the reference and probe-microphones, is also applicable here. The radius of the duct is $r = 0.15$ cm. The cut-off frequency ($f_{1,0}$) is 63.5 kHz, and the characteristic impedance, $Z_0 = 576$ dyn-s/cm⁵. The impedance of the reference microphone was previously calculated to be $Z_{rm} = (2.24 \times 10^9)/f$ dyn-s/cm⁵; thus the ratio $|Z_{rm}/Z_0| = (3.9 \times 10^6)/f$. Again, we find that for audio frequencies the pressure distribution is equal to that for a tube with a rigid termination. The distance from the tip of the probe tube to the diaphragm of the reference microphone is $y = 0.15$ cm. The magnitude ratio of the pressure at the probe-tip to that at the reference microphone is $\cos\{(2\pi yf)/c\} = 0.819$ or -1.7 dB for $f = 22.4$ kHz. The frequency, 22.4 kHz, was used in this calculation because it is the high-frequency limitation imposed upon these measurements by artifact of the source (i.e., for P_d measurements, CHAPTER I, FIGURE 10). Artifact level for the MEC probe-microphones under calibration conditions was determined by measurement of the probe output when the probe-tip was mechanically plugged. The unplugged pressure magnitude was 10 dB above the plugged signal level for all frequencies below 40 kHz. Noise floor measurements indicated that the artifact level was 10 dB above the noise floor of the probe-microphone for frequencies above 2 kHz. Therefore, the pressure ratios, P_t/P_d and P_b/P_d , are limited by the P_d artifact rather than by artifact of the MEC probe-microphones.

Measurements were made in the calibration cavity to determine the pressure change resulting from the insertion of a probe-microphone. This effect was termed "loading". The volume of the calibration cavity is 0.15 cc; the equivalent volumes of the 1" and 1/8" diameter microphones are 0.12 cc and 10^{-4} cc, respectively. Thus, the total effective volume of the calibration cavity is 0.27 cc, which is comparable to that of the smaller MEC of the cat (i.e., the tympanic cavity, $0.12 < V_t < 0.30$ cc). The equivalent volume of the calibration set-up was decreased for some measurements to 0.16 cc by using a 1/2" condenser microphone; the results reported here are for the 1" microphone. Pressure at the 1/8" reference microphone was measured for two conditions: 1) with a pressure-probe microphone present in the cavity, and 2) with it removed, and the hole in the calibration cavity rigidly plugged. These two measurements agreed within ± 0.2 dB and $\pm 2.8^\circ$ for frequencies between 33 Hz and 17 kHz. The maximum magnitude difference over the entire frequency range ($10 \text{ Hz} < f < 40 \text{ kHz}$) was observed at 17 Hz and was 0.4 dB. Thus, for measurements in the MECs these pressure-probe microphones will have negligible "loading" effects.

The precision of the calibration is probably within ± 0.8 dB and $\pm 3.2^\circ$ at low frequencies where the pressures at the probe-tip and 1/8" reference microphone are equal. At 22.4 kHz the magnitude precision may be degraded to ± 2.5 dB by the spatial variation in pressure (1.7 dB) between these microphones. Loading of the cavity impedances by the probe-microphones is insignificant for frequencies above 30 Hz. It is important to note that the MEC pressure probes were calibrated relative to the same reference microphone used for the P_d calibration. If

different reference microphones had been used, errors in the P_b/P_d , P_t/P_d ratios could arise caused by differences in the measured absolute sensitivities of the two references. Although not important in our procedure, repeatable (± 0.1 dB) absolute sensitivity readings for the 1/8" reference microphone were obtained using a pistonphone with a specially designed adapter which precisely couples the reference microphone in a repeatable manner.

3. Measurement Procedure

Measurement of the MEC pressure ratios, P_t/P_d and P_b/P_d , was performed at constant values of stimulus pressure magnitude, $|P_d|$. A frequency response measurement of P_d/E_o was first made at constant $|E_o|$. This measurement was then used to program the computer system to adjust the voltage stimulus, E_o , to provide a specified, constant $|P_d|$ at each frequency. One channel of the measurement system was used to measure P_b or P_t ; the other channel measured the actual value of P_d . Ratios of the pressure measurements, P_t/P_d or P_b/P_d , were then computed. A level of $|P_d| = 93$ dB SPL was used for the measurements reported here. P_t , P_b , or P_d data were accepted only if the S/N > 10 dB.

E. VOLUMETRIC MEASUREMENTS OF CAVITY VOLUMES

The volumes of both middle-ear cavities were volumetrically measured

in 12 animals. Colored saline was injected into each cavity using a calibrated syringe. A different color was used for the tympanic and bulla cavity measurements so that "leaks" past the foramen plug could be detected. A 0.1 cc syringe graduated at 0.001 cc increments (Hamilton Co., #1710) was used to measure the tympanic cavity volume, V_t , and also bulla volume, V_b , in cases where $V_b < 0.5$ cc. If $V_b > 0.5$ cc, a 0.5 cc syringe with graduations of 0.01 cc (Hamilton Co., #1750) was used to inject the initial 0.5 cc; the 0.1 cc syringe was then used to add the fluid required to fill the cavity. The 0.1 cc syringe was also used to measure the earcanal volume, V_{ec} , between the tympanic membrane and acoustic source.

The fluid measurement procedure was the following: All operations were observed with a dissecting microscope. Bulla volume was measured first; the hole through which fluid was injected was less than 0.5 cm in diameter. The foramen was plugged by a small amount of silicone stopcock grease, which often covered most of the round-window membrane. This type of grease was quite easily removed. The skull of the animal was oriented such that the hole was located at the "highest" point of the bulla. Colored saline (made using food coloring) was warmed to the temperature of the room ($30 \pm 3^\circ$ C) and slowly injected until a convex meniscus was formed at the fill hole. Care was taken in all fluid measurements to insure that air bubbles did not form in the fluid. A small tube with light suction was used to remove the fluid. The measurement was usually repeated several times.

Measurement of the tympanic cavity volume was more difficult. The head was reoriented so that the probe-microphone hole became the highest

point of the cavity, and fluid was injected. The injection was observed through both the fill hole and the tympanic membrane to insure that air bubbles were not present. Fluid was slowly added until its level was flush with the external surface of the hole. The foramen plug was then removed and much of the fluid flowed from the tympanic cavity into the bulla; suction was carefully applied through both the fill hole and foramen to remove the excess fluid. Usually, we replugged the foramen and repeated the measurement.

V_{ec} was measured after the acoustic source was removed. The tip of the source sound tube always left a clear indentation upon the earcanal. The skull was reoriented with the earcanal upward. Colored saline was injected until the fluid level reached the plane where the tip of the sound tube had contacted the earcanal. The fluid did not appear (under the dissecting microscope) to distort the shape of the tympanic membrane. Fluid was removed with a cotton wick. Several measurements were always made.

TABLE I summarizes the average value of V_t , V_b , and V_{ec} for each animal. The number of trials for each type measurement (N_t , N_b , N_{ec}) and the animal weight are also given. The first trial usually produced the largest result (for V_t or V_b). Variation among trials was less than 2.6 % for V_b . Intertrial variation for V_t was less than 8.6 %, except for two animals (TJL-38 and TJL-42); for these animals we have chosen the largest V_t measurement for inclusion in TABLE I. Intertrial variation for V_{ec} measurements was generally less than 6%; the largest variations observed (for TJL-43, having the smallest V_{ec} among these cats) were less than 20%. Average middle-ear cavity volumes, \bar{V}_t and

\bar{V}_b , were computed from volumetric measurements in 12 ears (TABLE I). Results are $\bar{V}_t = 0.217$ cc and $\bar{V}_b = 0.675$ cc, with standard deviations of 0.056 cc and 0.141 cc, respectively. The volumes ranged between $0.120 \text{ cc} < V_t < 0.298 \text{ cc}$ and $0.401 \text{ cc} < V_b < 0.900 \text{ cc}$.

III. RESULTS

A. ADMITTANCE MEASUREMENTS

1. Correction for the Source-Tympanic Membrane Coupling Space

To account for the coupling space between the acoustic source and tympanic membrane, we represented the space by a circularly symmetric, lossless tube (i.e., transmission line, CHAPTER I, Equation 14). Thus, all admittance measurements at the tympanic membrane presented in this report have been "corrected" using the following procedure. {Two exceptions are the direct acoustic measurement of this coupling space (FIGURE 5) and the direct measurement of bullae admittance (FIGURE 12).} The volume of the coupling space, V_{ec} , was volumetrically determined in every animal (except TJL-42; FIGURE 22). Cross-sectional area of the tube was assumed equal to that of the source, $A = 0.119 \text{ cm}^2$. The portion of V_{ec} resulting from the P_d probe-tube extension (length = 0.15 cm, $A = 0.119 \text{ cm}^2$, volume = 0.018 cc) was subtracted, and the resulting volume, $V'_{ec} = V_{ec} - 0.018$, was divided by A to obtain the transmission line length, $l' = (V'_{ec})/A$. Values of l' ranged from 0.12 cm to 0.48 cm (TABLE I). The uncorrected "load" admittance measurement, Y_L , and the parameters A and l' were used in Equation (14) of CHAPTER I to calculate the "corrected" admittance estimate, Y'_L . The prime notation will be used only in this section to distinguish "corrected" and "uncorrected" admittance measurements.

The effects of this procedure are illustrated in FIGURE 4. The uncorrected measurement chosen is the admittance at the tympanic membrane with the MEC's open, Y_{doc} . Y_{doc} is compliance dominated at low frequencies (C_{doc} = acoustic compliance), having magnitude slope of 6 dB/octave and angle of -90° . It is clear from CHAPTER I, Equation (14) that at low frequencies, the transmission line correction reduces to the subtraction of an admittance, $j\omega C_{\text{ec}}$ ($C_{\text{ec}} = V'_{\text{ec}}/\rho c^2$), from the measured admittance, Y_L . The Y'_{doc} result shows a 0.7 dB decrease in acoustic compliance relative to C_{doc} (i.e., $C'_{\text{doc}} = C_{\text{doc}} - C_{\text{ec}}$, and $20\log_{10}\{C'_{\text{doc}}/C_{\text{doc}}\} = -0.7$ dB). Variation of $\pm 10\%$ in the value of V'_{ec} results in ± 0.1 dB variation in C'_{doc} . The magnitude of the correction and its sensitivity to imprecision in the value of V'_{ec} are dependent upon the value of C_{doc} relative to C_{ec} . For example, the compliance change for data with somewhat smaller compliances (such as the results from the plugged foramen condition, FIGURE 7) is 2.6 dB. A $\pm 10\%$ variation in V'_{ec} for this situation results in ± 0.3 dB change in "corrected" value of compliance.

Effects of the TL correction are larger for frequencies above 6 kHz, especially for the angle. This is mainly caused by the fact that $|j\omega C_{\text{ec}}|$ is comparable to $|Y_{\text{doc}}|$ at these frequencies (FIGURE 4); note, however, that their angles differ by approximately 45° . The resulting Y'_{doc} appears to be consistent with the notion that at most high frequencies, the effect of the TL correction is still the subtraction of $j\omega C_{\text{ec}}$. We found that $\pm 20\%$ variation in the line parameters A or l' , with the volume $V'_{\text{ec}} = l'A$ constant, had small effect upon the Y'_{doc} result (maximum changes of 1.8 dB and 12.6° at any frequency). Thus, it is

important to precisely know the volume of the earcanal coupling space; the TL parameters of A and l' are relatively unimportant because our coupling space is quite small relative to a wavelength even at 20 kHz.

In Section II E we concluded that most volumetric measurements of V_{ec} were precise to within 6%, with the largest intertrial variation being 20%. We have acoustically measured the admittance of the earcanal coupling space by filling the open middle-ear cavities with saline and measuring the input admittance at the tympanic membrane (FIGURE 5). The result appears compliance dominated for $f < 100$ Hz and $f > 1$ kHz. At low frequencies this measurement is approximately equal to Y_{doc} ; for frequencies $100 < f < 1$ kHz there is a resonance, probably caused by the mass loading by the fluid upon the tympanic membrane. For $f > 250$ Hz, the admittance of the ear with fluid becomes mass dominated and decreases. At frequencies between 850 Hz and 15 kHz the measured admittance is within 2 dB of the volumetrically determined admittance ($j\omega V'_{ec}/\rho c^2$) of the earcanal space. Thus, the volumetric determination of the admittance of coupling space is accurate with $\pm 20\%$. The effect upon Y'_{doc} of a $\pm 20\%$ variation in volume is shown in FIGURE 6. The volume variation was produced through changes in the value of A , keeping $l' = 0.38$ cm. The magnitude and angle changes are less than 4 dB and 22° at any frequency. Volume variations ($\pm 20\%$) with $A = 0.119$ cm² and l' variable produced slightly smaller effects.

In summary, we have assumed that we may characterize the coupling space as a rigid cylindrical tube (a lossless transmission line) to correct for the effects of this space. Since the volume of the coupling space was small, the sensitivity of our results to the detailed values of

the TL model parameters (A and l') was not great. For most purposes it is necessary to know only the coupling volume precisely.

We have not attempted to account for the irregular geometry of the coupling space. The tympanic membrane is not planar nor is it perpendicular to the longitudinal axis of the ear canal; rather, it obliquely terminates the canal. Additionally, the non-uniform motion of the cat tympanic membrane (Khanna, 1970; Tonndorf and Khanna, 1970; Khanna and Tonndorf, 1972) quite possibly excites higher-order modes in the sound field near the tympanic membrane. The propagation of these modes in the earcanal is discussed in Section IV. Our acoustic measurement of the admittance of the coupling space (FIGURE 5) clearly indicates that losses in this earcanal space are relatively small up to 20 kHz. In most of our preparations the earcanal became dry and firm after exposure to the environment.

2. Stability

Initial Y_d measurements were made to assess the stability of the preparation and of the acoustic source when placed in the ear. Several measurements were first made with the bulla hole open. If these measurements were repeatable, measurements with the hole sealed and hole open were alternately made. Typical results for both conditions are shown in FIGURE 7. At low frequencies the admittance, Y , is compliance dominated with the admittance magnitude depending on the modification of the cavities. Above 3 kHz the curves are similar. Changes in these two

frequency regions were used as an indication of instability. The bulla was usually opened, to relieve possible static pressure, after each hole-sealed measurement. In some instances successive measurements were made without venting to determine the length of time required for noticeable changes to occur. Small differences (usually less than 1 dB) in the measurements of the hole-sealed condition were sometimes apparent at low frequencies; if this occurred, the static pressure vent-tube was sealed into the bulla, and the measurements were repeated. The initial Y_d measurements were quite repeatable in animals for which results are reported here. In general, the stability of the preparation was excellent throughout the measurement session. Characteristics of source instability when placed in the ear were previously described in CHAPTER I. Quite often these changes limited the duration of the measurement session to 6 - 14 hours. Source stability was determined by measuring P_r/E_o for one of the reference cavity loads and comparing the result to the original measurement used for source specification. For many of the results reported here, the source was demonstrably stable. However, in some other cases, small changes in P_r/E_o (less than 3 dB) were observed. We have chosen to include admittance measurements from these sessions, because it is likely that the changes occurred at the end of the session and were possibly caused by contamination of the source during its removal from the earcanal.

3. Y_d : Manipulations of the Middle-Ear Cavities

The input admittance at the tympanic membrane, Y_d , was measured for the "normal" (intact MEC's, Y_{di}) and three "experimentally modified" states of the MECs (Y_{dob} , Y_{dpf} , Y_{doc} , FIGURE 2). Typical results are shown in FIGURE 8. For frequencies below 1 kHz, all four admittances are compliance-like, i.e., the magnitude slope is 6 dB/octave and the angle is near 90° . The compliances of Y_{doc} and Y_{dob} are essentially identical. The compliance of the intact ear is slightly less ($\cong 3$ dB), while that of the plugged foramen condition is roughly 9 dB smaller. These low-frequency effects may be explained by the addition of a series impedance, $Z_{mec} \cong 1/j\omega(C_b + C_t)$, or $Z_{mecx} \cong 1/j\omega C_t$ to $Z_{doc} \cong 1/j\omega C_{doc}$ for the condition of intact MEC's or plugged foramen, respectively.

Near 4.5 kHz the admittance magnitude of Y_{di} sharply decreases by 18 to 20 dB and the angle increases from -60° to $+60^\circ$. This results from the parallel resonance of the MEC compliances with the acoustic mass of the foramen. With the bulla open (Y_{dob} , FIGURE 8) the frequency of this resonance is lowered to 3.1 kHz (0.5 x 0.4 cm hole). Opening the bulla as widely as possible¹ had the effect of placing a resonance near 3.6 kHz. These effects and those of the smaller bulla holes (FIGURES 7 and 11) can be qualitatively explained by placing an acoustic mass (M_h , of the hole) in parallel with C_t in the model of FIGURE 1D. Thus, increasing the hole from 0.5 x 0.4 cm to "widely open" reduces the acoustic mass of the "hole" (roughly $\rho l/A$, where l = hole length, A = hole area), which is effectively in series with M_f , therefore raising the resonant frequency.

For frequencies above 6 kHz, Y_{di} , Y_{dob} , and Y_{dpf} have similar magnitudes and angles. Their magnitudes are roughly constant at 1/450 mho or 2.2 mmho, while the angles decrease from $+20^\circ$ through 0° to -40° as frequency increases. Y_{doc} , on the other hand, has smaller admittance magnitude and angle in this frequency region. The $|Y_{doc}|$ slope is roughly -3 dB/octave ($1 \text{ kHz} < f < 10 \text{ kHz}$); the angle passes through 0° near 2.5 kHz and decreases to -40° at higher frequencies.

A complete series of the four admittance measurements (Y_{dx}) was performed in five other cats. Measurements in two of the five animals were performed with the acoustic source in a configuration different from that described in CHAPTER I; imprecision in the source specification for this configuration imposed a frequency limitation of $10 \text{ Hz} < f < 3 \text{ kHz}$ for admittance measurements. MEC pressure measurements were also made in one of these two animals. Results from these five other animals are consistent with the qualitative aspect of the description given above. Admittance results from TJJ-53 were chosen for presentation because both MEC pressure and Y_{dx} admittance measurements were obtained over a larger bandwidth ($10 \text{ Hz} < f < 22.4 \text{ kHz}$) in this animal.

4. Y_d and Y_{doc} : Measurement Summary Across Cats

Measurements of Y_d , the admittance of the intact ear at the tympanic membrane, are summarized in FIGURE 9. Typical curves from six ears (five cats) are shown. It is clear that all curves are compliance dominated at low frequencies ($f < 700 \text{ Hz}$). The acoustic compliances² range in value

from 1.63×10^{-7} to $3.29 \times 10^{-7} \text{ cm}^5/\text{dyn}$, having a range of 6.1 dB. The average³ value of compliance is $2.36 \times 10^{-7} \text{ cm}^5/\text{dyn}$. In the vicinity of 2 kHz the admittance becomes resistive with nearly constant average magnitude $\cong 1/630 \text{ mho} = 1.6 \text{ mmho}$ and angle approximately equal to 0° . Between 4.0 kHz and 4.5 kHz there is a relative minimum in the admittance magnitude and the angle changes sign; this resonance is caused by a parallel resonance of the middle-ear cavities and foramen. The $Q_3 = (\text{center frequency})/(-3 \text{ dB bandwidth})$ of these resonances vary from animal to animal (11.0, 11.4, 13.4, 14.9, 15.2, 18.3) with the average being $Q_3 \cong 14.0$. For frequencies between 6 kHz and 15 kHz the admittance appears to be approximately resistive with average magnitude of $1/630 \text{ mho} = 1.6 \text{ mmho}$ and angle averaging near -18° . For frequencies between 15 kHz and 22.4 kHz, the average admittance magnitude increases by 6 dB and the average angle increases to $+18^\circ$.

The input admittance with the cavities widely opened, Y_{doc} , is summarized for 5 cats in FIGURE 10. Y_{doc} is also compliance dominated at low frequencies with $2.68 \times 10^{-7} < C_{\text{doc}} < 6.35 \times 10^{-7} \text{ cm}^5/\text{dyn}$, a range of 7.5 dB. The average value of compliance is $4.2 \times 10^{-7} \text{ cm}^5/\text{dyn}$. In the frequency range between 900 Hz and 4 kHz the admittance is approximately resistive with nearly constant average magnitude (1/475 mhos, 2.1 mmho) and an angle near 0° . Note, however, that the admittance magnitudes have a small negative slope (-3 dB/octave) in the frequency region 1.5 kHz to 12 kHz. Three of the curves have a small relative minimum in $|Y_{\text{doc}}|$ near 12 kHz. Also, between 4 kHz and 11 kHz the average angle is about -20° . The trends are less clear at the highest frequencies (11 kHz to 22.4 kHz): two of the curves steadily increase in magnitude; the other

three have a relative maximum between 16 kHz to 18 kHz.

FIGURE 11 summarizes measurements of admittance at the tympanic membrane for the condition of an open bulla hole in six ears. The low frequency compliance of these measurements ranges from 2.90×10^{-7} to $6.20 \times 10^{-7} \text{ cm}^5/\text{dyn}$ (range of 6.6 dB), and has an average value of $4.5 \times 10^{-7} \text{ cm}^5/\text{dyn}$. The resonance at 1.3 kHz to 1.6 kHz is introduced by the acoustic mass of the bulla hole resonating with the bulla compliance. For frequencies above 2.5 kHz these data are very similar to the Y_d curves of FIGURE 9. We have included these measurements because they provide another estimate of C_{doc} at low frequencies, since the open bulla hole "shorts" the impedance of the MEC's. Note that these measurements were made prior to MEC manipulations, whereas the Y_{doc} curves were taken (many hours later) after the bulla, foramen, and tympanic cavity manipulations. Differences in MMSE acoustic compliance estimates for these two conditions were 0.2, 0.3, 0.7, 0.8, 1.9 dB for the corresponding pairs of curves from FIGURES 10 and 11. Some atypical compliance shifts were observed during the measurement session in which the difference is largest (TJL-53).

The differences among individual admittance curves for each of the above conditions (FIGURES 9, 10, and 11) mainly result from inter-animal variation. The precision of any individual admittance measurement is within the limits established in CHAPTER I for "test loads" (i.e., rms errors less than 1 dB and 7° , over 10 Hz to 22.4 kHz). For $f > 10$ kHz, precision at a given frequency may not be 1 dB, but is probably within the limits observed for high-frequency measurements in test loads ($\cong 3$ dB).

5. Bulla Admittance: Y_b

In one animal we plugged the foramen, sealed the acoustic source into the bulla cavity, and measured bulla admittance, Y_b . The source was placed on the posterolateral portion of the ventral surface of the bulla. The tip of the source sound-tube (CHAPTER I, FIGURE 2A) was sealed with silicone grease to the external boney surface surrounding an enlarged hole ($\cong 0.4$ cm diameter). Thus, the probe tube extended into the bulla about 0.1 cm. After the source was removed, the bulla volume was volumetrically determined to be $V_b = 0.708$ cc. An admittance prediction from the volumetric measurement was calculated as $j\omega V_b / \rho c^2$. FIGURE 12 indicates that the measured and predicted admittances are in excellent agreement. The rms differences between these results are 0.5 dB and 8.6° for the bandwidth, 10 Hz to 3 kHz.

At frequencies above 3 kHz the measured admittance shows resonances that are similar to those observed in test cavities (CHAPTER I, Section III), but the resonant frequencies are inharmonically related. The specific frequencies of resonance are probably a function of the position of the point of measurement (by the acoustic source) relative to the bulla. In particular, for $f > 3$ kHz this measurement probably does not accurately represent the driving point admittance of the bulla at the foramen.

6. Tympanic Membrane Holes and Z_{mec}

We have measured Y_d in several animals in which holes were present in the tympanic membrane. We have not systematically studied the effects of such holes, but we report some observations.

In one case Y_d was measured with the foramen open and the bulla widely open. The tympanic membrane hole was relatively "small" (diameter $\cong 0.07$ cm) and was located ventral to the manubrium of the malleus. The input admittance appeared resistive (1/500 mhos, 2 mmho) for $30 \text{ Hz} < f < 200 \text{ Hz}$; at higher frequencies ($200 \text{ Hz} < f < 1.5 \text{ kHz}$) the magnitude was similar, but the angle approached -90° . With the bulla and foramen open, this result implies that the admittance of the TM hole is mainly resistive at frequencies below 200 Hz and hints that it may have a mass component at higher frequencies. The hole was plugged with a small amount of silicone grease and the input admittance was measured. The admittance appeared compliant for $10 < f < 1 \text{ kHz}$ and had an admittance magnitude that was 3 dB larger than that measured before the hole was made. Thus, the "small" hole had resistive behavior at low frequencies and when plugged, the low frequency compliance nearly returned to its pre-hole value.

In another case a relatively "large" (diameter $\cong 0.2$ cm) tympanic membrane hole was located in the center of the TM near the tip of the manubrium. Both cavities were "shorted" at low frequencies by the presence of several holes. The input admittance for this condition was primarily that of an acoustic mass of approximate value 0.018 g/cm^4 for $100 \text{ Hz} < f < 2 \text{ kHz}$; below 400 Hz a resistive component of the admittance was also evident. Thus, the "large" hole (plus the mass effects of the

bullae and tympanic cavity holes) combined to give a mass dominated input admittance. Measurements with the MECs closed imply that the mass contribution of the hole is less than 20% of the above total mass ($\approx 0.004 \text{ g/cm}^4$).

Admittance measurements were also made in one other animal (FIGURE 13) with a TM hole present and the MECs sealed. The hole was located in the anteroventral edge of the TM near the tympanic ring and was approximately intermediate in size relative to the two holes previously described. Note that the normal Y_d and the hole-present measurement are nearly identical in the region of resonance near 4.2 kHz (FIGURE 13). For frequencies below 5 kHz the hole-present admittance is similar in many respects to an estimate of middle-ear cavity admittance, Y_{mec} , presented in Section IV, FIGURE 24. This implies that the admittance of the hole is somewhat larger than Y_{mec} at most frequencies. The largest differences occur 1) in the frequency region of the admittance maximum near 1 kHz (FIGURE 13; corresponding to the impedance minimum near 2 kHz of FIGURE 24) and 2) at frequencies above the MEC resonance (i.e., $f > 5 \text{ kHz}$). We have a hypothesis which may explain these effects. The low Q of the resonance near 1 kHz (FIGURE 13) relative to the Z_{mec} measurement of FIGURE 24 probably results from the resistance and mass of the TM hole in series with the impedance of the MECs alone, Z_{mec} . At higher frequencies ($f > 5 \text{ kHz}$) the impedance of the hole (which is in parallel with the impedance of box 2, FIGURE 1A) may become high relative to Z_{doc} (FIGURE 1A), and the hole-present measurement may "approach"⁴ the normal Y_d , which is controlled by Y_{doc} at these frequencies.

B. MIDDLE-EAR CAVITY PRESSURE MEASUREMENTS

A complete series of P_b/P_d and P_t/P_d measurements for the "normal" and "experimentally" modified states of FIGURE 2 was made in three animals. Measurements of P_b/P_d were made in 5 other ears. The results shown in Sections 1 and 2 below, for cat TJL-53, are representative of all the results. Inter-animal variations and differences resulting from the location of the bulla probe-microphone are discussed.

1. Intact Middle-Ear Cavities

Measurements of P_t/P_d and P_b/P_d for the condition of intact MECs are shown in FIGURE 14. The tip of the bulla probe-microphone was located approximately 0.5 cm from the foramen. The two pressure ratios have identical magnitude and angle for frequencies below 500 Hz. The magnitudes are constant with value near -10 dB; the angles are approximately 0° . This response is consistent with the model of FIGURE 1D. At low frequencies, $Z_{mec} \cong 1/j\omega(C_t + C_b)$ and $Z_{doc} = 1/j\omega C_{doc}$. The model predicts that

$$P_t/P_d = Z_{mec}/(Z_{mec} + Z_{doc}) = C_{doc}/(C_{doc} + C_t + C_b) \quad (5)$$

$$\text{and } P_b/P_d = (P_b/P_t)(P_t/P_d) = (Z_b/(Z_b + Z_f))(P_t/P_d) . \quad (6)$$

Since $|Z_f| \ll |Z_b|$ at low frequencies, $P_b/P_d \cong P_t/P_d$.

$|P_b/P_d|$ remains nearly constant to 4 kHz; however, a large (180°) phase lag occurs. Near 8 kHz there is a minimum in $|P_b/P_d|$ as the

magnitude decreases $\cong 37$ dB and the angle passes through 0° . Note that for the pronounced resonance at 11.3 kHz, $|P_b/P_d|$ and $|P_t/P_d|$ are approximately equal with value -5 dB. At frequencies just below this resonance ($\cong 10.5$ kHz), the angles are also equal; however, the angle of P_b/P_d increases approximately 180° as frequency increases past resonance. Another minimum in $|P_b/P_d|$ occurs near 15 kHz; the magnitude again increases for frequencies above 15 kHz as the magnitude and angle of both pressure ratios become nearly equal in the vicinity of 20 kHz. The model of FIGURE 1D does not predict these large variations in P_b/P_d for frequencies above 7 - 8 kHz.

For P_t/P_d a clear resonance occurs at 2100 Hz; there is a sharp magnitude decrease of approximately 20 dB, and the angle changes by 180° . The series resonance of C_b and M_f (FIGURE 1D) is responsible for this behavior. The parallel resonance of Z_{mec} causes $|P_t/P_d|$ to exceed 0 dB between 4 - 6 kHz and the angle becomes 0° at 4.5 kHz. $|P_t/P_d|$ decreases at higher frequencies until becoming equal to $|P_b/P_d|$ at 11.3 kHz where it has a small, sharp magnitude peak ($\cong 7$ dB increase). P_t/P_d has a broader magnitude peak near 16.5 kHz. Near 20 kHz there is a sharp magnitude decrease of 10 dB.

2. Manipulations of the Middle-Ear Cavities

Measurements of P_t/P_d for intact MECs, widely opened bulla, and plugged foramen are shown in FIGURE 15. At low frequencies, opening the bulla produces a large pressure loss ($\cong 46$ dB at 119 Hz) and $|P_t/P_d|$ has

a slope of 12 dB/octave and angle of 180° . This result is also compatible with the model of FIGURE 1D: Opening the bulla results in $Z_b \cong 0$; $Z_f \cong j\omega M_f$ is much smaller than $Z_t = 1/j\omega C_t$ at low frequencies and, therefore, $Z_{mec} \cong Z_f$. Substitution into Equation (5) results in $P_t/P_d \cong \omega^2 M_f C_{doc} / (\omega^2 M_f C_{doc} - 1)$, which is approximately $-\omega^2 M_f C_{doc}$ at low frequencies. At higher frequencies the magnitude of the pressure ratio exceeds 0 dB at 3.4 kHz and 6 kHz, where two relative maxima in the ratio occur; the angle passes through 0° near 3.8 kHz.

P_t/P_d for the condition of plugged foramen is similar to the intact MECs result in that at low frequencies ($f < 3$ kHz) the magnitude is constant ($\cong -4.6$ dB) and the angle is 0° . Since $Z_{mec} \cong 1/j\omega C_t$ for this condition, this result is also consistent with the model prediction $P_t/P_d \cong C_{doc} / (C_{doc} + C_t)$.

For frequencies above 6.5 kHz, the three P_t/P_d ratios are generally similar in magnitude and angle, with the following exceptions: The resonant peak at 11.3 kHz observed in the intact pressure ratios (for $|P_t/P_d|$ and $|P_b/P_d|$) is not present in either the open bulla or plugged foramen measurement. This observation suggests that this peak in tympanic cavity pressure is a result of the presence of the intact bulla cavity (FIGURE 14). At 16.5 kHz there are small magnitude peaks (5 - 8 dB) in both the intact and plugged foramen measurements; a larger peak (10 - 12 dB) in the open bulla measurement occurs at a slightly higher frequency (18.5 kHz). In addition, the 10 dB magnitude decrease observed at 20 kHz for the intact measurement was not observed in either the open bulla or plugged formamen measurements.

The gradual magnitude decrease ($\cong -6$ dB/octave) observed in all

three pressure ratios for frequencies above 6.5 kHz is generally consistent with the model of FIGURE 1D. The measurements of FIGURE 10 show Z_{doc} to be approximately resistive (R_{doc}) for $6.5 < f < 12$ kHz, with more complex behavior at higher frequencies. If $Z_{mec} \cong 1/j\omega C_t$ at these frequencies, then $P_t/P_d \cong 1/(1 + j\omega C_t R_{doc})$; when $\omega C_t R_{doc} \cong (0.9 \times 10^{-3})f \gg 1$, the pressure ratio will decline at -6 dB/octave.

3. P_b/P_d : Effect of Bulla Pressure Probe Location

P_b/P_d transfer ratios were measured in eight ears (six animals). In three of these ears, measurements were made using one bulla hole (location) and varying the depth of insertion of the probe-microphone tip; at least two different depths were examined in these cases. FIGURE 16 illustrates P_b/P_d for three depths with a bulla hole on the posterolateral portion of the ventral surface of the bulla. Three effects are evident as the probe tip location is changed from near the cavity wall to the vicinity of the foramen: 1) the low-frequency ($f < 1$ kHz) value of $|P_b/P_d|$ increases approximately 0.5 to 2 dB; 2) the frequencies of the pressure minima are lowered (first minima: 7.6 kHz to 6.8 kHz to 5.7 kHz; second minima: 14.9 kHz to 14.1 kHz to 13.3 kHz); and 3) the frequencies of the pressure "maxima" (11.2 kHz and 18.8 kHz) remain essentially constant.

In another ear simultaneous pressure measurements were made at two somewhat different locations (one location was near the foramen with the

probe tip inserted 0.1 to 0.15 cm; the other was near the cavity wall at a more medial and ventral location). For low frequencies the ratio of $|P_b/P_d|$ measurements, $|P_{b1}/P_{b2}|$, was less than 0.5 dB in this case. At higher frequencies the alternating minima and maxima were observed for the measurement near the foramen; however, the maximum in the 12 kHz region was not present in the measurement near the cavity wall. This is the only case for which deviations from the above behavior were observed; all other results in which probe location was varied are consistent with FIGURE 16.

The change observed at low frequencies in $|P_b/P_d|$ for the other two animals for which pressure measurements vs depth were made was less than 0.5 dB. Thus, the differences at low frequencies in FIGURE 16 are larger than those observed in the other three cases (≈ 0.5 dB). These increases in $|P_b/P_d|$ at low frequencies for deeper probe insertions are consistent, qualitatively, with the notion that the probe tube volume displaces bulla cavity volume as the probe tube is inserted. However, quantitatively, analysis of this situation predicts that the change in $|P_b/P_d|$ for the maximum probe insertion (0.49 cm) is approximately 0.1 dB, which is much smaller than the 0.5 to 2 dB observed in the measurements. Thus, the source of this magnitude increase is not clear.

The behavior of P_b/P_d for frequencies above 8 kHz (effects 2 and 3 above) indicates that the wave properties of sound propagation in the bulla are important; large spatial variations in the pressure field exist, since P_b/P_d was found to be a strong function of probe location at these frequencies. The largest "dimension" of the bulla cavity is approximately 2 cm (\approx quarter wavelength at 4.3 kHz). Thus, we expect

significant spatial variations in bulla cavity pressure near or above 4 kHz. We have not attempted to systematically map the pressure distribution of the bulla. However, it is clear that the "desired" P_b measurement for the purpose of determining the driving point impedances of the cavities (see Introduction) is the pressure measured at the bullar edge of the foramen.

We have not investigated spatial variations in tympanic cavity pressure, P_t . The largest tympanic cavity dimension is approximately 0.7 cm (\cong quarter wavelength at 12.3 kHz). Thus, it is likely that significant spatial variations in tympanic cavity pressure also occur at frequencies near or above 12 kHz. Kruger and Tonndorf (1977) found spatial variations in $|P_t|$ to be less than 1 dB for frequencies below 4 kHz. At high frequencies it is not clear that one can define a location corresponding to the P_t "node" in the network of FIGURE 1B & C. The "node" should theoretically be at the "entrance" to the tympanic cavity, which is in fact, the medial side of the tympanic membrane. The TM is clearly not localized spatially to a point; furthermore, its complex vibration pattern (Khanna and Tonndorf, 1972) is likely to generate higher-order modes in the near-field. Thus, validity of computations of cavity impedances, \hat{Z}_{mecx} (Equation 4), may be limited to frequencies below 12 kHz because of the likelihood of spatial variations in the sound pressure in the tympanic cavity.

4. Measurements with a Tympanic Membrane Hole

In one cat, measurements of P_t/P_d and P_b/P_d were made with a relatively "large" hole in the tympanic membrane. For $f < 400$ Hz, $|P_t/P_d| = |P_b/P_d| = 1$ (0 dB) and the angles of both pressure ratios were 0° . Since $|P_t/P_d| = 1$, the TM hole provided a relatively low impedance (short circuit) which is in parallel with Z_{doc} . For $f > 400$ Hz the frequency dependence of each pressure ratio is somewhat different from the corresponding pressure ratio for the intact TM condition. However, the ratio P_b/P_t is virtually identical to the ratio obtained with the TM intact (FIGURE 23); this result is consistent with the model prediction of FIGURE 1C (see Section I) that $P_b/P_t = Z_b/(Z_b + Z_f)$ independent of Z_{doc} and the state of the TM. Y_d measurements were also made in this animal over a limited bandwidth; a more detailed description of the effects of this TM hole may be possible through analysis of both pressure and admittance measurements.

IV. DISCUSSION

A. INTERPRETATION OF MEASUREMENTS AS ACOUSTIC ADMITTANCE

According to Beranek (1954), "acoustic impedance at a given surface is defined as the complex ratio of effective sound pressure averaged over the surface to effective volume velocity through it." The interpretation of our results as acoustic impedance assumes that P_d measurements made at a point near the center of the earcanal represent the average sound pressure over the earcanal cross-section. This assumption appears to be justified for the "test loads" described in CHAPTER I, since good agreement was found between measurement and theory in these cases for $f < 22.4$ kHz. However, because these loads were cylindrically symmetric, non-uniform (higher-order) modes should not be excited. In contrast, motion of the cat tympanic membrane is known to be non-uniform for frequencies between 385 Hz and 6 kHz (Khanna and Tonndorf, 1972). For $f < 2$ kHz there are peak displacement regions both anterior and posterior to the malleus. At frequencies above 4 kHz the displacement pattern becomes complex with many sections of the TM vibrating with local displacement maxima. Therefore, it is likely that higher-order modes exist in the sound field near the TM at frequencies above 4 kHz.

The importance of higher-order modes in our pressure measurement depends upon the degree to which they are propagated from the TM to the point of measurement. If one models the earcanal coupling space by a cylindrical, rigid-walled tube of diameter $d \cong 0.5$ cm, the cutoff

frequencies are $f_{1,0} = (1.84c)/\pi d = 40$ kHz for the first asymmetric mode, and $f_{0,1} = (3.83c)/\pi d = 84$ kHz for the first circularly symmetric mode. Therefore, for our measurement frequency range ($f < 22.4$ kHz), these higher order modes are below cutoff, i.e., they are evanescent. We calculate the space constant, S , for the $f_{1,0}$ mode to be

$$S = ((d/2)/1.84)\{1 - (f/f_{1,0})^2\}^{-0.5},$$

which results in $S = 0.14$ cm for $f \ll f_{1,0}$. The pressure of this mode is attenuated by the factor, $e^{-x/S}$, where x is distance from the TM. Space constants for higher-order modes are smaller than that of the $f_{1,0}$ mode. We have used values of $x = l'$ between 0.12 cm and 0.48 cm (TABLE I; mean value = 0.38 cm) to characterize the distance between the P_d probe-microphone tip and the TM. Thus, in theory, the higher-order modes are appreciably attenuated between the TM and probe-microphone. At present, it is not possible to come to a quantitative conclusion concerning the effects of these higher modes because their relative amplitudes are not known. However, the observation by Kruger and Tonndorf (1977) that differences in measurements of $|P_t|$ "were generally less than 1 dB" for $200 < f < 4$ kHz, as the probe position was varied throughout the tympanic cavity suggests that these issues are not important for $f < 4$ kHz. Also, the TM vibration patterns reported by Khanna and Tonndorf (1972) indicate that higher modes become more prominent for frequencies above 4 kHz. The good agreement obtained between our Y_d and P_t/P_d measurements in Section IV C strongly suggests that the effects of these higher modes are not particularly significant in our results for $f > 4$ kHz.

In conclusion, the placement of our acoustic system a few mm from the TM may help to reduce the problems associated with higher-order modes. Our results may clearly be interpreted as acoustic impedance for $f < 4$ kHz. It is likely that this interpretation is valid for frequencies well above 4 kHz; measurements of the spatial distribution of the pressure in the earcanal coupling space are needed to resolve this issue. We will report the computed admittances for frequencies to 22.4 kHz.

B. COMPARISONS TO PREVIOUS MEASUREMENTS

1. Impedance Measurements

Previous measurements of input impedance at the cat tympanic membrane have been reported by Møller (1963, 1965), Tonndorf and Khanna (1967), Khanna and Tonndorf (1972), and Margolis et al., (1978). Results from these studies are compared with our measurements below.

The most comprehensive measurements are those of Møller (1963, 1965). Although Møller's system for impedance measurement is similar in principle to ours, it was calibrated over a much smaller bandwidth. Also, his plane of impedance measurement was 1.8 cm from the TM compared to $l' = 0.12$ to 0.48 cm in our measurements. Møller accounted for the effects of this coupling space by assuming that it could be represented by a lossless uniform transmission line. However, as Møller pointed out, the long length used in his measurements makes it "important to

determine the plane of the eardrum with great precision" (Møller, 1965, p. 131). Because of the large coupling space his results are very sensitive to small percentage changes in the length in the frequency region near 7 kHz. In contrast, we have demonstrated (Section III A) that our results are not very sensitive to TL length, even at very high frequencies (to 22.4 kHz). Therefore, our improved ability to make high-frequency measurements results mainly from 1) significantly smaller coupling space and 2) precise source specification over a broader bandwidth. Z_d and Z_{doc} results from the two studies are compared in FIGURES 17 and 18, respectively, and are discussed below.

The agreement for the Z_d measurements is quite close. FIGURE 17 compares two⁴ curves from Møller (1965) with a "typical" curve from FIGURE 9. Results from both studies show compliance-like behavior at low frequencies, with similar $|Z_d|$ and angles near -90° . The angle measurements of the two studies are in general agreement. In the frequency region 1.5 to 3 kHz, Møller's curves have $|Z_d|$'s that are somewhat more constant than our "typical" curve. Some of our results (FIGURE 9) do have this character. We observed variations in the frequency of the MEC resonance of 4.0 to 4.5 kHz; Møller's results have resonances at 3.4 kHz and 4.2 kHz. In general, our resonances are somewhat sharper and have larger $|Z_d|$ increases than those of Møller. Note that at frequencies above resonance, Møller's magnitude decreases slightly, whereas ours is approximately constant.

Møller's (1963, 1965) Z_{doc} measurements (five curves) are compared to our average result in FIGURE 18. The "Lynch average" was computed using the five curves of FIGURE 10. For $f < 3$ kHz, the results from the

two studies are quite similar. At low frequencies the curves are compliance dominated. In the range 700 Hz to 4 kHz all curves exhibit a broad magnitude minimum and the angle passes through 0° . Note that Møller's angles are significantly larger than our average in this frequency region (by as much as 60°). For $f > 4$ kHz the differences between the angle results decrease, but the magnitude differences increase and differ by as much as 10 dB from our average at 7 kHz.

We noted above that Møller's $|Z_d|$ and $|Z_{doc}|$ results decrease as frequency is increased above 3-4 kHz. Also, the differences between his results and ours are largest at these frequencies. Our measurements are quite precise in this frequency region; imprecision in Møller's correction for his large coupling space is probably the source of these differences.

Møller (1963, 1965) also reports two curves of input impedance with the bulla and foramen open (Z_{dob}). These results are similar to that of FIGURE 8. In one case, opening the bulla shifted the MECs resonance from 4.5 kHz to 3.8 kHz which is consistent with our results. However, the Q and impedance magnitude at the resonant peak were substantially reduced, effects that we have not observed.

Margolis et al. (1978) were primarily concerned with changes in Z_d with static pressure changes (tympnograms), and used a commercially available impedance device (Grason Stadler 1720B) to perform the measurements at two frequencies (220 and 660 Hz). Their results for intact MECs are in good agreement with our measurements. They also reported an average change of less than 0.5 dB in $|Z_d|$ resulting from the drilling and sealing of holes in the tympanic cavity. This result is

also consistent with our measurements.

Tonndorf and Khanna (1967) inferred acoustic input-impedance magnitude, in one cat, from displacement measurements of the manubrium of the malleus for constant $|P_d|$ stimuli. Volume velocity was calculated assuming that "all points of the tympanic membrane vibrate in phase and that its displacement is coneshaped". They used an "effective area" of the TM as determined by Wever and Lawrence (1954). Single curves of $|Z_d|$ and $|Z_{dob}|$ are reported for frequencies approximately between 50 Hz and 8 kHz. These results are in general agreement with our measurements in that 1) for $f < 800$ Hz they have approximate slope of -6 dB/octave, 2) opening of the bulla causes the input-impedance magnitude to decrease, and 3) the MEC resonance frequency shifts to a lower frequency when the bulla is opened. However, their $|Z_d|$ measurement indicates that the MECs resonance is near 2 kHz, a result that is lower than our lowest measurement of resonant frequency by a factor of two. In addition, as frequency increases above 3 kHz, both $|Z_d|$ and $|Z_{dob}|$ increase dramatically ($\cong 30$ dB), which is not consistent with our measurements, Møller's measurements, or their own subsequent measurements (Khanna and Tonndorf, 1972). It is likely that this behavior results from the invalidity of their assumptions used to calculate TM volume velocity. Vibration patterns of the TM (Khanna and Tonndorf, 1972) indicate that the vibration amplitude of the TM generally exceeds that of the manubrium. Thus, use of manubrium displacement to calculate TM volume velocity could result in estimates that are too small.

Khanna and Tonndorf (1972) determined the vibration pattern of the TM in cat using time-averaged holography. Measurements were obtained at

several frequencies (385 Hz to 5.9 kHz) and sound-pressure levels, $|P_d|$. They calculated TM volume displacement (for constant $|P_d|$) from their TM displacement patterns assuming pressure linearity and that "all points on the TM vibrate in phase". Results for three cats were compared to two Z_d results from Møller (1963, 1965) (i.e., volume displacement/ $|P_d| = 1/j\omega Z_d$) and were found to be in "close agreement". The large magnitude increase for $f > 3$ kHz observed by Tonndorf and Khanna (1967) was not present in the 1972 results. In summary, the Khanna and Tonndorf (1972) results are in general agreement with our Z_d measurements and probably represent an improvement in precision and bandwidth over the 1967 results.

Guinan and Peake (1967) reported curves of transmission change resulting from 1) opening the bulla, 2) opening both middle-ear cavities, and 3) from removing the septum in an ear in which the bulla was previously open. The ratio, cochlear potential/ P_d , was used to assess transmission change. They found that opening the bulla or both MECs increased the transmission by ≈ 5 dB for all frequencies below 600 Hz; transmission was also increased over a narrow bandwidth near 4 kHz by as much as 12 dB. At frequencies slightly above and below this 4 kHz region, transmission was decreased. Removing the septum with the bulla previously opened produced no change in transmission at low frequencies; near 3 kHz a large transmission increase was found (≈ 15 dB) over a narrow bandwidth. Transmission was slightly decreased for frequencies slightly above and below the 3 kHz frequency region. The qualitative description of these results is consistent with our measurements of input impedance; Z_{di} , Z_{dob} , and Z_{doc} (FIGURE 8) can be used to calculate the

impedance changes (Z_{di}/Z_{dob} , Z_{di}/Z_{doc} , and Z_{dob}/Z_{doc}) resulting from these "experimental modifications" of the MECs. If the "series" model of FIGURE 1B is valid (see Section IV C), these changes in transmission will equal the corresponding changes in input impedance. Comparison of the impedance curves of FIGURE 8 indicates that these impedance ratios correspond closely to the transmission changes observed by Guinan and Peake. We observed a range in $|Z_{di}/Z_{doc}|$ or $|Z_{di}/Z_{dob}|$ (at low frequencies) of 3 to 8 dB; Guinan and Peake's value of transmission increase (5 ± 2 dB) falls within this range. Also, the magnitudes and frequencies of the large peaks in transmission (3 kHz and 4 kHz) are in excellent agreement with the peaks in the impedance ratios.

2. MEC Pressure Measurements

Preliminary measurements of P_t/P_d and P_b/P_d for the various "normal" and "experimentally modified" states of the MECs have been previously made in this laboratory (Geisser, 1972; Miller, 1973). These results are generally consistent with those shown in FIGURES 14 and 15. However, significant improvements have been made in P_t , P_b , and P_d probe-microphone construction (stability, high impedance to eliminate "loading") and the associated calibration procedures. Additionally, the precision of the measurement system has been improved. These efforts have allowed us to make more accurate pressure measurements over a wider frequency range.

Kruger and Tonndorf (1977) measured $|P_t|$ and $|P_d|$ for constant

round-window cochlear-potential magnitude. Frequencies examined were between 200 Hz and 4 kHz at third-octave intervals. The ratio $|P_t/P_d|$ calculated from their results is roughly constant at -4 dB between 200 and 400 Hz, increases to 0 dB at 800 Hz, has a minimum of -20 dB in the 2 kHz region, and increases to +3 dB at 4 kHz. This general behavior vs frequency is somewhat similar to our results (FIGURE 15). Our low-frequency $|P_t/P_d|$ (or $|P_b/P_d|$) measurements ranged in value from -5 dB to -12 dB for measurements in eight ears. Thus, their value is 1 dB larger than our largest value. Their frequency sampling is not fine enough to precisely measure the minimum in $|P_t/P_d|$ near 2 kHz, but their result does show a minimum. Also, near 4 to 5 kHz our measurements show $|P_t/P_d|$ exceeding 0 dB; their data point at 4 kHz is consistent with this result.

C. WIDEBAND TEST OF THE SERIES MODEL

In Section I B we noted that the "series" model structure could be tested using measurements of transmission $(P_t/P_d)_x$ and admittance Y_{dx}/Y_{doc} to obtain independently each side of Equation (3),

$$1 - (P_t/P_d)_x = Y_{dx}/Y_{doc} , \quad (3)$$

for the three conditions of 1) intact MECs, 2) bulla cavity widely open with the foramen open, and 3) plugged foramen.

FIGURES 19, 20, and 21 compare computations of each side of Equation (3) for each of the three conditions. The quantity $1 - (P_t/P_d)_x$

is very sensitive to errors in $(P_t/P_d)_x$ when $|(P_t/P_d)_x| \cong 1$. We have, therefore, denoted these frequency regions (i.e., where $|(P_t/P_d)_x| \geq 0.3$, near 5 kHz) by horizontal bars in FIGURES 19 - 21. At most frequencies, errors in $1 - (P_t/P_d)_x$ are quite small, since $|(P_t/P_d)_x|$ is considerably less than 1.

The agreement is excellent for frequencies below 2 kHz; magnitude differences are less than 1 dB and the angles are nearly indistinguishable except for FIGURE 21, where the difference is about 9° . Relatively good agreement for the frequency regions where $|(P_t/P_d)_x| > 0.3$ is also observed. The largest magnitude discrepancies in each of the three figures occur near 13 kHz (6.5, 10, 9 dB, for FIGURES 19 - 21, respectively). Approximately 6 dB may be accounted for by possible errors in the admittance measurements. Since the agreement between theory and measurement for test loads (CHAPTER I, Section III) is within $\cong 3$ dB at high frequencies (CHAPTER I, FIGURE 9), the admittance ratios might be in error by 6 dB. All three admittance ratios are larger than the corresponding $1 - (P_t/P_d)_x$ curve for $f > 8$ kHz. A small increase in $|Y_{doc}|$ in this frequency region would tend to decrease these differences. It is possible that our Y_{doc} measurements with the MECs widely open contain a small series impedance component resulting from sound pressure on the medial side of the tympanic membrane. That is, opening the middle-ear cavities may not effectively "short" Z_{mec} . If this impedance were known and could be accounted for (i.e., subtracted from Z_{doc}), $|Y_{doc}|$ might be slightly larger at high frequencies, thus improving the above agreement. If it is assumed that this impedance results primarily from constriction

in a pathway between the tympanic membrane and "free" space, then this hypothesis could possibly account for the result that $|Y_{doc}|$ is less than $|Y_{di}|$, $|Y_{dob}|$, and $|Y_{dpf}|$ at high frequencies (FIGURE 8). Measurements of Y_{doc} and the admittance with the MECs opened "more" widely or measurements of sound pressure on the medial side of TM with the cavities open are needed to test this hypothesis.

In summary, with the exception of the frequency region near 13 kHz, these tests imply that the "series" model of FIGURE 1 is a valid description of the MECs and ossicular chain for $10 \text{ Hz} < f < 22 \text{ kHz}$. This result is significant because it allows us, in principle, to determine the components of one impedance (Z_{mec} or Z_{doc}) independent of the other. It also implies that modifications of the middle-ear cavities should make equal changes in input impedance, Z_d , and transmission. The good agreement between our Y_d changes for MEC manipulations and the transmission changes reported by Guinan and Peake (1967) (see Section IV B) support this conclusion.

D. CORRELATION OF MIDDLE-EAR CAVITY ADMITTANCE AND MIDDLE-EAR CAVITY VOLUMES

In this section we examine the correlation between acoustic and volumetric measurements of bulla and tympanic cavity volumes. In doing so, we use the series model to make predictions of V_t and $V_{mec} = V_t + V_b$ using acoustic admittance measurements at low frequencies. These predictions are compared with volumetric measurements and are in

excellent agreement, which indicates that the effects of the cavities at low frequencies can be predicted from the cavity volumes.

Acoustic and volumetric measurements of bulla cavity volume for one animal were compared in FIGURE 12 (Section III A 5) and found to be in excellent agreement. This is the only case in which we have a comparison between a direct acoustic measurement and the corresponding volumetric measurement. We can, however, estimate V_t and the total MEC volume, $V_{mec} = V_t + V_b$, from a series of acoustic admittance measurements such as those of FIGURE 7 or 8. We have made measurements that allow acoustic estimates of V_{mec} (seven cats) and V_t (five cats) which may be compared to the corresponding volumetric results.

Since the "series" model is clearly valid at low frequencies, we have $Z_{mec} = Z_{di} - Z_{doc}$ and $Z_t = Z_{dpf} - Z_{doc}$. It is clear that at low frequencies each of these impedances is compliance dominated and may be represented by an equivalent volume, $V = C_{pc}^2$. Therefore, we may estimate the acoustic volumes V_{mec} and V_t by

$$V_{mec} = (V_{doc} V_{di}) / (V_{doc} - V_{di}) \quad \text{and}$$

$$V_t = (V_{doc} V_{dpf}) / (V_{doc} - V_{dpf}) ,$$

using values of V_{doc} , V_{di} , and V_{dpf} computed from MMSE compliance estimates of the respective acoustic impedance measurements. The MMSE estimates were computed using magnitude data for frequencies generally less than 500 Hz. Since at low frequencies Z_{doc} is equal to Z_d with an open bulla hole (see Section III A), we used Z_d with an open bulla hole to calculate the above acoustic estimates, because it was available in a larger number of animals.

Acoustic estimates and volumetric measurements are compared in FIGURE 22 and are in excellent agreement for both V_{mec} and V_t . The vertical "error" bars indicate the change in the acoustic estimate for a 1 dB variation in both acoustic admittance measurements used in the computation. For example, an upper error bar for a V_{mec} estimate was computed substituting $V_{doc}/1.12$ and $1.12 V_{di}$ in the above equation. In Section II E we found the intertrial variation in volumetric measurements of V_t to be less than 8.6%, and 2.6% for V_b . If these variations are representative of the errors in our volumetric measurements, the precision of the volumetric measurements will be $\cong 0.03$ cc for both V_t and V_b . Thus, possible "errors" in the acoustic estimates are much larger than "errors" in volumetric measurements.

The acoustic estimates of V_{mec} appear to be consistently smaller than the corresponding volumetric measurements. Reasons for this are unclear. This trend is not consistent with "underfilling" of the cavities caused by trapped air bubbles, etc. It is consistent with the hypothesis that the measured acoustic admittance magnitudes are all slightly smaller by a fixed fraction than the true magnitudes. Note, however, that this hypothesis is not supported by the V_t results.

We may also examine the correlation between low-frequency acoustic measurements and volumetric results using the MEC pressure measurements. Since Z_{doc} , Z_{mec} , and Z_t are compliance dominated at low frequencies, the model of FIGURE 1D predicts the pressure ratio for the intact MECs to be $P_t/P_d = C_{doc}/(C_{doc} + C_{mec})$, and for the plugged foramen condition $P_t/P_d = C_{doc}/(C_{doc} + C_t)$. Thus, substituting the MMSE compliance estimate for C_{doc} (obtained from a Z_{doc} impedance measurement) and the

volumetric data for V_t and V_{mec} (i.e., compliances computed using $C = V/\rho c^2$) we obtain predictions of P_t/P_d for the two conditions. These predictions for TjL-53L are in agreement with MMSE estimates of the low-frequency values of the measured pressure ratios to within 0.3 dB to 0.6 dB for the intact MECs, and 0.3 dB to 0.7 dB for the plugged foramen condition.

In summary, the correlation of volumetric measurements with low-frequency acoustic measurements of both admittance and MEC pressure indicates that the middle-ear cavities are accurately represented by $C = V/\rho c^2$ for low frequencies.

E. NETWORK MODEL OF THE MIDDLE-EAR CAVITIES

1. The Pressure Ratio: P_b/P_t

Some aspects of the detailed MEC model of FIGURE 1D can be tested by comparing the measured pressure ratio, P_b/P_t , to the model prediction, $P_b/P_t = Z_b/(Z_b + Z_f)$. P_b/P_t was computed from measurements of P_t/P_d and P_b/P_d for the condition of intact MECs (FIGURE 23). According to the model, this pressure ratio should depend only upon the properties of the foramen and the bulla cavity, being independent of the impedance of the ossicular chain (Z_{doc}) and the tympanic cavity. Assuming $Z_b = 1/j\omega C_b$, and $Z_f = R_f + j\omega M_f$, the model predicts

$$P_b/P_t = \frac{1}{(1 - \omega^2 M_f C_b) + j\omega R_f C_b} \quad (8)$$

At low frequencies the model prediction is $|P_b/P_t| = 1$ with angle of 0° . At $\omega = 1/(M_f C_b)^{0.5}$ there is a maximum in $|P_b/P_t|$ and a 180° shift in angle due to the pole. The damping at resonance is controlled by R_f . For frequencies somewhat above this resonance, $|P_b/P_t|$ decreases at -12 dB/octave and the angle becomes -180° . These trends are in qualitative agreement with the P_b/P_t measurement for frequencies below 6 to 7 kHz. However, at higher frequencies the measurements have additional maxima and minima which are not predicted by this model. These large maxima and minima mainly result from the P_b measurement (note that the direct measurement of Z_b (FIGURE 12) had similar variation) and may be accounted for by a more complicated model for Z_b , such as $Z_b = (1/j\omega C_b)H(\omega)$, where $H(\omega)$ is a rational function of ω having two damped second-order poles and zeros at the appropriate frequencies. To precisely quantify the high-frequency behavior of Z_b , measurements of P_b or bulla impedance, Z_b , must be made at the foramen.

2. Estimates of MEC Model Impedances

The impedance of the middle-ear cavities, Z_{mec} , can be estimated by combining input impedance and MEC pressure measurements (i.e., $Z_{dx}(P_t/P_d)_x = \hat{Z}_{mecx}$, Equation 4). For one animal (TJL-53L) we have made computations for three experimental conditions: 1) intact

MECs, 2) bulla open widely with the foramen open, and 3) plugged foramen. Note that for condition (1) the \hat{Z}_{mec} estimate is that of the total middle-ear cavities impedance, Z_{mec} ; for condition (2), $\hat{Z}_{mec} = Z_t Z_f / (Z_t + Z_f)$; for condition (3), $\hat{Z}_{mec} = Z_t$. These estimates are shown in FIGURES 24, 25, and 26, respectively.

Responses of an electric network analog are compared to the \hat{Z}_{mecx} estimates in FIGURES 24 - 26. The network is that of FIGURE 1D, but with the resistance of R_f being proportional to $\omega^{0.5}$. Element values were chosen as follows: Volumetric measurements of $V_b = 0.780$ cc and $V_t = 0.247$ cc were used to calculate the corresponding acoustic compliances ($C = V/\rho c^2$), $C_b = 5.55 \times 10^{-7}$ and $C_t = 1.75 \times 10^{-7}$ cm⁵/dyn. The minimum in the \hat{Z}_{mec} estimate (FIGURE 24) corresponds to the series resonance of Z_b and Z_f ; therefore, this frequency is $f_s = 1/\{(2\pi)(M_f C_b)^{0.5}\}$. Substituting $f_s = 2125$ Hz (from FIGURE 24) and the volumetrically predicted C_b , we calculate $M_f = 1.01 \times 10^{-2}$ g/cm⁴. At 2125 Hz, the \hat{Z}_{mec} estimate is resistive and approximately equal to 10 ohms. We therefore chose $R_f(f) = 0.216(f)^{0.5}$ ($R_f(\omega) = 0.086(\omega)^{0.5}$) so that its value equals 10 ohms at 2125 Hz.

In general, the agreement between model and measurement for the three conditions is quite good. The rms differences between the model and \hat{Z}_{mec} estimate for the total MEC impedance (FIGURE 24) are 1.5 dB in magnitude and 7.2° in angle for $10 \text{ Hz} < f < 10 \text{ kHz}$. The total MEC impedance estimate is compliance dominated for $f < 1 \text{ kHz}$ and $6 \text{ kHz} < f < 11 \text{ kHz}$. The model prediction from volumetric measurements ($V_t + V_b$, $f < 1 \text{ kHz}$) is in excellent agreement with the \hat{Z}_{mec} estimate.

The model predicts the shape of the curve near the series resonance at 2125 Hz and also precisely fits the measurements in the vicinity of the parallel resonance near 4.5 kHz. This is significant since it is an independent test of the model. The model and measurement are also in good agreement for $6 \text{ kHz} < f < 11 \text{ kHz}$, where the response is dominated by C_t . At 11.3 kHz there is a small magnitude peak ($\cong 8 \text{ dB}$ magnitude change) and angle variation in the \hat{Z}_{mec} estimate that results from the peak in the P_t/P_d measurement (Section III B 1); the model does not predict this peak, but use of a more complicated Z_b model (see the previous section) can account for this behavior. For frequencies above 16 kHz the angle of \hat{Z}_{mec} becomes much less than -90° , which is inconsistent with the interpretation of this result as an impedance. The model remains compliance dominated by C_t in this frequency region.

The \hat{Z}_{mec} estimates for the condition of open bulla and foramen are in good agreement with the model response for most frequencies (FIGURE 25) using the model element values given above. {Note that the appropriate comparison at low frequencies is between the model response and the curve denoted "bulla hole open" (see footnote 1).} The model impedance is

$$\hat{Z}_{\text{mec}} = \frac{Z_f Z_t}{Z_f + Z_t} = \frac{R_f(\omega) + j\omega M_f}{\{1 - \omega^2 M_f C_t\} + j\omega C_t R_f(\omega)} . \quad (9)$$

The pole places a maximum in the model response at 3.8 kHz; the value of $R_f(\omega)$ in this frequency region controls the impedance magnitude at the peak. The \hat{Z}_{mec} estimate and model agree well for both magnitude

and angle in the frequency region near resonance ($1 \text{ kHz} < f < 5 \text{ kHz}$).

At very low frequencies ($\omega M_f \ll R_f(\omega)$, or $f \ll 30 \text{ Hz}$) the model impedance is dominated by $R_f(\omega)$; we have no P_t/P_d measurements at these low frequencies. For frequencies well above the 30 Hz break frequency, but well below the resonant frequency, the frequency dependence of the model is approximately $j\omega M_f$. The "bulla hole open" estimate is in excellent agreement with the model response in this frequency region. The frequency dependence of the resistance, $R_f(\omega)$, is necessary to fit the angle measurements of FIGURE 25 at frequencies below 700 Hz. Use of a constant 10 ohm resistance results in an angle of approximately 35° at 120 Hz; the frequency dependence of the resistance decreases its effect at low frequencies, thus making the angle much closer to 90° at low frequencies.

At very high frequencies the model response becomes $1/j\omega C_t$. The \hat{Z}_{mec} estimate is in fair agreement with the model for $6 \text{ kHz} < f < 15 \text{ kHz}$. Maximum differences in magnitude or angle are $\cong 6.5 \text{ dB}$ and $\cong 40^\circ$. Note, however, that the angle becomes less than -90° in this frequency region. Also, a 14 dB discrepancy in magnitude exists near 18 kHz. Since the model predicts that Z_t controls in this frequency region, this discrepancy may result from inadequacy in the Z_t model specification (see the discussion of FIGURE 26 below for further evidence for this conclusion).

The estimate $\hat{Z}_{\text{mec}} = Z_t$ (FIGURE 26) is clearly compliance-like for $f < 3 \text{ kHz}$, with magnitude slope of -6 dB/octave and angle near -90° . The model response is in good agreement with these data for $f < 3 \text{ kHz}$. For $3 \text{ kHz} < f < 13 \text{ kHz}$ the magnitude and angle deviate somewhat from

compliant behavior with the largest magnitude difference being 8 dB (6 kHz) and with angle differences approaching 45° (6.7 kHz). There is some evidence⁶ that these effects may be due to static pressure build-up during the measurements of P_t and Z_{dpf} used to compute the Z_t estimate. We did not use a static pressure vent when making these measurements. Near 17 kHz the Z_t estimate has a large peak and the angle changes by roughly 180° . The wave properties of the sound field in the tympanic cavity may become important at these high frequencies, thus causing effects similar to those observed in the bulla impedance and pressure measurements. Clearly, the model of $Z_t = 1/j\omega C_t$ will not account for this behavior.

In summary, the model parameters C_t and C_b were determined from volumetric measurements. M_f was calculated using C_b and the frequency of the series resonance taken from the \hat{Z}_{mec} estimate (FIGURE 24). $R_f(\omega)$ was chosen to fit these same measurements at the series resonance; the form of the frequency dependence (i.e., $\omega^{0.5}$) is reasonable, based on known acoustical properties of "intermediate-sized tubes" (Beranek, 1954). The good agreement between model and measurements for the three \hat{Z}_{mec} estimates indicates that this model provides a precise description of the acoustics of the MECs for frequencies below 10 kHz. The rms differences between model and measurement for the total MEC impedance (FIGURE 24) are 1.5 dB and 7.2° for $10 \text{ Hz} < f < 10 \text{ kHz}$. It may be possible to obtain a better fit between model and measurements by modification of Z_b and Z_t to include the effects of the wave nature of sound propagation in the bulla and tympanic cavities at higher frequencies.

3. Correlation of Foramen Geometry with M_f and $R_f(\omega)$

We have made measurements of foramen "diameter" and "length" using several skulls from our experimental animals. The tissue lining the foramen and MECs had been removed during the procedure used to clean the skulls. The foramen geometry is complicated and not precisely described in terms of a "length" and "diameter"; however, the MEC model elements, M_f and $R_f(\omega)$, can be roughly estimated from these mechanical dimensions.

The acoustic impedance of an "intermediate-sized tube" is given by Beranek (1954, p. 137) to be $R_f(\omega) + j\omega M_f$ ($45 \text{ Hz} < f < 6.7 \text{ kHz}$), with $M_f = (\rho/\pi r^2)(L + 1.7r)$, and $R_f(\omega) = (\rho/\pi r^2)(L/r + 2)(2\mu\omega)^{0.5}$. The parameter $\mu = 0.156 \text{ cm}^2/\text{s}$ is the kinematic coefficient of viscosity, r = tube radius in cm, and L = tube length (cm). This model includes the effects of two end corrections for a flanged tube. Foramen measurements on five skulls indicate that the "diameter" is approximately 0.2 to 0.3 cm, with the "length" being 0.15 to 0.2 cm. Dimensions for TJL-53L are $r = 0.15 \text{ cm}$ and $L = 0.2 \text{ cm}$. Substituting values for TJL-53L we have $M_f = 0.8 \times 10^{-2} \text{ g/cm}^4$, which is 20% smaller than the model value of $1.01 \times 10^{-2} \text{ g/cm}^4$. The resistance is $R_f(\omega) = 0.031(\omega)^{0.5}$ and is a factor of 2.8 smaller than the model value of $0.086(\omega)^{0.5}$. The normal tissue of the foramen passage would tend to decrease the radius, thus decreasing these differences. Note that approximately half of the mass estimate results from the end corrections.

4. Comments Concerning M_f

The good agreement between the \hat{Z}_{mec} estimate (TJL-53L) and model response ($120 \text{ Hz} < f < 2 \text{ kHz}$) for the open bulla condition (FIGURE 25) indicates that the foramen mass, M_f , is constant with value $1.01 \times 10^{-2} \text{ g/cm}^4$ in this frequency range. The following measurements in the 3.6 kHz to 4.5 kHz range also support this conclusion. The parallel resonance of the intact MECs at 4.5 kHz (FIGURE 8) is given by the model to be $f_p = 1/\{2\pi(M_f C_{eq})^{0.5}\}$, where $C_{eq} = C_b C_t / (C_b + C_t)$. The resonance in the Y_{dob} measurement for the bulla open widely condition is at 3.6 kHz; the model predicts this frequency to be $f_{ob} = 1/\{2\pi(M_f C_t)^{0.5}\}$. The ratio f_p/f_{ob} , computed from the measured frequencies, is 1.25. Assuming that M_f is the same for the two different experimental conditions, the model prediction is $\{(C_t + C_b)/C_b\}^{0.5}$, which may also be expressed in terms of the cavity volumes as $\{(V_t + V_b)/V_b\}^{0.5}$. Substituting the TJL-53L volumetric measurements for V_t and V_b (TABLE I), we have $f_p/f_{ob} = 1.15$. These two f_p/f_{ob} ratios agree within 8%. Results from two other cats indicate agreement within 8% and 5%. We have no direct experimental evidence that M_f remains constant at frequencies above 4.5 kHz. It is likely that at higher frequencies the acoustic impedance of the foramen and bulla contains a frequency dependent mass component, since there is a relatively large change in "diameter" at the junction of the foramen and the bulla cavity (Ingard, 1948; Burkhard and Sachs, 1977).

V. SUMMARY

Admittance at the tympanic membrane, Y_d , and the pressure transfer ratio, P_t/P_d , were measured for "normal" and "experimentally modified" states of the middle-ear cavities. These input-admittance and transmission measurements were used to test a proposed "series" model of the middle ear, $Z_d = Z_{mec} + Z_{doc}$. The model consists of the MECs impedance, Z_{mec} , in series with the impedance measured with the cavities widely opened, Z_{doc} , (i.e., essentially the impedance of the ossicular chain). The tests show the model to be valid for frequencies between 10 Hz and 22 kHz, except possibly in the frequency region near 13 kHz.

A lumped-element network model containing four elements (C_t , C_b , M_f , and $R_f(\omega)$) provides a good description of the impedance components of Z_{mec} for $10 \text{ Hz} < f < 10 \text{ kHz}$. Volumetric measurements of bulla and tympanic cavity volumes are in excellent agreement with the acoustic measurements of the compliances C_t and C_b indicating that the MECs are accurately represented by $C = V/\rho c^2$. Average volumetric results (12 ears) are $\bar{V}_t = 0.22 \text{ cc}$ and $\bar{V}_b = 0.66 \text{ cc}$. Fair agreement was found between foramen dimensions and the model elements M_f and $R_f(\omega)$.

Results were also presented concerning the spatial variation in bulla cavity pressure, input admittance and MEC pressures with tympanic membrane perforations, and the effects of the earcanal coupling space.

Measurements of the input admittance with the MECs opened widely, Y_{doc} , may be tentatively interpreted as the input impedance of the ossicular chain. However, the impedance of the "remaining" MECs and the

tissue surrounding the TM and ossicles may contribute a measurable component to Y_{doc} for frequencies above 3 kHz. Systematic measurements of Y_{doc} for various "experimental modifications" of the ossicular chain and cochlea are presented in the next chapter.

FOOTNOTES

(1) FIGURE 8 shows the Y_{dob} measurement with a 0.5 x 0.4 cm hole rather than with the bulla widely opened. This was done because a small shift in compliance was apparent for the single measurement taken with bulla widely open (see also Section III A 4); we, therefore, chose not to use these data for low frequencies. The data shown in FIGURE 8 clearly make the point that at low frequencies $Y_{doc} \cong Y_{dob}$. However, they do not accurately represent the widely opened bulla results in the frequency region near resonance because the size of the hole influences the frequency of resonance; at frequencies above the resonance frequency the two measurements are generally similar. Therefore, subsequent calculations involving Y_{dob} (Section IV) will be performed using both measurements and appropriate frequency regions of validity.

(2) Compliance estimates, C , were computed by minimizing the mean square magnitude error (MMSE) between the measured admittance curve and the function ωC over some specified low-frequency bandwidth (generally 10 Hz to 200-600 Hz). Unless otherwise noted, reported compliance values were computed in this manner.

(3) Average compliance was computed by averaging magnitude data (in dB) from N animals at individual frequencies; the MMSE compliance was then calculated from the average curve using the algorithm previously described.

(4) The admittance of the hole-present condition is certainly much closer in magnitude and angle to the normal Y_d and Y_{doc} than to Y_{mec} in this frequency range.

(5) Møller (1963, 1965) reports three curves of Z_d for intact ears. We have arbitrarily chosen two curves from the 1965 study (FIGURE 2, K42; FIGURE 4, unknown cat number) for comparison. The third curve (1963, FIGURE 4, K19) does not differ significantly from the ones chosen, and its frequency of MEC resonance is 4.5 kHz. We have not summarized results from the two studies by averaging, since this process will not preserve the sharpness of the MEC resonance.

(6) Repeated measurements without venting of the tympanic cavity showed increases in $|Y_{dpf}|$ (as large as 8 dB) for $4 \text{ kHz} < f < 7 \text{ kHz}$. Similar measurements of P_t/P_d without venting were not made. Repeated Y_{dpf} and P_t/P_d measurements, with venting between measurements, showed only small differences (less than 3 dB over the same frequency range), which appeared to result from slight shifts in the frequencies of the small peaks and dips. Results in this report are those for which cavity venting was performed just before measurement. It is possible that some small changes could occur during the time required to perform the frequency sweep. If $|P_t/P_d|$ increased in the same manner as $|Y_{dpf}|$ when the cavity is not vented, then it would be possible for these effects to roughly cancel in the $Z_{dpf}(P_t/P_d)_{pf}$ result.

TABLE I
SUMMARY OF VOLUMETRIC MEASUREMENTS

| CAT NUMBER | CAT WEIGHT (kg) | NUMBER OF TRIALS $N_t/N_b/N_{ec}$ | AVERAGE TYMPANIC VOLUME (cc) | AVERAGE BULLA VOLUME (cc) | AVERAGE EARCANAL VOLUME (cc) | T. LINE LENGTH $l' = V'_{ec} / A$ ($\frac{cc}{cm}$) |
|------------|-----------------|--------------------------------------|------------------------------|---------------------------|------------------------------|---|
| TJL-38R | 3.8 | 4/3/0 | 0.133 | 0.628 | --- | --- |
| TJL-40L | 2.9 | 3/3/0 | 0.181 | 0.900 | --- | --- |
| TJL-42R | 2.4 | 3/3/0 | 0.174 | 0.546 | --- | --- |
| TJL-43R | 2.1 | 3/3/4 | 0.200 | 0.401 | 0.032 | 0.12 |
| TJL-44R | 2.1 | 1/3/3 | 0.120 | 0.612 | 0.050 | 0.27 |
| TJL-45R | 3.9 | 3/3/3 | 0.239 | 0.708 | 0.073 | 0.47 |
| TJL-46R | 3.4 | 0/0/3 | --- | --- | 0.069 | 0.43 |
| TJL-47R | 2.1 | 1/3/3 | 0.236 | 0.615 | 0.062 | 0.37 |
| TJL-48R | 3.3 | 0/0/3 | --- | --- | 0.074 | 0.47 |
| TJL-49L | 2.9 | 3/3/3 | 0.242 | 0.568 | 0.055 | 0.31 |
| TJL-50R | 3.8 | 3/3/0 | 0.243 | 0.738 | --- | --- |
| TJL-51L | 3.2 | 3/2/3 | 0.298 | 0.740 | 0.070 | 0.44 |
| TJL-52L | 2.4 | 2/2/2 | 0.285 | 0.865 | 0.075 | 0.48 |
| TJL-53L | 3.5 | 2/2/3 | 0.247 | 0.780 | 0.062 | 0.37 |
| TJL-53R | 3.5 | 0/0/2 | --- | --- | 0.074 | 0.47 |

FIGURE CAPTIONS

FIGURE 1: A network model for the middle ear. The form of the model is that of an electric network analog, where voltage is analogous to sound pressure (P) and current to volume velocity (U). Part A: The input impedance at the tympanic membrane (TM), $Z_d = P_d/U_d$, is the ratio of complex amplitudes of sound pressure at the TM, P_d , to TM volume velocity, U_d . Z_{doc} is the input impedance at the TM when the middle-ear cavities (MECs) are widely opened (i.e., $Z_{mec} = 0$). P_t is sound pressure in the tympanic cavity. Part B is the "series" form of the model in A. Boxes 2 through 8 have been replaced by the equivalent input impedance, Z_{doc} . Part C is a more detailed model for the total middle-ear cavities impedance (Z_{mec}) in terms of the component impedances of the bulla cavity (Z_b), tympanic cavity (Z_t), and foramen (Z_f). In Part D the impedances of C are represented by network elements corresponding to the acoustic compliances of the bulla (C_b) and tympanic (C_t) cavities, and the acoustic mass (M_f) and resistance (R_f) of the foramen.

FIGURE 2: Schematic diagram of the experimental arrangement of the "normal" and "experimentally modified" states of the middle-ear cavities (MECs). Part A: The "normal" condition of intact MECs with pressure measurements at the tympanic membrane (TM) (P_d), tympanic cavity (P_t), and bulla cavity (P_b). The P_d measurement is used to compute the input admittance at the TM with the MECs intact, Y_{di} . Part B: The measurement condition for bulla opened widely (indicated by the heavy dashed line). P_t and P_d are measured (and input admittance at the TM is calculated from

P_d) for two conditions: 1) foramen open (Y_{dob}) and 2) foramen plugged (Y_{dpf}) (indicated by the dashed plug). Part C: P_d is measured and input admittance (Y_{doc}) is computed for the condition of widely opened MECs, indicated by the dashed line. The four sets of measurements were usually obtained without removal of the sound source from the earcanal.

FIGURE 3: Frequency response calibrations for the bulla, $E_b(f)/P(f)$, and tympanic cavity, $E_t(f)/P(f)$, probe-microphones. $E(f)$ and $P(f)$ are complex amplitudes of the probe output voltage and input pressure, respectively. Magnitudes are reported in dB, i.e., $20\log_{10}\{|E/P|\}$. All of the frequency response measurements in this paper are made up of straight-line segments connecting data points with a density of 40 points/decade. Symbols are only used to delimit different curves.

FIGURE 4: Effects on Y_{doc} of the correction for the source-tympanic membrane coupling space. Cat numbers, where appropriate, are usually placed in the lower right corner of the plot; R or L refers to right or left ear, respectively.

FIGURE 5: Comparison of acoustic and volumetric measurements of the earcanal coupling space. The curve labeled "FLUID IN MEC" is assumed to be an acoustic measurement of the coupling space for $f > 1$ kHz; $j\omega V'_{ec}/\rho c^2$ is the volumetric result.

FIGURE 6: Sensitivity of the admittance Y'_{doc} (Y_{doc} corrected for the coupling space) to a $\pm 20\%$ variation in coupling space volume. The volume change was produced by variation of the area, A , about the nominal value 0.119 cm^2 .

FIGURE 7: A comparison of typical input admittance measurements. " Y_{di} " and Y_d "BULLA HOLE OPEN" measurements are used to assess stability of the preparation and/or the acoustic source. Comparison to Y_{dpf} at low frequencies illustrates the approximate range in admittance magnitude encountered for these measurements.

FIGURE 8: Input admittance at the tympanic membrane for the "intact" (Y_{di}) and "experimentally modified" states of the middle-ear cavities. The modifications are: bulla open widely with the foramen open (Y_{dob}), foramen plugged (Y_{dpf}), and middle-ear cavities opened widely (Y_{doc}). These results are for one animal.

FIGURE 9: Summary of input admittance measurements at the tympanic membrane (middle-ear cavities intact), Y_{di} , from five cats. Cats included are: TJL-46, 47, 48, 52, 53R, 53L. (One of the curves for both magnitude and angle has a sharp decrease near 1.8 kHz; these measurements are for the same animal (TJL-53R). The reasons for this decrease are unknown.)

FIGURE 10: Summary of measurements of input admittance at the tympanic membrane with the middle-ear cavities widely open, Y_{doc} . Cats included are: TJL-46, 47, 48, 52, 53L.

FIGURE 11: Measurement summary of input admittance at the tympanic membrane with an open bulla hole. Results are from five cats: TJL-46, 47, 48, 52, 53R, 53L.

FIGURE 12: Comparison of a direct "ACOUSTIC" measurement of bulla cavity admittance (Y_b) and the prediction from volumetric results. The

acoustic measurement was obtained with a slightly different configuration of the acoustic source (i.e., R_2 resistor removed). The precision of the high-frequency results is therefore degraded relative to that obtained with our normal source configuration. In this and in subsequent figures, angle scales for plots of admittance or impedance extend over the range $\pm 90^\circ$, although the measurements sometimes exceed this range. Impedance or admittance angle results greater than $\pm 90^\circ$ result from measurement imprecision.

FIGURE 13: Effects of a tympanic membrane (TM) perforation. Both curves are measurements of input admittance at the tympanic membrane with the middle-ear cavities intact.

FIGURE 14: Measurements of bulla (P_b) and tympanic cavity (P_t) pressures relative to the pressure at the tympanic membrane (P_d) with the middle-ear cavities intact. The magnitude ratio is expressed in dB, i.e., $20\log_{10}\{|P/P_d|\}$. The P_t/P_d result is an average of two frequency response measurements.

FIGURE 15: Measurements of tympanic cavity pressure relative to that at the tympanic membrane (P_t/P_d) for the "INTACT" and experimentally modified states of the middle-ear cavities. The "INTACT" measurement is the curve from FIGURE 14. The foramen was open during the "BULLA OPEN WIDELY" measurement. Each curve was obtained by averaging two frequency response measurements.

FIGURE 16: Spatial variation in bulla cavity pressure. The pressure ratio P_b/P_d was measured for three insertion depths of the

probe-microphone. The measurement at 0.03 cm is near the bulla cavity wall, while that at 0.49 cm is near the foramen.

FIGURE 17: Comparison of measurements of the input impedance at the tympanic membrane with intact middle-ear cavities. The "LYNCH" result is a typical curve in that its magnitude is close to the average of all the curves of FIGURE 9. The "MØLLER" results are from his FIGURE 2 (the curve with no angle measurement) and FIGURE 4.

FIGURE 18: Comparison of measurements of the input impedance at the tympanic membrane with middle-ear cavities opened. The "LYNCH AVERAGE" was obtained by averaging the results of FIGURE 10. The "MØLLER" curves are a summary of his measurements for this experimental condition. Five individual magnitude and angle measurements are shown. These curves were taken from Møller, 1963, FIGURES 3, 5; and Møller, 1965, FIGURES 4, 8, 13.

FIGURE 19: Wideband test of the "series" model structure for the condition of intact middle-ear cavities (MECs). Measurements of input admittance, Y_{di} , and the pressure transfer ratio, P_t/P_d , were made with the MECs intact. Y_{doc} is input admittance with the MECs widely opened. Two curves of each of these results were averaged and used in the computations.

FIGURE 20: Wideband test of the "series" model structure for the bulla open condition. Measurements of input admittance were made for two conditions: 1) with a 4 x 5 mm hole in the bulla (reported for $10 \text{ Hz} < f < 1.7 \text{ kHz}$), and 2) with the bulla open widely. The valid

admittance ratio at low frequencies is the curve with filled circles (see text for discussion). The pressure ratio, P_t/P_d , was measured with the bulla open widely. Y_{doc} is input admittance with the middle-ear cavities widely opened. Two curves of each of these results were averaged and used in the computations with the exception of the bulla open widely admittance for which a single frequency response was used.

FIGURE 21: Wideband test of the "series" model structure for the plugged foramen condition. Measurements of input admittance, Y_{dpf} , and the pressure transfer ratio, P_t/P_d , were made with the foramen mechanically plugged. Y_{doc} is input admittance with the MECs widely opened. Two curves of each of these results were averaged and used in the computations.

FIGURE 22: Correlation of acoustic admittance and volumetric measurements of middle-ear cavity (MEC) volumes. The top plot is the acoustic admittance prediction of total MEC volume ($V_t + V_b$) vs the volumetric result for seven cats. The line with unity slope indicates perfect correlation. The lower plot is the acoustic prediction of tympanic cavity volume (V_t) vs the volumetric result in five cats. Open symbols denote estimates from acoustic data obtained using an acoustic source configuration which limited measurements to frequencies below a few kilohertz. Results obtained with the normal source configuration are indicated by closed symbols.

FIGURE 23: Measurement of P_b/P_t , the ratio of bulla-cavity pressure to tympanic-cavity pressure with intact middle-ear cavities. The result for one animal is shown; measurements in two other animals were quite

similar.

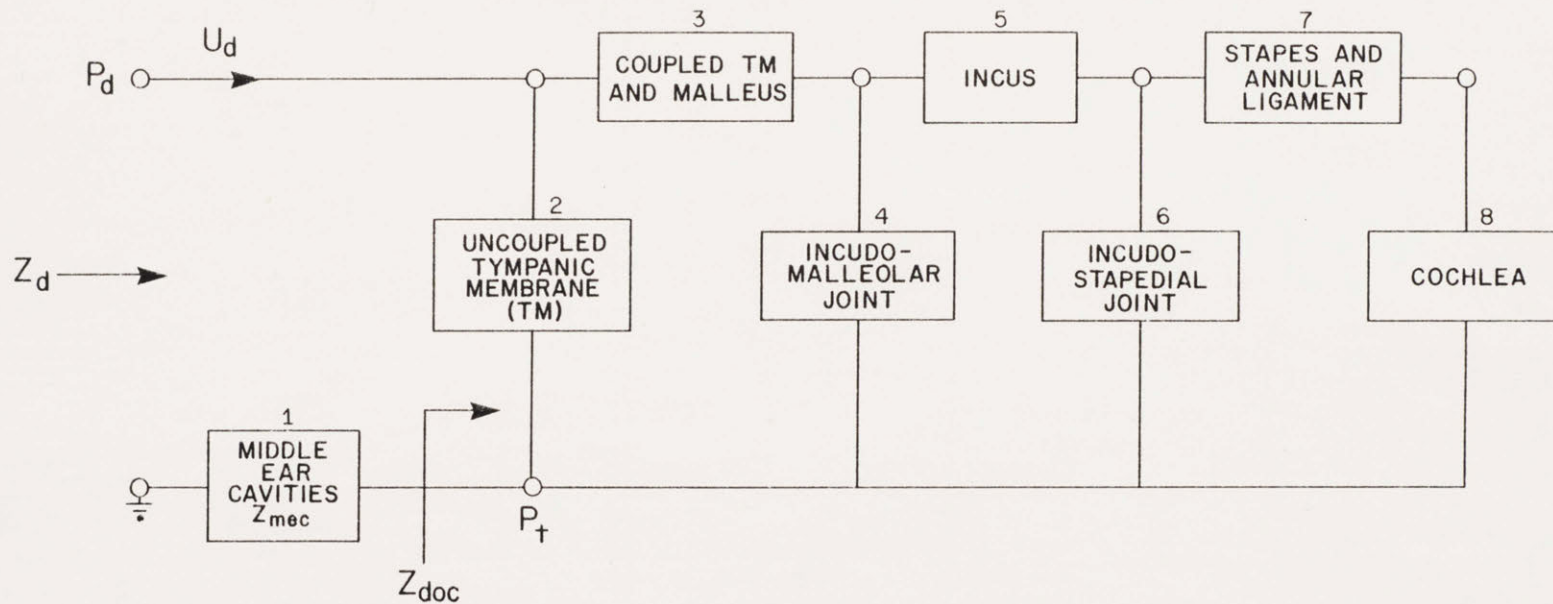
FIGURE 24: Comparison of the total acoustic impedance of the middle-ear cavities, Z_{mec} , from measurements and model. Two curves of each Z_{di} and $(P_t/P_d)_i$ were averaged and used to compute the "MEASUREMENT" result.

FIGURE 25: Comparison of the acoustic impedance of the parallel combination of foramen impedance, Z_f , and tympanic cavity impedance, Z_t , from measurements and model. Two curves of each Z_{dob} and $(P_t/P_d)_{ob}$ were averaged and used to compute the "BULLA HOLE OPEN" result. A single curve of Z_{dob} and the $(P_t/P_d)_{ob}$ average were used to compute the "BULLA WIDELY OPEN" result.

FIGURE 26: Comparison of the tympanic cavity acoustic impedance, Z_t , from measurements and model. Two curves of each Z_{dpf} and $(P_t/P_d)_{pf}$ were averaged and used to compute the "MEASUREMENT" result.

A.

A MIDDLE-EAR NETWORK MODEL



B.

"SERIES" MODEL

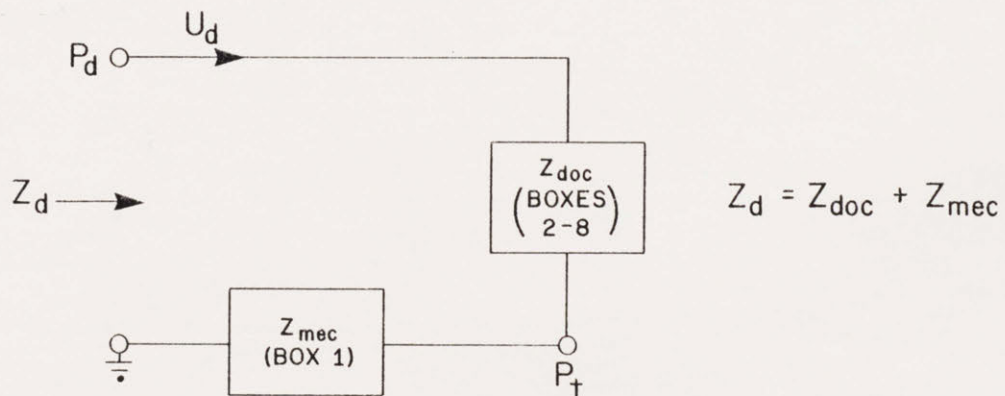


FIGURE 1

DETAILED MIDDLE-EAR CAVITIES MODEL

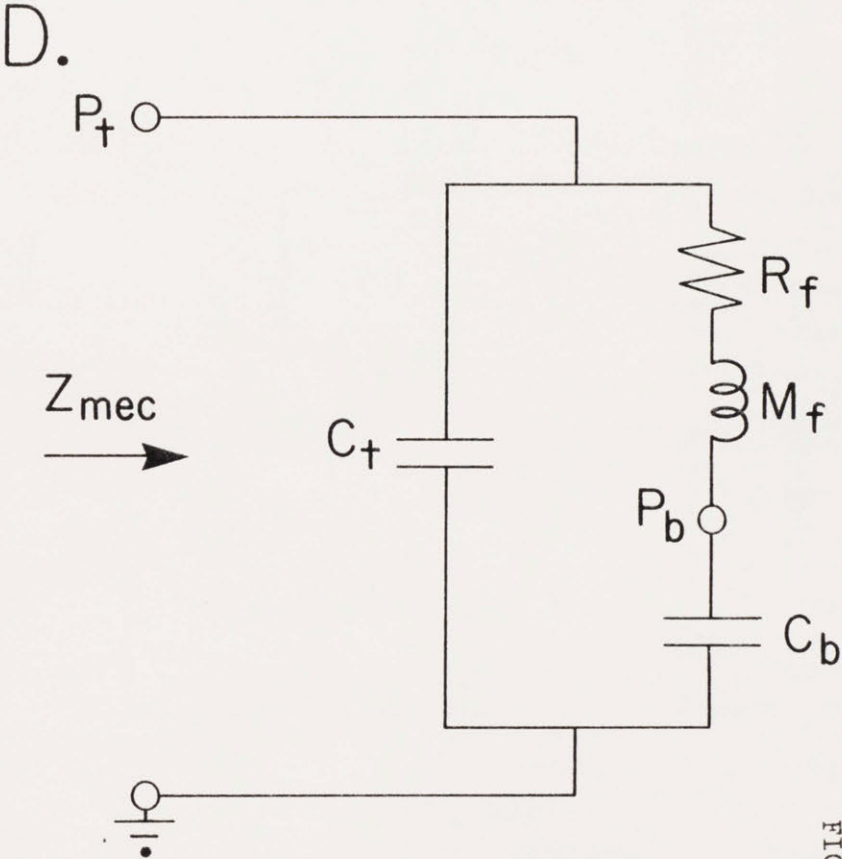
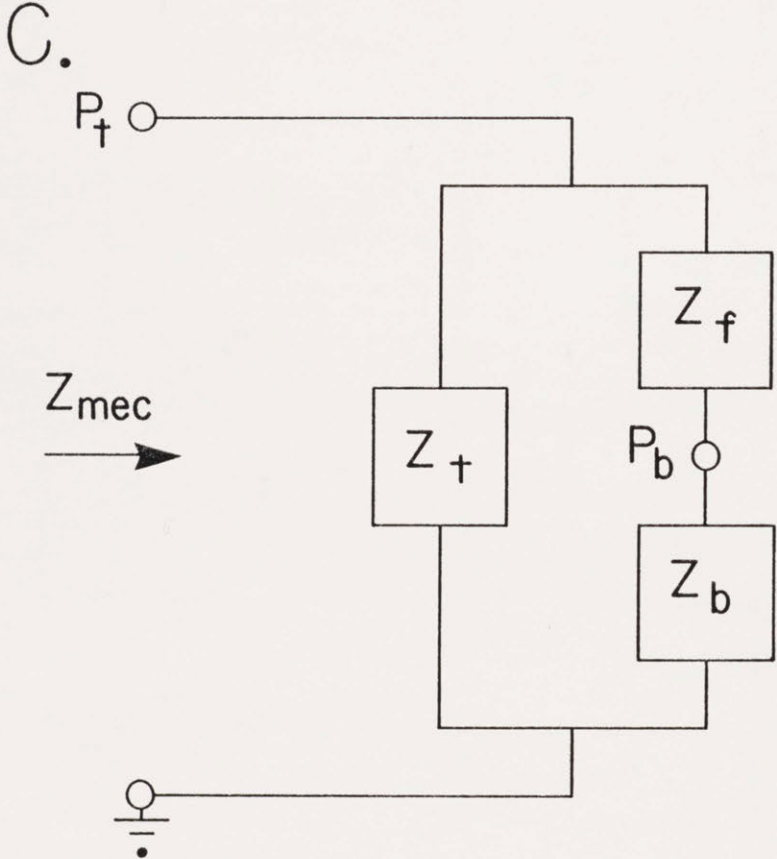
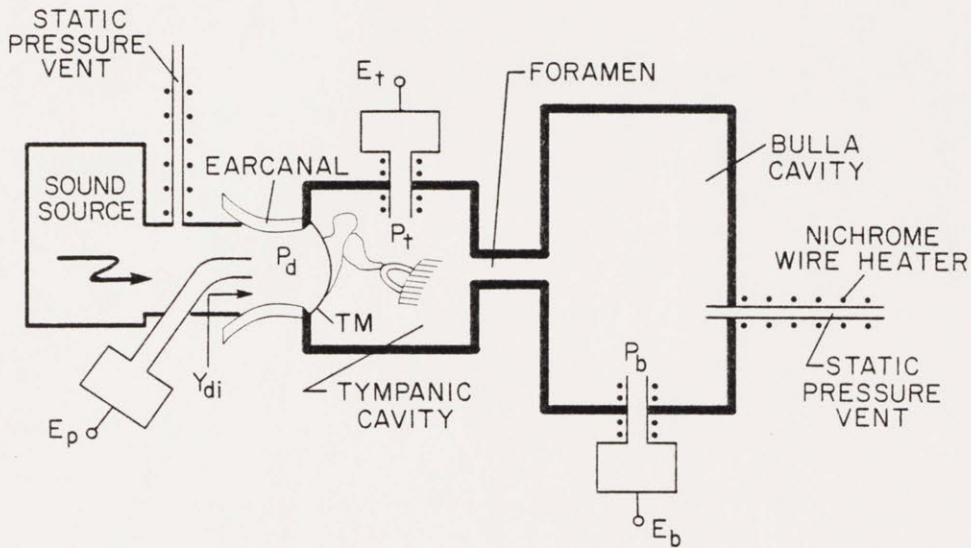


FIGURE 1

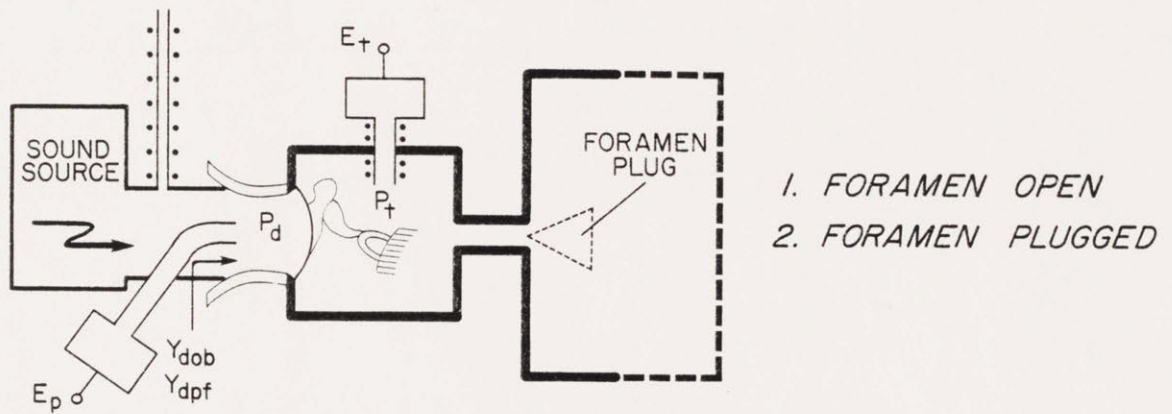
DIAGRAM OF THE
EXPERIMENTAL ARRANGEMENT

FIGURE 2

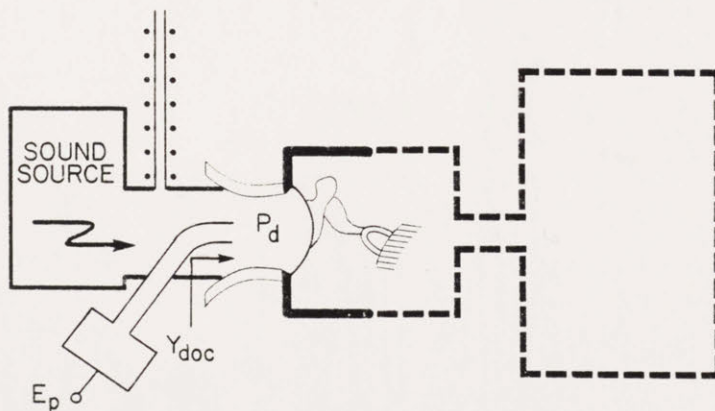
A. MIDDLE-EAR CAVITIES INTACT



B. BULLA OPEN WIDELY



C. MIDDLE EAR CAVITIES OPEN WIDELY



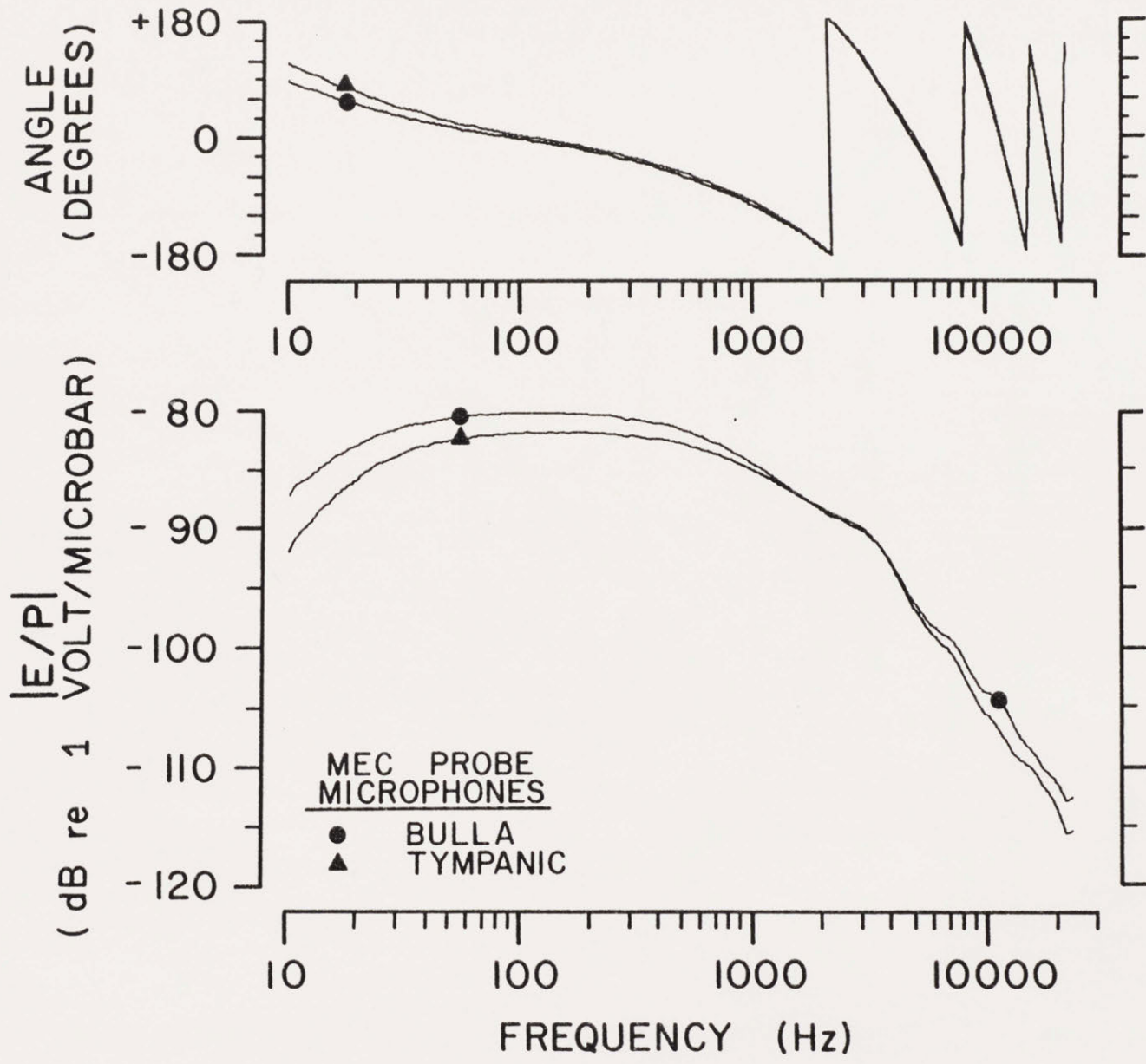


FIGURE 3

FIGURE 4

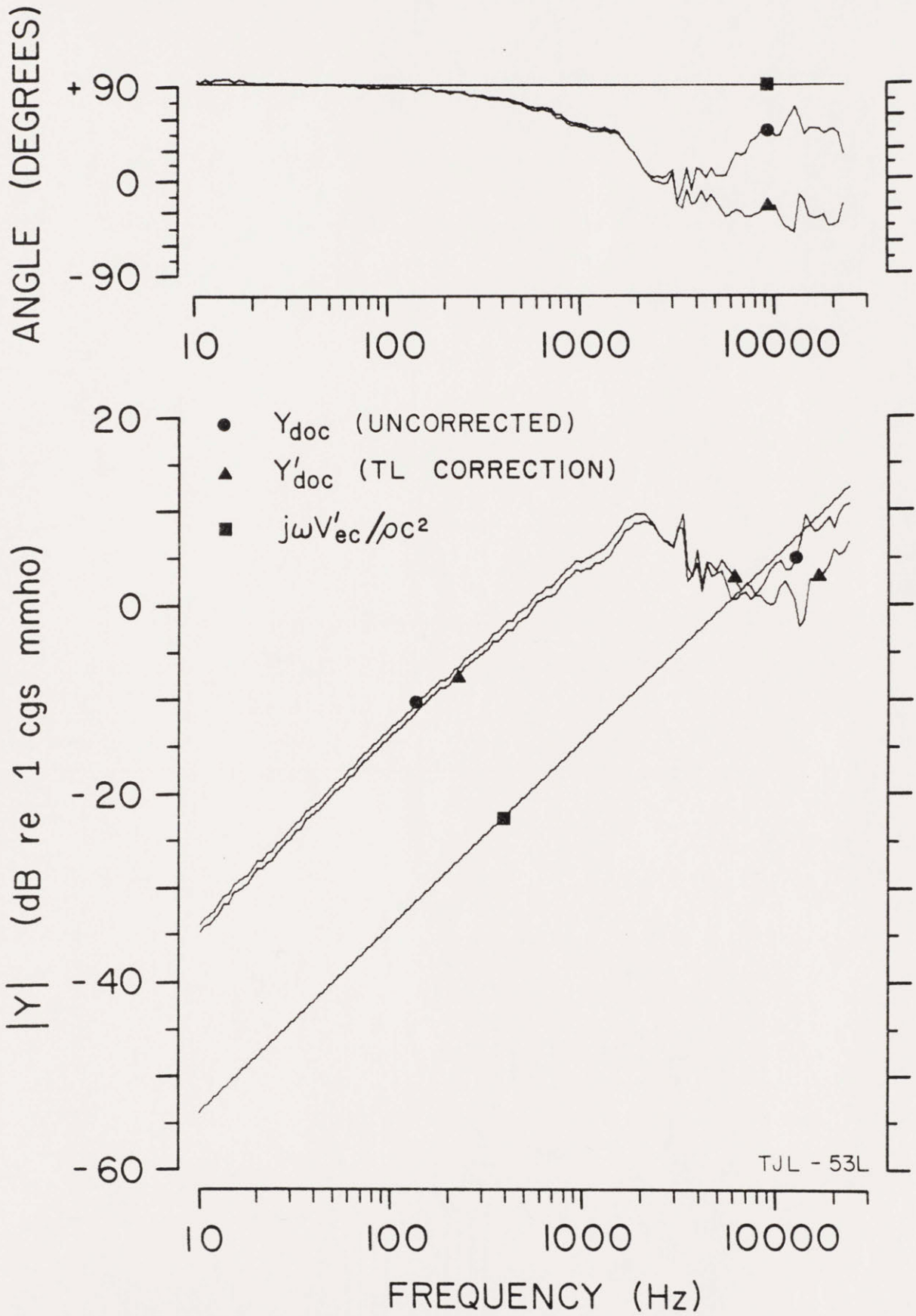


FIGURE 5

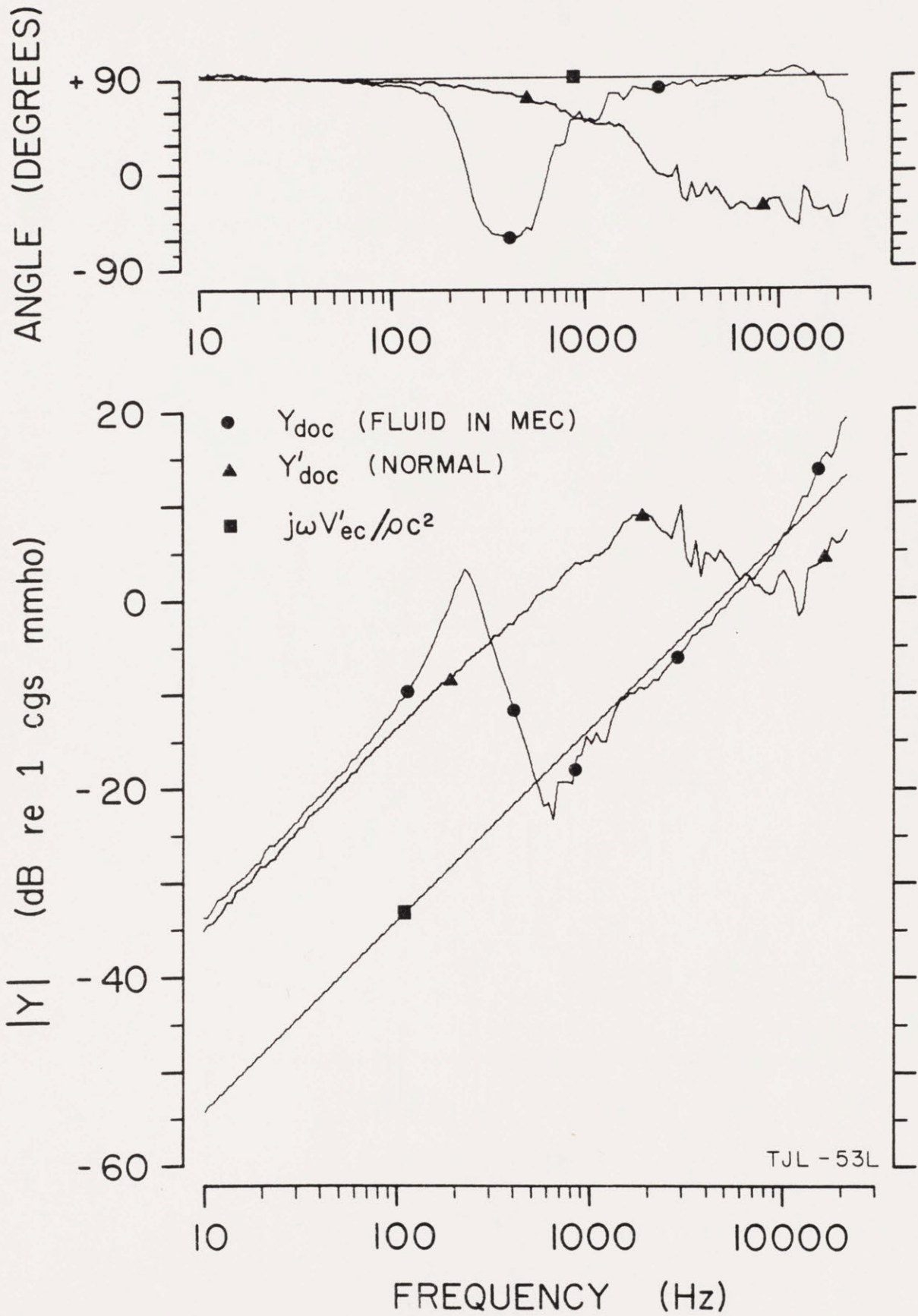


FIGURE 6

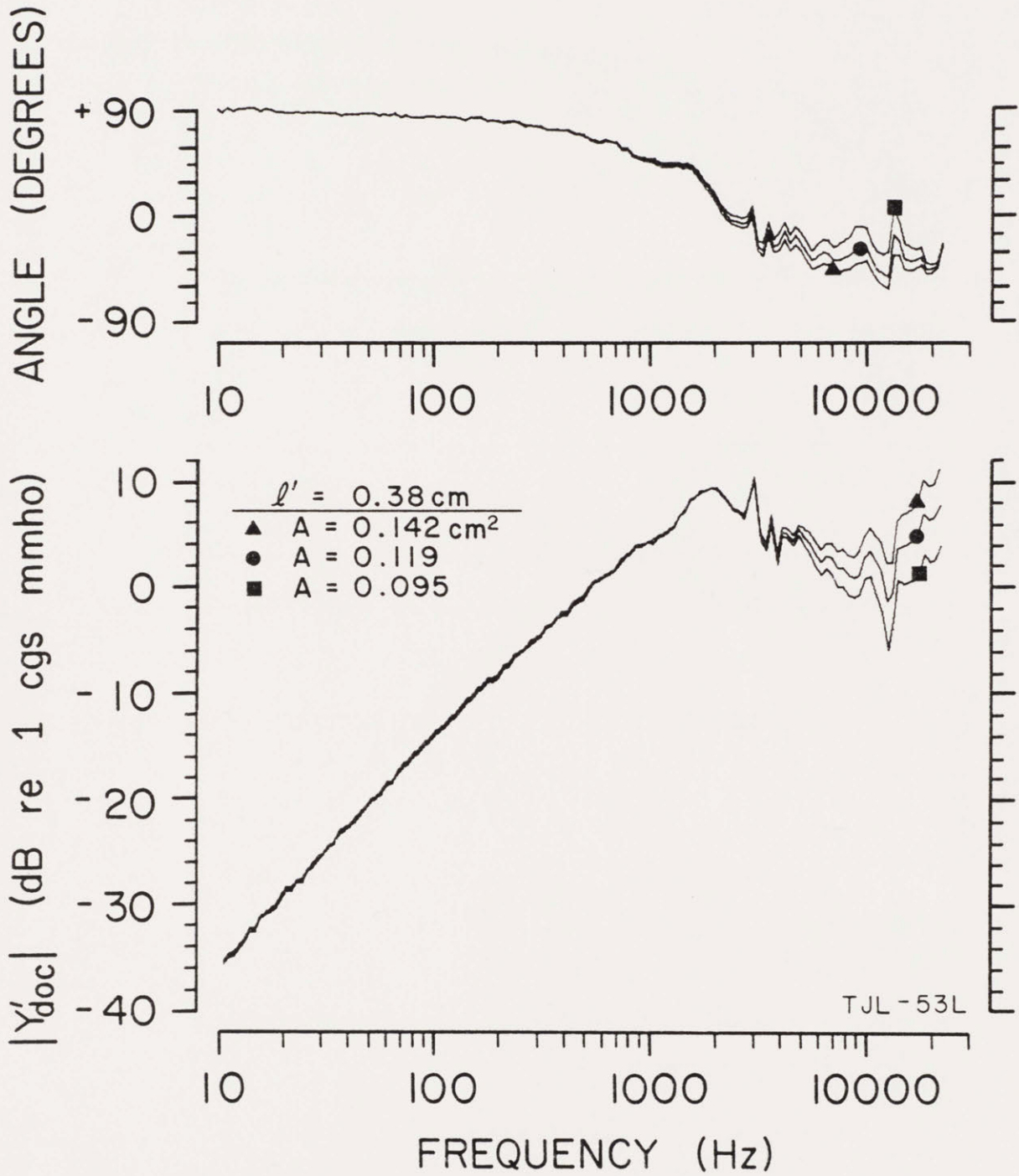


FIGURE 7

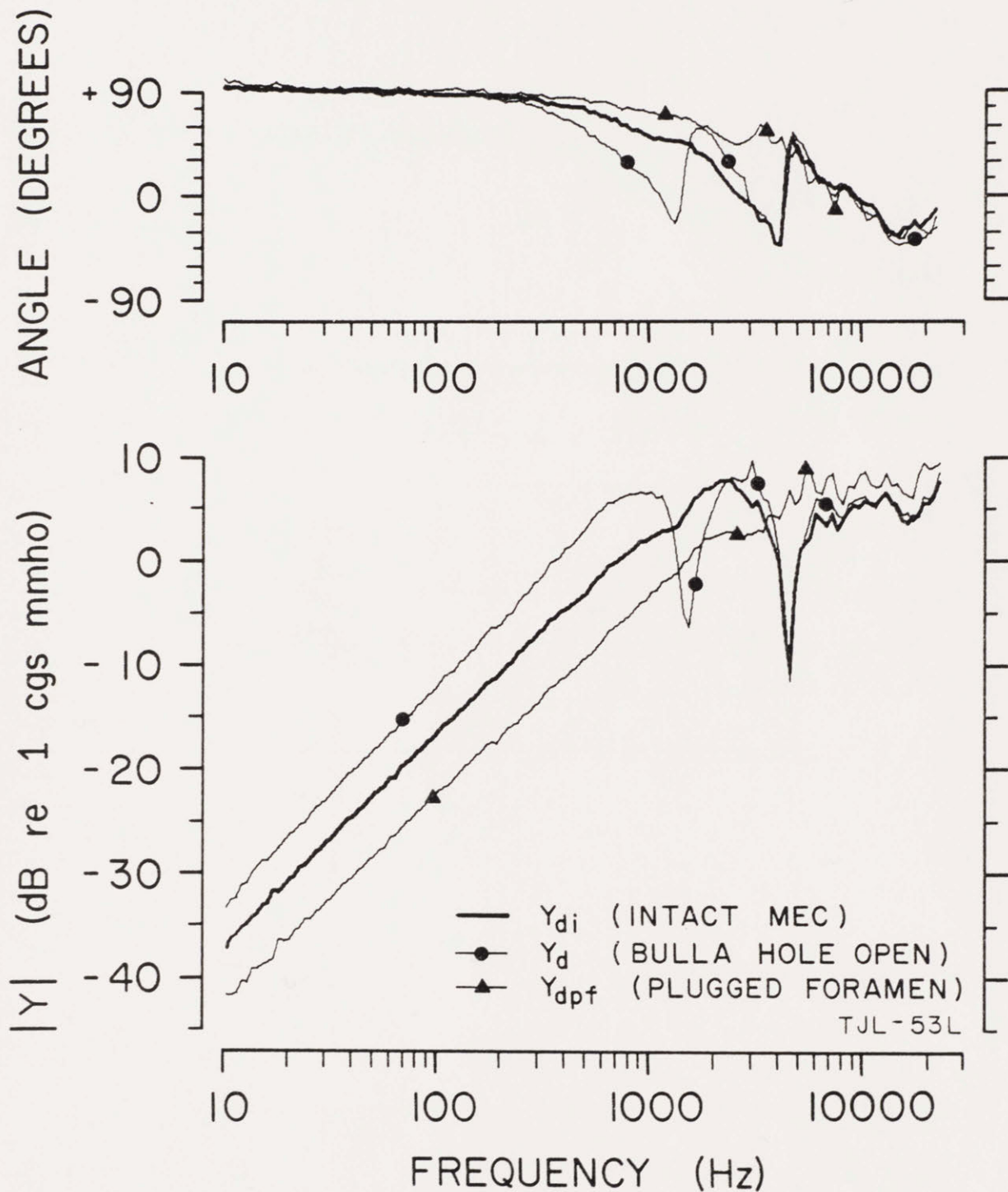


FIGURE 8

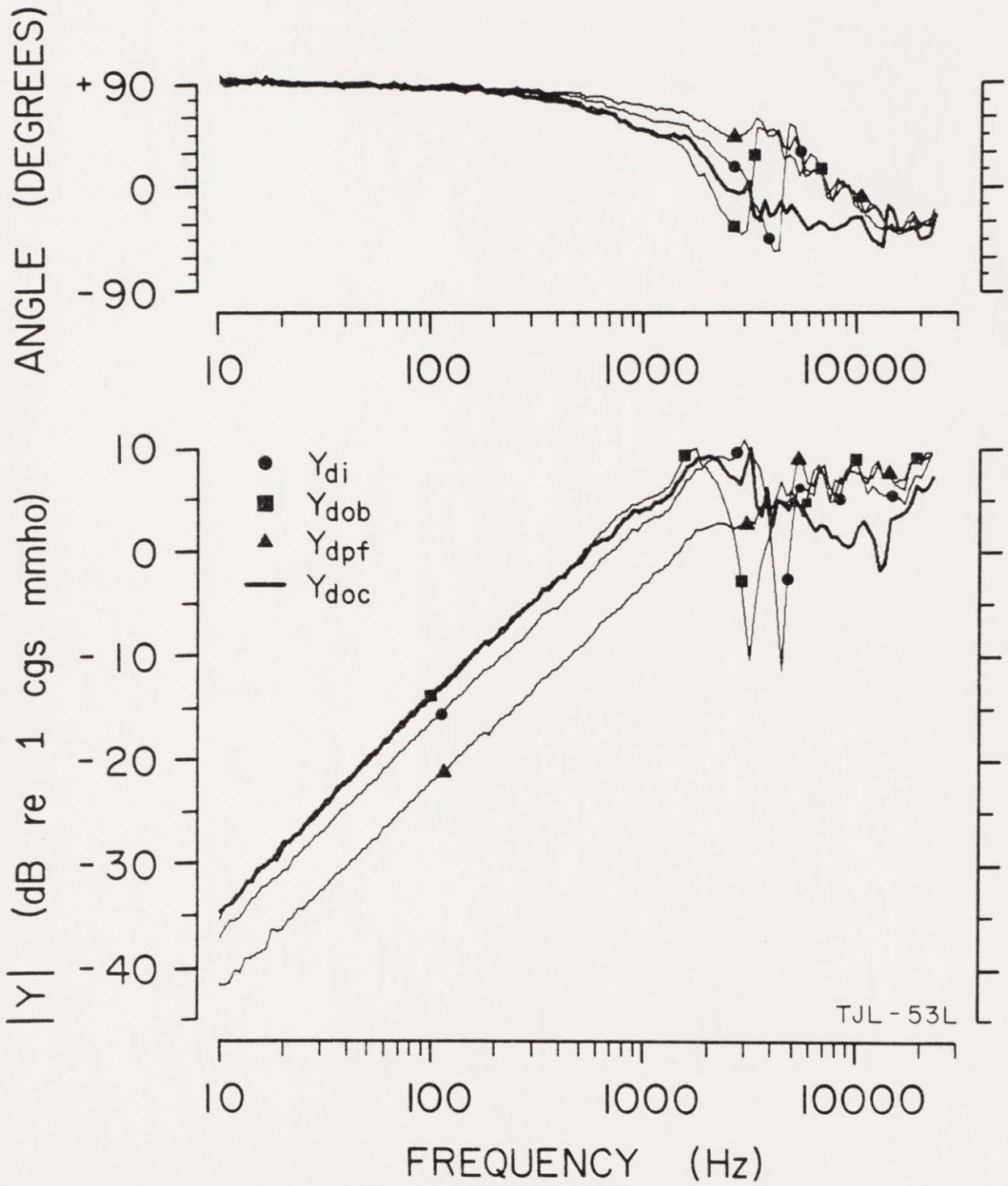


FIGURE 9

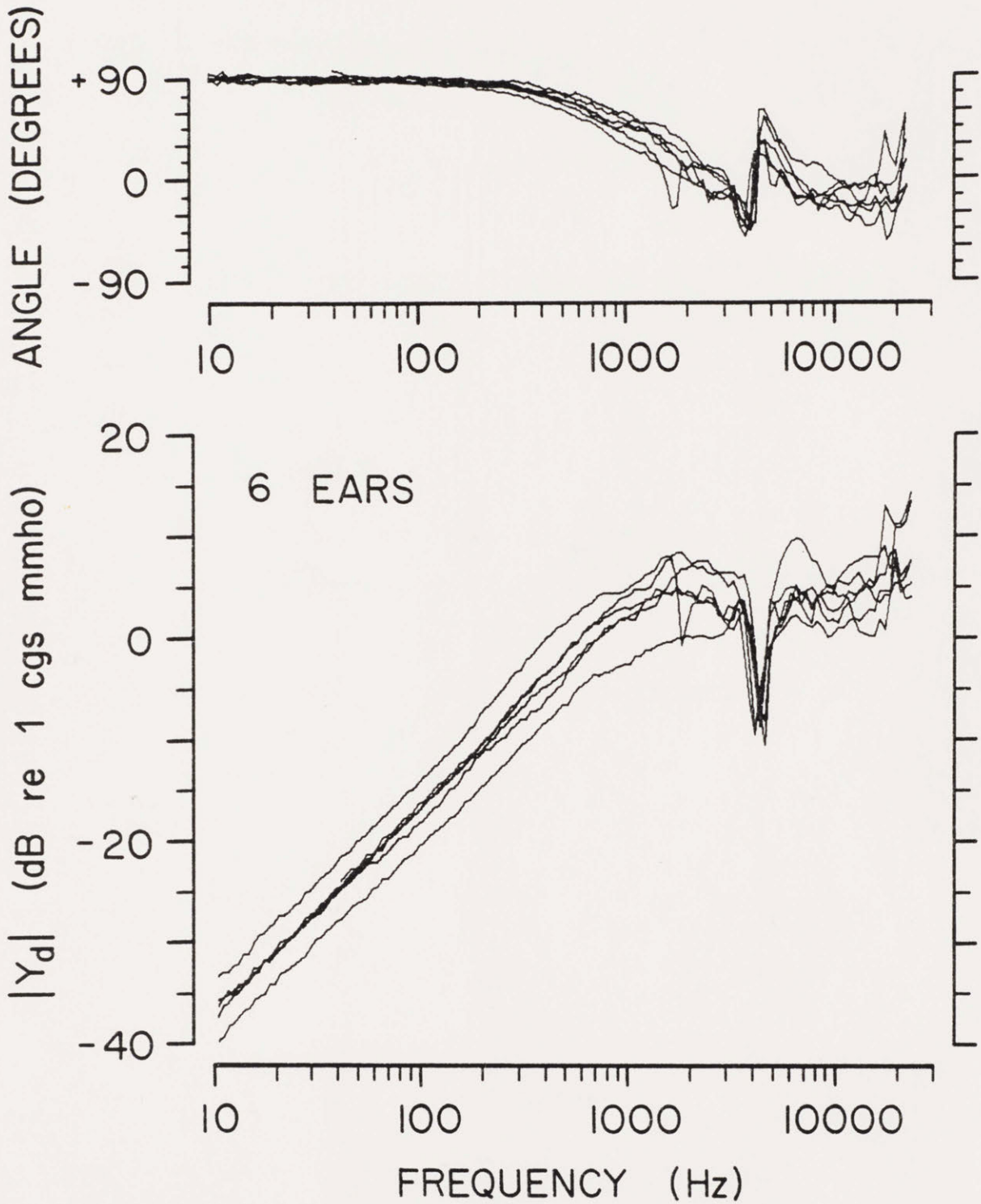


FIGURE 10

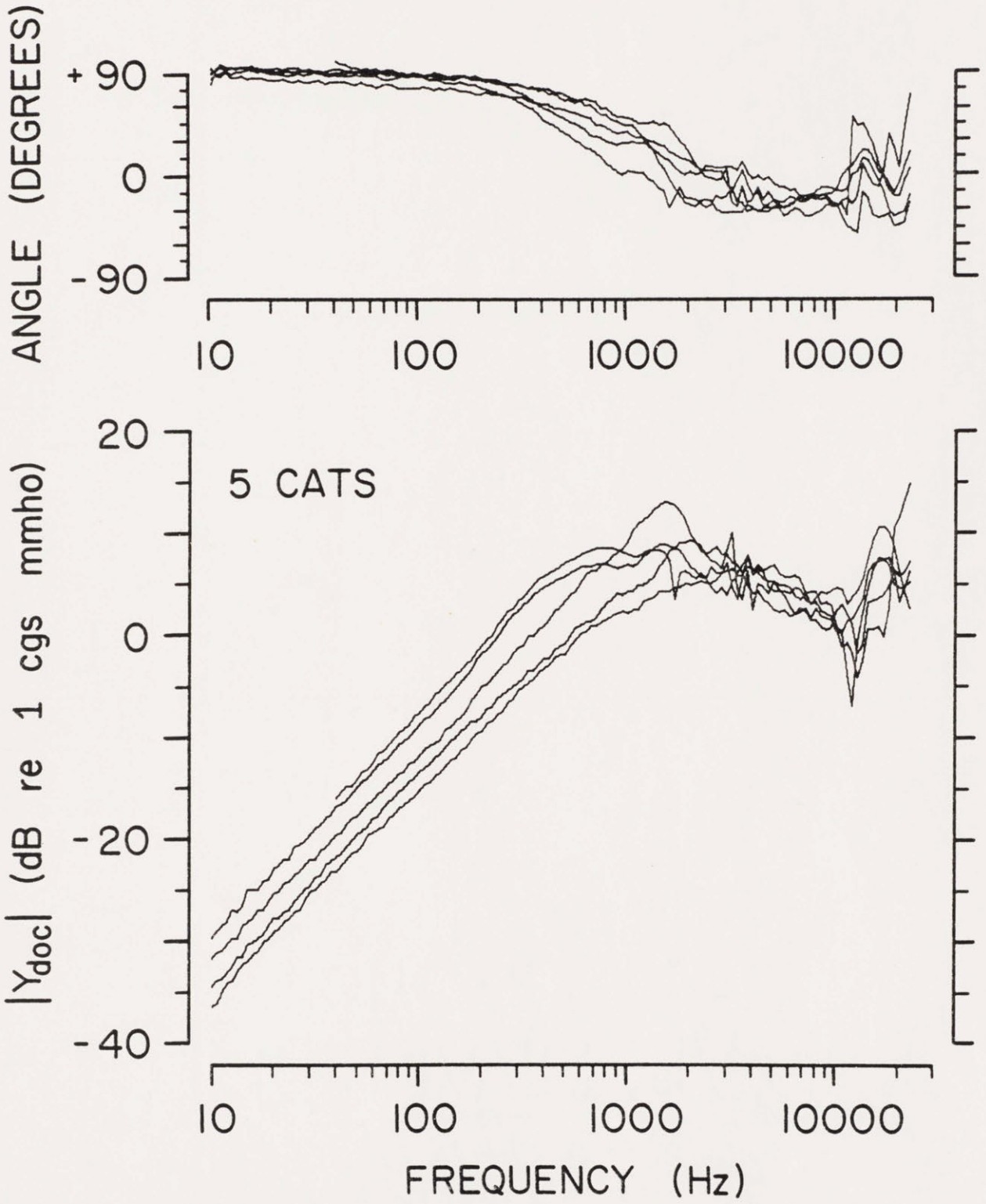


FIGURE 11

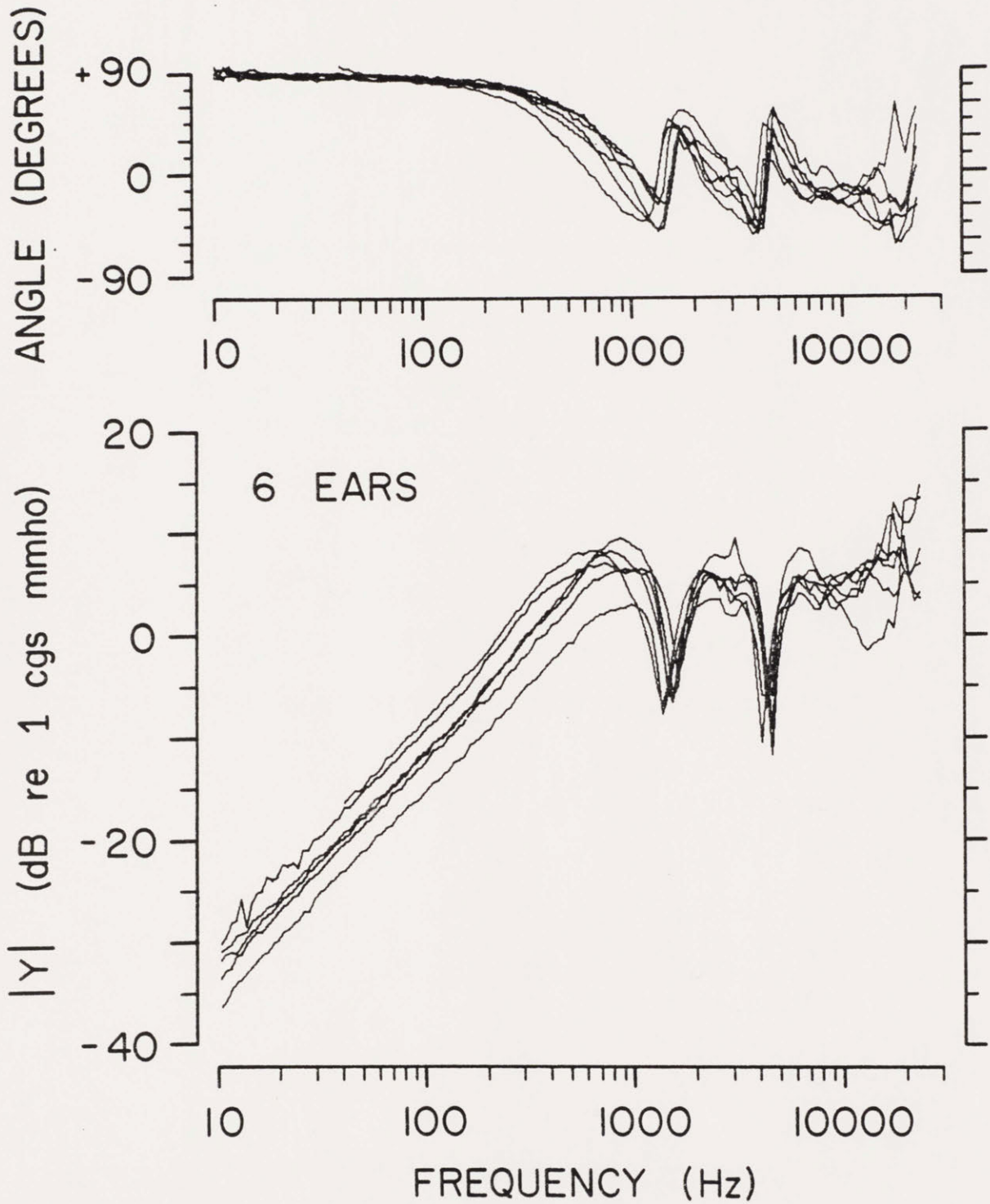


FIGURE 12

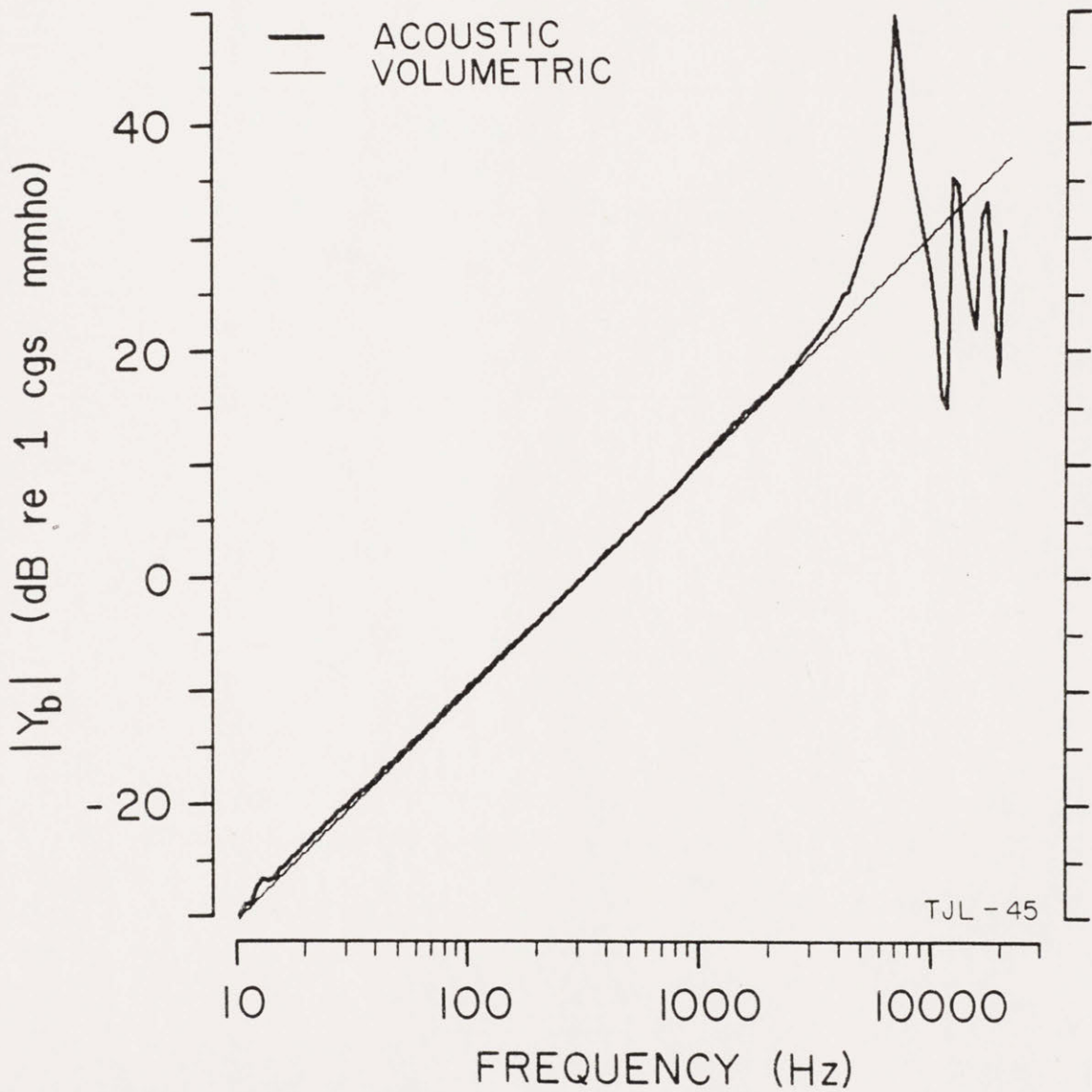
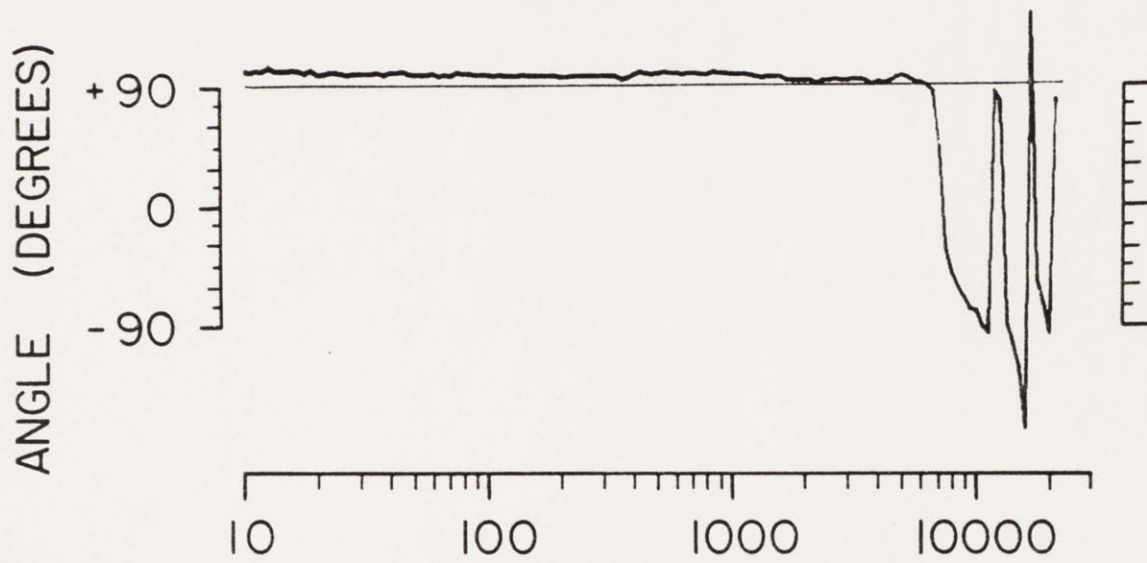
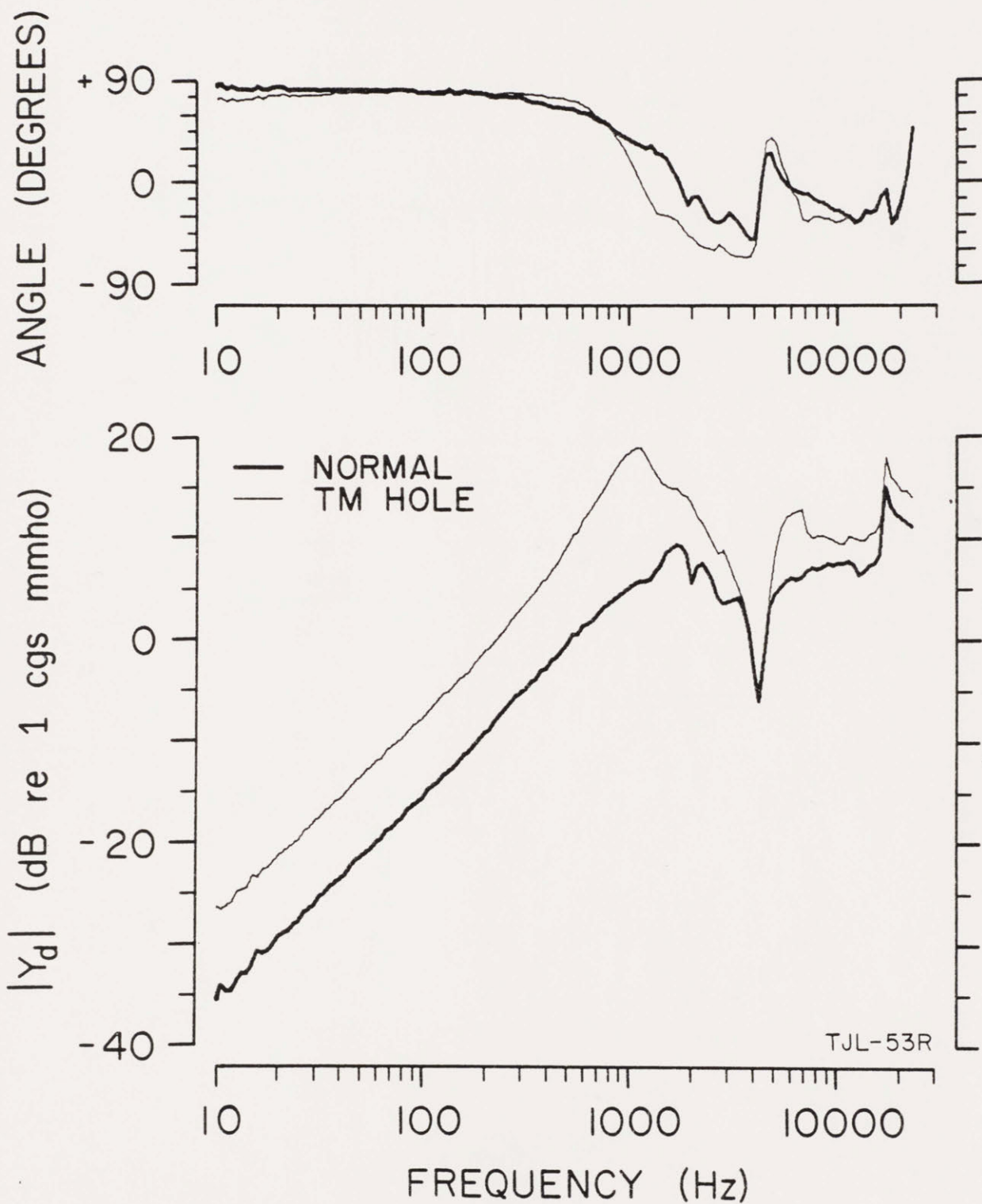


FIGURE 13



TJL-53R

FIGURE 14

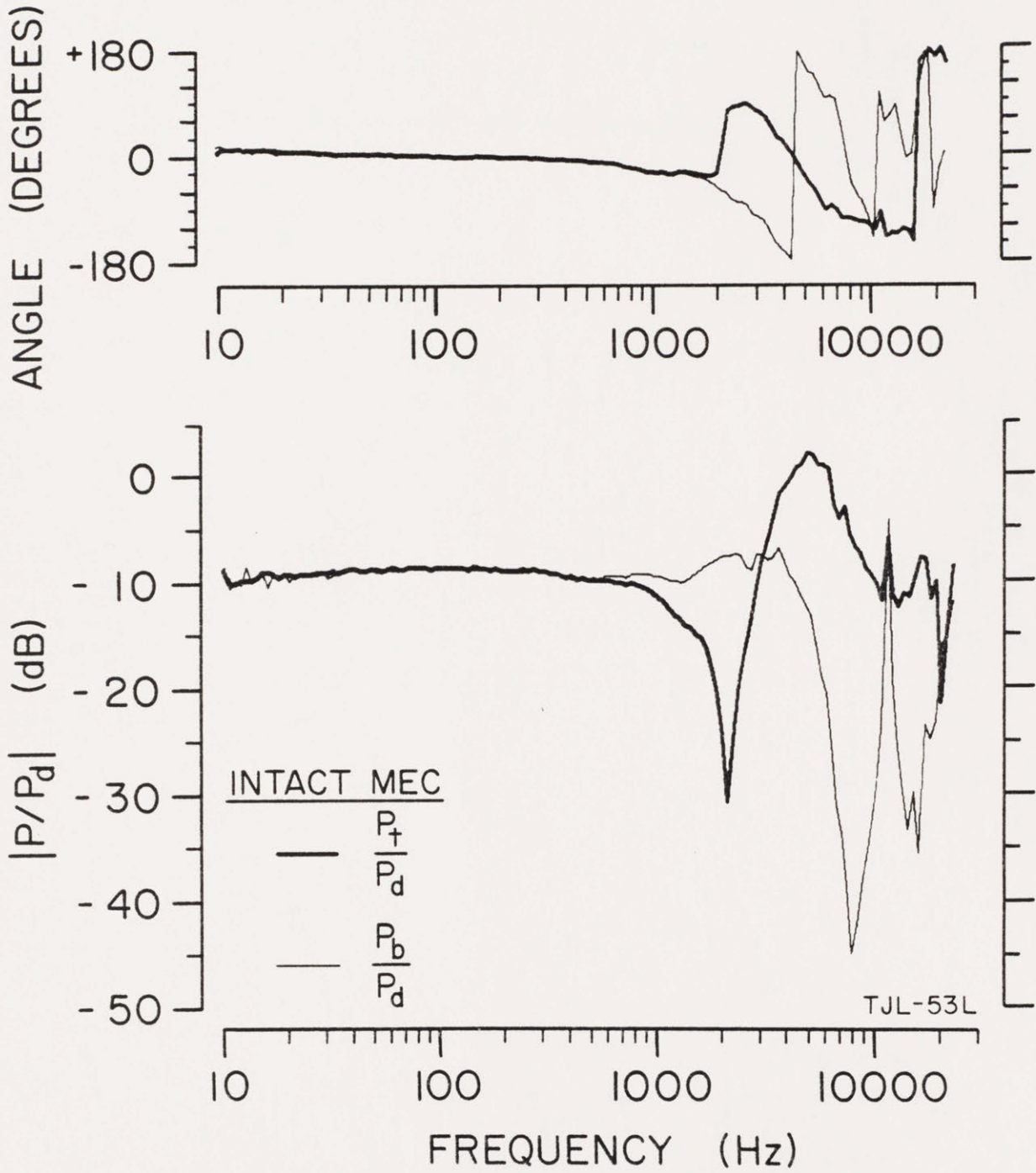


FIGURE 15

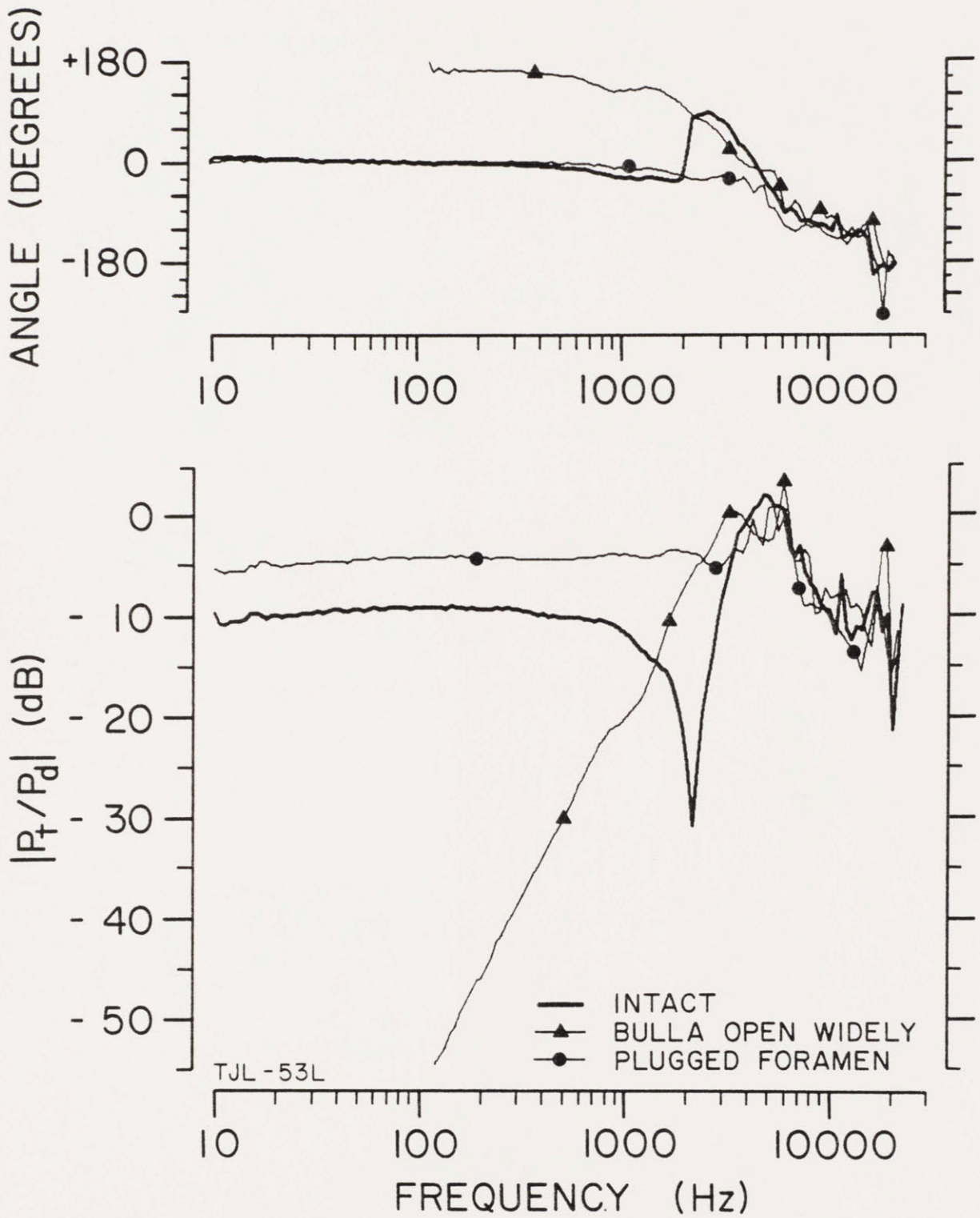


FIGURE 17

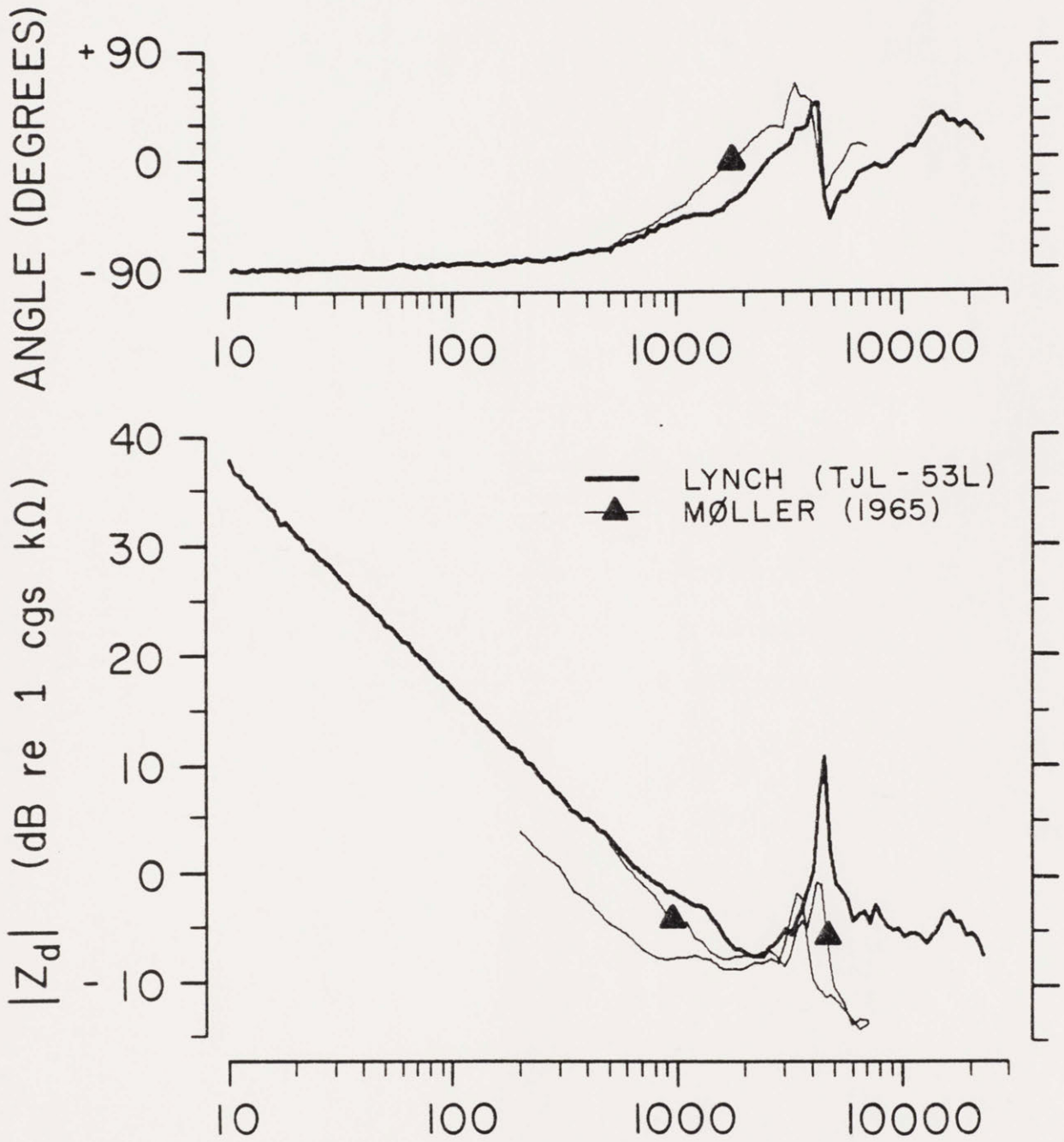


FIGURE 18

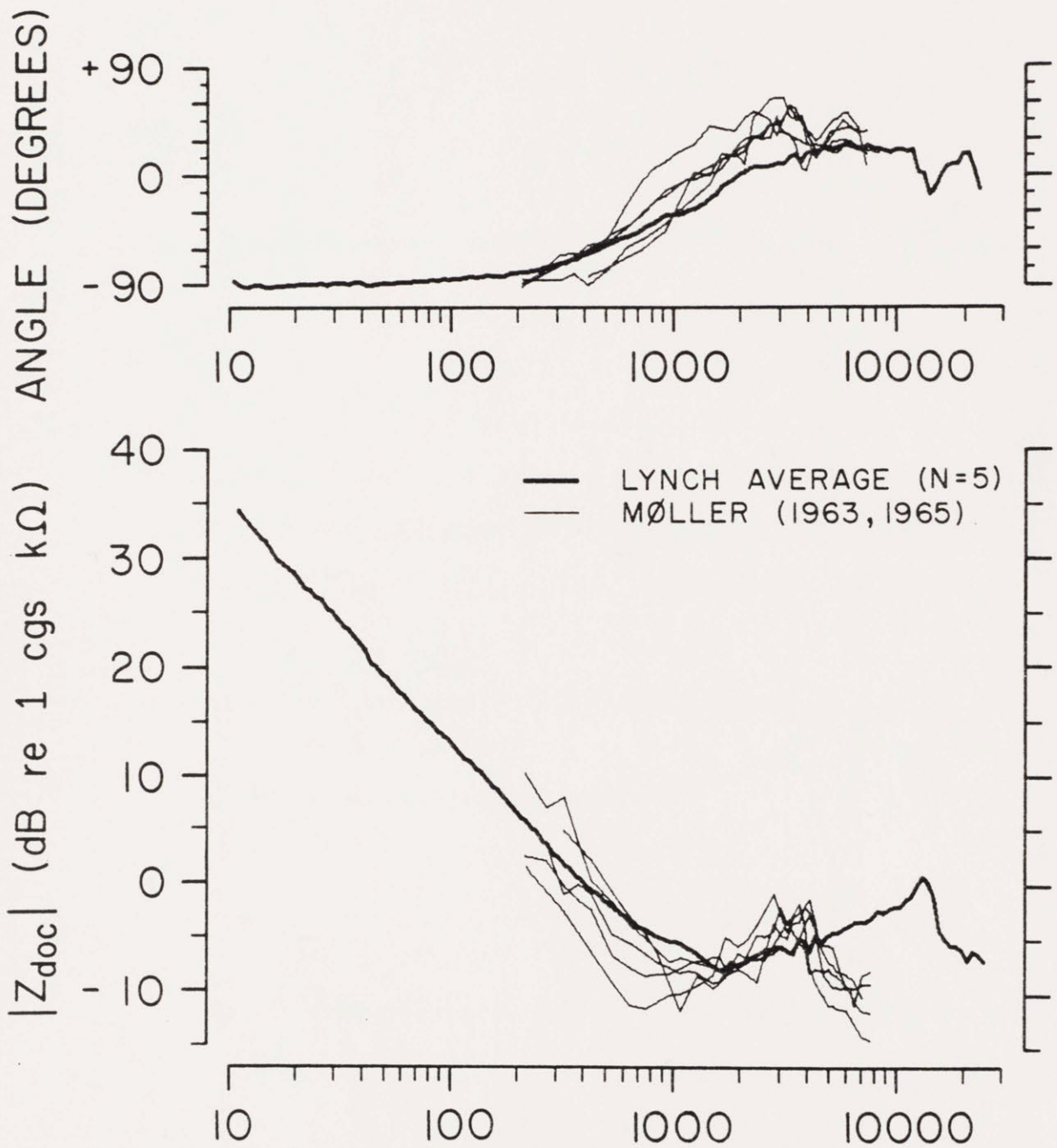


FIGURE 19

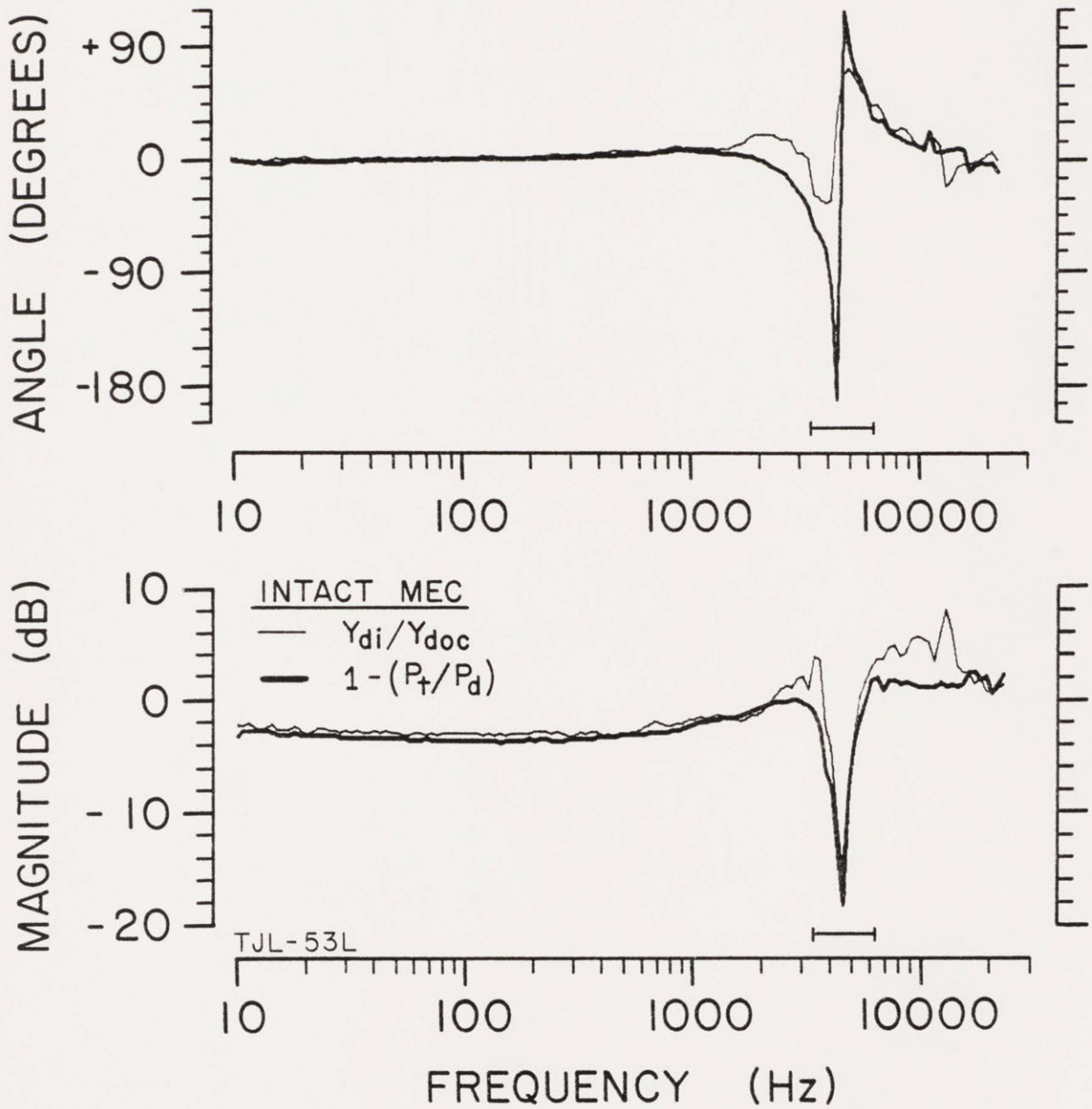
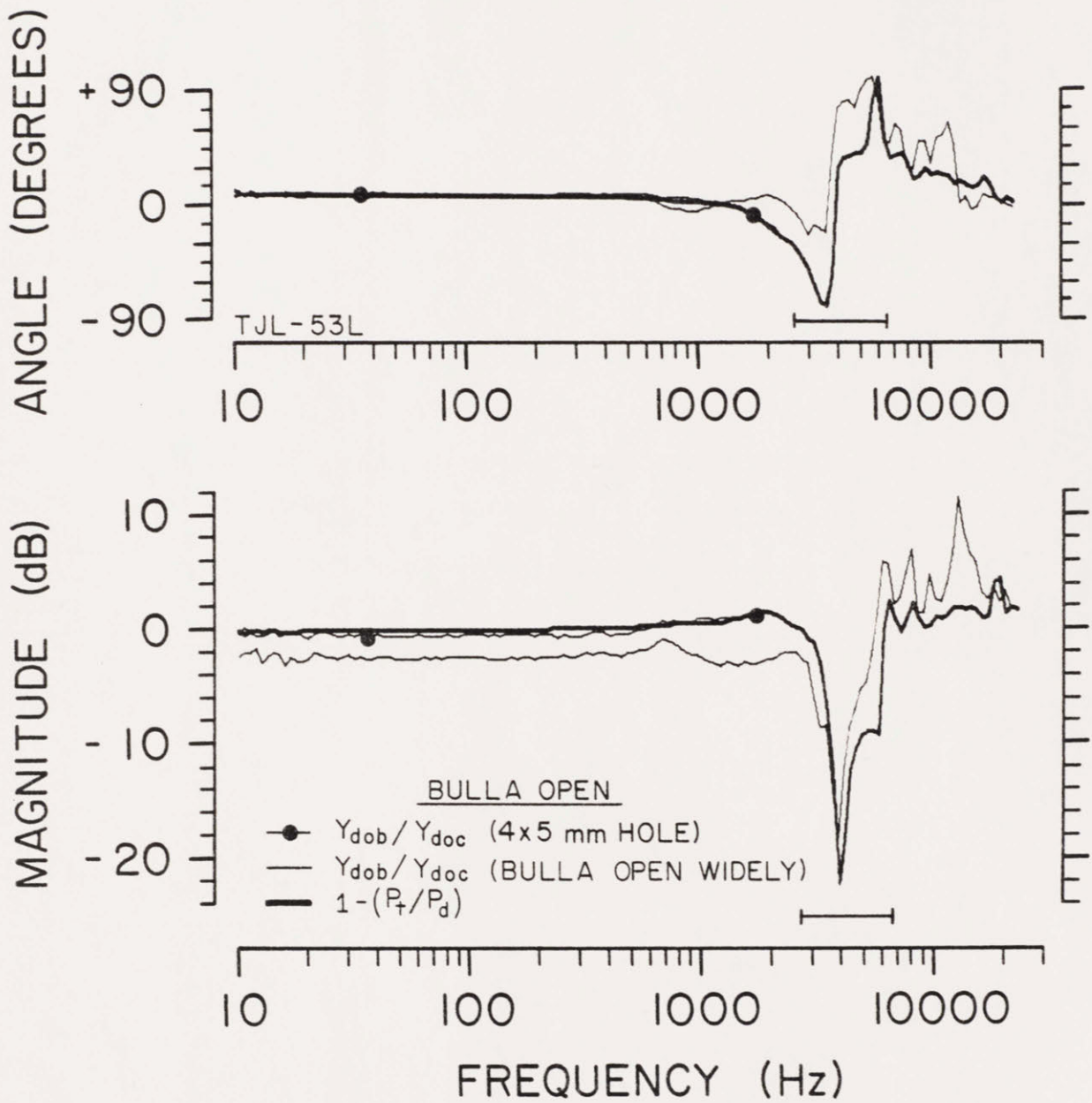


FIGURE 20



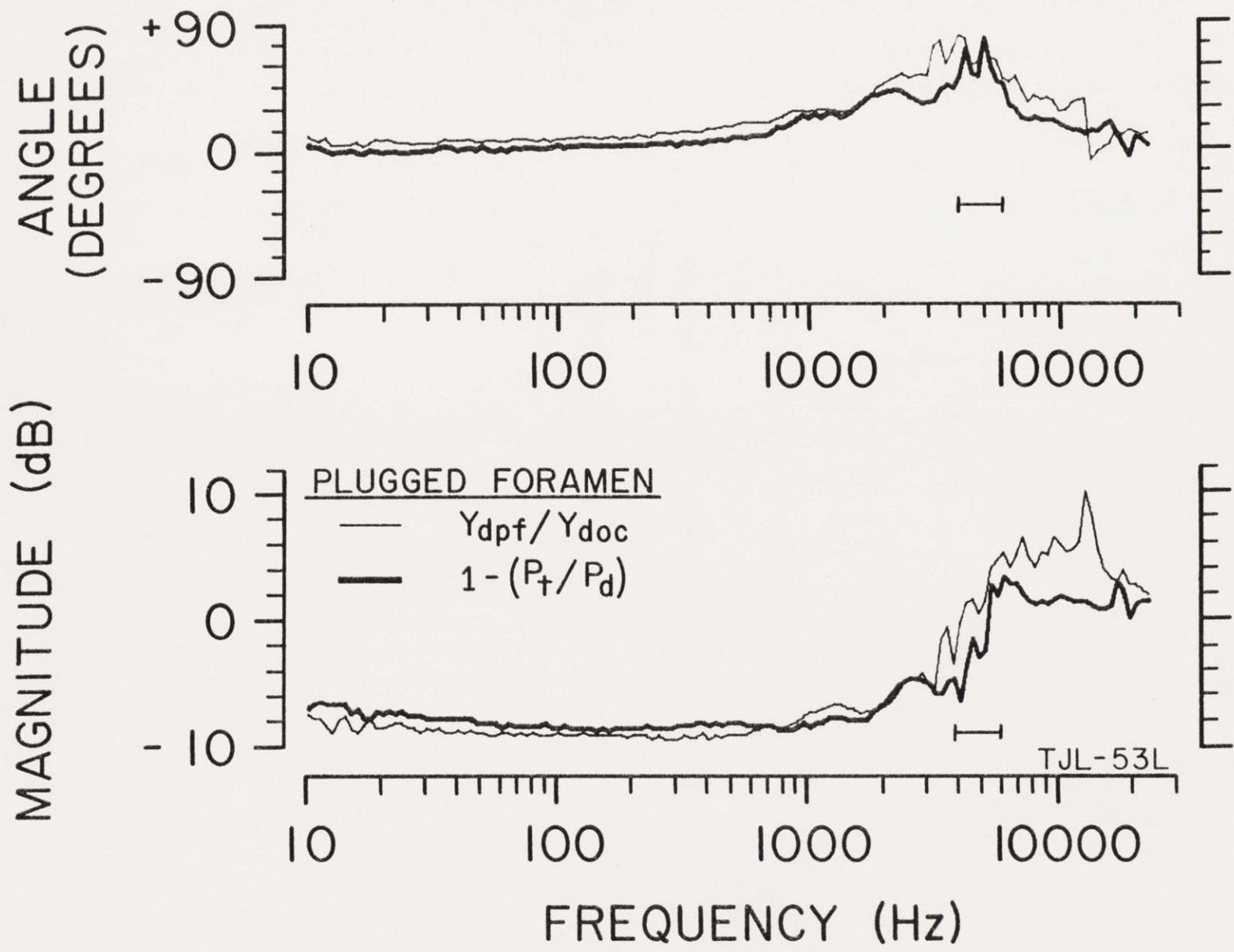


FIGURE 21

FIGURE 22

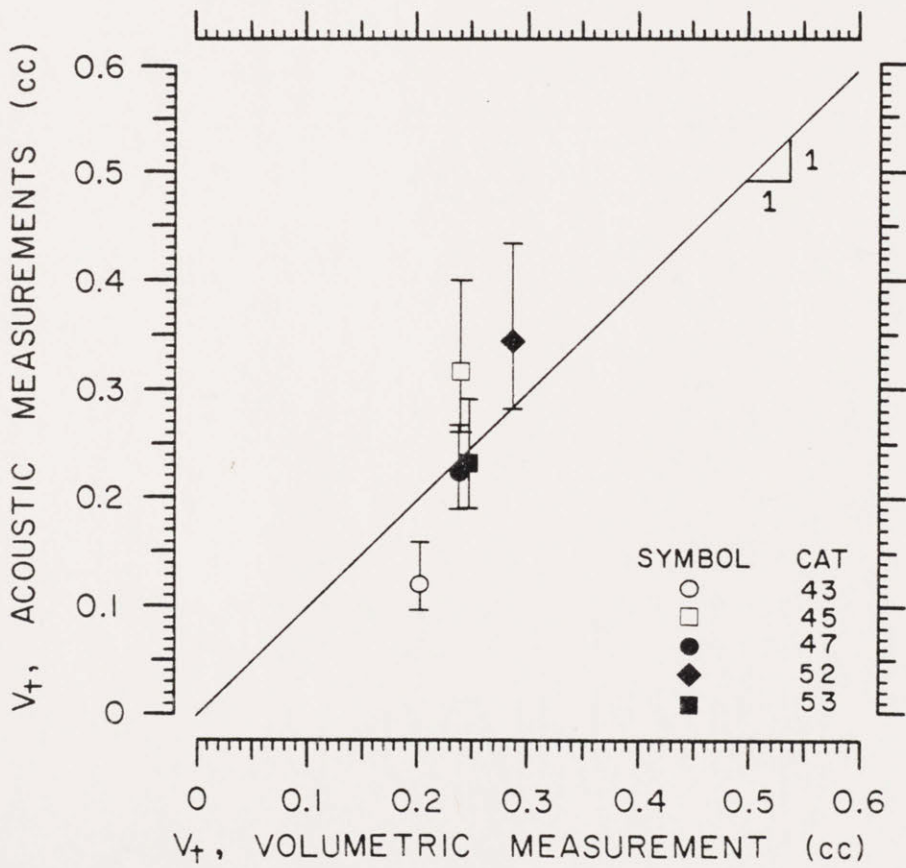
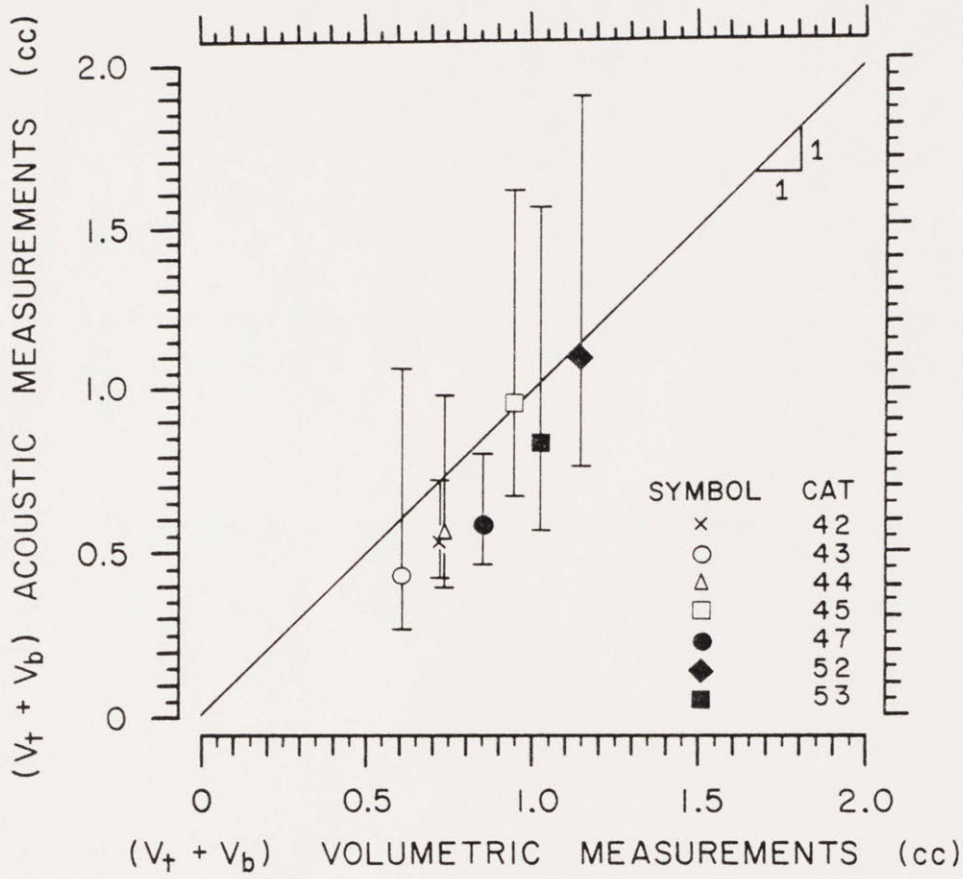


FIGURE 23

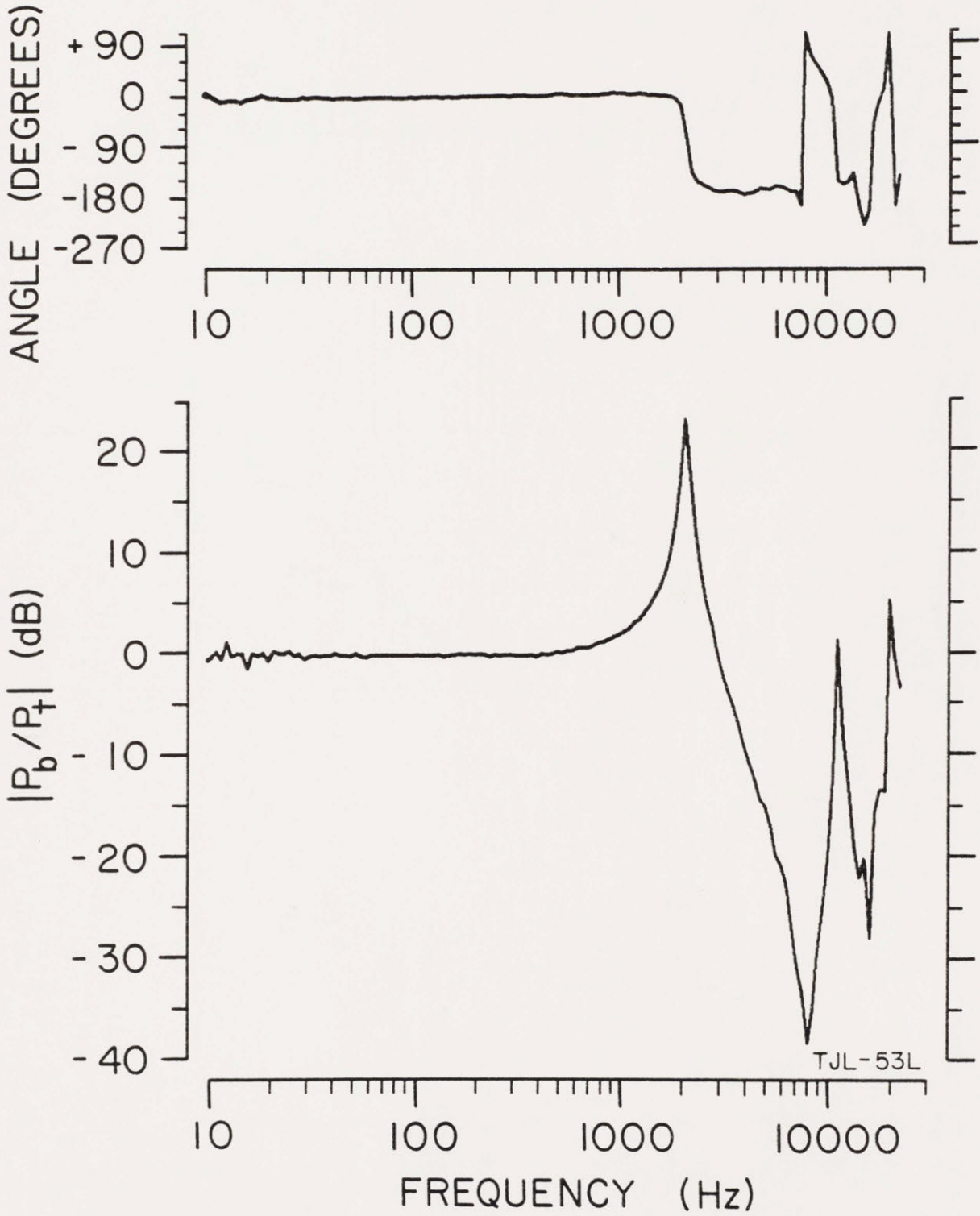


FIGURE 24

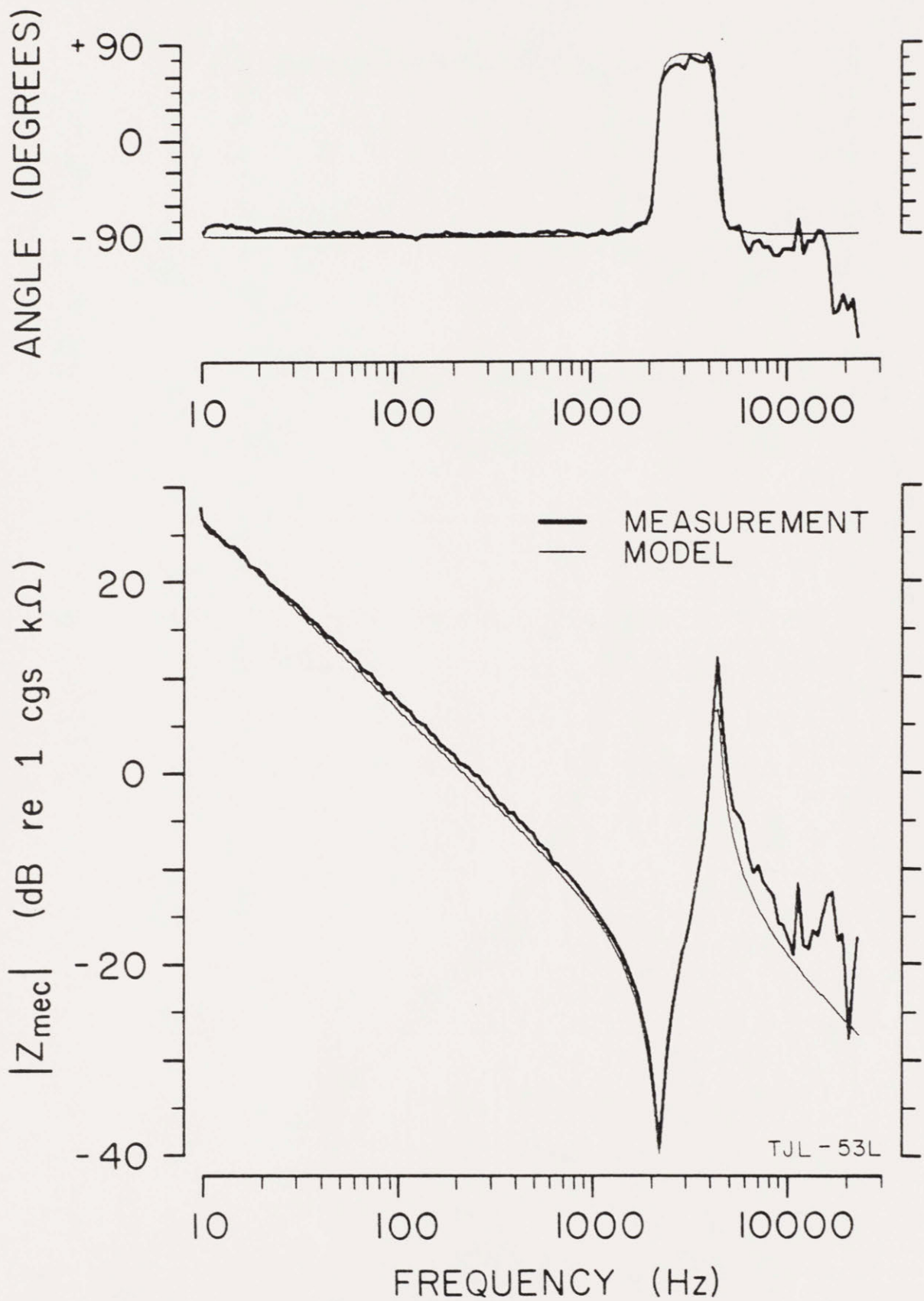


FIGURE 25

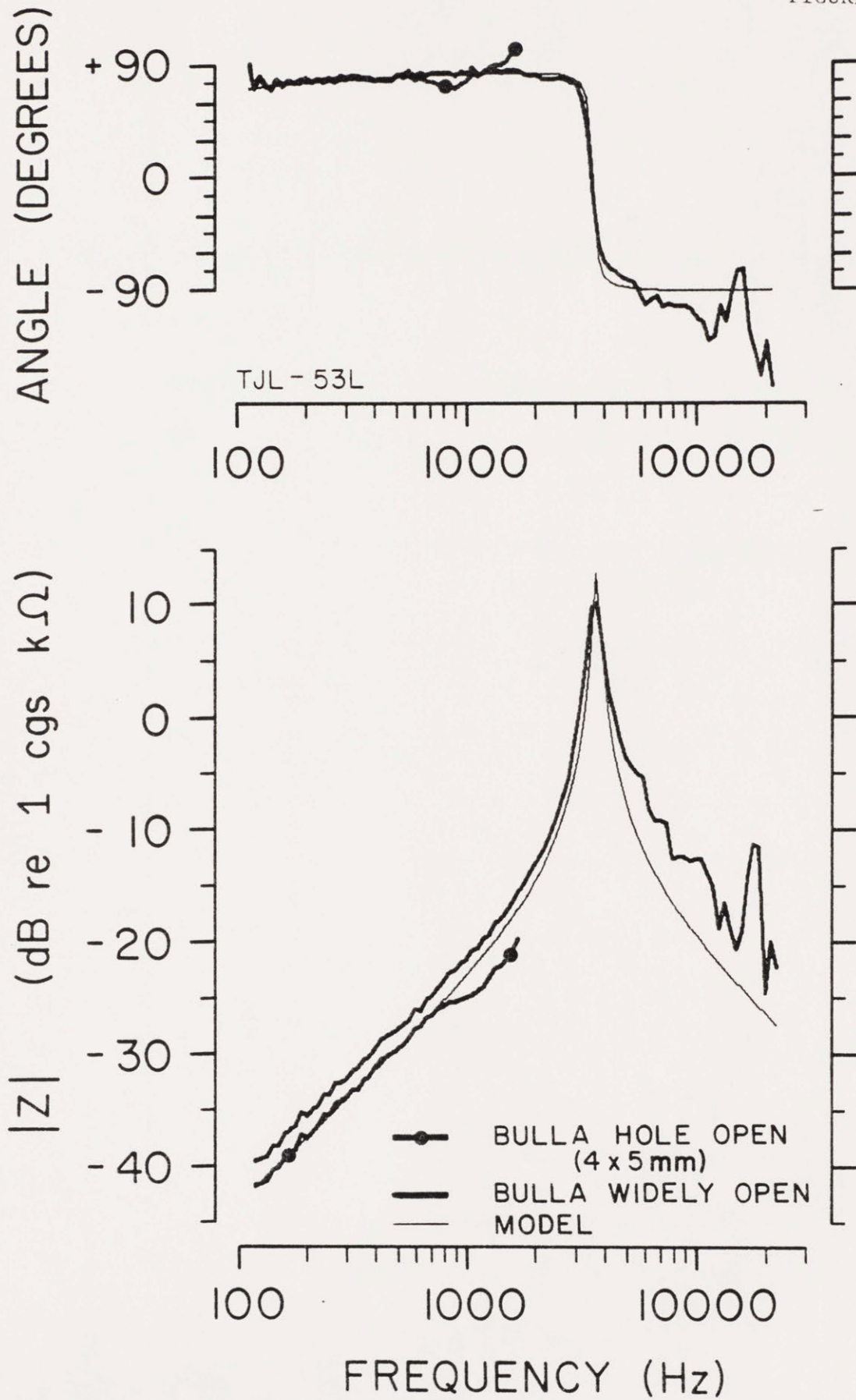
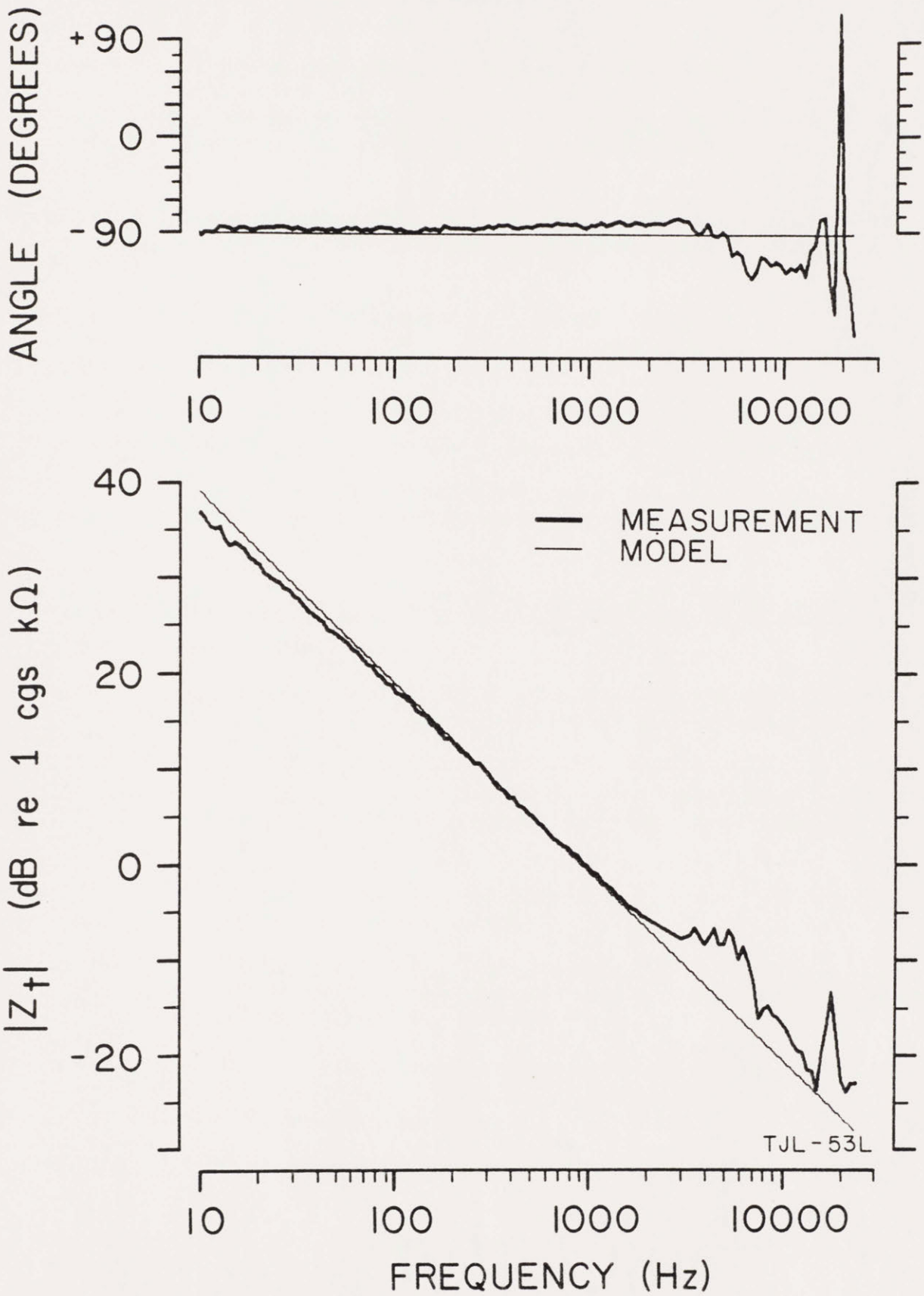


FIGURE 26



REFERENCES

- Beranek, L.L. (1954). Acoustics (McGraw-Hill, New York).
- Burkhard, M.D., and Sachs, R.M. (1977). "Sound pressure in insert earphone couplers and real ears," *J. Speech & Hear. Res.* 20(4), 799-807.
- Geisler, C.D., and Hubbard, A.E. (1975). "The compatibility of various measurements on the ear as related by a simple model," *Acustica* 33, 220-222.
- Geisser, D.I. (1972). "Measurements of Sound Pressure in Middle-Ear Cavities of Cats," S.B. Thesis, Massachusetts Institute of Technology, Cambridge, Ma., 121 pp.
- Guinan, J.J., Jr., and Peake, W.T. (1967). "Middle-ear characteristics of anesthetised cats," *J. Acoust. Soc. Am.* 42, 1237-1261.
- Ingard, U. (1948). "On the radiation of sound into a circular type, with an application to resonators," *J. Acoust. Soc. Am.* 20(5), 665-682.
- Khanna, S.M. (1970). "A holographic study of tympanic membrane vibrations in cats," Ph.D. Thesis, The City University of New York, New York, pp. 1-197.
- Khanna, S.M., and Tonndorf, J. (1972). "Tympanic membrane vibrations in cats studied by time-averaged holography," *J. Acoust. Soc. Am.* 51(6; Pt. 2), 1904-1920.
- Kruger, B., and Tonndorf, J. (1977). "Middle ear transmission in cats with experimentally induced tympanic membrane perforations," *J. Acoust. Soc. Am.* 61(1), 126-132.
- Lynch, T.J., III, Nedzelnitsky, V., and Peake, W.T. (in preparation). "Input impedance of the cochlea in cat."
- Margolis, R.H., Osguthorpe, J.D., and Popelka, G.R. (1978). "The effects of experimentally-produced middle ear lesions on tympanometry in cats," *Acta Otolaryngol.* 86, 428-436.
- Miller, S.P. (1973). "An Investigation of Middle Ear Pressure Measurements in Cats," B.S. Thesis, Massachusetts Institute of Technology, Cambridge, Ma., 69 pp.
- Møller, A.R. (1961). "Network model of the middle ear," *J. Acoust. Soc. Am.* 33 (2), 168-176.
- Møller, A.R. (1963). "Transfer function of the middle ear," *J. Acoust. Soc. Am.* 35(10), 1526-1534.

- Møller, A.R. (1965). "An experimental study of the acoustic impedance of the middle ear and its transmission properties," *Acta Otolaryngol.* 60, 129-149.
- Mundie, J.R. (1963). "The impedance of the ear--a variable quantity," (Middle Ear Function Seminar, May, 1963, Ft. Knox, Kentucky), U.S. Army Med. Res. Lab. Report No. 576, pp. 63-85.
- Nedzelnitsky, V. (1971). "Measurements of sound pressure in the cochleas of anesthetized cats," Sc.D. Thesis proposal, Massachusetts Institute of Technology, Cambridge, Massachusetts, pp. 1-108.
- Nedzelnitsky, V. (1980). "Sound pressures in the basal turn of the cat cochlea," *J. Acoust. Soc. Am.* 68(6), 1676-1689.
- Nuttall, A.L. (1974). "Measurements of the guinea-pig middle-ear transfer characteristic," *J. Acoust. Soc. Am.* 56(4), 1231-1238.
- Onchi, Y. (1949). "A study of the mechanism of the middle ear," *J. Acoust. Soc. Am.* 21(4), 404-410.
- Onchi, Y. (1961). "Mechanism of the middle ear," *J. Acoust. Soc. Am.* 33(6), 794-805.
- Peake, W.T., and Guinan, J.J. (1967). "Circuit model for the cat's middle ear," M.I.T. Research Laboratory of Electronics, Quarterly Prog. Rep. No. 84, 320-326.
- Tonndorf, J., and Khanna, S.M. (1967). "Some properties of sound transmission in the middle and outer ears of cats," *J. Acoust. Soc. Am.* 41(2), 513-521.
- Tonndorf, J., and Khanna, S.M. (1970). "The role of the tympanic membrane in middle ear transmission," *Ann. Otol. Rhinol. & Laryngol.* 79, 743-753.
- Wever, E.G., and Lawrence, M. (1954). Physiological Acoustics (Princeton University Press: Princeton).
- Zwislocki, J. (1957). "Some impedance measurements on normal and pathological ears," *J. Acoust. Soc. Am.* 29(12), 1312-1317.
- Zwislocki, J. (1962). "Analysis of the middle-ear function. Part I: Input impedance," *J. Acoust. Soc. Am.* 34(8; Pt. 2), 1514-1523.
- Zwislocki, J. (1963). "Analysis of the middle-ear function. Part II: Guinea-pig ear," *J. Acoust. Soc. Am.* 35(7), 1034-1040.

Chapter III

COMPONENTS OF THE ADMITTANCE OF THE CAT OSSICULAR CHAIN

I. INTRODUCTION

Our approach to understanding the mechanics of the middle ear was discussed in the introduction of CHAPTER II. The measurements of CHAPTER II determine the impedance of the middle-ear cavities and a model of this impedance. The input impedance of the annular ligament and stapes (Z_s), and cochlea (Z_c) have also been measured and modeled (Lynch et al., 1981). This report is concerned with the next step, namely, the determination of the properties of the tympanic membrane (TM) and ossicular chain.

A proposed network model of the middle ear with the middle ear cavities (MECs) completely removed is shown in FIGURE 1. The input admittance at the tympanic membrane for this condition will be referred to as Y_{doc} . In CHAPTER II we demonstrated the validity of the "series" model of CHAPTER II, FIGURE 1B (i.e. $Z_d = Z_{doc} + Z_{mec}$). Thus, we may determine the properties of the TM and ossicular chain independent of the impedance of the middle-ear cavities. We have measured Y_{doc} for various "experimental modifications" of the anatomical components of FIGURE 1 (e.g., removal of the cochlear "load", joint interruption, mass loading of the ossicles, fixation of the incus and stapes or malleus). These measurements can be used to determine or infer details concerning the mechanics of some of these anatomical components.

We have also determined the input admittance at the tympanic membrane with the MECs intact, Y_d , when static pressures were applied to the MECs. Since it is unlikely that the static pressures significantly affect the impedance of the middle-ear cavities, Z_{mec} , these results can be interpreted as effects upon Z_{doc} .

This chapter is a survey of some results concerning the mechanics of the TM and ossicular chain. Some of the "experimental modifications" were only performed in one animal; however, our confidence in the surgical manipulations and acoustic measurement results is the same as for results previously described in CHAPTERS I and II. Discussion and interpretation of these results and their integration into a complete network model for the cat middle ear remains to be done. A substantial amount of work concerning the modelling of some of these results and those of Guinan and Peake (1967) has been performed but is not reported here.

II. METHODSA. INPUT ADMITTANCE AT THE TM, Y_d , AND STATIC MEC PRESSURE

The Y_d admittance measurement system and the "correction" for the earcanal coupling space have been previously described in CHAPTERS I and II. Measurements reported here have been corrected for earcanal coupling space.

In two experiments Y_d was measured with static pressures applied to the middle-ear cavities. The equipment used to generate static pressures (Grason-Stadler 1720 otoadmittance meter) and to measure them (differential pressure transducer, Statham Instruments PM₊1-350) have been previously used for measurements in human (Rabinowitz, 1977). The DC output voltage of the pressure transducer was interfaced to a gain and offset control circuit (Rabinowitz, 1977) which was connected to a digital voltmeter (Hickok, 3400) so that DC pressure (re ambient) could be directly indicated in mm H₂O. A long length (2.2 m) of plastic tubing (\cong 0.2 cm i.d.) was used to connect the pressure source to the measurement transducer. Another tube (length = 2.2 m) of smaller diameter (0.08 cm i.d.) was placed between the transducer and bulla hole (0.15 cm diameter). The hole was placed on the medioventral surface of the bulla cavity. When changing the pressure source output, sufficient time was allowed for the pressure in the MECs to equalize to the new value. Static pressures (\pm 10 cm H₂O) were maintained constant with variations being less than \pm 0.1 cm H₂O.

B. SURGICAL PREPARATION AND EXPERIMENTAL MODIFICATIONS

The surgical procedures used to open the middle-ear cavities were described in Chapter II. For some of the measurements reported here, the styloid projection and the chorda tympani had been removed. Measurements of Y_{doc} before and after their removal indicated no significant change. In some instances we cut the ligament between the tensor tympani and malleus. The incudo-stapedial joint was interrupted using a miniature scalpel to separate the stapes from the sesamoid bone. The sesamoid bone was either removed completely or retracted onto the lenticular process of the incus. For the "interrupted manubrium" condition, we separated the manubrium from the rest of the malleus using a special tool to break the bone. The manubrium and its connection to the TM were left intact. Tissue glue (HISTOACRYL tissue adhesive, B. Braun Melsungen AG, Melsungen, W. Germany) was used to "reconnect" the incudo-stapedial joint after interruption or to "block" the ossicles (*i.e.*, affix them to the cavity wall). In one case we used zinc cement (S.S. White) to "block" the malleus, incus, and stapes. When gluing ossicles to the cavity wall with HISTOACRYL the periosteum on the wall surface was left intact. It was removed when using zinc cement. The integrity of the "block" appeared visually to be quite good. A relatively large force could be applied to the blocked ossicles (using a dental tool) without detecting any motion. Petrolatum was used to couple the 5.4 mg mass to the manubrium for measurements of "mass loading". The mass was always placed on the ventral surface of the manubrium midway between the umbo and the posterior end of the manubrium and did not touch the tympanic

membrane.

C. MEASUREMENTS OF OSSICULAR MASS

Ossicular masses were measured in five cats (nine ears). Results are listed in TABLE I. Ossicles were removed from live animals and measurements were usually made soon thereafter (i.e., within 2 hours). Cat 1968 is an exception; measurements were made 2 days after removal. A Mettler balance (Type M5SA, 50g maximum mass) having one microgram resolution was used. Measurements were repeatable to within 50 micrograms for the malleus and several micrograms for the incus and stapes. These measurements of stapes mass (average = 0.530 mg, with values ranging between 0.498 to 0.599 mg) are in good agreement with previously reported results (Lynch, 1974; Lynch et al., 1981) (average = 0.521 mg for six stapes with range of values between 0.422 to 0.618 mg). We also used this balance to determine the mass of the lead weight (5.4 mg) used to "load" the malleus.

III. RESULTS

A. EXPERIMENTAL MODIFICATIONS OF THE COCHLEA AND JOINTS

In this section we describe Y_{doc} measurements for which a component impedance of FIGURE 1 has been set to "zero" by an "experimental modification". Three cases are considered: 1) complete removal of the "cochlear load", i.e., $Z_c = 0$, 2) interruption of the incudo-stapedial joint, $Z_{\text{jis}} = 0$, and 3) interruption of the manubrium of the malleus ("shorting" a component of the total malleus impedance, Z_m , to acoustic ground).

1. Removal of the Cochlear "Load"

In one animal we measured the input admittance at the tympanic membrane, Y_{doc} , before and after removing the round window-membrane, scala vestibuli and tympani fluids, and basal portion of the basilar membrane (FIGURE 2). Comparison with the "NORMAL" result indicates that removal of the "cochlear load" produces a pronounced resonance at 1.9 kHz with $|Y_{\text{doc}}|$ increasing about 15 dB relative to the "NORMAL" result. Thus, the cochlear input impedance, Z_c , clearly has an effect upon the input impedance at the tympanic membrane for $800 \text{ Hz} < f < 2.8 \text{ kHz}$. At low frequencies the admittances are compliance dominated and are essentially identical. For frequencies between 2 to 4 kHz, the "COCHLEAR

LOAD REMOVED" result is predominantly mass controlled. At higher frequencies the magnitude and angle approach that of the "NORMAL" condition. Note however that for most frequencies in the range $4 \text{ kHz} < f < 12 \text{ kHz}$ the "NORMAL" $|Y_{\text{doc}}|$ is 3 dB to 4 dB larger.

2. Interruption of the Incudo-Stapedial Joint

FIGURE 2 also illustrates Y_{doc} obtained when the incudo-stapedial joint (ISJ) was interrupted after the "cochlear load" had been removed. The interrupted joint result is essentially identical to that with the cochlear load removed. The sesamoid bone was completely removed in this animal.

FIGURE 3 shows Y_{doc} before ISJ interruption ("NORMAL"), with the ISJ interrupted, and with the incus and stapes glued together with HISTOACRYL cement. The "NORMAL" and "RECONNECTED" measurements are quite close, indicating that the interruption did not otherwise alter the system and demonstrating the reversibility of this experimental modification. These results also suggest that the impedance of the incudo-stapedial joint, Z_{jis} , (for the normal or glued state) is much higher than that of the stapes and cochlea, $Z_{\text{sc}} = Z_{\text{s}} + Z_{\text{c}}$.

We have investigated the effects of interruption of the incudo-stapedial joint in four animals. Comparison of FIGURES 2 and 3 indicates some distinct differences between results from TJL-46 (FIGURE 2) and TJL-52 (FIGURE 3). 1) The low frequency compliance clearly changes for ISJ interruption in TJL-52 whereas essentially no

change was observed for TJL-46. 2) The increase in $|Y_{\text{doc}}|$ (≈ 22 dB) near 1.4 kHz for joint interruption is somewhat larger (≈ 7 dB) for TJL-52. 3) The interrupted ISJ measurement of TJL-52 contains a significant mass component (note the large negative angle) over a wider frequency range (i.e. $2 \text{ kHz} < f < 7 \text{ kHz}$). 4) The large magnitude minimum at 7.5 kHz with an associated 90° angle increase is only apparent for TJL-52.

Such comparisons can be conveniently observed in FIGURE 4 for all four animals. Incudo-stapedial joint interruption resulted in a 15 dB to 22 dB increase in $|Y_{\text{doc}}|$ for frequencies between 1.3 kHz to 2.2 kHz for these cats. Changes in the compliance at low frequency ranged from a 2 dB $|Y_{\text{doc}}|$ decrease to a 3.5 dB increase. Interruption generally decreased $|Y_{\text{doc}}|$ in the frequency region 3.5 kHz to 10 kHz, but tended to increase it slightly for frequencies above 10 kHz to 13 kHz.

Møller (1965) reports one measurement of Y_{doc} for the interrupted ISJ condition for $200 \text{ Hz} < f < 7 \text{ kHz}$. His result is quite similar to ours. He observed a ≈ 4 dB compliance increase at low frequencies, with the maximum increase in $|Y_{\text{doc}}|$ being 19.5 dB at 800 Hz. Above 4 kHz, his interrupted joint $|Y_{\text{doc}}|$ decreased relative to the intact measurement with the difference being about 8 dB at 6 kHz. Møller's frequency of maximum $|Y_{\text{doc}}|$ increase is roughly a factor of two smaller than our smallest frequency and is the only significant difference between results from these two studies.

3. Interruption of the Manubrium of the Malleus

We report measurements for the interrupted manubrium modification (IM) for only one cat (TJL-52). We have results for one other cat in which the incus and malleus were separated at the incudo-malleolar joint. Results from this manipulation were similar in nature to the IM results described below. Several experimental manipulations of the ossicular chain were made before the IM modification. The temporal sequence was as follows. Y_{doc} was first measured for the "NORMAL" and interrupted ISJ conditions (FIGURES 5 and 3). The stapes and incus were then reconnected (FIGURE 3) and subsequently glued to the cavity wall (FIGURE 8). At this point the malleus was interrupted at the manubrium (FIGURE 5).

From FIGURE 5 it is clear that the compliance at low frequencies with the manubrium interrupted decreased relative to the "NORMAL" value by approximately 3 dB. The frequency of the maximum in admittance magnitude is 1.5 kHz compared to 1.3 kHz for the interrupted ISJ condition. {This frequency shift is consistent with the observed compliance change assuming that a series mass-compliance model is valid and that the mass term remains constant; see Section IV B 4.} A mass component is clearly indicated in the IM results for frequencies above the resonance to 3 kHz. Note that the IM admittance magnitude has a relatively sharp admittance minimum near 3.3 kHz and that the angle increases nearly 90° in this region. This type behavior is also observed for the ISJ condition, but at a much higher frequency (7.5 kHz). For $4 \text{ kHz} < f < 10 \text{ kHz}$ the "NORMAL" and IM results are nearly identical. At higher frequencies the IM result has another magnitude minimum at 12 kHz,

and roughly parallels the "NORMAL" magnitude curve, at a lower admittance level; angle measurements are quite close for $f > 10$ kHz. It is also interesting to note the small relative minimum and maximum in $|Y_{doc}|$ near 2.3 kHz (IM condition) and 2.6 kHz (ISJ condition) with associated angle variations. A resonance and anti-resonance is apparently occurring at these frequencies. It is clear that similar behavior is seen in some Y_{doc} measurements for the condition of intact ossicular chain (e.g., FIGURE 2 and CHAPTER II, FIGURE 10).

B. "MASS LOADING" OF THE MANUBRIUM

A 5.4 mg piece of lead (rough dimensions are 0.2 cm x 0.07 cm x 0.07 cm) was used to experimentally "load" the manubrium of the malleus under two conditions: 1) intact ossicular chain, and 2) interrupted incudo-stapedial joint. The purpose of these tests was to manipulate the mass component of the ossicular chain. This mass is approximately half that of the malleus (see TABLE I). There is some evidence that the mass of the malleus and incus affect middle-ear transmission in cat. The model of Peake and Guinan (1967) required mass components for the malleus and incus to fit their transmission measurements. Preliminary measurements (Kopec, 1973) in which a mass was placed on the malleus (and TM) indicate that 1) the input impedance at the TM may be changed at some frequencies, and 2) significant transmission reductions can occur at both low and high frequencies. However, a measurement of transmission with and without mass loading of

the guinea pig stapes (Johnstone and Taylor, 1971) indicated no detectable change in transmission. In summary, direct measurements of the effects of mass loading of ossicular chain are almost nonexistent. There is interest in this issue since prosthetic ossicles are often used in surgical modifications of the human middle-ear.

1. "Mass Loading" of the Intact Ossicular Chain

In one animal we placed the mass on the manubrium when the ossicular chain was intact (FIGURE 6). The primary effect of this "mass loading" was to decrease $|Y_{doc}|$ (by as much as 8 dB) in the frequency region 1.5 kHz to 3.5 kHz. The angle was significantly changed over a broader frequency range. It appears that this manipulation introduced a mass component in Y_{doc} near 2 kHz since both magnitude and angle decrease and the angle becomes negative. The "MASS REMOVED" curve is very close to the "NORMAL" result in this frequency region which indicates the reversibility of the manipulation. There is essentially no change in low-frequency compliance resulting from the addition of the mass. It is interesting to note (and quite hard to see in FIGURE 6) that the addition of the mass caused nearly all of the small peaks and dips observed in the "NORMAL" curve (both magnitude and angle for $f > 3.5$ kHz) to shift to slightly higher frequencies. In summary, it is clear that this manubrium "loading" for an intact ossicular chain introduces an inertial component to the malleus impedance, Z_m , which is detectable in the input impedance at the tympanic membrane.

2. "Mass Loading" on the Interrupted Manubrium

We also placed the mass on the manubrium in an animal which had previously had its manubrium interrupted (FIGURE 7). This manipulation clearly increased the mass component of the admittance, with $|Y_{doc}|$ decreasing approximately 15 dB for $1.5 \text{ kHz} < f < 2.0 \text{ kHz}$. The frequency of the admittance maximum is lowered from 1.5 kHz to 1.1 kHz and corresponding angle changes occur. The relative admittance minimum near 3.3 kHz was also lowered to 2.1 kHz. The "MASS REMOVED" result indicates that the manipulation was essentially reversible. Note however, that the addition of the mass caused a 1 dB decrease in compliance at low frequencies which did not return to its pre-mass condition when the mass was removed. Thus, it appears that this "mass component" which must result from the mass of the manubrium and tympanic membrane, can be significantly increased by manubrium "loading" with a 5.4 mg mass.

C. "BLOCKING" OF THE OSSICLES

Measurements of admittance at the tympanic membrane with the ossicles "blocked" (i.e., rigidly glued to the boney wall) were made in two cats. In both cases we blocked the incus and stapes by gluing the region of their connection (ISJ) to the cavity wall. In one cat we also blocked the manubrium.

The effect of blocking the incus and stapes (with HISTOACRYL) is shown in FIGURE 8. A large decrease ($\cong 15 \text{ dB}$) in low frequency

compliance is the primary effect; the "NORMAL" compliance is $C_{\text{doc}} = 6.0 \times 10^{-7} \text{ cm}^5/\text{dyn}$ and the "BLOCKED" incus and stapes compliance is $C = 1.1 \times 10^{-7} \text{ cm}^5/\text{dyn}$. The "NORMAL" and "BLOCKED" results are generally similar in magnitude for $f > 2\text{kHz}$ with angle measurements being in good agreement for $f > 5 \text{ kHz}$. In principle, the Z_{doc} measurement with the incus and stapes blocked should be the parallel combination of Z_{tmu} and the impedance $(Z_{\text{tmc}} + Z_{\text{m}} + Z_{\text{jim}})$ (FIGURE 1).

Results from the other cat were obtained with a different configuration of the acoustic source which limited measurements to $f < 2 \text{ kHz}$. Blocking of the incus and stapes in this cat (zinc cement) resulted in a decrease in low frequency compliance of 16.5 dB. The normal compliance is $C_{\text{doc}} = 5.3 \times 10^{-7} \text{ cm}^5/\text{dyn}$, and the blocked incus and stapes compliance is $C_{\text{bis}} = 8.0 \times 10^{-8} \text{ cm}^5/\text{dyn}$. {Thus, the C_{doc} values and the compliance changes for both cats are quite similar.} Subsequent blockage of the manubrium decreased the low-frequency compliance to $C_{\text{tmu}} = 5.3 \times 10^{-8} \text{ cm}^5/\text{dyn}$, a 3.6 dB decrease relative to that with the incus and stapes blocked. The model of FIGURE 1 predicts that Z_{doc} for the condition of blocked malleus is a direct measurement of the "uncoupled tympanic membrane" impedance, Z_{tmu} . Therefore C_{tmu} is the compliance component of this impedance.

Møller (1965) reports one case for which the malleus was immobilized by fixation to the middle-ear walls with dental cement. For $f < 2.5 \text{ kHz}$ his input-impedance magnitude was larger than his "normal" impedance, and for $3 \text{ kHz} < f < 7 \text{ kHz}$ the normal and blocked input-impedances were similar in magnitude. This result is generally similar to our blocked incus/stapes measurement (FIGURE 8) for

3 kHz $< f < 7$ kHz. However, the detailed frequency dependence of his blocked result is considerably different from our measurements at low frequencies. Our results for blocked manubrium or blocked incus/stapes are clearly compliance like at low frequencies with 6 dB/octave slope in $|Y|$ and angle of 90° . Møller's result has angles between 60° and 90° (he did not report angles at some frequencies) with magnitude slope of 6 dB/octave in one frequency region and slope of 18 dB/octave at the lowest frequencies.

D. EFFECTS OF POSITIVE AND NEGATIVE STATIC MEC PRESSURES

Y_d , the input admittance with MECs intact was measured in two cats for which the static middle-ear cavity pressure was manipulated. We report here the results for one live animal. The other cat died suddenly at the beginning of the measurement session. In this case a 4.5 dB decrease in low-frequency compliance, C_{doc} , (i.e., the compliance with bulla hole open) was observed upon death (within 10 minutes). Otherwise, results for the dead cat (for $f < 4$ kHz) are similar to those reported for the live cat. A larger range of static pressures (± 30 cm H_2O) was used for the dead cat.

FIGURE 9 illustrates frequency responses of Y_d taken at various negative and positive static pressures in the range ± 10 cm H_2O . FIGURE 10 displays these same data in terms of admittance and impedance "tympograms". It is quite clear that changes in static pressure (re ambient) decrease the low-frequency $|Y_d|$ and hence, compliance

(FIGURE 10A). Larger changes occur for all positive MEC pressures except +1.0 cm H₂O. Note that MEC pressure variations have little effect on Y_d in the frequency region near 4 kHz (FIGURE 9) where Y_d is dominated by the impedance of the middle-ear cavities, Z_{mec} , rather than by that of the TM and ossicular chain, Z_{doc} (see Chapter II). In the frequency region $1 \text{ kHz} < f < 3.6 \text{ kHz}$ the effects are more complicated. Tympanograms for $f = 1 \text{ kHz}$ and $f = 2 \text{ kHz}$ (FIGURES 10B, 10C) indicate that the $|Y_d|$ maximum occurs at a static pressure other than zero. Note that the plots of $|Y_d|$ vs static pressure for these two curves are "bell shaped". This behavior disappears as one approaches frequencies just below the MEC resonance at 4 kHz. For example, at $f = 3.35 \text{ kHz}$ (FIGURE 10D) $|Y_{doc}|$ increases for larger negative pressures and a mass component becomes noticeable. This mass component becomes more prominent at frequencies above the MEC resonance (FIGURE 10E).

IV. DISCUSSION

A. ON THE "TRANSFORMER RATIO" OF THE MIDDLE EAR

The simple conception of the middle ear as a mechanical transformer which "matches impedances" between the "low" acoustic impedance of air and the "high" acoustic impedance of the cochlear fluid is quite prevalent in the literature on middle-ear mechanics (Wever and Lawrence, 1954). Siebert (1973) and Schubert (1978) have noted significant problems with this point of view. Siebert (1973) concludes that "matching is achieved at best over the limited frequency range 3-5 kHz" and that "to consider the middle ear as just an impedance matching device is to oversimplify effects that are much more subtle".

The effects of the middle-ear cavities, which were presented in CHAPTER II, are clearly a feature of middle-ear signal transmission which is not included in the transformer model. The extent to which the middle-ear functions as an "ideal" transformer (IT) can be determined from our impedance measurements. If the middle ear were an IT then input impedance at the tympanic membrane Z_{doc} , would be a scaled version of the input impedance of the cochlea, Z'_c (this notation is not consistent with Lynch et al., 1981) for all frequencies. That is, $Z_{\text{doc}}(f) = Z'_c(f)/T^2$ where T , the transformer ratio, is a real number independent of frequency; note that, in general Z'_c and Z_{doc} are complex numbers. Our measurements of Z_{doc} for interrupted ISJ or cochlear "load" removed (FIGURES 2, 3, 4) clearly indicate that Z_{doc} is controlled by the

cochlear impedance only for a range of frequencies between 500 Hz and 3 kHz. Outside this frequency region Z_{doc} is apparently influenced by the ossicular chain and tympanic membrane (see Section IV B).

We can calculate a transformer ratio, T , from our previous measurements of cochlear impedance (Lynch et al., 1981) and our present Z_{doc} measurements (CHAPTERS II and III). Lynch et al. found Z'_c to be resistive with value $R_c = 1.2 \times 10^6 \text{ dyn-s/cm}^5$, for $500 \text{ Hz} < f < 5 \text{ kHz}$ and demonstrated that it is "primarily determined by the basilar membrane and cochlear fluids". The "NORMAL" and "COCHLEAR LOAD REMOVED" measurements of FIGURE 2 show that in this experiment the cochlear impedance controls Z_{doc} only over the frequency range $800 \text{ Hz} < f < 2.8 \text{ kHz}$. Furthermore, only in the upper part of this frequency range ($2.1 \text{ kHz} < f < 3.0 \text{ kHz}$) is the "NORMAL" Z_{doc} resistive (i.e., angle $0^\circ \pm 9^\circ$), with $R_{\text{doc}} = 560 \text{ dyn-s/cm}^5$. Since both Z_{doc} and Z'_c are resistive we can compute a "transformer ratio", $T = \{R_c/R_{\text{doc}}\}^{0.5} = 46$, which approximately represents middle-ear mechanical behavior over a small frequency range $2.1 \text{ kHz} < f < 2.8 \text{ kHz}$.

From FIGURE 4 it is clear that the frequency for which interruption of the ISJ makes the largest change in $|Z_{\text{doc}}|$ varies from animal to animal ($1.3 \text{ kHz} < f < 2.2 \text{ kHz}$). Our average Z_{doc} results (CHAPTER II, FIGURE 18) have resistance $R_{\text{doc}} = 445 \text{ ohms}$ with angle $0^\circ \pm 9^\circ$ for $1.6 \text{ kHz} < f < 3.0 \text{ kHz}$. Using the average R_{doc} value we compute $T = 52$. Thus, the "average" middle ear has a transformer ratio of $T \cong 52$ which approximately characterizes the mechanics for frequencies in the vicinity of 2 kHz to 3 kHz.

Another issue that arises in connection with the transformer ratio

is its interpretation in terms of the anatomical and mechanical properties of middle-ear components. The transformer ratio can be written as, $T = A_d l_m / A_s l_i$, where A_d and A_s are the "effective" eardrum and stapes footplate areas and l_m/l_i is the ratio of "effective" lever arm lengths of the malleus and incus respectively. The anatomical area of the TM in cat is 0.36 cm^2 to 0.465 cm^2 with the average value (of four ears) being 0.418 cm^2 (Wever et al., 1948). A_s has been previously determined (Wever et al., 1948; Guinan and Peake, 1967; Lynch et al., 1981) and is $1.26 \times 10^{-2} \text{ cm}^2$ assuming the stapes footplate motion is piston-like translation. Guinan and Peake (1967) determined a value of $l_m/l_i = 2$ for cat from measurements of displacement at the tip of the manubrium and at the incudo-stapedial joint. If we assume 2 is the "effective" lever ratio and use $T = 52$ and $A_s = 1.2 \times 10^{-2} \text{ cm}^2$, the "effective" eardrum area is, $A_d = (TA_s)(l_i/l_m) = 0.31 \text{ cm}^2$. Thus, we obtain an "effective" area of the TM that is 74% of the average anatomical area.

In summary, the "transformer action" of the cat middle ear is the dominant property only for a narrow range of frequencies near 2 kHz to 3 kHz. It is clear that outside this frequency range models of the mechanical operation of the middle-ear must include impedances of the tympanic membrane and/or the ossicular chain and middle-ear cavities in addition to the transformer. The precise mechanical mechanisms that are involved in determining the "transformer ratio" and possible frequency dependence of the ratio remain to be determined.

B. Z_{doc} : IMPLICATIONS FOR MODELS OF CAT MIDDLE-EAR MECHANICS

We can use our measurements of admittance at the tympanic membrane for the "normal" and "experimentally modified" states of the middle ear to determine the influence of the component impedances of FIGURE 1 upon normal middle-ear mechanics. The middle-ear model of FIGURE 1 is similar in structure to that of Peake and Guinan (1967), which was constructed to fit their measurements of middle-ear transmission. Note that in both models all the impedances have been referred through whatever transformer mechanisms are present to the tympanic membrane (e.g., the acoustic impedance of the stapes, annular ligament and cochlea are scaled by $1/T^2$, $Z_s = Z'_s/T^2$, $Z_c = Z'_c/T^2$, FIGURE 1). Conversion of the Peake-Guinan model and the model of FIGURE 1 into equivalent acoustic impedance forms (in which the transformer is explicitly shown) has been previously discussed in detail (Lynch, 1978).

1. Z_{jis} : The Incudo-Stapedial Joint Impedance

Available evidence (for cat) indicates that the impedance of the incudo-stapedial joint is high relative to that of the stapes, annular ligament and cochlea, $Z_{sc} = Z_s + Z_c$ (FIGURE 1). Guinan and Peake (1967) state that their "measurements show no appreciable flexing of the incudo-stapedial joint for displacements in the linear range" and therefore Z_{jis} was not included in their middle-ear model (Peake and Guinan, 1967). This view is consistent with our Z_{doc} impedance results

(FIGURE 3) where we found no significant difference between "NORMAL" or "RECONNECTED" states of the ISJ. Presumably, the joint was quite rigidly fixed by cement used to "reconnect" the incus and stapes. Furthermore, in this cat we had also measured Y_{doc} with the ISJ clearly interrupted, but with the sesamoid bone in place so that the incus and stapes were in contact. Y_{doc} for this condition was nearly identical to the "NORMAL" result, with the only significant difference being a 1 dB decrease in low-frequency compliance relative to the "NORMAL" curve for $f < 600$ Hz (i.e., a compliance very close to the compliance of the "RECONNECTED" curve). Apparently the static forces acting on the joint in this instance were sufficient to provide coupling between the stapes and incus; the relatively large magnitude of Z_{jis} was not dependent on the integrity of the connective tissue between the stapes and incus. In summary, Z_{jis} is apparently a high "shunt" impedance and therefore need not be considered in subsequent discussions of the model of FIGURE 1.

2. Components of the Low-Frequency Compliance, C_{doc}

For low frequencies we can use a simplified form of the model of FIGURE 1 and determine the components of the input compliance, C_{doc} , for the intact ossicular chain. We will ignore Z_{jis} , for reasons given in the preceding section, and will assume that the compliance of the incus impedance, Z_i , is negligible. The impedances Z_{tmu} , Z_{jim} , Z_{sc} and $(Z_{tmc} + Z_m)$ are represented by compliances C_{tmu} , C_{jim} , C_{sc} and C_{eq} respectively, which are estimated below.

The compliance of the annular ligament is $C'_{sc} = 0.36 \times 10^{-9} \text{ cm}^5/\text{dyn}$ (Lynch et al., 1981) which becomes $C_{sc} = T^2 C'_{sc} = 9.7 \times 10^{-7} \text{ cm}^5/\text{dyn}$ ($T = 52$) when referred to the TM side of the transformer (assuming the transformer ratio is independent of frequency). Our measurement of Z_{doc} with manubrium blocked yields an estimate of the impedance Z_{tmu} (Section III C). For $f < 2 \text{ kHz}$ the result indicates that $C_{tmu} = 5.3 \times 10^{-8} \text{ cm}^5/\text{dyn}$ which is a factor of 10 smaller than the compliance measured for the intact ossicular chain, $C_{doc} = 5.3 \times 10^{-7} \text{ cm}^5/\text{dyn}$. The compliance measured at the tympanic membrane with the incus and stapes blocked is $C_{bis} = 8.0 \times 10^{-8} \text{ cm}^5/\text{dyn}$. The above values of C_{sc} , C_{tmu} , C_{doc} and C_{bis} can be used to calculate C_{eq} and C_{jim} using the following procedure. The input compliance with the incus and stapes blocked, C_{bis} , is predicted by the model to be

$$C_{bis} = C_{tmu} + \frac{C_{eq} C_{jim}}{C_{eq} + C_{jim}} . \quad (1)$$

Similarly, the input compliance for the intact ossicular chain is

$$C_{doc} = C_{tmu} + \frac{C_{eq} (C_{jim} + C_{sc})}{C_{eq} + C_{jim} + C_{sc}} . \quad (2)$$

Substituting the above values for C_{sc} , C_{tmu} , C_{doc} and C_{bis} into Equations (1) and (2) and solving for C_{eq} and C_{jim} (we have a second order equation in either unknown compliance and take the positive root) we obtain the result, $C_{eq} = 9.1 \times 10^{-7} \text{ cm}^5/\text{dyn}$ and $C_{jim} = 2.7 \times 10^{-8} \text{ cm}^5/\text{dyn}$. Thus, the "shunt" compliances C_{tmu} and C_{jim} are much smaller than the "series"

compliances C_{eq} and C_{sc} . We can therefore think of the resulting model as consisting primarily of two series "stiffness" elements ($K = 1/C$); one resulting from the annular ligament, $K_{sc} = 1/C_{sc} = 1.0 \times 10^6 \text{ dyn/cm}^5$ and the other from the coupled TM and malleus suspension, $K_{eq} = 1.1 \times 10^6 \text{ dyn/cm}^5$, which total (approximately) to the input stiffness, $K_{doc} = 1/C_{doc} = 1.9 \times 10^6 \text{ dyn/cm}^5$ of the intact ossicular chain.

In conclusion, it is apparent that at low frequencies the "shunt" elements of C_{tmu} and C_{jim} provide high impedances and therefore have only small "shunting" effects; the low-frequency stiffness of the annular ligament and coupled TM/malleus are comparable. The above numerical values predict that if the ISJ were "interrupted", the resulting change in input-compliance at the TM, C_{doc} , would be an increase of 5.6 dB which is roughly consistent some of the results of FIGURE 4. This type of model can only predict increases in C_{doc} for ISJ interruption. In cases where C_{doc} was decreased by ISJ interruption, it is possible that large displacements during the manipulation caused a relatively "long term" change in stiffness of the TM or malleus/incus suspension. We noted "long term" changes in stiffness (when manipulating static MEC pressures) that could be eliminated by alternately applying decreasing positive and negative MEC pressures. Another possibility might involve the effects of perilymphatic pressure upon static position of the annular ligament, (Lynch et al., 1981)

3. High Frequencies: Effects of Z_{tmu}

At high frequencies Z_{tmu} may play a significant role. Our one direct measurement of Z_{tmu} (blocked malleus) was valid only for $f < 2\text{kHz}$. The blocked incus and stapes measurements of FIGURE 8 are an indirect test of the "shunting" issue. However, they are consistent with the view that "shunting" by Z_{tmu} , is significant at medium to high frequencies. The "NORMAL" and "BLOCKED INCUS AND STAPES" measurements have similar magnitudes for $f > 2\text{ kHz}$ with angle measurements being in good agreement for $f > 5\text{ kHz}$. The "approximate" agreement of these results for $f > 2\text{ kHz}$ implies that the input-impedance to the right of node B of FIGURE 1, Z_{NB} , for the "NORMAL" condition is roughly equivalent to an open circuit (i.e., the "BLOCKED" condition) in its effect on Z_{doc} . However, the results of Guinan and Peake (1967) indicate that $|Z_{jim}| \cong |Z_{NB}|$ for frequencies near 10 kHz; thus, Z_{jim} cannot be ignored when modelling middle-ear transmission (Peake and Guinan, 1967). These impedance and transmission results could be consistent if both Y_{doc} measurements of FIGURE 8 are primarily determined by Z_{tmu} at high frequencies. A high-frequency measurement of Z_{doc} with the malleus blocked is needed to resolve this issue.

There are other indications that the Z_{tmu} controls Z_{doc} at high frequencies. For $4\text{ kHz} < f < 10\text{ kHz}$ the IM and "NORMAL" results are nearly identical (FIGURE 5). Measurements with IM (FIGURE 7) clearly have a mass component in the 1.5 kHz to 3 kHz region. This presumably results from a component of the malleus impedance which is due to the manubrium ($Z'_m = j\omega M'$). For this experimental condition, Z_{tmu} is

effectively in parallel with $Z'_m + Z_{tmc} = j\omega M' + 1/(j\omega C_{tmc})$. Manipulation of Z'_m by the addition of the 5.4 mg mass causes the resonance in Z_{doc} to shift to a lower frequency (consistent with the mass addition). For frequencies above the resonance $Z'_m + Z_{tmc} \cong j\omega M'$. If $|Z_{tmu}| \gg |Z'_m|$ then the resulting Z_{doc} measurement should be mass dominated at all frequencies above the resonance. Close comparison of FIGURES 5 and 7 indicates that the "NORMAL" $|Z_{doc}|$ and the mass-loaded impedance magnitudes are quite close for $f > 3$ kHz. Thus, Z_{tmu} must control this Z_{doc} for frequencies above 3 kHz to 4 kHz. This view is also supported by the results with a mass added to the manubrium for the condition of intact ossicular chain. The significant mass component of Z_m which appears for the mass loading result of FIGURE 6 also disappears for $f > 3.8$ kHz, presumably because $|Z_m|$ becomes much larger than $|Z_{tmu}|$ at higher frequencies. The fact that the interrupted ISJ results of FIGURE 4 become negative above 3 kHz to 4 kHz but are near 0 dB at very high frequencies also supports the above "shunting" conclusion.

4. Inertial Effects of the Malleus and Incus

The "mass loading" effects observed for the condition of intact ossicular chain (FIGURE 6) and interrupted manubrium (FIGURE 7) suggest that the mass component of the malleus impedance, Z_m , does not significantly contribute to the input impedance, Z_{doc} , of the intact middle ear. We can estimate the inertial effects of the ossicles using the measurements with interrupted ISJ and mass loading with intact

ossicular chain.

For a rotational system such as the ossicular chain, acoustic mass (M^a) and mechanical mass (M^m) are related by $M^a = (M^m k^2) / (A_d l_m)^2$, where k is radius of gyration. The product, $A_d l_m$, can be calculated as $A_d l_m = T A_s l_i = 0.125 \text{ cm}^3$ using $T = 52$, $A_s = 1.2 \times 10^{-2} \text{ cm}^2$, and an estimate of the effective torque arm of the incus, $l_i = 0.2 \text{ cm}$, based on an approximate measurement. Manubrium loading by the $M^m = 5.4 \text{ mg}$ mechanical mass (intact ossicular chain) produced an acoustic mass component in the admittance measurement (FIGURE 6) at 2.2 kHz of $M^a = 1/(|Y|\omega) = 0.072 \text{ g/cm}^4$. Using these values we calculate the radius of gyration, $k = 0.46 \text{ cm}$ which appears to be quite reasonable considering the geometry and dimensions of the malleus and the location of the 5.4 mg mass upon the manubrium.

We can also estimate the radius of gyration for the malleus and incus using an estimate of acoustic mass derived from the ISJ admittance measurement of FIGURE 5. Assuming that this result can be represented by a series mass-compliance (MC) network with resonant frequency $f = 1/\{2\pi(MC)\}^{0.5}$, we can calculate the acoustic mass component using the measured resonant frequency and low-frequency compliance. This computation results in an acoustic mass estimate of $M^a = 0.022 \text{ g/cm}^4$ for interrupted ISJ. Using the above value for $A_d l_m$ and our average measurements of malleus and incus mass ($11.1 + 4.3 = 15.4 \text{ mg}$, TABLE I) we calculate $k = 0.15 \text{ cm}$. The moment of inertia of the malleus and incus is ($k^2 M^m$) is 0.35 mg-cm^2 . These values are in reasonable agreement with those of Funnell (1975) who used a "geometrically simplified model" of the cat ossicles with an estimated incudo-malleolar mass of 11 mg to

estimate the moment of inertia for various rotational axes. He found the moment of inertia to be approximately 0.12 mg-cm^2 "for reasonable axis locations" with $k = 0.1 \text{ cm}$. The results of FIGURE 5 indicate that the mass component with the ISJ interrupted is roughly equal to that with the manubrium interrupted. This implies that the manubrium and TM are the major source of the mass component for the ISJ condition.

C. IMPLICATIONS FROM MEASUREMENTS OF STATIC MEC PRESSURE

In Section B 2 we concluded that at low frequencies the total middle ear stiffness, $K_{\text{doc}} = K_{\text{eq}} + K_{\text{sc}}$, is the sum of the stiffness of the coupled TM/malleus (K_{eq}) and annular ligament (K_{sc}). The results of FIGURES 9 and 10 indicate that static middle-ear cavity pressures dramatically increase the total stiffness K_{doc} . Since the above analysis indicated that $K_{\text{eq}} \cong K_{\text{sc}}$, we cannot simply attribute these changes to manipulation of one stiffness or the other. It is possible that static MEC pressure affects both stiffnesses.

It is interesting to note that the low-frequency compliance changes vs static MEC pressures are asymmetrical with respect to positive and negative MEC pressures. Lynch et al., (1981) found the incremental stiffness of the annular ligament to be a function of the static pressure difference across the stapes footplate. The ossicular chain (except stapes) was removed in their preparation and the static perilymphatic pressure was thought to displace the stapes "outwards" (e.g., into the tympanic cavity); a minimum value of annular ligament stiffness was

found when a static MEC pressure of 7 cm H₂O was applied. {It is not known if the minimum would occur at 7 cm H₂O for the condition of an intact ossicular chain.} Changes in annular ligament stiffness appeared to be symmetrical about the minimum value. It is likely that the incremental stiffness of K_{eq} is also a function of static middle ear pressure. The asymmetry in K_{doc} might be explained if the incremental stiffness of K_{eq} were asymmetrical for positive and negative pressures and/or if the minimum in K_{eq} vs static MEC pressure occurred at a pressure substantially different from that of the K_{sc} curve (for intact ossicular chain).

Margolis et al., (1978) report tympanograms for $f = 220$ Hz and $f = 660$ Hz for an intact middle ear. Their results are in good agreement with our measurements. Our results are also in general agreement with those of Møller, 1965. His plots of acoustic impedance magnitude vs static MEC pressure for $f = 500$ Hz, 1.0 kHz, 2.0 kHz, and 3.0 kHz are quite similar to our results. Both Møller's results and ours show the resistive component of the impedance to be asymmetrical in that the resistance decreased more for negative than for positive pressures. Møller reports this result at one frequency (1 kHz); we found it to be true at most frequencies (FIGURES 10A to E). For positive pressure the resistance increases for many conditions.

FIGURES 9 and 10D indicate that changes in Y_{doc} vs static MEC pressure occur even at very high frequencies (near 10 kHz). Note that Y_{doc} has a negative angle in this frequency region in contrast to the positive angle ($\approx 90^\circ$) seen at low frequencies. In the preceding section we concluded that the uncoupled TM impedance, Z_{tmu} , significantly

affects the input impedance, Z_{doc} , at these frequencies. We therefore conclude that static MEC pressures probably affect Z_{tmu} for frequencies in the 5 kHz to 12 kHz region.

TABLE I
SUMMARY OF OSSICULAR MASS MEASUREMENTS

| CAT NUMBER | MALLEUS MASS (mg) | INCUS MASS (mg) | STAPES MASS (mg) |
|-----------------------|-------------------------|-----------------------|------------------------|
| 1818-R | 11.095 | --- | --- |
| 1859-R | 10.586 | 4.029 | 0.599 |
| 1859-L | 11.655 | 4.369 | --- |
| 1963-R | 10.630 | 4.300 | --- |
| 1963-L | 10.450 | 4.408 | --- |
| 1968-R | 11.035 | 3.941 | 0.490 |
| 1968-L | 12.325 | 3.955 | 0.531 |
| 1993-R | 11.294 | 4.684 | --- |
| 1993-L | --- | 4.819 | 0.498 |
| AVERAGE | 11.134 | 4.313 | 0.530 |
| STANDARD DEVIATION | 0.627 | 0.328 | 0.050 |

FIGURE CAPTIONS

FIGURE 1: A network model for the middle ear with middle-ear cavities removed. The form of the model is that of an electric network analog, where voltage is analogous to sound pressure (P) and current to volume velocity (U). The input impedance at the tympanic membrane (TM) with the MECs open, $Z_{doc} = P_d/U_d$, is the ratio of complex amplitudes of sound pressure at the TM, P_d , to TM volume velocity, U_d . Nodes are labeled A through D. Symbols for acoustic impedance of the corresponding anatomical components are given at the bottom of each box. Dashed boxes indicate impedances that have been previously determined.

FIGURE 2: Effects upon Y_{doc} resulting from the "removal" of the cochlear load and interruption of the incudo-stapedial joint. Data points are connected by straight-line segments and have a density of 40 points/decade in this and all subsequent frequency response plots. Symbols are used only to identify different curves.

FIGURE 3: Demonstration of the reversibility of the effects of interruption of the incudo-stapedial joint. Admittance measurements, Y_{doc} , were made at the tympanic membrane with the middle-ear cavities completely removed for 1) ossicular chain intact ("NORMAL"), 2) with "INTERRUPTED INCUDO-STAPEDIAL JOINT", and 3) with the joint "RECONNECTED" with cement.

FIGURE 4: Change in input admittance at the tympanic membrane, ΔY_{doc} , resulting from interruption of the incudo-stapedial joint in

four cats. The magnitude and angle of the complex ratio, ($Y_{\text{doc}} \text{ joint interrupted} / Y_{\text{doc}} \text{ normal}$), is plotted. Magnitude is expressed in dB, i.e., $20 \log_{10} \{\text{the ratio}\}$.

FIGURE 5: Effects upon Y_{doc} of interrupting the incudo-stapedial joint and subsequent interruption of the manubrium of the malleus.

FIGURE 6: Effects of mass loading of the malleus manubrium for the condition of intact ossicular chain (middle-ear cavities removed). The "NORMAL" curve was obtained before the mass was attached to the manubrium. The "MASS REMOVED" curve demonstrates the reversibility of this experimental manipulation.

FIGURE 7: Effects of mass loading of the malleus manubrium for the condition of interrupted manubrium. The "INTERRUPTED MANUBRIUM" curve was taken before the mass was attached. The "MASS REMOVED" curve demonstrates the reversibility of this experimental manipulation.

FIGURE 8: Effects upon Y_{doc} of mechanical fixation of the incus and stapes. The middle-ear cavities were removed. The "BLOCKED INCUS AND STAPES" curve was obtained when glue was used to affix the stapes and incus to the external wall of the cochlea.

FIGURE 9: Y_{d} resulting from the application of positive and negative static pressures to the intact middle-ear cavities of one cat. Part A illustrates results for negative static pressures. The curve labeled 0 cm H₂O is the normal input admittance at the tympanic membrane with cavities intact and is plotted in both (A) and (B). Part B gives results for positive static pressures.

FIGURE 10: "Tymanograms" constructed from the measurements of FIGURE 9. Results are given for five frequencies (224 Hz, 1.0 kHz, 2.0 kHz, 3.35 kHz, and 9.44 kHz) in Parts (A) through (E). The left plot in each figure is admittance magnitude and angle vs static middle-ear cavity (MEC) pressure. Admittance magnitudes, $|Y|$, are given in dB re 1 cgs mho, i.e. $20\log_{10}\{|Y|/1 \text{ mho}\}$ where $1 \text{ mho} = 1 \text{ cm}^5/(\text{dyn-s})$. Thus, -60 dB is 1 mmho. The middle graph is the real (G) and imaginary (B) parts of the admittance plotted vs static MEC pressure. The plot on the right is the real (R) and imaginary (X) parts of the impedance vs static MEC pressure. Data points marked by an X in Part A represent points where the computed resistance or conductance was negative; the symbol was placed at $R = 0$ or $G = 0$ when this situation occurred.

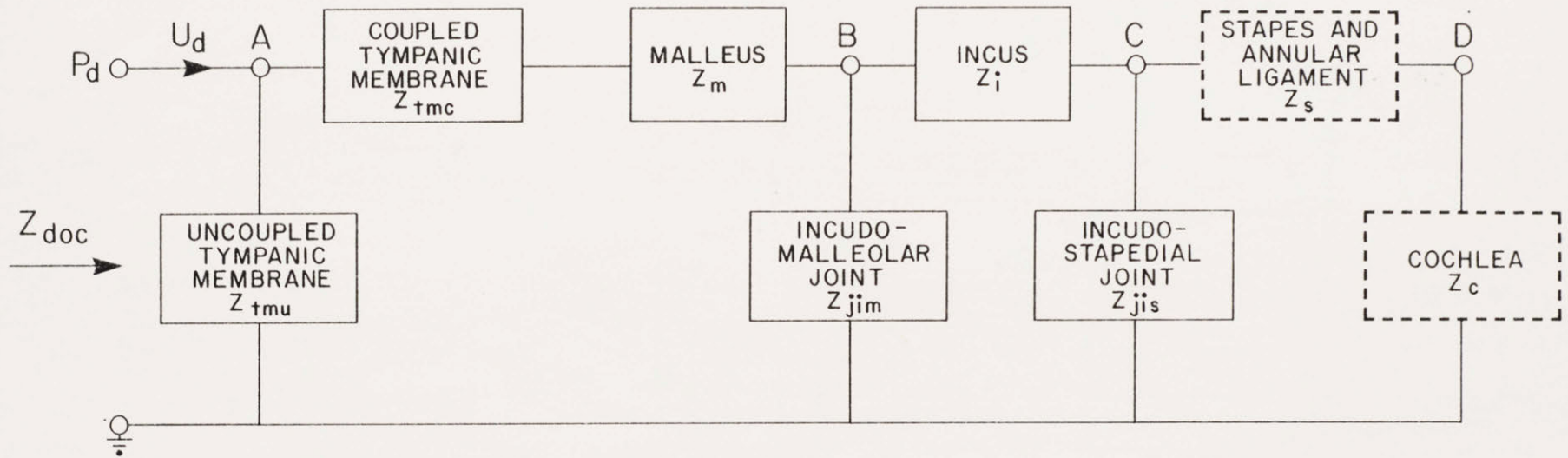


FIGURE 1

FIGURE 2

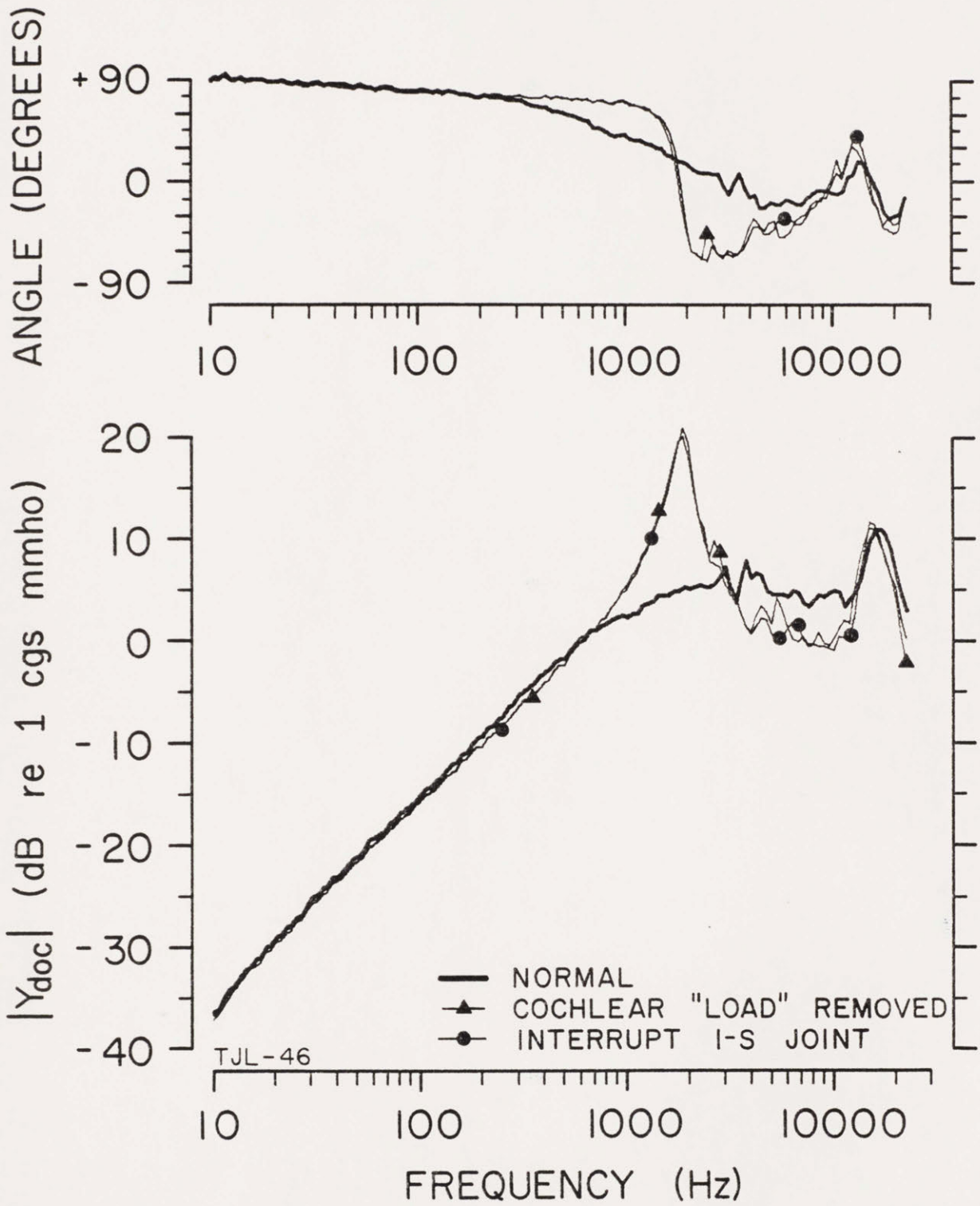


FIGURE 4

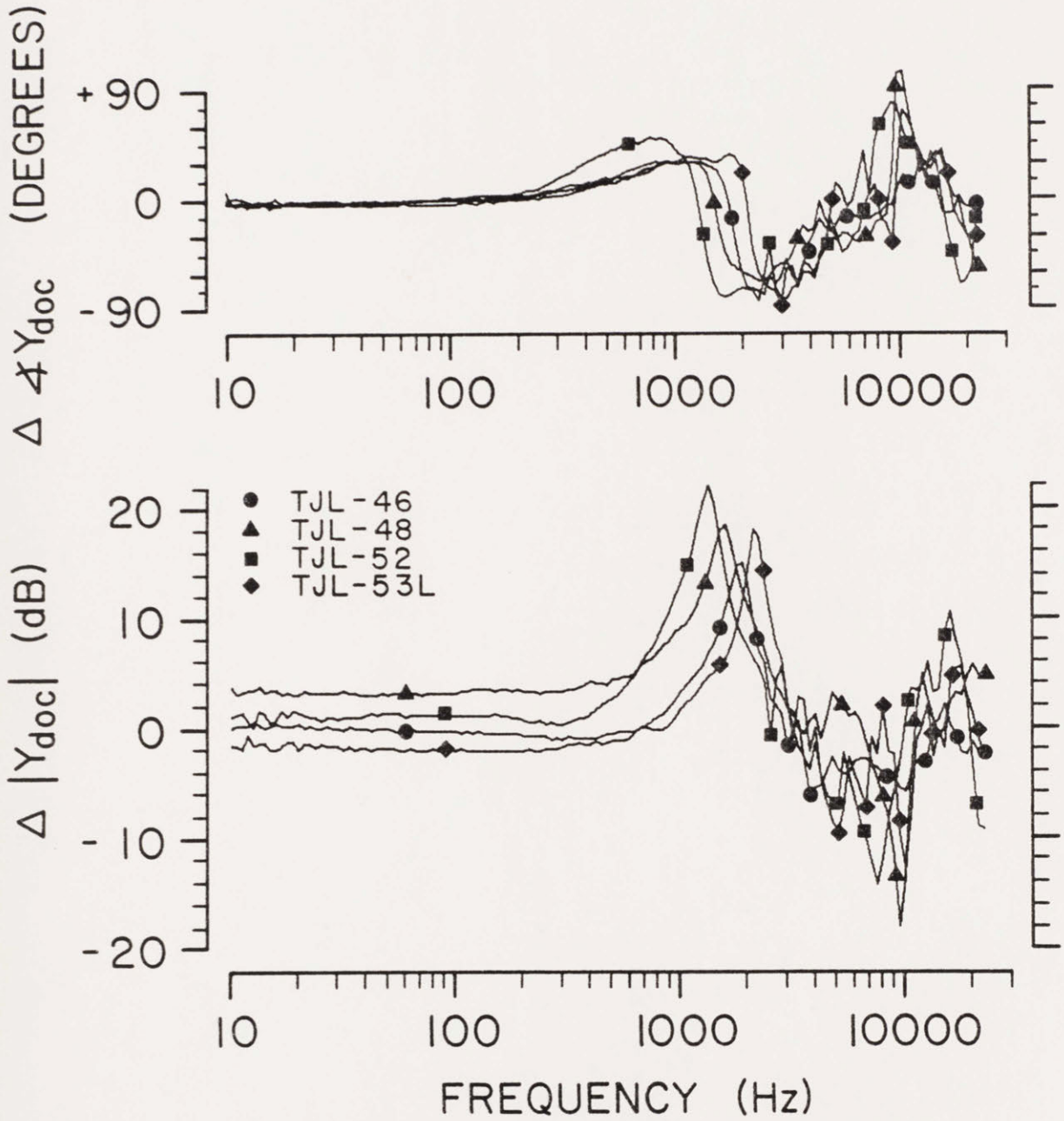


FIGURE 5

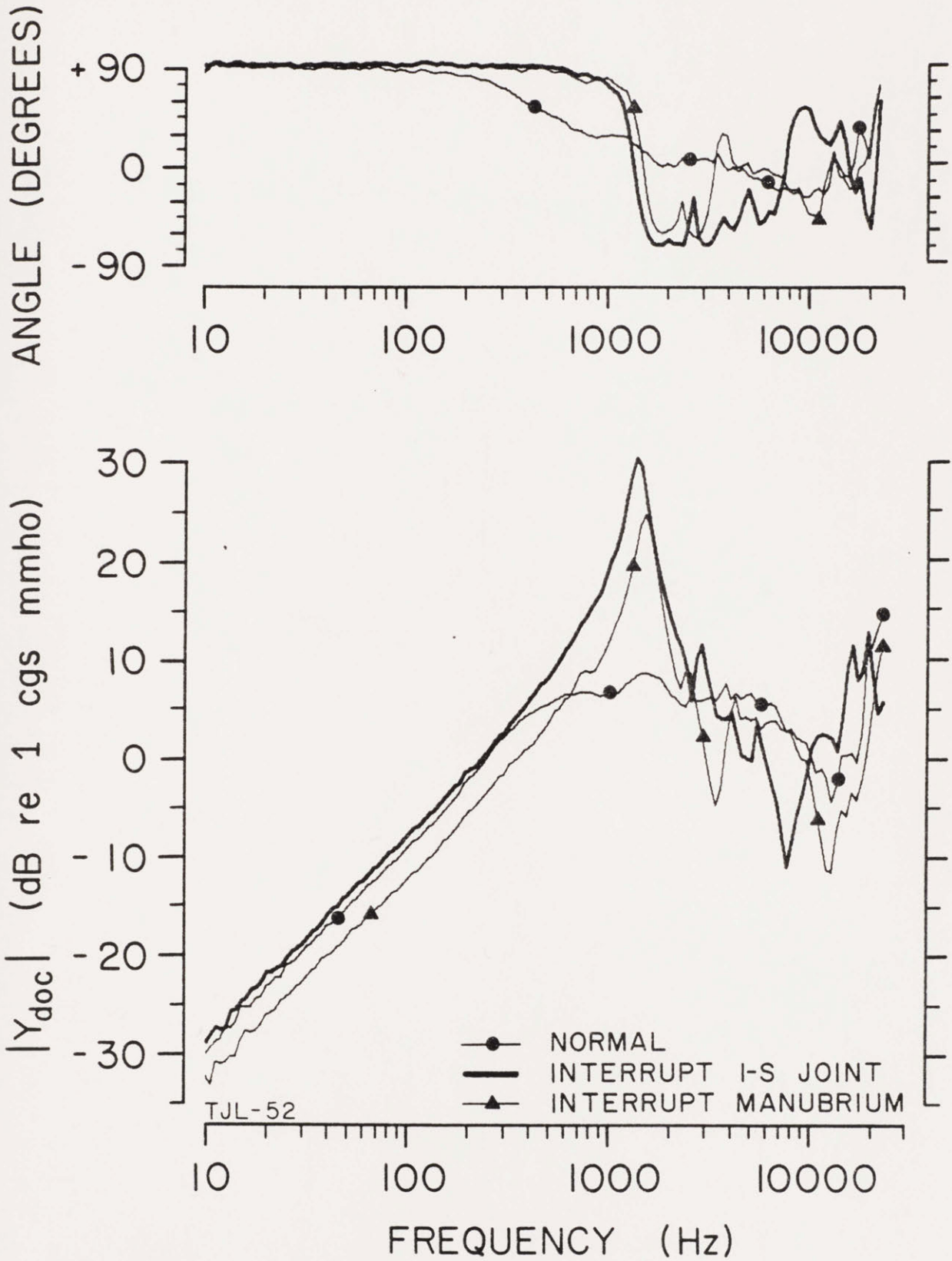


FIGURE 6

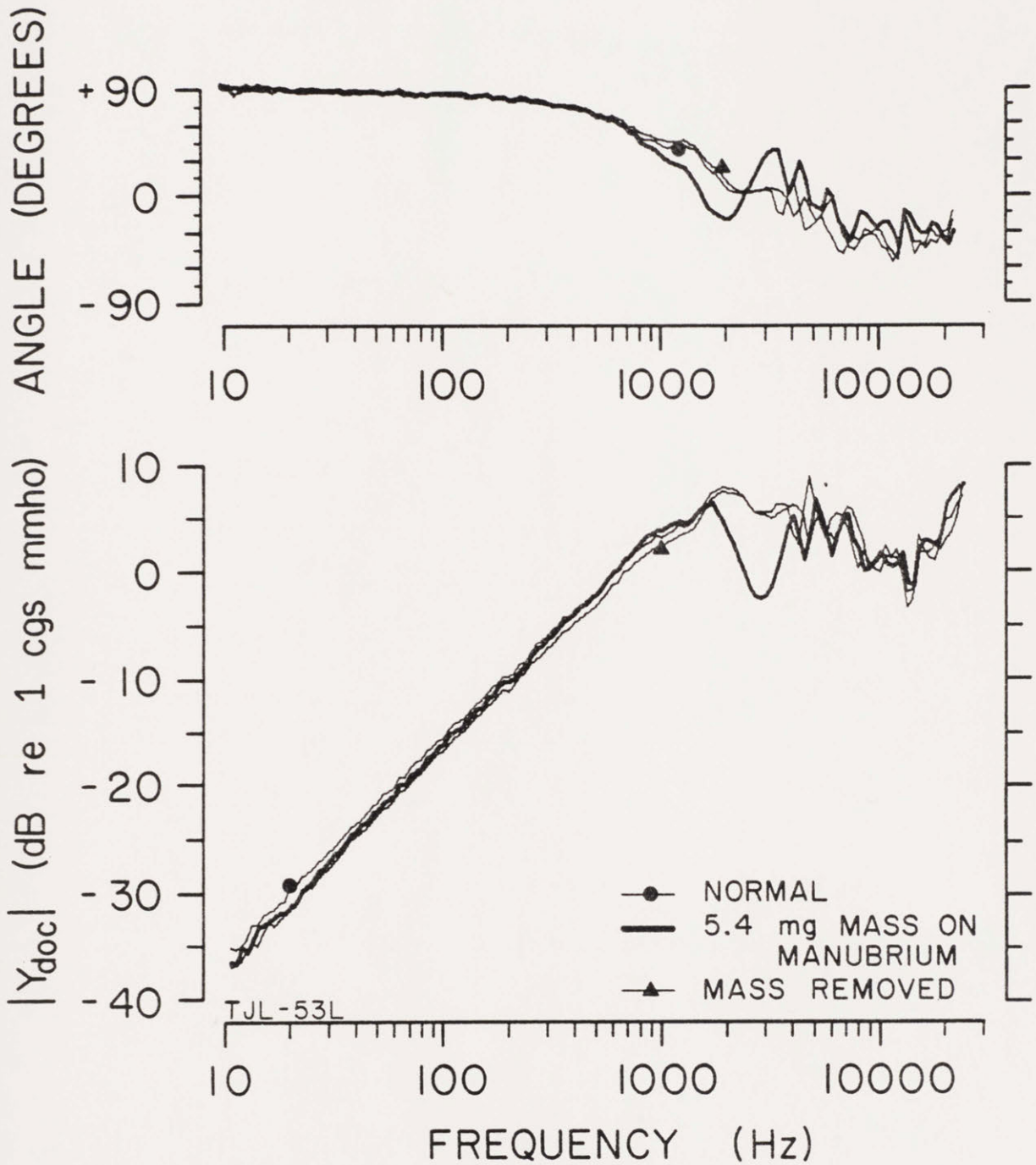


FIGURE 7

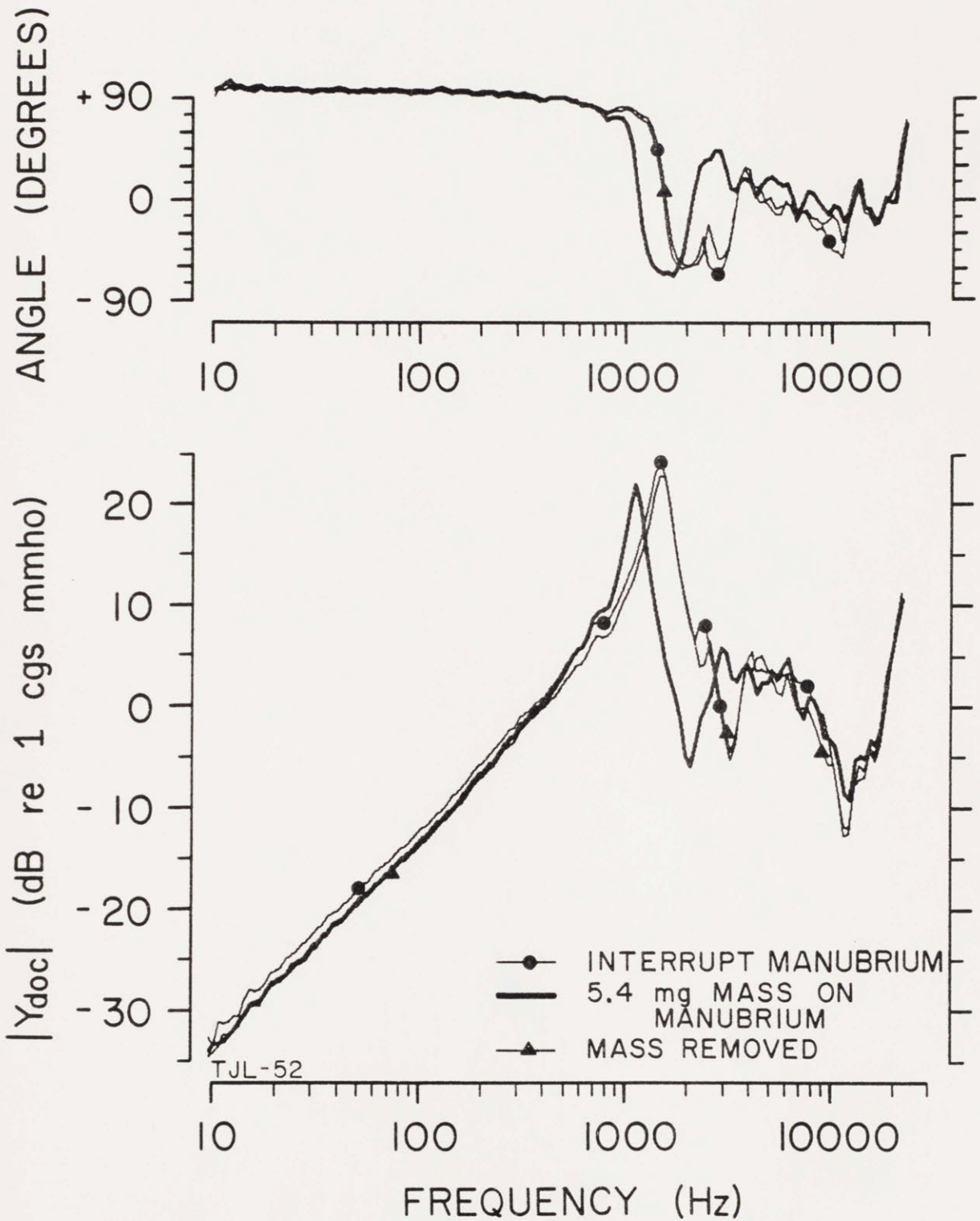


FIGURE 8

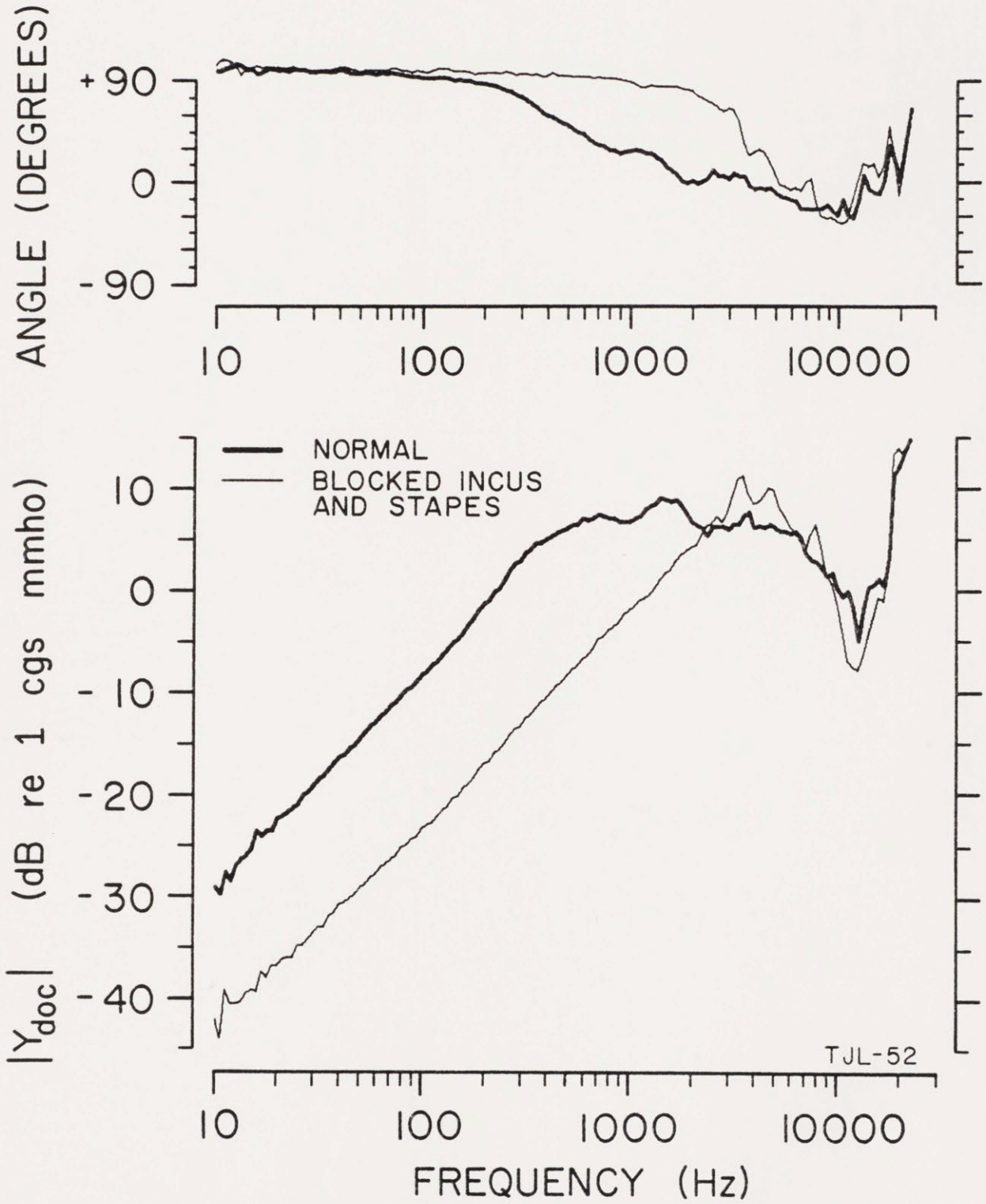


FIGURE 9A

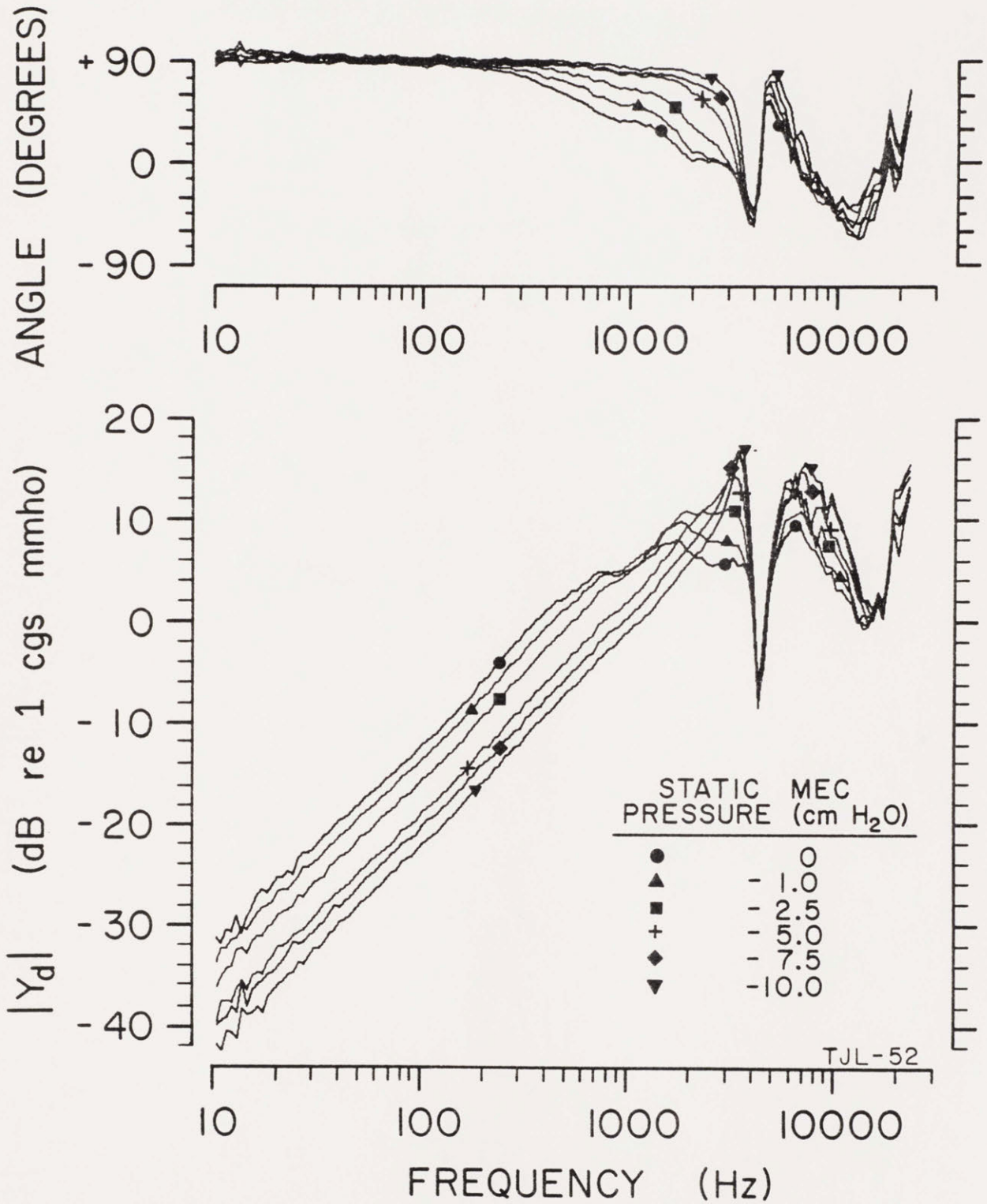
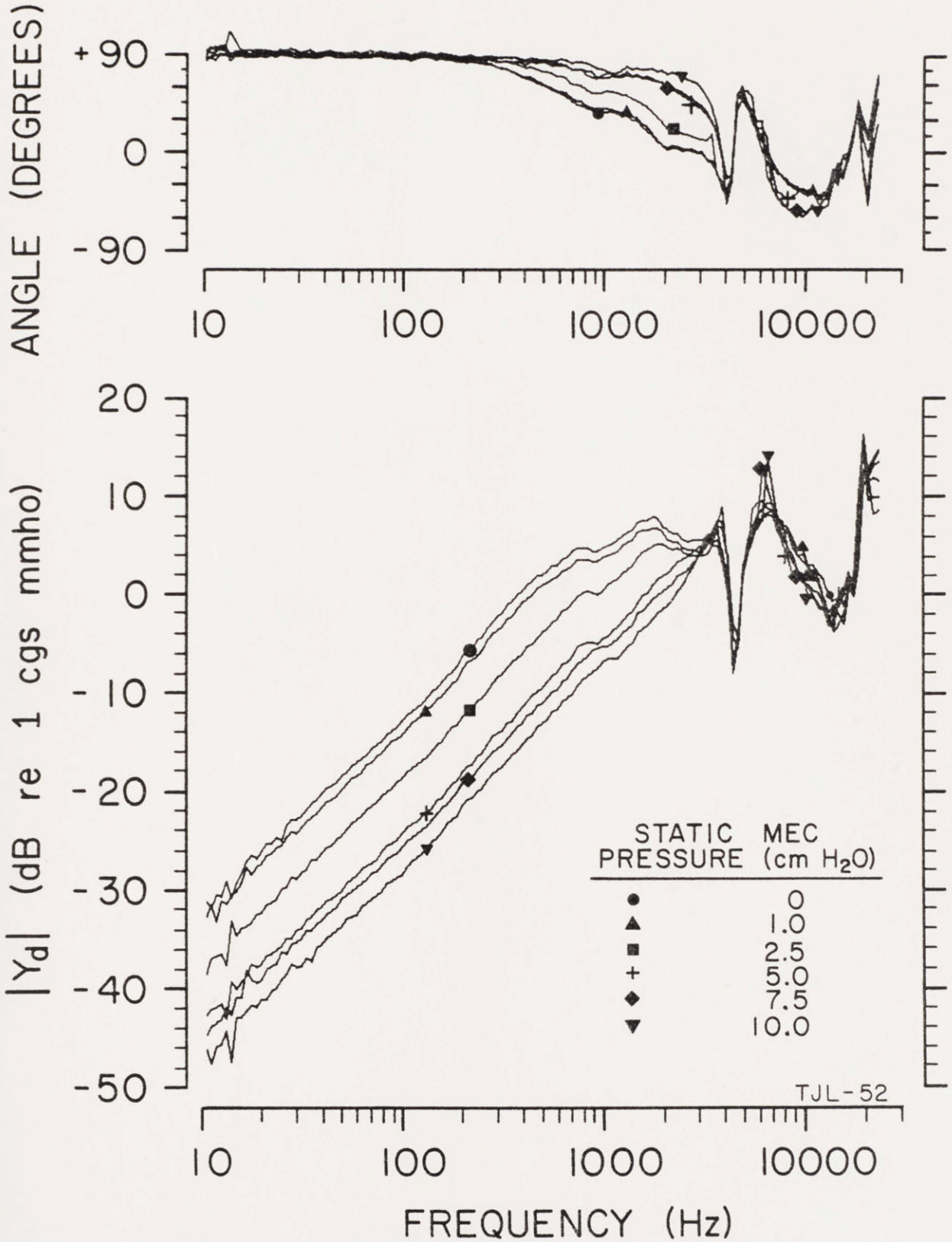


FIGURE 9B



TYMPANOGRAMS (f = 224 Hz)

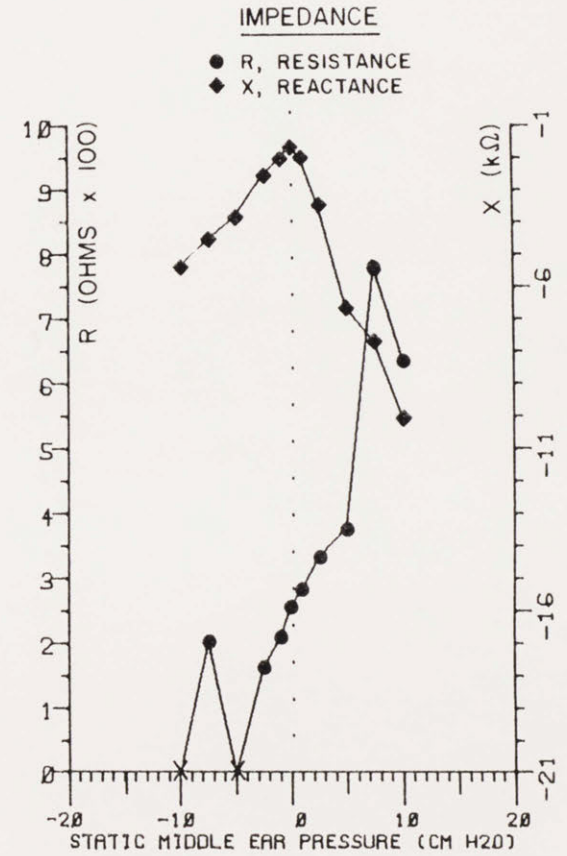
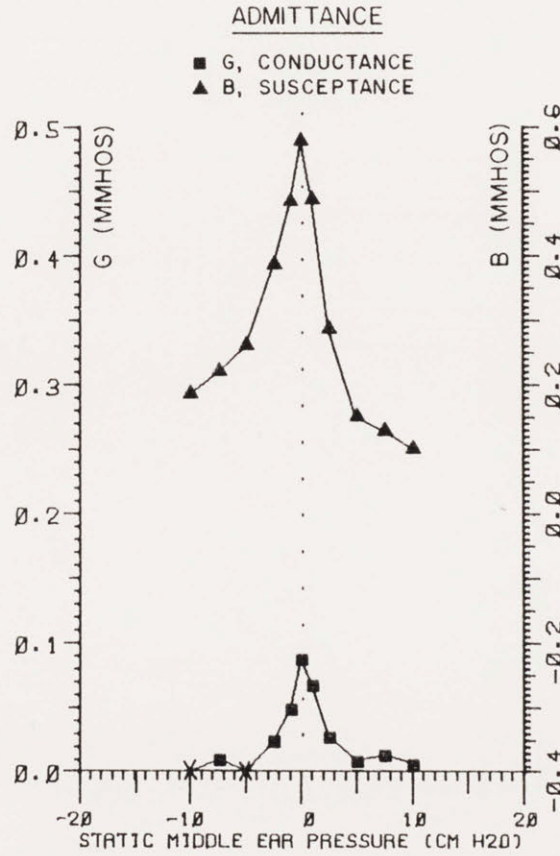
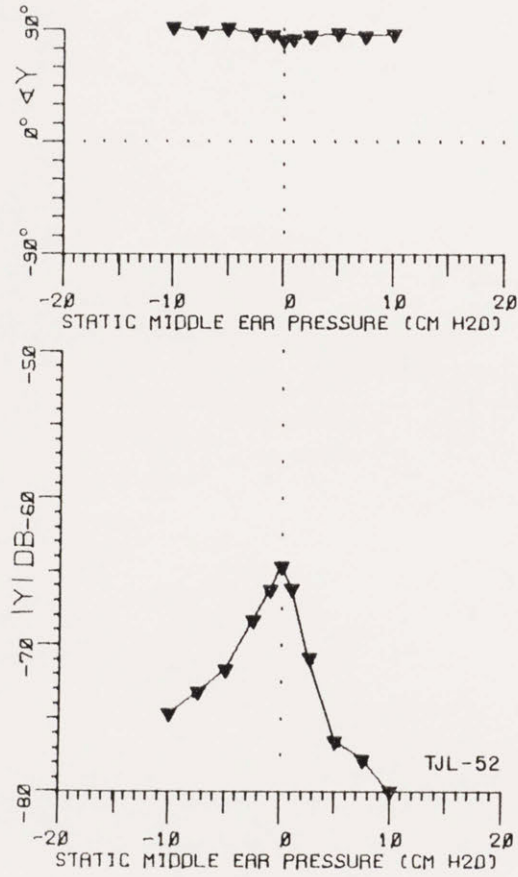


FIGURE 10A

TYMPANOGRAMS (f = 1.0 kHz)

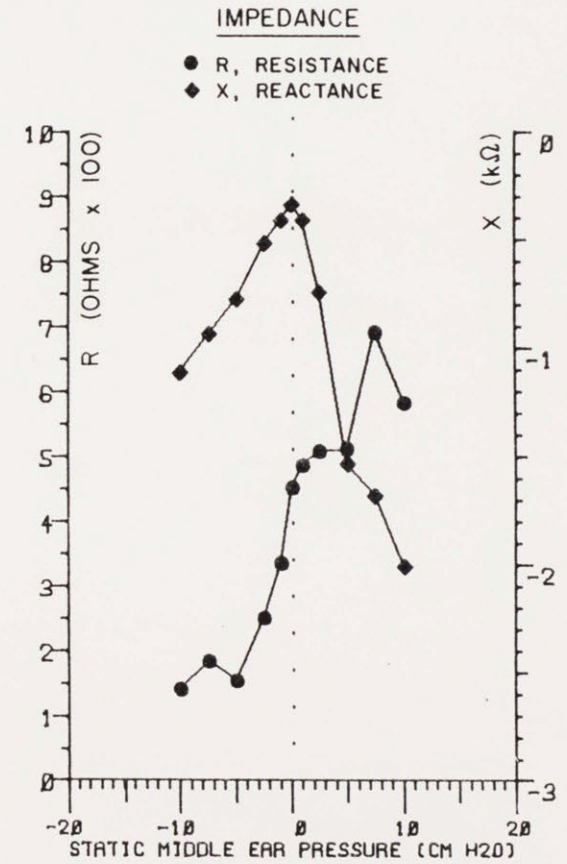
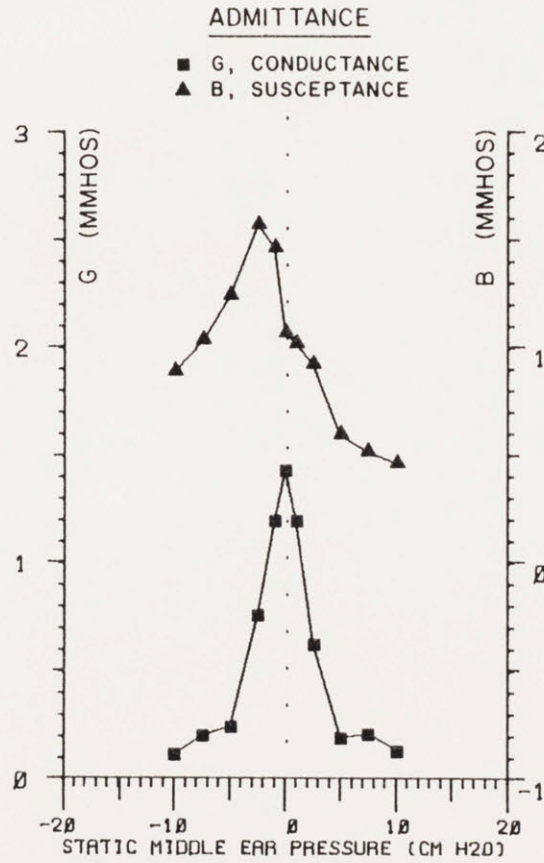
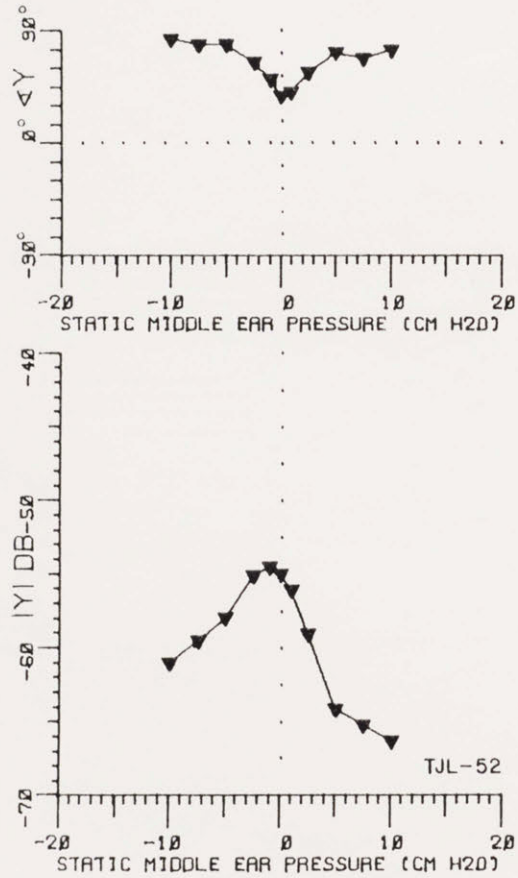


FIGURE 10B

TYMPANOGRAMS (f = 2.0 kHz)

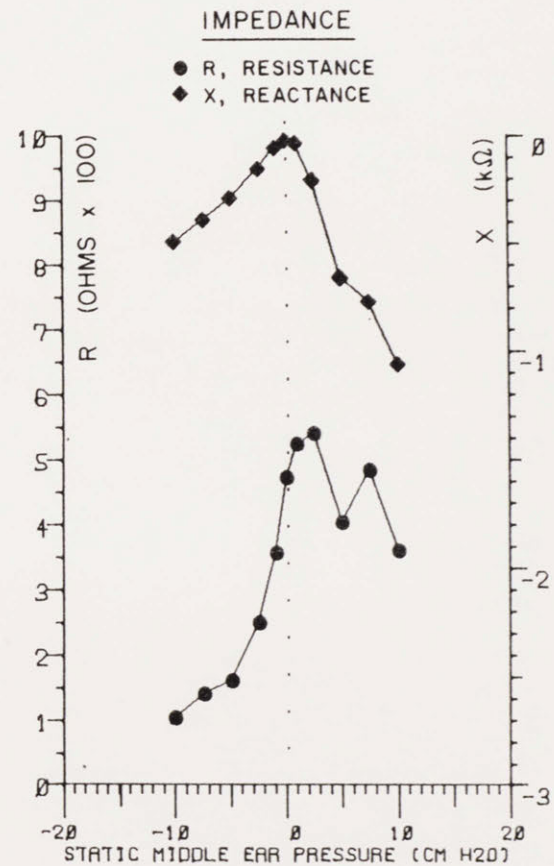
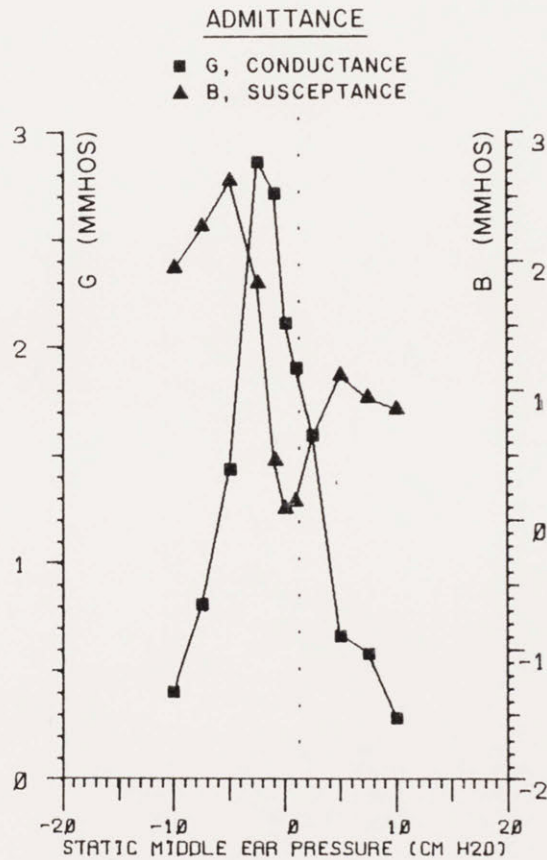
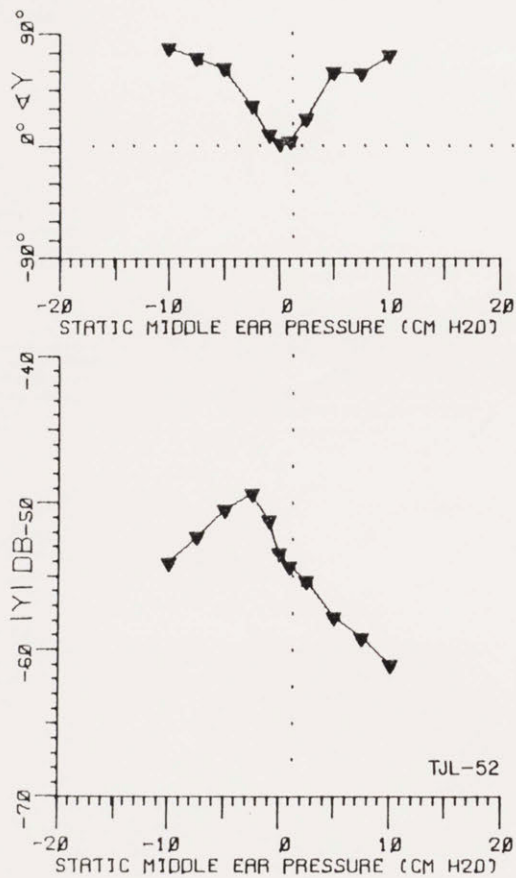


FIGURE 10C

TYMPANOGRAMS (f = 3.35 kHz)

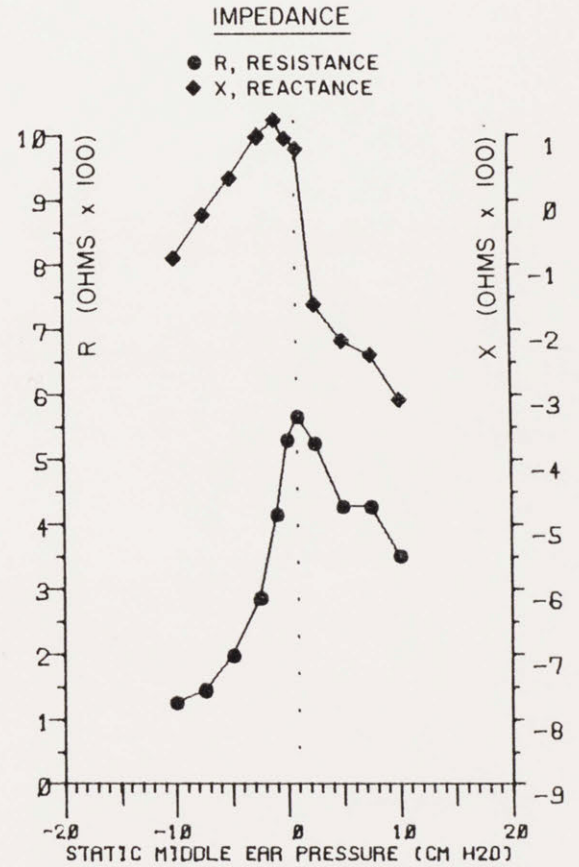
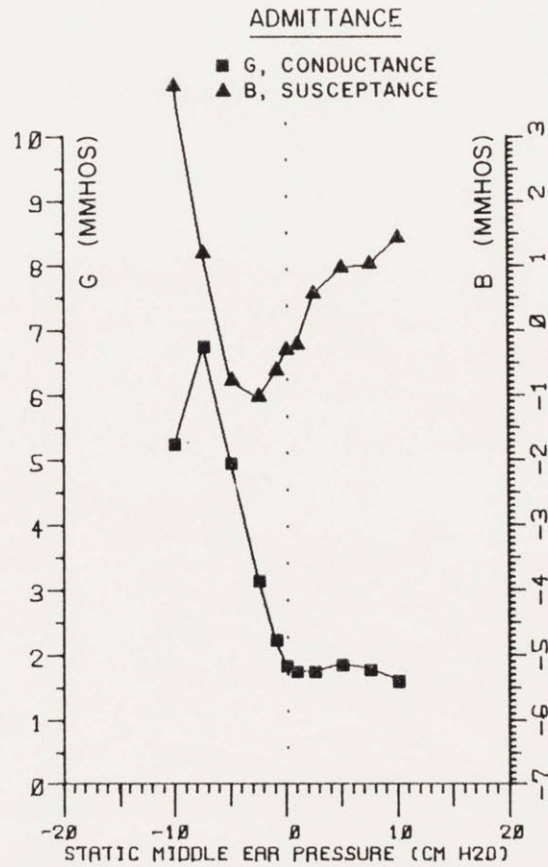
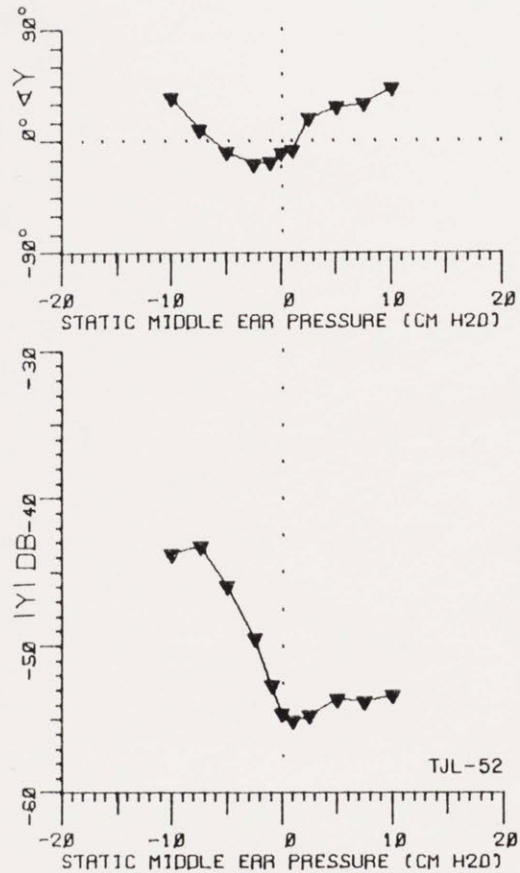


FIGURE 10D

TYMPANOGRAMS (f = 9.44 kHz)

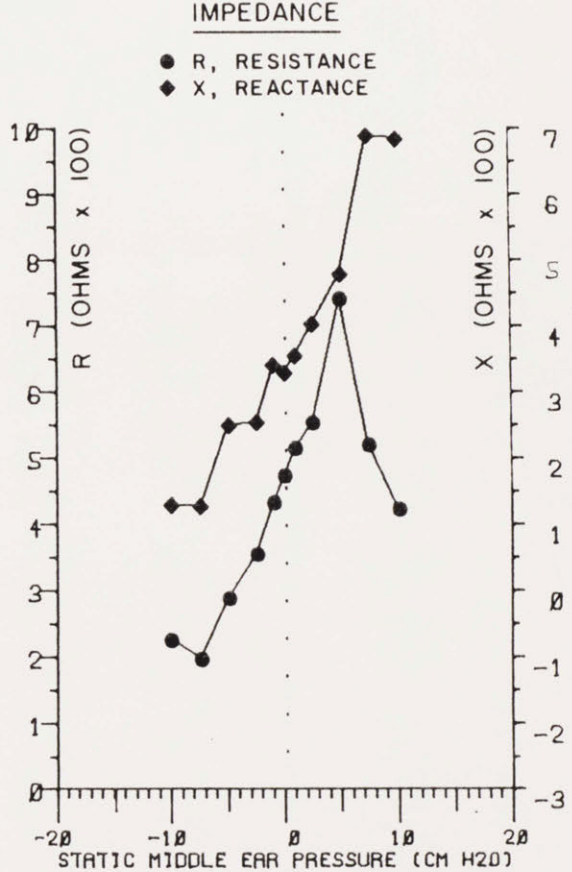
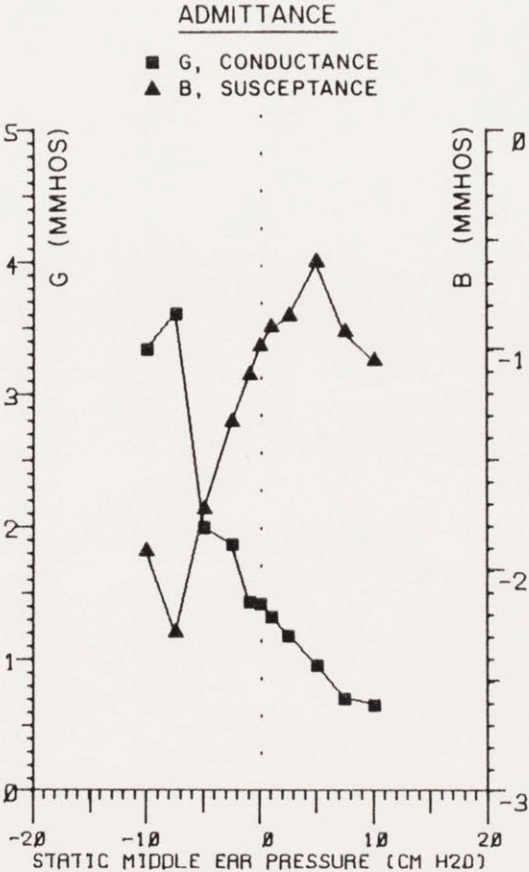
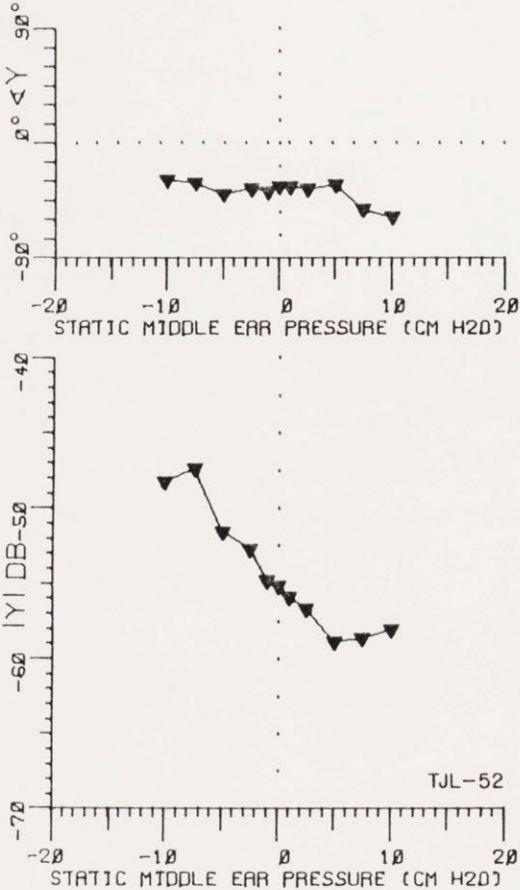


FIGURE 10E

REFERENCES

- Funnell, W.R.J. (1975). "A Theoretical Study of Eardrum Vibrations Using the Finite-Element Method," Ph.D. Thesis, McGill Univ., Montreal, Canada, pp. 1-199.
- Guinan, J.J., Jr., and Peake, W.T. (1967). "Middle-ear characteristics of anesthetized cats," *J. Acoust. Soc. Am.* 42, 1237-121.
- Johnstone, B.M., and Taylor, K.J. (1971). "Physiology of the middle ear transmission system," *J. Oto-Laryngol. Soc. of Australia* 3, 226-228.
- Kopec, G.E. (1973). "Cochlear Potential Change After Increasing Middle Ear Inertia," S.B. Thesis, Massachusetts Institute of Technology, Cambridge, Ma., pp. 1-44.
- Lynch, T.J., III. (1974). "Measurements of Acoustic Input Impedance of the Cochlea in Cats," S.M. Thesis, Massachusetts Institute of Technology, Cambridge, Ma., pp. 1-180.
- Lynch, T.J., III. (1978). "An Analysis of the Signal Transmission Properties of the Cat Middle Ear," Ph.D. Thesis proposal, Massachusetts Institute of Technology, Cambridge, Ma., pp. 1-248.
- Lynch, T.J., III, Nedzelnitsky, V., and Peake, W.T. (in preparation). "Input impedance of the cochlea in cat."
- Margolis, R.H., Osguthorpe, J.D., and Popelka, G.R. (1978). "The effects of experimentally-produced middle ear lesions on tympanometry in cats," *Acta Otolaryngol.* 86, 428-436.
- Møller, A.R. (1965). "An experimental study of the acoustic impedance of the middle ear and its transmission properties," *Acta Otolaryngol.* 60, 129-149.
- Peake, W.T., and Guinan, J.J. (1967). "Circuit model for the cat's middle ear," M.I.T. Research Laboratory of Electronics, Quarterly Prog. Rep. No. 84, 320-326.
- Rabinowitz, W.M. (1977). "Acoustic-Reflex Effects on the Input Admittance and Transfer Characteristics of the Human Middle-Ear," Ph.D. Thesis, Massachusetts Institute of Technology, Cambridge, Ma., pp. 1-250.
- Schubert, E.D. (1978). "History of research on hearing," In: Handbook of Perception, Vol. IV, Hearing, edited by E.C. Carterette and M.P. Friedman (Academic, New York), pp. 41-80.
- Siebert, W.M. (1973). "Hearing and the Ear", In: Engineering Principles in Physiology, Vol. I (Academic, New York/London), pp. 139-184.

Wever, E.G., and Lawrence, M. (1954). Physiological Acoustics
(Princeton Univ., New Jersey).

Wever, E.G., Lawrence, M., and Smith, K.R. (1948). "The middle ear in
sound conduction," Arch. Otolaryngol. 48, 19-35.

BIOGRAPHICAL NOTE

Thomas Joseph Lynch III

Born:

October 7, 1949
Hartford, Connecticut

Education:

| | |
|----------|---|
| B.S.E.E. | University of Cincinnati, 1972 |
| S.M. | Massachusetts Institute of Technology, 1974 |
| E.E. | Massachusetts Institute of Technology, 1975 |

Research and/or Professional Experience:

| | |
|----------------|--|
| 1973 - present | Research Assistant in Otolaryngology, Eaton-Peabody Laboratory Massachusetts Eye and Ear Infirmary |
| 1973 - 1975 | Teaching Assistant in Electrical Engineering Massachusetts Institute of Technology |
| 1975 | Electrical Engineer Comsat Laboratories Clarksburg, Maryland |
| 1970 - 1972 | (Cooperative Student) |
| 1968 - 1970 | Cooperative Student Ohio Valley Electric Corporation Piketon, Ohio |
| 1972 | Electronics Technician Hobart Manufacturing Company Hillsboro, Ohio |

Awards

Tau Beta Pi, Eta Kappa Nu, Sigma Xi
Whitaker Health Sciences Fund Fellow, 1977 - 1979
College of Engineering Academic Achievement Award, 1970
Ohio Association of Emblem Clubs Scholarship, 1967

Publications

Lynch, T.J., III, Nedzelnitsky, V., Peake, W.T. (1976). "Measurements of Acoustic Input Impedance of the Cochlea in Cats", Journal of the Acoustical Society of America, 59, S30(A).
Lynch, T.J., III, Nedzelnitsky, V., Peake, W.T. "Input Impedance of the Cochlea in Cat", (in preparation for Journal of the Acoustical Society of America)